KAUNAS UNIVERSITY OF TECHNOLOGY

RENJI R. REGHU

SYNTHESIS AND PROPERTIES OF ELECTRON-DONOR FUNCTIONALIZED CHARGE-TRANSPORTING COMPOUNDS CONTAINING AROMATIC OR HETEROAROMATIC CORES

Doctoral dissertation
Technological sciences, Materials engineering (08T)

2012, Kaunas

The research was carried out at Kaunas University of Technology, Department of Organic Technology in the period of 2009-2012. It was supported by FP-7 PEOPLE PROGRAMME, Marie Curie Actions – ITN Grant No. 215884.

Dissertation defended externally

Scientific advisor:

Prof. Dr. Habil. Juozas Vidas Gražulevičius (Kaunas University of Technology, Technological Sciences, Materials Engineering – 08T).

The dissertation is available on the Internet:

http://en.ktu.lt/research/dissertations/view-of-all-dissertations

Reviewed by:

Prof. Dr. Šarūnas Meškinis (Kaunas University of Technology, Technological Sciences, Materials Engineering – 08T).
Prof. Dr. Saulius Grigalevičius (Kaunas University of Technology, Technological Sciences, Materials Engineering – 08T).

ISBN xxxx-xxxx

KAUNO TECHNOLOGIJOS UNIVERSITETAS

RENJI R. REGHU

ELEKTRONŲ DONORINĖMIS GRUPĖMIS FUNKCIONALIZUOTŲ ORGANINIŲ PUSLAIDININKIŲ, TURINČIŲ AROMATINES IR HETEROAROMATINES ŠERDIS, SINTEZĖ IR SAVYBĖS

Daktaro disertacija
Technologijos mokslai, Medžiagų inžinerija (08T)

2012, Kaunas

Disertacija parengta 2009-2012 metais Kauno technologijos universiteto Cheminės technologijos fakultete, Organinės technologijos katedroje. Mokslinius tyrimus rėmė 7-BP Žmonių programa, Marie Curie veikla – ITN granto Nr. 215884.

Disertacija ginama eksternu

Mokslinis konsultantas:

Prof. habil. dr. Juozas Vidas Gražulevičius (Kauno technologijos universitetas, technologijos mokslai, medžiagų inžinerija – 08T).

Interneto svetainės, kurioje skelbiama disertacija, adresas:

http://ktu.lt/kas-kur-kada?tipas=disertacija

Recenzavo:

Prof. dr. Šarūnas Meškinis (Kauno technologijos universitetas, technologijos mokslai, medžiagų inžinerija – 08T).
Prof. dr. Saulius Grigalevičius (Kauno technologijos universitetas, technologijos mokslai, medžiagų inžinerija – 08T).

ISBN xxxx-xxxx

List of Abbreviations

A-D-A	Acceptor-donor-acceptor
Alq_3	Tris(8-hydroxyquinoline) aluminium
α	Pool-Frenkel parameter
BHJ	Bulk heterojunction
CV	Cyclic voltametry
Col_h	Columnar hexagonal
CT	Charge transfer
^{13}CNMR	Carbon nuclear magnetic resonance
CIE	Commission Internationale d'Eclairage
DSSCs	Dye-sensitized solar cells
DSC	Differential scanning calorimetry
D-A	Donor-acceptor
D-A-D	Donor-acceptor-donor
DPV	Differential pulse voltametry
DMF	Dimethylformamide
DMSO	Dimethylsulfoxide
DCM	Dichloromethane
DPB	4-(Diphenylamino)phenylboronic acid
DFT	Density functional theory
dppe	1,2-Bis(diphenylphosphino)ethane
dba	*E*,*E*-dibenzylideneacetone)
d	doublet
dd	doublet of doublet
EDOT	3, 4-Ethylenedioxy thiophene
EL	Electroluminescence
E_g^{opt}	Optical band gap
E_g^{ele}	Electrochemical band gap
E_{red}	Reduction potential
E_{oxi}	Oxidation potential
E_A	Electron affinity
η_{ext}	External quantum efficiency
η_p	power efficiency
FMO	Frontier molecular orbital
FIrpic	Iridium(III)[bis(4,6-difluorophenyl)-pyridinato-*N*,$C^{2'}$]picolinate
HOMO	Highest Occupied Molecular Orbital
^{1}H NMR	Proton nuclear magnetic resonance
ICT	Intramolecular charge transfer
I_P	Ionization potential
ITO	Indium tin oxide
LUMO	Lowest Unoccupied Molecular Orbital
Liq	8-hydroxyquinolinolato lithium
λ_{em}	Emission maximum

λ_{abs}	Absorption maximum
MALDI-TOF	Matrix-Assisted Laser Desorption/Ionization-Time of Flight
4-MTP	4-methoxythiophenol
MEH-PPV	Poly[2-methoxy-5-(2-ethyl-hexyloxy)-1,4-phenylene-vinylene]
μ_o	Zero field mobility
μ	Charge carrier mobility
NBS	N-Bromosuccinimide
NMP	N-methyl pyrrolidone
NPB	*N, N '*-diphenyl-*N, N'*-bis(1-naphthyl)-(1,1 '-biphenyl)-4, 4'-diamine
OFETs	Organic field-effect transistors
OLEDs	Organic light emitting diodes
OPVs	Organic photovoltaic devices
PL	Photoluminescence
PEDOT	Poly (3, 4-ethylenedioxythiophene)
PSS	Poly (styrenesulfonate)
PLED	Polymer light emitting diode
PBI	Perylene bisimide
$PPy)_2Ir(acac)$	Iridium(III) bis(2-phenylpyridinato-*N*,$C^{2'}$) acetylacetonate
PS	polystyrene
PC-Z	bisphenol Z polycarbonate
PTC	Phase transfer catalyst
PFBT	Pentafluorobenzenthiol
PCE	Power conversion efficiencies
PBI-F	*N,N'*-bis(2,2,3,3,4,4,5,5,5-nonafluoropentyl)-3,4:9,10-perylene-tetracarboxylicacid bisimide
Φ_F	Fluorescence quantum yield
SCLC	Space-charge limited current
SAM	Self-assembled monolayer
TGA	Thermogravimetric analysis
TPA	Two-photon absorption
TPD	*N*,*N*-bis(3-methylphenyl)-*N*,*N*-diphenylbenzidine
THF	Tetrahydrofuran
TB	2, 5-Thiophenediylbisboronic acid
TPZ	2, 4, 6-triphenyl-1, 3, 5-triazine
TfOH	Trifluoromethane sulfonicacid
TBAF	Tetra-n-butylammonium fluoride
T_g	Glass transition temperature
T_D	Thermal decomposition onset
T_m	Melting transition
T_{cr}	Crystallization temperature
τ	Fluorescent decay time constant
XRD	X-ray diffraction
XTOF	Xerographic time-of-flight

Contents

1. INTRODUCTION

Symmetry has fascinated chemists from earlier times. In addition to the inherent beauty of symmetric molecules, symmetry plays a significant role in important chemical topics such as supramolecular self-assembly, chemical selectivity or synthesis including asymmetric synthesis and asymmetric catalysis. Symmetric conjugated organic materials, for example, star-shaped compounds, starbursts or dendrimers, exhibit a great variety of technologically relevant properties like absorption and emission of light or electrical and photoconducting properties; thus making them useful materials for the application in electronic and optoelectronic devices such as organic field-effect transistors (OFETs), organic light emitting diodes (OLEDs) and organic photovoltaic devices (OPVs).

Symmetrical compounds containing arylene imide, pyrene, triphenylamine and triazine moieties as the central core have been explored extensively as organic luminescent and charge transporting materials for organic electronics and optoelectronics. Moreover, these central cores provide the opportunity for multifunctionalization with other conjugated molecular moieties and thus, afford the tunabitity of the properties such as photoelectrical, optical, photoluminescent, redox and/or thermal characteristics. Electron-donor chromophore, for example, carbazolyl, fluorenyl, phenothiazinyl *etc*, substitutions to these molecular cores could extent the conjugation length of their derivatives which in turn change the aforementioned properties.

Charge-transport is an important property for the opto-electronic device applications. Charge-transporting compounds can be of *p*-type (hole transporting), *n*-type (electron transporting), or ambipolar (capable of transporting both holes and electrons). Extensively used practical devices are based mainly on hole-transporting materials as active layers. However the demand for efficient electron-transporting and ambipolar organic materials cannot be overestimated.

Perylene bisimide and triazine moieties can serve as electron-deficient molecular cores whereas pyrene and triphenylamine derivatives are electron-rich compounds. Electron-donor substitutions to the electron-deficient/rich central cores not only alter the molecular orbitals in order to match the work functions of the commonly used electrodes but also tune the semiconducting characteristics. Perylene bisimide and triazine core functionalization of electron-donors can produce electron-transporting or ambipolar organic electroactive materials. On the other hand, electron-donor chromophores attached to pyrene and triphenylamine central-core can yield hole-transporting compounds with interesting redox-properties and luminescent characteristics. The compounds synthesized in this work are intended mainly for the two areas of organic electronics, i.e. OFETs and OLEDs.

The charge-transporting properties are not only depending on the intrinsic electronic properties of the materials but also rely on the microscopic and macroscopic order of the materials in the solid state. Most of the low-molar-mass charge transporting materials are not capable of forming thin, neat, homogenous layers, and must be used in combination with polymeric hosts. The presence of a large proportion of polymer host in the compositions, leads to considerable decrease

of charge carrier mobility. Hence, low-molecular-weight materials that form stable glasses having glass transition temperatures above room temperature are of interest. Moreover, room temperature organic liquid crystals with dendritic architecture are also of interest since the molecular order in the mesophase enhances the charge-transport and the dendritic shape improves the processability. Solution processable film-forming organic materials are particularly interesting in the context of cost-effective device fabrication.

The number of air stable organic semiconductors showing ambipolar behaviour is limited because of the critical position of their molecular orbitals; i.e. such kind of molecules should have low laying HOMO (slightly lower than -5.0 eV) and LUMO (below -3.9 eV with respect to the vacuum level) energy levels. Moreover, some of organic ambipolar materials are hardly soluble and for this reason difficult to be used in large area printed electronics. In this viewpoint, solution processable ambipolar organic materials are of great interest.

Symmetric luminescent organic materials with high emission quantum yields and substituent dependant emission behaviour are also of interest in the standpoint of structure-property relationship and the possible application in OLEDs.

The main aims of this work were:

1. Synthesis and studies of the properties of new solution processable electron-transporting and ambipolar donor-acceptor hybrids for organic electronics.
2. Synthesis and investigation of the properties of dendritic charge-transporting materials possessing luminescence and redox characteristics which make them promising for the application in optoelectronics.

The tasks proposed for the achievement of the above stated aims were as follows:

1. Synthesis and investigation of thermal, electrochemical, photoelectrical and photophysical properties of donor-substituted arylene imides.
2. Synthesis and investigation of the properties of pyrene, triazine and triphenylamine core-centred organic materials containing electron-donor chromophores.
3. Testing of the synthesized materials in the structures of electronic and optoelectronic devices.

The main statements of doctoral dissertation are:

1. The newly synthesized solution processable bay carbazol-2-yl or -3-yl substituted perylene bisimides are applicable as ambipolar organic semiconductors with complementary charge-transporting properties.
2. Bay triphenylamino substituted perylene bisimide is relevant for the fabrication of solution processable ambipolar organic field-effect transistor.
3. Electron-donor functionalized pyrene, triazine and triphenylamine core-centred organic materials exhibiting good luminescence, charge-transport and redox characteristics are appropriate for application in optoelectronic devices.

2. LITERATURE REVIEW

Symmetric organic electroactive materials containing electron-donors

2.1. Introduction

Electronic and optoelectronic devices using organic materials as active layer(s), for example; electrophotographic photoreceptors, organic light-emitting diodes, organic photovoltaic devices or organic field-effect transistors, have recently been received enormous interest from both the academia and industry from the standpoint of potential technological applications as well as fundamental sciences [1,2,3,4]. The devices using organic materials are attractive because they can take advantage of organic materials such as light weight, potentially low cost, and capability of thin-film, large-area, flexible device fabrication. Photoreceptors in electrophotography using organic photoconducting materials have already established wide markets of copying and laser printers [5,6]. OLEDs have also found practical applications in small displays such as mobile phones, digital camera finders, car audios and lighting [7]. Organic photovoltaic devices are viewed as one of the most promising candidates for low cost energy sources because of the possibility of a production on flexible and large-area substrates by solution processing that should dramatically reduce the manufacturing costs [3,8]. OFET-driven displays have also been applied in low-cost electronics like logic circuits for radiofrequency identification tagging, smart cards, and chemical and biological sensors [9,10,11,12].

The development of high performance charge-transporting materials is a key issue for the fabrication of organic electronic and optoelectronic devices with better performance since the charge-transport is an as an essential operational process in these devices. Charge-transporting organic materials are mostly based on π-electron systems, which are characterized by properties such as light absorption and emission in the ultraviolet-visible-near infrared wavelength region, charge-carrier generation and transport, nonlinear optical properties *etc*. Organic charge-transporting materials include small molecules (i.e. molecular materials), dendrimers and polymers [13,14,15,16].

Electron-donors are regarded as electron-rich chemical entities or compounds that donate electrons to other moieties. They are widely employed in the synthesis of charge-transporting materials, particularly, hole-transporting and ambipolar (transporting both holes and electrons) organic materials for electronic and optoelectronic applications. The electron-rich chromophores such as carbazole, triphenylamine, phenothiazine, thiophene, fluorene, alkoxy-phenyl *etc*, and their derivatives have the capability of donating electrons and have extensively been exploited in the synthesis of organic p-type semiconductors [17,18,19,20,21,22]. Though these compounds can transport holes inherently, the electronic properties can be changed according to the application by functionalizing with other electron-donors. Dendritic charge-transporting materials are particularly interesting since their nano dimension, monodisperse characteristics and the extended conjugation brings unique photophysical and photoelectrical properties important for device

fabrication. By applying strategized synthetic approaches and employing wide variety of synthetic protocols, ambipolar charge-transporting materials can be produced; in which the electron-deficient molecular moieties, for example; arylene bisimides, may be functionalised with electron-donors.

In this review, the recent contributions to the synthesis and properties of organic materials having dendritic architecture or electron-transporting/ambipolar characteristics applicable in optoelectronics will be discussed.

2.2. Dendritic organic materials for optoelectronic applications

Dendrimers are repeatedly branched, roughly spherical large molecules. The term dendrimer is derived from the Greek words: *dendrons* –tree and *meros* –part. A dendrimer is typically symmetric around the core, and often adopts a spherical three-dimensional morphology (Figure 2.1). It usually consists of three components: (1) the core which is located in the geometrical centre or focus and usually determines the most important function of the dendrimer; (2) the surrounding dendrons which contain branching points and the branching level defines the dendrimer generation; (3) the surface groups which are covalently grafted onto the periphery of the dendrons to tune the solubility and processability of the dendrimer. The dendritic architectural feature allows a variety of possible combinations of core, dendrons and surface groups and makes it feasible to tune each of the three functional parts independently without sacrificing others.

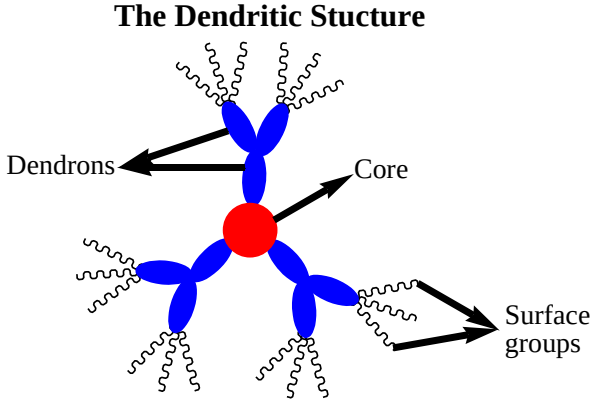

Figure 2.1 Schematic representation of dendritic structure

Dendritic charge-transporting materials can be generated by symmetrical multi-fuctionalization of polycyclic or heterocyclic aromatic core by various electro-active molecular moieties, for example; electron donors, and thus, the molecular properties can be tuned in the standpoint of device fabrication. Due to careful structural design, dendrimers can combine the potential advantages of both small molecules and polymers. First, like small molecules, dendrimers possess a well-defined structure and monodispersity. This ensures the batch to batch reproducibility unlike polymers in terms of monodispersity and chemical purity; both are essential factors for determining device performance. At the same time, the good solubility and

appropriate viscosity of dendrimers in common organic solvents make them suitable for solution processing by using methods such as spin-coating and ink-jet printing to fabricate thin films for devices, avoiding the expensive and high-temperature vacuum evaporation technique which is applied for small molecular materials. Moreover, dendrimers containing photoactive components, in the core and/or in the branches, are particularly interesting since: 1) luminescence signals offer a handle to better understand the dendritic structures and superstructures; 2) cooperation among the photoactive components can allow the dendrimer to perform useful functions such as light harvesting; 3) changes in the photophysical properties can be exploited for sensing purposes with signal amplification; and 4) photochemical reactions can change the structure and other properties of dendrimers and could also lead to a controlled release of molecules [23,24,25]. These advantages of dendrimers over polymers as well as low molar mass compounds, of course, influence the synthetic strategies of the chemists working on the synthesis of organic materials relevant to optoelectronics.

2.2.1. Electron-donor-functionalized dendritic pyrene derivatives

Pyrene is a flat aromatic system consisting of four fused benzene rings; termed as smallest peri-fused (one where the rings are fused through more than one face) polycyclic aromatic hydrocarbon (PAH). Moreover since pyrene is peri-fused, the aromatic core is well resonance-stabilized. Electron-donors functionalized pyrene based materials, with their extended delocalized π-electrons, discotic shape, high photoluminescence efficiency, and good hole-injection/transport properties, have the potential to be a very interesting class of organic semiconductors for optoelectronic applications; in particular for OLED applications [26,27].

Most of the dendritic materials based on pyrene core are tetrafunctional derivatives. Practical precursor of pyrene to tetrafunctional derivatives is 1,3,6,8-tetrabromopyrene; which has been produced easily on the gram scale since 1937 by the bromination of pyrene at elevated temperatures in nitrobenzene [28,29]. Bromine substitutions are often achieved by S_NAr or by metal-catalyzed C-C bond coupling procedures.

Z. Zhao and coworkers [30] reported an excellent example of pyrene core based stiff dendrimers containing carbazole/fluorene electron-donors as dendrons for OLED applications (Figure 2.2). A Pd/Cu-catalyzed Sonogashira coupling reaction [31] was used as a key reaction to construct these acetylene-linked dendrimers (**Ia-Ie**). As visualized by theoretical method, the dendrimers **Ia** and **Ib** exhibited an X shape with a calculated length of about 5 and 7 nm, respectively, and **Ic**, **Id** and **Ie** showed a dense “pancake-like” shape with a calculated diameter of about 9, 11, and 14 nm, respectively. Since **Ie** possessed many arms at its periphery, its dendrons were distorted in order to avoid the involved steric crowdedness. The whole molecule thus was “thick” in the periphery and “thin” in the centre, which hampered the pyrene ring from another molecule to get close to form excimer.

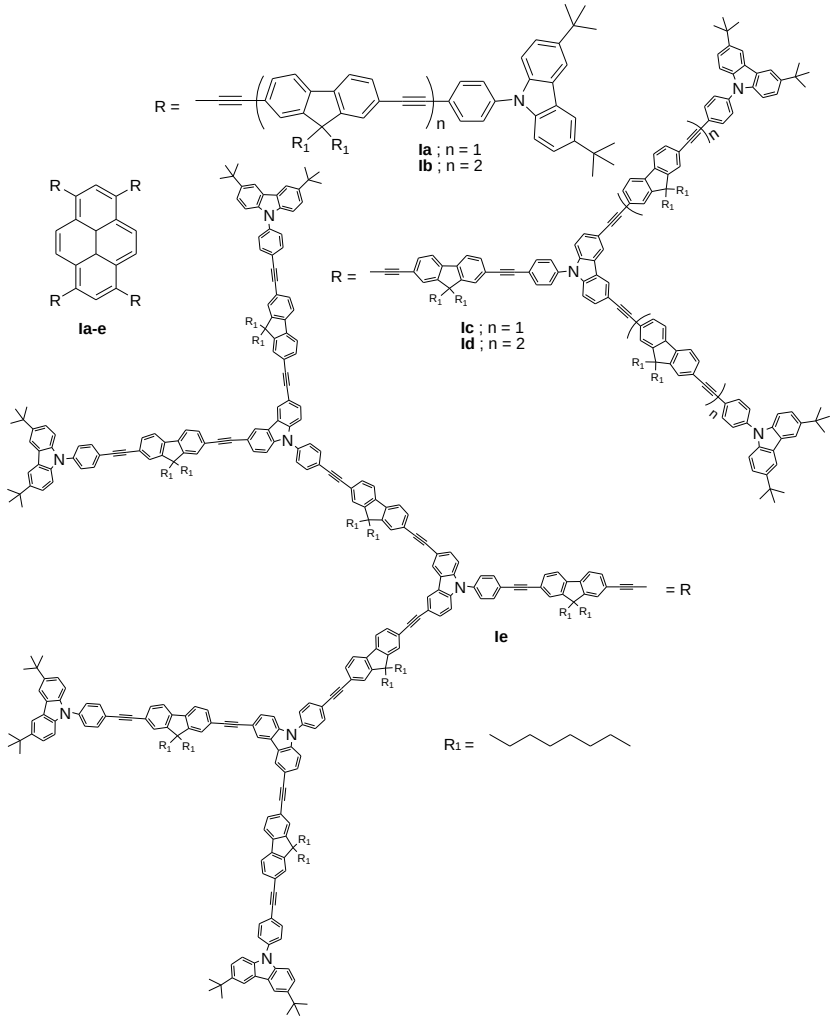

Figure 2.2 Structures of pyrene dendrimers **Ia-e**

All the dendrimers exhibited high glass transition temperatures and enjoyed high thermal stability, with decomposition temperatures in the range of 425-442 °C. The dendrimers **Ia-Ib** were highly fluorescent in both solutions and solid states. The PL quantum yields of the dendrimers were much higher than that of 1,3,6,8-tetrakis(phenylethynyl) pyrene [32]. The quantum yield was found to be decreased with increase in dendrimer generation. The energy transfer efficiency might be decreased as the generation increases since some of the arms were far away from the core [33]. The dendrimer generation effect on the EL property was tested in single-layer devices with a configuration of ITO (120 nm)/PEDOT (25 nm)/dendrimer/Cs_2CO_3 (1 nm)/Al (100nm) [34]. Compounds **Ia** and **Ib** showed greenish yellow EL at 576 and 572 nm with CIE chromaticity coordinates of (0.48, 0.51) and (0.47, 0.52), respectively. **Id** showed yellow EL (CIE: 0.51, 0.49) at 560 nm. However, **Ie** exhibited a narrow yellowish green (CIE: 0.39, 0.59) EL at 530 nm

with a weak emission at ~560 nm, which was comparable to its PL in both solutions and solid states. Compound **Ic**-based OLED exhibited yellow EL (CIE: 0.49, 0.50) with a maximum brightness of 5590 cd/m^2 at 16 V, a high current efficiency of 2.67 cd/A at 8.6 V, and a best external quantum efficiency of 86%. Gigantic two-photon absorption and strong two-photon excited fluorescence in these dendrimers have also been reported [35].

Pd/Cu-catalyzed Sonogashira coupling reaction was employed by J. Hu *et.al* [36] for the synthesis of cruciform-shaped pyrene derivatives **IIa-d** (Scheme 2.1). Although **IIa-c** and **IId** contains same numbers of *p*-functionalized phenylethynyl groups, their molecular structures were quite different as a result of introducing substituents at different positions on the pyrene scaffold. Compounds **IIc** and **IId** were also different in the length and shape of their conjugation pathways.

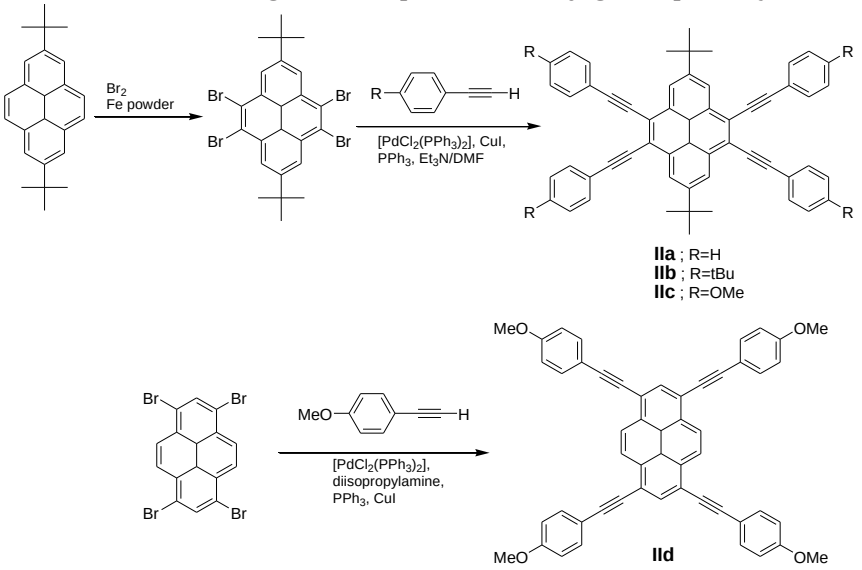

Scheme 2.1 Synthesis of pyrene derivatives **IIa-d**

Inspection of the absorption and emission spectra of these compounds indicated that the extension of π-conjugation in these pyrene chromophores through phenylethynyl substituents served to shift the wavelength of absorption and fluorescence emission into the pure-blue visible region. Single-crystal X-ray analysis indicated that two bulky *t*-Bu groups on the pyrene moiety at the 2- and 7-positions play a significant role in inhibiting the π-stacking interactions between neighbouring pyrene units. These molecules emitted very bright, pure-blue fluorescence and showed good solubility in common organic solvents, and high stability.

A series of materials for OFETs, with pyrene moiety at the core and four substituted thiophene arms of different lengths (1–3 thiophene units) have been synthesized using Suzuki cross-coupling reaction by P. Anant *et.al* (Scheme 2.2) [37,38]. Pyrene functionalized at the 1,3,6,8-positions with unsubstituted thiophene units has previously been reported [39], but suffered from poor solubility. The

presence of alkyl-chains at the termini of all oligothiophene substituents in **IIIa-c** improved the solubility in organic solvents, permitting ready characterization and processing for device construction.

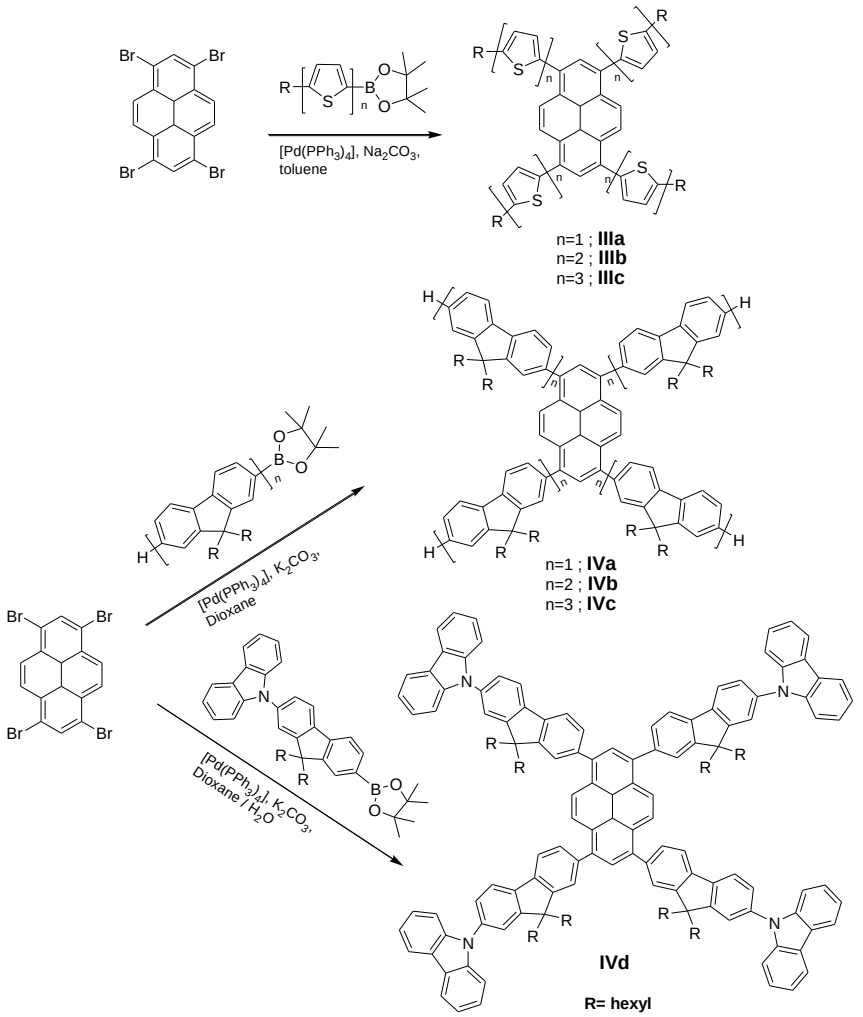

Scheme 2.2 Synthesis of donor substituented pyrene derivatives **IVa-d**

UV–visible absorption and photoluminescence spectra of compounds **IIIa-c** studied in both solution and thin film showed red-shifted absorption and emission maxima as the oligothiophene length increased. X-ray solid-state study of **IIIa** showed that it forms a layered structure with regions of alkyl chain and thiophene/pyrene, and despite these segregation, intermolecular contacts between the thiophene and pyrene components was limited to edge-to-face interactions not involving sulphur. Hole transporting (p-channel) field-effect transistors based on drop cast films of compound **IIIc** were fabricated and characterized under N_2 environment. The charge mobility of 1.9×10^{-5} cm^2/Vs was obtained following

annealing, but was lower than the mobility measured for single crystals or films of the related tetra(2-thienyl)pyrene compounds [39].

F. Liu *et.al* [40] reported pyrene centred oligofluorenes **IVa-c** with good film forming ability and sky blue fluorescence. Carbazole end-capped pyrene based material **IVd** possessing enhanced electrochemical stability and device performance was also reported by the same research group [41]. These pyrene derivatives were synthesized by suzuki-coupling reactions (Scheme 2.2). Compounds **IVa-c** showed high thermal stability with T_D that ranged from 377 to 391 ^oC. The T_D increased when the oligofluorene chain increased. T_D of **IVd** was 299 ^oC, which was lower than that of the oligofluorenes-armed pyrene derivatives and was attributed to the length of the arms. In DSC analysis, for the short arm species **IVa** and **IVb**, a phase transition at about 200 ^oC was observed in the first heat trace. For **IVc**, which has longer oligofluorene arms, no phase transition was observed upon heating to 300 ^oC; which indicated that it was morphologically stable. These pyrene derivatives also possessed glass transition temperatures above room temperature [40]. However, at 192 ^oC, some crystallization was observed in DSC heat trace of **IVd** [41].

As observed by photoluminescence studies of **IVa-c**, the emission peak was red-shifted upon increasing the arm length. The difference between the emission peaks for **IVa** and **IVb** was 11 nm, and for **IVb** and **IVc** was 1 nm, which indicated that the effective conjugation saturated quickly when the arm length increased. Compared with oligofluorenes functionalized pyrene derivatives **IVa-c**, **IVd** showed similar photophysical properties. Absolute quantum yield of **IVd** spin-coated film reached 71% measured in the integrating sphere, which was a good value for light-emitting materials. The oligofluorene derivatives exhibited high solid-state PL quantum efficiencies (>90%) and near single-exponential PL decay transients with excited state lifetimes of ~1.4 ns [42].

Compared with pyrene-centred starbursts containing oligofluorenes arms, compound **IVd** with carbazole end capping unit showed improved hole-injection ability and electrochemical stability [41]. Because of good hole-injection ability, no additional hole-injection/transporting layer was required for the electroluminescent device fabrication with **IVc-d**. Single-layered electroluminescent device fabricated with **IVd** as host material took on stable blue emission with a peak current efficiency of 0.84 cd/A. The peak efficiency reached 3.28 cd/A and the maximum brightness was over 2200 cd/m^2. Single-layered device made of **IVc** had a maximum brightness of over 2700 cd/m^{-2} and a maximum current efficiency of 1.75 cd/A [40]. Distributed-feedback lasers with low optical pumping thresholds were also constructed based on these pyrene derivatives [42].

P. Sonar and coworkers [43] reported soluble pyrene based organic semiconductors. Electron-rich chromophores like bithiophene, phenylene, thienothiophene or benzothiadiazole-thiophene were selected as tetra substituents for the synthesis of pyrene core functionalized derivatives **Va-d** (Figure 2.3). The compounds were synthesized by Stille and Suzuki-Miyaura cross-coupling routes [38,44]. To achieve solution processability, alkyl groups were incorporated to the conjugated moieties.

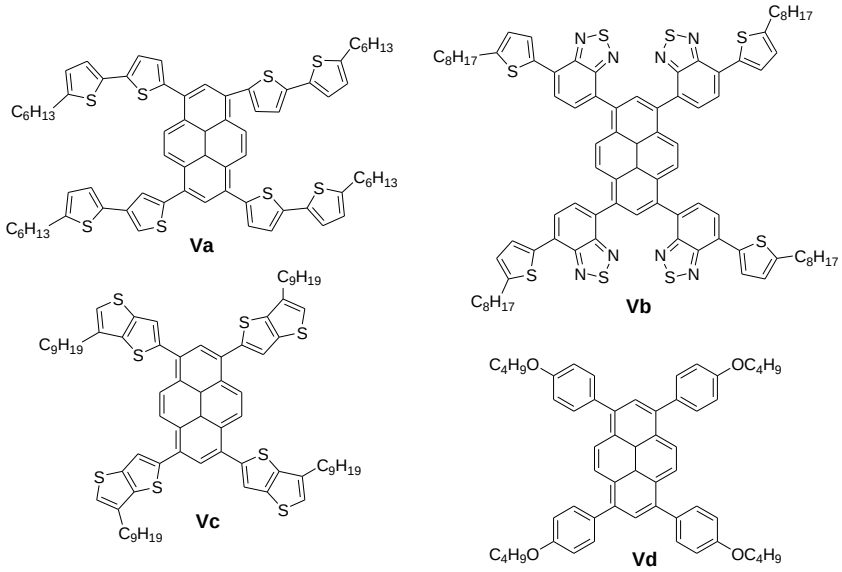

Figure 2.3 Structures of pyrene derivatives **Va-d**

Solution PL spectra for **Vc** and **Vd** showed deep blue and sky blue emission, respectively, with the maxima at 433 and 490 nm, whereas **Va** and **Vb** exhibited green and orange emission with the maxima at 530 and 541 nm, respectively. The calculated HOMO values were in the range of -5.15 to -5.33 eV; which match quite well with commonly used hole injection/transport layers and anodes such as PEDOT:PSS (-5.1 eV) and ITO (-4.9 eV). **Vc** and **Vd** showed melting points at 252 and 100 °C, respectively, in DSC heating cycles up to 300 °C. The thermal decomposition temperatures were observed above 400 °C for all compounds except **Vc**, which showed T_D onset at 299 °C. OLED based on **Vd** as the active emitter showed efficiencies of 2.56 cd/A, deep blue emission (CIE: 0.15, 0.18), low turn-on voltages (3.0 V), and a maximum brightness of 5015 cd m^{-2} at 11 V [43].

Dendrimers **VIa-b** consisting of a polysulfurated pyrene core with appended poly(thiophenylene) dendrons possessing remarkable luminescent and electrochromic properties was reported by M. Gingras *et.*al (Figure 2.4) [45]. The photophysical and redox properties of these dendrimers were depend on the length of their branches: 1) the dendron localized absorption band at *ca.* 260 nm increased strongly in intensity and moved slightly to the red on increasing dendrimer generation; 2) in dichloromethane solution, the quantum yield and lifetime of the fluorescence band and the values of the half-wave potentials increased with increase in dendrimer generation; 3) the dendrimer branches partially protected the core from oxidation by $AuCl^{4-}$. These compounds showed strong blue fluorescence and the yellow to deep blue colour change upon reversible one-electron oxidation.

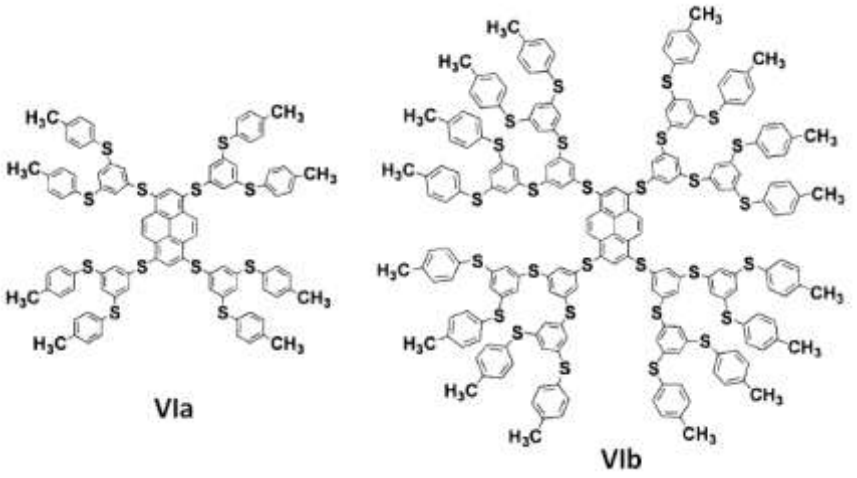

Figure 2.4 Structures of pyrene dendrimers **VIa** and **VIb**

Using 1,3,6,8-tetraethynylpyrene as a core, a series of polyphenylene dendrimers was prepared in high yield by combining divergent and convergent growth methods by S. Bernhardt *et.al* [46]. The fluorescence quantum yields of dilute solutions were excellent (*ca.* 90%) and were independent of the size of the polyphenylene shell. The authors [46] suggested the application of these materials in OLEDs since they combine excellent optical features and an improved film-forming ability.

2.2.2. Triphenylamine based dendritic organic materials for optoelectronics

In contrast to the aliphatic amines, aromatic amines are non basic compounds. Triphenylamino compounds are mainly used in organic electronics because of their ability for the formation of stable aminium radical cation. Triphenylamine based molecules have attracted enormous research interests, in particular, for the solution-processable organic optoelectronic device applications, because of their good solution processability benefiting from the three-dimensional propeller structure of triphenylamino moiety. Because of the excellent charge-transporting characteristics, triphenylamine based compounds were widely employed in electro-photographic photoconductors [47,48].

N. Metri *et.al* [49] recently reported triphenylamine-core based derivatives containing alkyl thieno [3,2*b*] thiophene and thiophene units (Figure 2.5). Suzuki and Stille coupling methods were used for the preparation of **VIIa-e** according to the position of the alkyl chain relative to the triphenylamine core. According to the reactivity of the different entities, two experimental conditions were also used. Compounds **VIIa-e** showed significant thermal stability, with T_D values higher than 300 ^oC. DSC analysis revealed that some of the compounds existed as molecular glasses with glass transition temperatures ranging from 27 to 57 ^oC.

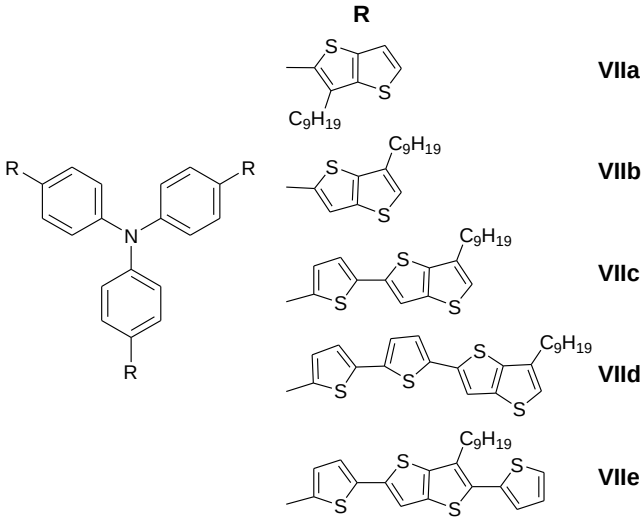

Figure 2.5 Structures of triphenylamine derivatives **VIIa-e**

Extended oligothiophene-triphenylamine hybrid conjugated systems **VIIIa-d** with internal charge transfer for the application in solution processed organic solar cells were reported by E. Ripaud *et.al* (Figure 2.6) [50]. Stille coupling reactions and triethylamine assisted condensations with malonodinitrile were performed for the synthesis of these compounds.

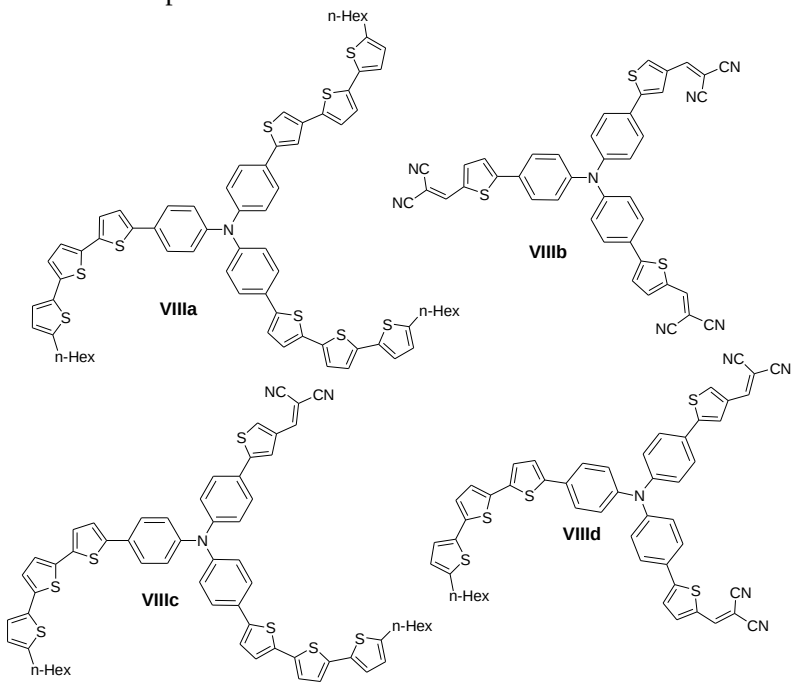

Figure 2.6 Structures of triphenylamine derivatives **VIIIa-d**

Branched triphenylamine-based conjugated structures associating terthienyl chains and dicyanovinyl acceptor groups displayed broad absorption bands, high molar absorption coefficients and low lying HOMO levels. Intramolecular charge transfer between the thienyl-substituted triphenylamine block and the terminal groups was observed in triphenylamine derivatives **VIIIc-d**. The relative intensity of CT band increased with the number of electron acceptor groups and became predominant for compound **VIIId** containing two electron acceptor moieties. Hole mobility of the triphenylamine-based donors measured by space-charge limited current technique were found to be 2.9×10^{-5} cm^2 V^{-1} s^{-1}, 3.9×10^{-5} cm^2 V^{-1} s^{-1} and 5.6×10^{-5} cm^2 V^{-1} s^{-1} , respectively, for compounds **VIIIb** , **VIIIc** and **VIIId**. The derivatives **VIIIc** and **VIIId** tested in solar cells revealed combined effects of internal charge transfer and improved hole-mobility which lead to devices with very high open-circuit voltage and PCE values [50].

The same research group also synthesized the conjugated systems consisting of dicyanovinyl electron-acceptor units connected to a triphenylamine core by means of thiophene, thienylenevinylene and bithiophene conjugating spacers (Figure 2.7) [51]. Compounds **IXa-c** were synthesized by Wittig-Horner reactions [52]. The electronic properties of these compounds analyzed by UV-Vis absorption spectroscopy, cyclic voltametry and theoretical calculations revealed that these properties were depending on the length and rigidity of the conjugating spacers.

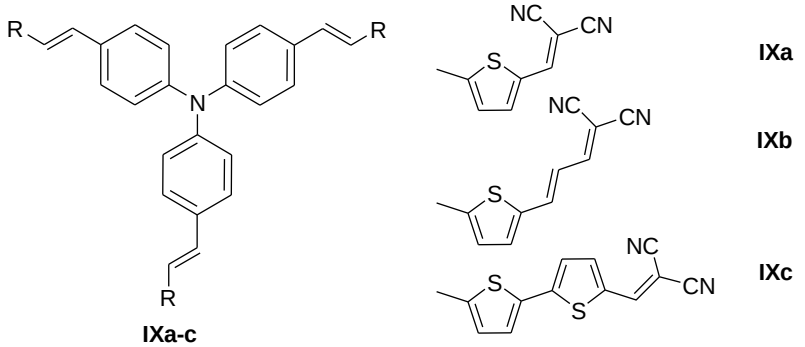

Figure 2.7 Structures of cyanovinyl functionalized triphenylamine derivatives **IXa-c**

A. Cravino and coworkers [53] synthesized hole-transporting "hybrid" systems **Xa-b** consisting of a triphenylamine core carrying π-conjugated terthienyl branches for optoelectronics (Figure 2.8).

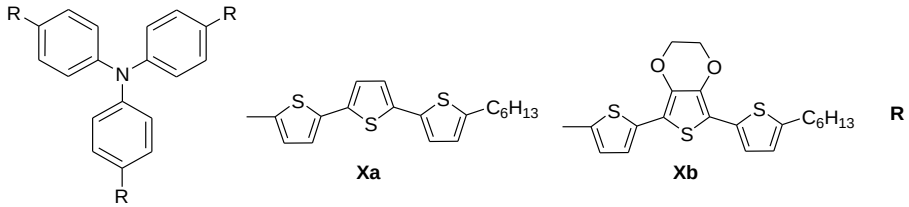

Figure 2.8 Structures of triphenylamine derivatives **Xa** and **Xb**

Thermal analysis and X-ray diffraction studies of compounds **Xa** and **Xb** revealed their amorphous character and cyclic voltametric studies showed their

electron donating capability. Compounds **Xa** and **Xb** showed fluorescence emission quantum yields of 22% and 17%, respectively, in solution. The semiconducting potentialities of these compounds were evaluated by their implementation in very simple prototype devices that display electroluminescence at low voltage as well as a photovoltaic effect. In compound **Xb**-based OLEDs, the turn-on voltage values were in the range of 1.9-3 V and the emitted green light was detectable by the naked eye ~ 2 V. Compounds **Xa** and **Xb** were tested as donor materials in bilayered heterojunction devices using fullerene C_{60} as the electron acceptor. A clear photovoltaic effect established under illumination suggested the occurrence of a photoinduced electron transfer from **Xa** and **Xb** to C_{60}. Power conversion efficiencies of the solar cells fabricated using **Xa** and **Xb** were found to be 0.32% and 0.14%, respectively. OFETs fabricated by spin coating from **Xa** and **Xb** showed hole-mobility values in the order of 10^{-5} cm^2 V^{-1} s^{-1}. The evaporation of **Xa** allowed for the attainment of reproducible sets of devices that display considerably higher charge mobility. Field-effect mobility established for the devices fabricated using vacuum evapourated films of **Xa** reached values up to 1.1×10^{-2} cm^2 V^{-1} s^{-1}. Since this material has been found amorphous which did not depend on the deposition technique, this higher mobility measured in evaporated films might be due to the formation of more dense structure, not attainable by spin casting, beneficial for intermolecular contacts [53].

J. Zhang *et.al* [54,55] reported solution processable dendritic compounds with triphenylamine core and different chromophore arms for organic photovoltaic applications (Figure 2.9). Compounds **XIa-b** were synthesized by Knoevenagel condensation [56] of malononitrile with the appropriate aldehydes and the compound **XIc** was prepared by palladium-catalyzed Heck reaction [57].

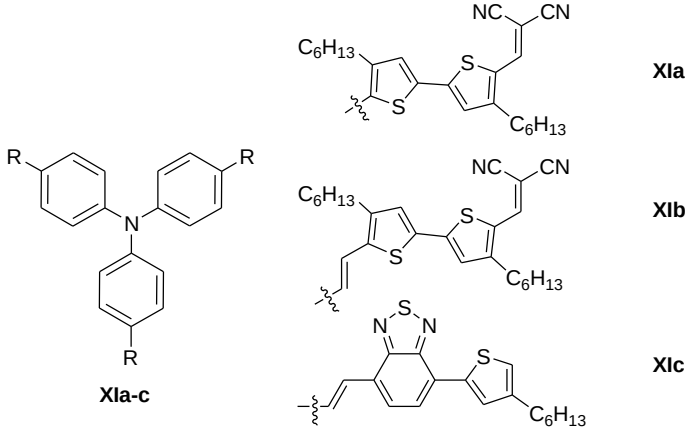

Figure 2.9 Structures of triphenylamine derivatives **XIa-c**

Compounds **XIa-b** were found to be thermally stable. Temperatures of 5% weight loss were 358 ^oC for **XIa,** 347 ^oC for **XIb**, and 303^oC for **XIc**, respectively. UV-Vis absorption spectra of compounds **XIa-c** suggested the occurring of intramolecular charge transfer between the triphenylamine core and the thiophene derived substituents. Absorption peaks of the films were red shifted in comparison

with those of their solutions. The absorption spectrum of **XIa** film covered a broad wavelength ranged in the visible region from 380 to 750 nm. It was red-shifted by *ca.* 40 nm with respect to that of the **XIb** film, due to the presence of the vinylene bridges between triphenylamine and bithiophene units. **XIc** film exhibited broad and strong absorption peaks in the range of 300-630 nm. PL spectra of the chloroform solution and the film of **XIc** showed a red emission with the peaks at 656 and 657 nm, respectively. The power conversion efficiencies of the bulk heterojunction solar cells based on **XIa** and **XIb** as donor materials reached 1.4% and 3.0%, respectively. Structural modifications with the hexyl side chains and the vinylene-bridge in the dicyanovinyl-containing compounds significantly improved the solution-processability, absorption and photovoltaic properties of compounds **XIa-b**. The photovoltaic device based on **XIc** showed a PCE of 2.39%. The photovoltaic properties of compounds **XIb-c** were reported to be among the best for solution-processable triphenylamine-containing organic molecules [54, 55].

Solution-processable dendritic N-atom-centred and phenyl-centred triphenylamine nonamers (containing 9 triphenylamine subunits) as hole-transporting and hole-injection materials for OLEDs were reported by M. Ichikawa *et.al* (Figure 2.10) [58]. Ionization potentials of the materials **XIIa** and **XIIb** were *ca.* 5.1 eV and *ca.* 5.3 eV, respectively and were close to that of ITO anode. Computational chemistry studies suggested that the *p*-phenylenediamine-like structure affected the ionization potential values. The compounds were very stable in their glassy states; T_gs were 188 ^oC for **XIIa** and 194 ^oC for **XIIb**. The N-atom centred nonamer **XIIa** showed poor performance as a hole-transporting material compared with phenyl-centred nonamer **XIIb**. The differences in the properties were resulted from the fractional difference of the central units of the molecular structures.

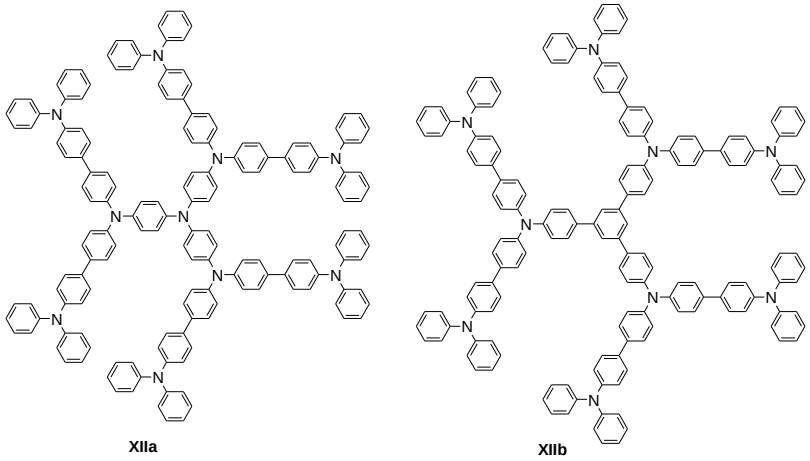

Figure 2.10 Structures of triphenylamine dendrimers **XIIa** and **XIIb**

M. Sonntag *et.al* [59] reported dendritic derivatives with triphenylamine as core and carbazole or fluorene electron-donor chromophores as side arms for solution processable OFETs (Figure.211). Compounds **XIIIa-f** were synthesized by Suzuki

cross-coupling reactions from the corresponding borolane derivatives and the triiodo derivative of triphenylamine as shown in Scheme 2.3.

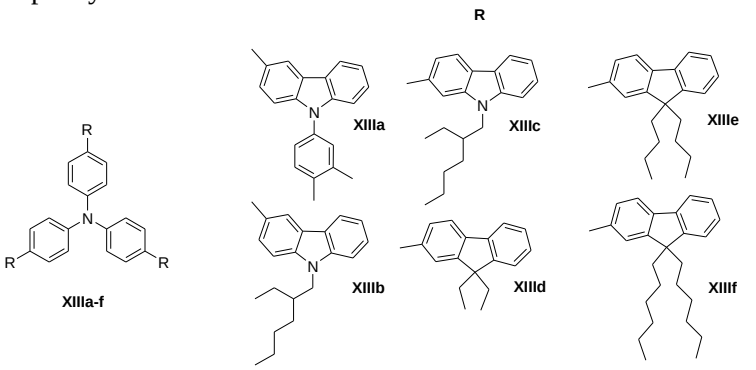

Figure 2.11 Structures of triphenylamine derivatives **XIIIa-f**

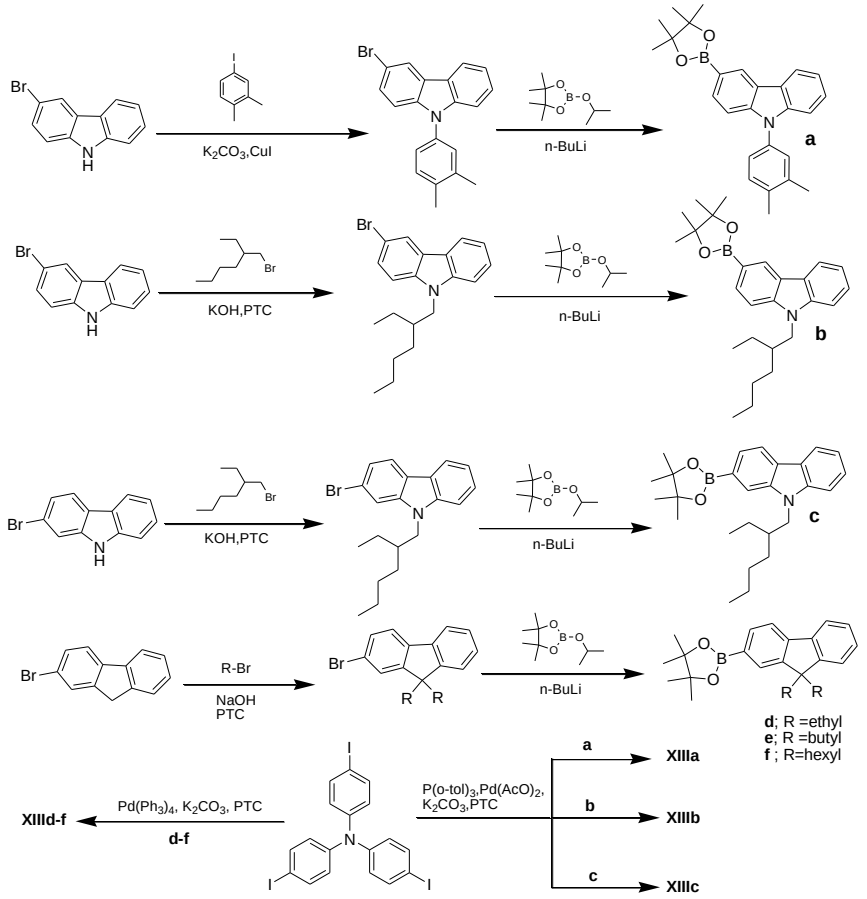

Scheme 2.3 Synthesis of triphenylamine derivatives **XIIIa-f**

Compounds **XIIIa-f** exhibited high thermal stability up to 495 °C as characterized by TGA. Except **XIIIc** all compounds formed molecular glasses with the glass transitions between 57 °C and 167 °C. **XIIIc** crystallized upon cooling and

showed a melting point at 223 °C. Absorption and fluorescence spectra were similar for the compounds **XIIIc-d** and might be due to the terphenyl-like structure of these compounds. In the case of **XIIIb**, the absorption and fluorescence maxima were shifted to shorter wavelengths and attributed to the benzidine-like structure of this compound. The fluoren-2-yl derivatives **XIIId-f** were quite stable in the electrochemical environment as characterized by cyclic voltametry. The carbazol-2-yl compound **XIIIc** was electrochemically unstable comparing to the carbazol-3-yl compounds **XIIIa-b** in cyclic voltametric studies. The HOMO energy levels of these compounds were in the range of -5.0 to -5.2 eV as determined from the oxidation onsets. Compounds **XIIIa-c** and **XIIIe** exhibited charge mobilities in the range of 10^{-4} cm^2 V^{-1} s^{-1} as tested in OFETs. Higher hole-mobility of 3×10^{-4} cm^2 V^{-1} s^{-1} was observed in the device prepared from **XIIIb** [59].

Aromatic hydrazones are usually used in electrophotographic photoreceptors as molecular dispersions in inert polymer hosts. To enhance the hole-transporting ability, new material systems that allow a decrease in the concentration of the inactive polymer components and thus provide a higher concentration of hydrazone moieties are required. Star-shaped low molar mass or dendritic molecular architectures are considered to be useful for this purpose. Dendritic structures exhibit a more stable amorphous nature due to the geometry of these molecules, which does not favour close packing.

Glass-forming hole-transporting triphenylamine-based trihydrazones **XIVa-d** were synthesized by condensation of tris(*p*-formylphenyl) amine with N-methyl-N-phenyl hydrazine, N,N-diphenylhydrazine, N-1-naphthyl-N-phenylhydrazine, or N-2-naphthyl-N-phenylhydrazine [60]. Tris(*p*-formylphenyl)- amine, synthesized through Vilsmeier–Haack reaction [61] of triphenylamine, reacted with different hydrazines yielding the corresponding hydrazones **XIVa-d**. Hole-transporting dendrimer **XIVe** was prepared in a multi-step synthesis by applying convergent method as shown in Scheme 2.4 [62].

Hydrazones **XIVa** and **XIVb** were obtained as crystalline compounds and showed clear endothermic melting peaks in the first DSC heating scans at 247 and 241°C, respectively. They formed glasses after cooling from the melt. Upon the second heating, they showed glass transitions at 74 and 81°C, respectively. Then, no crystallization was observed even when they were heated above T_g. Compounds **XIVc** and **XIVd** were obtained as amorphous materials and in DSC experiments showed only glass transitions at 86 and 87°C, respectively [60]. T_g of dendrimer **XIVe** was found to be 164°C. The films of dendrimer **XIVe** were found to be clear, transparent, homogeneous, and mechanically tough. UV-Vis absorption maximum was observed at 418 nm. Cut-off wavelength of the dendrimer **XIVe** was 487 nm corresponding to the HOMO to LUMO excitation energy of 2.5 eV [62].

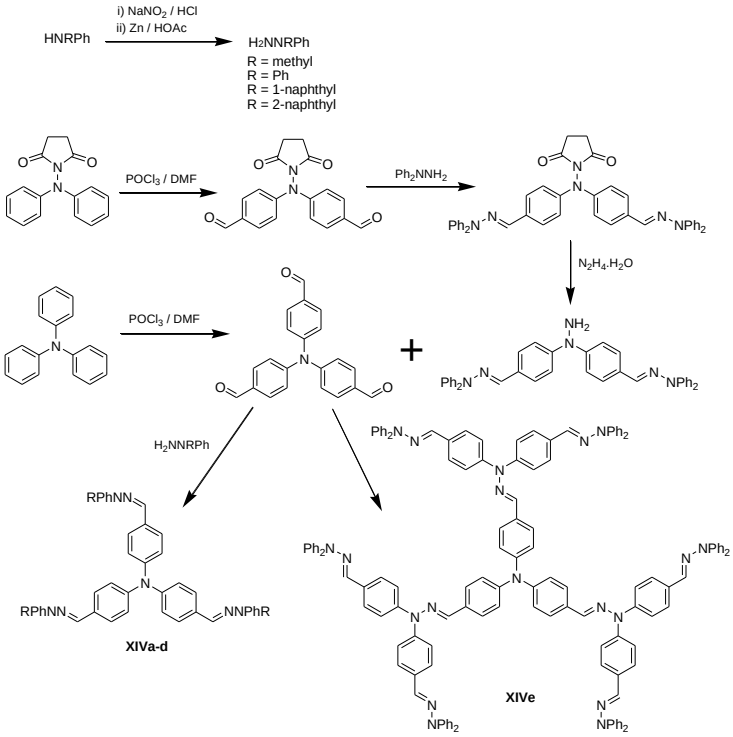

Scheme 2.4 Synthesis of triphenylamine derived hydrazones **XIVa-e**

Triphenylamine- cored alkynylruthenium dendrimers with nonlinear optical characteristics were reported [63,64]. The dendrimers **XVIa-c** were synthesized by Sonogashira coupling reaction (Figure 2.12). Impacts of π-system lengthening through the metal centre as well as the effect of generation increase in these dendrimers were investigated. The first wavelength-dependence study of refractive nonlinearity of N-cored dendrimers has revealed a trend in nonlinear refractive maxima. These N-cored alkynylruthenium dendrimers exhibited two-photon absorption behaviour at wavelengths below 1000 nm and three-photon absorption beyond 1000 nm.

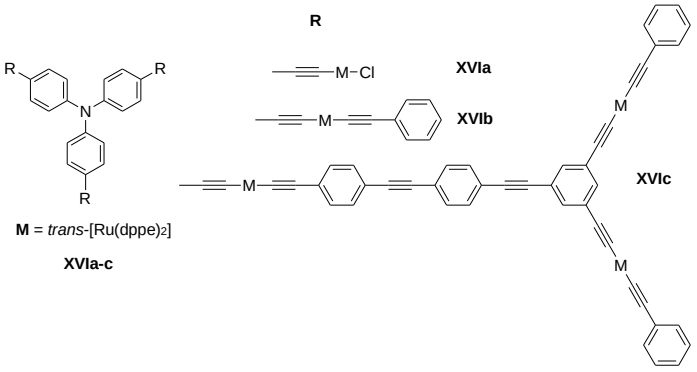

Figure 2.12 Structures of triphenylamine compounds **XVIa-c**

N. Satoh *et.al* [65] reported a series of charge-separable and hole-transporting phenylazomethine dendrimers **XVIIa-e** with a triarylamine core and evaluated their use as a charge separator in DSSCs (Figure 2.13). Compounds **XVIIa-e** were prepared by synthesizing upto five generations of dendrons using a convergent method *via* reaction of aromatic ketones with aromatic amines [66,67].

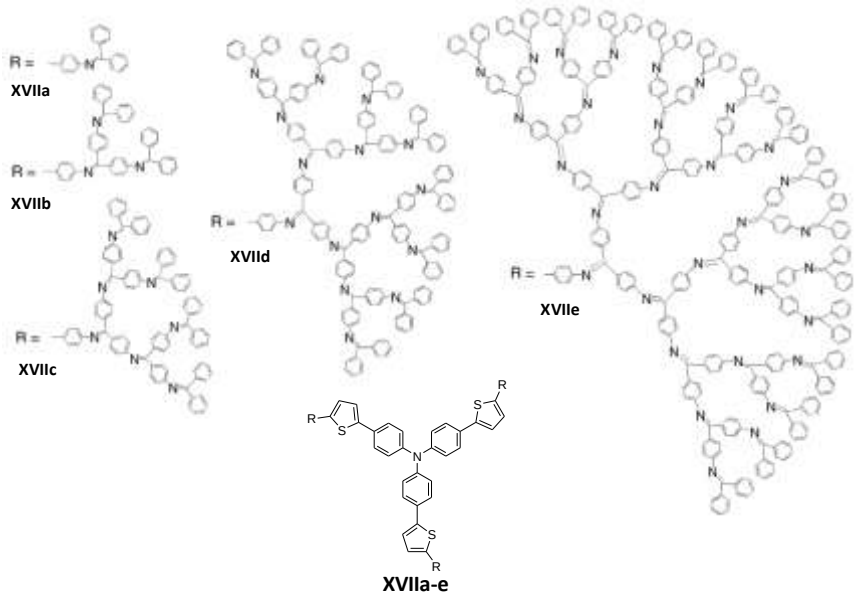

Figure 2.13 Structures of triphenylamine dendrimers **XVIIa-e**

Electrochemical analysis revealed that the π-conjugated dendron shells isolated the triphenylamine core at the centre of the dendrimer and that the triphenylamine core was oxidized through the dendron shell with an attenuation factor of 0.35. DSSCs prepared by casting these dendrimers onto dye-sensitized TiO_2 film exhibited a higher open-circuit voltage than the bare film through the suppression of back electron transfer. The energy conversion efficiency of the DSSC prepared using fifth-generation dendrimer **XVIIe** was 21% higher than that for the bare film and, when complexed with $SnCl_2$, provided a 34% improvement [65].

2.2.3. Electron-donors functionalised compounds containing triazine-core for optoelectronics

Triazine is an electron-deficient heterocyclic ring, analogous to the six-membered benzene ring but with three carbon atoms replaced by nitrogen atoms. 1,3,5-Triazine (s-triazine) derivatives have proven their great potential in the area of material chemistry, both for their π-interaction abilities, and for their aptitude to be involved in intricate H-bond networks [68,69]. They can be synthesized using simple protocols and widely employed in organic electronics. Moreover, the combination of electron-accepting triazine chromophores and electron-donating chromophores results in materials exhibiting ambipolar charge-transport.

Electron transport-type host materials for green phosphorescent organic light-emitting devices based on s-triazine and various aryl moieties **XVIIIa-c** were reported by H.-F. Chen *et.al* [70]. The Suzuki coupling reactions of bromo substituted triazine-core scaffold with various boronic acids yielded **XVIIIa** and **XVIIIb** (Scheme 2.5).

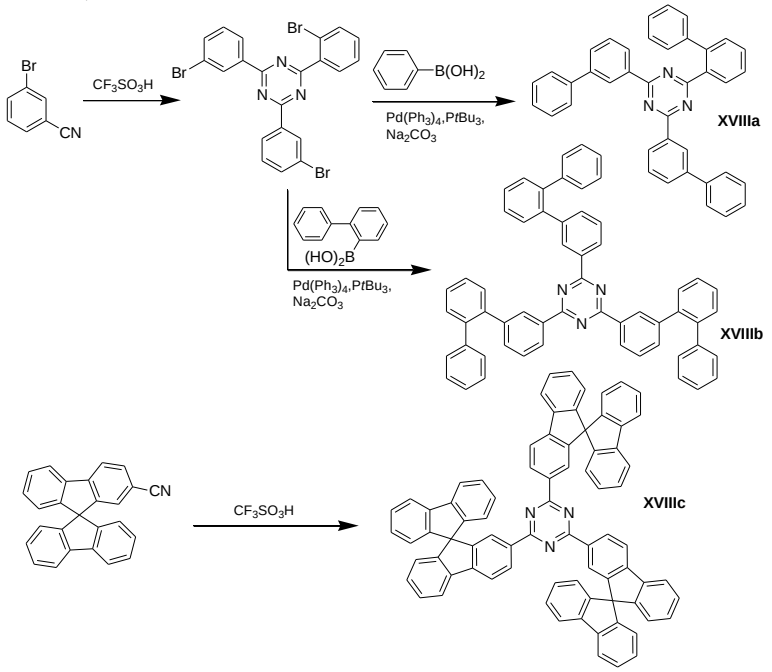

Scheme 2.5 Structures of triazine derived materials **XVIIIa-c**

Thermal, photophysical and charge-transporting properties as well as morphology of these materials were influenced by the nature of the aryl substituents attached to the triazine core. The *meta–meta* linkage between the 1,3,5-triazine core and the peripheral aryl moieties in **XVIIIa-b** limited the effective extension of their π-conjugation, leading to high triplet energies of 2.80 and 2.69 eV, respectively. Time-of-flight mobility measurements revealed good electron mobilities for these compounds (> 10^{-4} cm^2 V^{-1} s^{-1}), following the order **XVIIIb** > **XVIIIc** > **XVIIIa**. The electrophosphorescent device incorporating **XVIIIa** as the host, doped with $(PPy)_2Ir(acac)$ and 1,3,5-tris(N-phenylbenzimidizol-2-yl)benzene as the electron-transporting layer, achieved a high external quantum efficiency of 17.5% and a power efficiency of 59.0 lm W^{-1}. For the same device configuration, the **XVIIIb**-based device provided values of η_{ext} and η_p of 14.4% and 50.6 lm W^{-1}, respectively; the **XVIIIc**–based device provided values of 5.1% and 12.3 lm W^{-1}, respectively. The superior performance of the **XVIIIa** -based devices was due to the balanced charge recombination. The poor efficiencies of the **XVIIIc** -based devices was because of the relatively low triplet energy (2.54 eV) which did not allow efficient confinement of the triplet excitons on the green phosphorescent emitter

$(PPy)_2Ir(acac)$ [70]. Amorphous 2,4,6-tris[4-(1-naphthyl)phenyl]-1,3,5-triazine with electron drift mobility of 8×10^{-4} cm^2 V^{-1} s^{-1} was also reported [71].

Non-conjugated bipolar compound **XIXa** comprising triazine core and carbazole arms were synthesized and characterized for the fabrication of phosphorescent OLEDs by L. Zeng *et.al* (Scheme 2.6) [72].

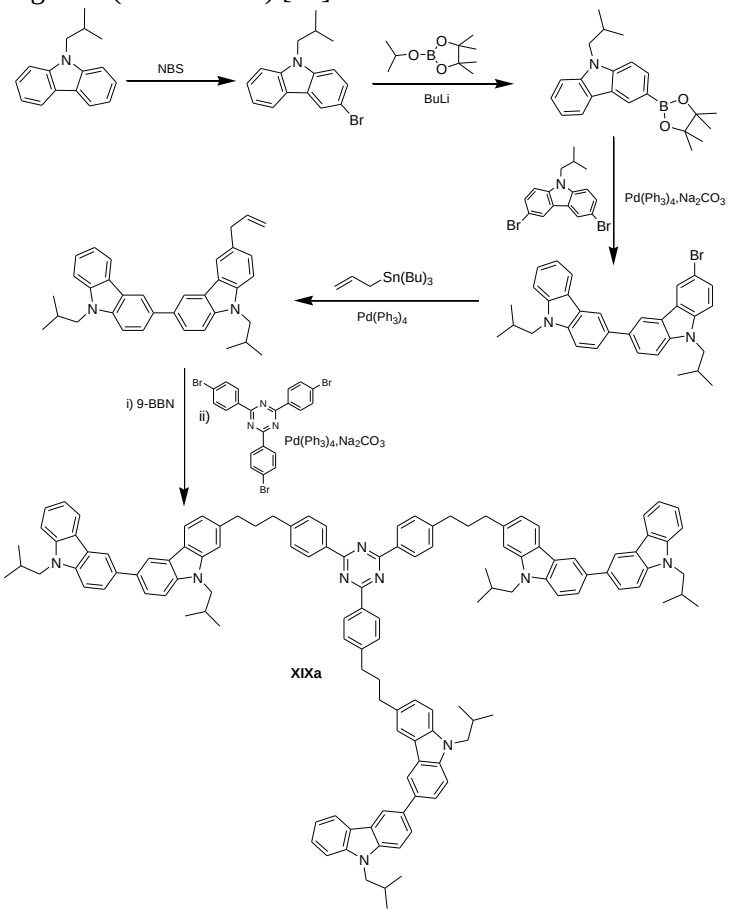

Scheme 2.6 Synthesis of dendritic triazine compound **XIXa**

The flexible linkages connecting the two charge-transporting moieties in the non-conjugated bipolar hybrid molecules served to increase entropy because of the more abundant conformations, which was favourable to solubility in organic solvents to facilitate materials purification and solution processing. Furthermore, the increased entropy with flexible linkages presented a higher free energy barrier to crystallization from a glassy state, thereby improving morphological stability against crystallization as compared to relatively rigid conjugated and non-conjugated bipolar hybrid molecules without flexible linkages. Because of the absence of π-conjugation between the two charge-carrier moieties; i.e., triazine and fluorene, the LUMO/HOMO levels and the triplet energies of the two moieties as independent entities were retained in the resultant non-conjugated bipolar compound **XIXa**. The

device with **XIXa** as the host possessed the current density of 0.5 mA/cm^2 and a luminance of 160 cd/m^2, corresponding to current efficiency of 32 cd/A, and external quantum efficiency of 9.2% [72]. The efficiency achieved with **XIXa** as the host was reported to be the best among the solution-processed phosphorescent OLEDs using bipolar hosts.

M. M. Rothmann and coworkers [73] reported a series of donor-substituted 1,3,5-triazine derivatives **XXa-f** prepared by nucleophilic substitution of cyanuric chloride with carbazole, 3-methylcarbazole, phenol, and 3,5-dimethylphenol (Scheme 2.7).

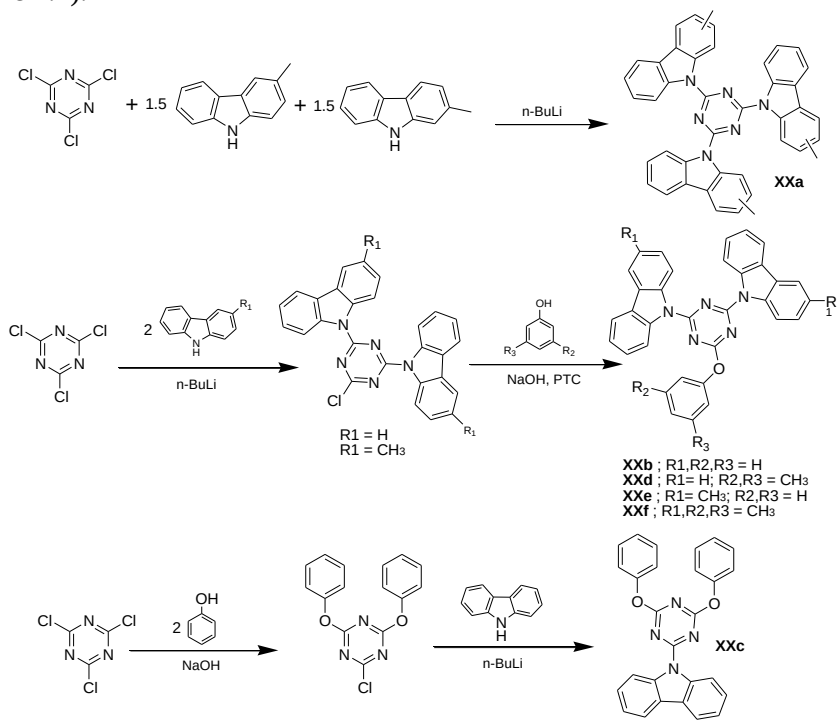

Scheme 2.7 Synthesis of triazine compounds **XXa-f**

Symmetric 2,4,6-triscarbazolyl-1,3,5-triazine reported by H. Inomata *et.al* [74] was highly crystalline with a melting point of 465^{o}C. The substitution of the s-triazine core with three 2-methylcarbazole units or three 3-methylcarbazole moieties still yielded materials with a high tendency to crystallize. Unsymmetrically substituted triscarbazolyl triazines were found to be more interesting. M. M. Rothmann *et.al* [73] were able to prepare various compounds with either two methylcarbazolyl substituents and one carbazole unit or three different methylcarbazolyl units. This strategy resulted in materials with slightly decreased crystallization tendencies. However, the glass formation properties of these triazines were still poor. Usage of stoichiometric mixture of 2-methylcarbazole and 3-methylcarbazole (1:1) as substituents was found to be the most effective way to obtain a less crystalline material.

Triazine derivatives **XXa-f** exhibited melting signals during the first DSC heating cycles. The melting temperatures ranged from 147 to 335 ^{o}C. Some of the derivatives formed glasses and the T_gs ranged from 80 to 170 ^{o}C. The triplet energies of the triazines **XXa-f** were in the range from 2.86 to 2.96 eV. The potential of this class of materials as hosts for blue phosphors has been tested. A maximum brightness of 6900 cd/m^2 and a maximum external quantum efficiency of 10.2% were reached using the blue emitter FIrpic [73].

Donor-acceptor molecules consisting of an electron-deficient 1,3,5-triazine core with three fluorene arms substituted with diarylamino **XXIa-c** or carbazolyl **XXId** electron donors were reported by K. M. Omer *et.al.* [75]. Compounds **XXIa-d** were synthesized by employing Suzuki conditions as shown in Scheme 2.8.

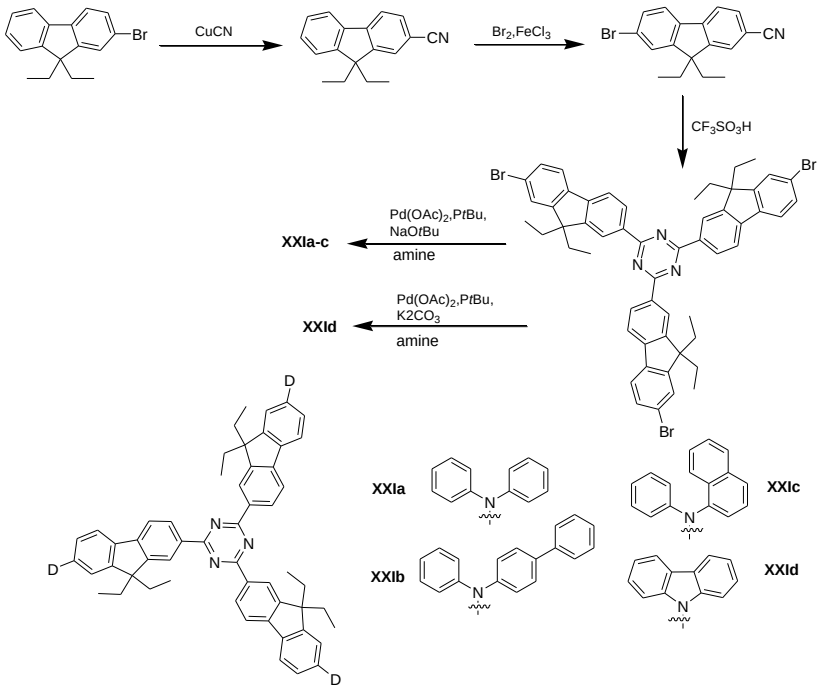

Scheme 2.8 Synthesis of dendritic triazine compounds **XXIa-d**

Cyclic voltametry of **XXIa-c** showed that the reduction consisted of one wave of single electron transfer to the core, while the oxidation exhibited a single peak of three sequential electron transfer processes, with the formation of a trication. The carbazolyl-containing molecule **XXId** after oxidation underwent a subsequent rapid chemical reaction to produce a dimer (*via* the overall coupling of two radical cations with the loss of two protons). The dimer was more easily electro-oxidized than the monomer **XXId**. With continuous cycling on the oxidation side, a conductive polymer film was formed on the surface of the working electrode. Because of the presence of the acceptor (triazine) centre and strong donors in the arms (diarylamines), **XXIa-c** exhibited large solvatochromic effects with emissions ranging from deep blue (428 nm) to orange-red (575 nm) depending on the solvent

polarity. These molecules in dilute solutions possessed high PL quantum yields of 0.70-0.81. The electro-generated chemiluminescence of **XXIa-c** in nonaqueous solutions showed strong chemiluminescence that could be seen with the naked eye in a well-lit room. The electro-polymerized polymer film of **XXId** exhibited electrochromic behaviour and found to be pale orange in the neutral state and dark green in the oxidized state [75].

Fluorene substituted triazine derivatives **XXIIa-b** with efficient hole-blocking ability were designed and synthesized by H. Zhong *et.al* [76]. The cyano derivatives were prepared by the standard Suzuki coupling reaction or the cyanation followed by the Suzuki reaction. The cyclization of the two cyano derivatives using trifluoromethane sulfonic acid gave **XXIIa-b** (Scheme 2.9).

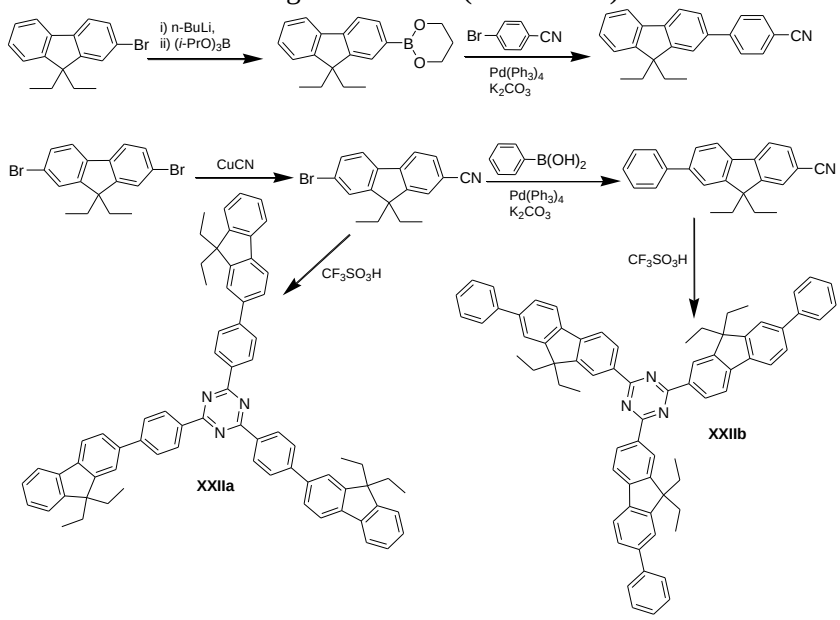

Scheme 2.9 Synthesis of fluorene containing triazines **XXIIa** and **XXIIb**

The absorption spectrum of **XXIIb** was red-shifted about 20 nm, compared with 350 nm of **XXIIa**. The presence of a charge-transferred electronic state in **XXIIb**, caused by the interaction between electron-donating fluorene moiety and electron-accepting triazine moiety was found to be well pronounced [77]. The presence of a phenyl spacer between fluorene moiety and triazine ring in **XXIIa** might be weakened the CT interaction and as a result, the absorption peak was located at shorter wavelength. The CT interaction was also observed in the PL spectra of the triazine derivatives. The electroluminescent devices based on **XXIIa-b** were fabricated with the following configuration: ITO/NPB/Alq_3/compounds containing triazine units/LiF/Al, where a 40 nm thickness layer of Alq_3 was used as the emitting layer and **XXIIa-b** were used as the electron-transporting/hole-blocking materials with a thickness of the layer of 20 nm. The devices based on Alq_3/**XXIIa** and Alq_3/**XXIIb** possessed high luminance of 13000 cd m^{-2} and 18000 cd m^{-2}; respectively. The maximum current efficiencies of the devices containing **XXIIa**

and **XXIIb** were remarkably improved from 3.1 cdA^{-1} of the comparative device with a configuration of ITO/NPB/Alq_3/Alq_3/LiF/Al to 4.0 and 4.9 cd A^{-1}, respectively. **XXIIa** and **XXIIb** enabled to improve the balance between hole- and electron- mobility in the devices. Compounds **XXIIa-b** were also tested in PLED for the improvement of the performance. The known PLED material MEH-PPV was used as light emitting layer and triazine molecules **XXIIa-b** as hole-blocking materials. The maximum luminance of device containing **XXIIa** and **XXIIb** were promoted from 1358 cd m^{-2} of comparative device MEH-PPV (without a hole-blocking layer) to 2327 and 2871 cd m^{-2}, respectively. Furthermore, devices containing **XXIIa** and **XXIIb** showed maximum current efficiencies of 0.97, and 1.37 cd A^{-1}, respectively; which were more than four times higher than 0.25 cd A^{-1} of device containing MEH-PPV [76].

B. Qu *et.al* [78] reported a red–orange light emitting material with a branched molecular structure, 2,4,6-tris[2-(N-ethyl-3-carbazole)carboxethenyl]-1,3,5-s-triazine (**XXIIIa**). Compound **XXIIIa** was assembled from s-triazine, acting as an acceptor group, vinylene conjugated connectors and N-ethylcarbazolyl groups, as donor peripheral groups by alkaline condensation reaction (Scheme 2.10).

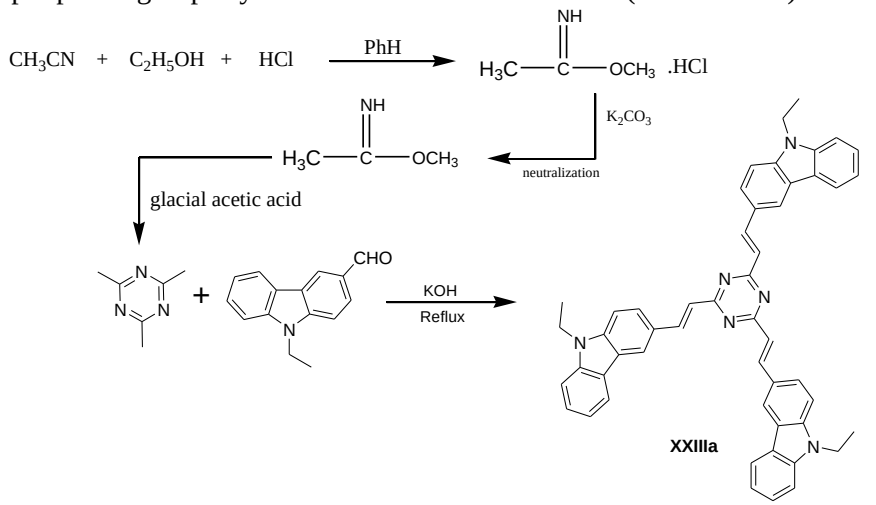

Scheme 2.10 Synthesis of triazine derivative **XXIIIa**

The absorption maximum of **XXIIIa** in dilute solution occurred at 394 nm, while the absorption maximum of the film occurred at 403 nm with a shoulder peak at 503 nm, which showed a red-shift (9 nm) with respect to the spectrum of the solution. The optical band gap of **XXIIIa** was found to be 2.77 eV. The PL spectrum of **XXIIIa** in dilute solution peaked at 474 nm. The PL spectrum of **XXIIIa** film showed two peaks at 483 and 569 nm, which were assigned to the monomer and excimer emissions [79,80], respectively. **XXIIIa** also showed two-photon absorption and two-photon excited fluorescence [81]. The HOMO level of **XXIIIa** was found to be about -5.2 eV. The white EL device was fabricated using **XXIIIa** as a red–orange emitter and 8-hydroxyquinolinolato lithium (Liq) as a blue–green emitter. N,N-bis(3-methylphenyl)-N,N-diphenylbenzidine (TPD) as the

adjustor for charge carrier mobility was introduced between the two emitting layers to improve the stability of the white emission colour on bias voltage. The EL devices of ITO/poly(N-vinylcarbazole): **XXIIIa** (56 nm)/TPD(5 nm)/Liq (30 nm)/Mg:Ag exhibited good quality white emission. The CIE chromaticity coordinates were 0.34 and 0.39 and were stable with respect of the bias voltage.

Multi-branched two-photon absorption triazine chromophores **XXIVa-d** with different donor strength, conjugation length, and direction of charge transfer were synthesized by Y. Jiang and co-workers **[**82**]**. Bromination of 2,4,6-tri(p-tolyl)-1,3,5-triazine afforded 2,4,6-tris(4-(bromomethyl)phenyl)-1,3,5-triazine, followed by reaction with trimethyl phosphate, yielding triazine derivative for Wittig reaction [83]. The condensation of the respective donor-aldehydes with triazine derivative by the Horner–Wadsworth–Emmons reaction [52] gave compounds **XXIVa-d** (Scheme 2.11).

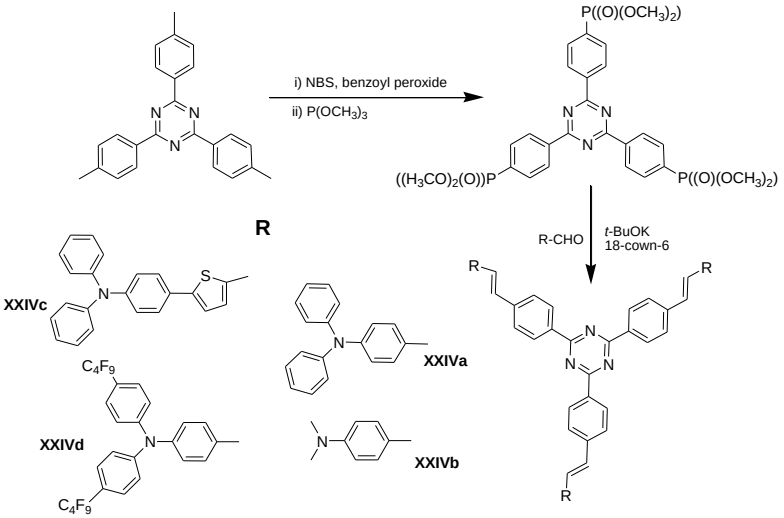

Scheme 2.11 Synthesis of triazine derivatives **XXIVa-d**

One-photon absorption and emission spectra revealed that the Stokes shifts for these compounds increased with an increasing extension of the π-systems and increase of electron-donating ability of the donors, whereas the fluorescence quantum yield exhibited large increase with the introduction of electron-accepting perfluoroalkyl as side groups to the end donor. Investigation of the nonlinear absorption properties of these chromophores revealed that their two photon absorption cross section values increased with increasing electron-donating strength of the end group, extending the conjugation length of the system, introducing electron-accepting perfluoroalkyl, and making ICT possible. In conjunction with the increased fluorescence quantum yield the multi-branched triazine derivative with perfluoroalkyl moiety would be able to provide potential application in two-photon fluorescence bioimaging. These molecules also exhibited good optical limiting properties; which made them potential candidates for optical limiters in the photonics field.

Triazine moiety as an electron-transporting central core, separated from thiophene, furan, or EDOT moieties by the *p*-phenylene spacers **XXVa-e** were synthesized by K. R. Idzik *et.al* [84]. The Stiile coupling reaction of bromo substituted triazine derivative yielded **XXVa-e** (Scheme 2.12).

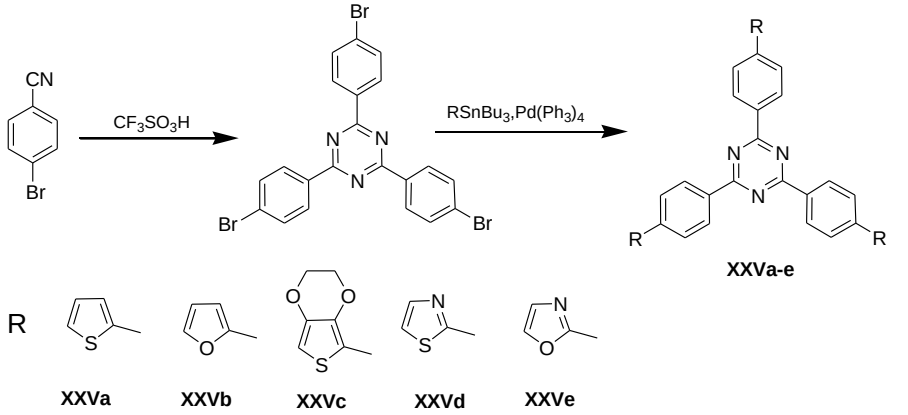

Scheme 2.12 Synthesis of triazine derivatives **XXVa-e**

XXVa-e displayed excellent redox stability. Spectroelectrochemical experiments confirmed reversible redox behaviour of the polymer of **XXVc** upon oxidation switching between all redox states even going up to tetracation. The dilute solutions of these derivatives exhibited fluorescence in the range from 395 to 465 nm with the quantum yield being in the range of 36 to 42%. The decay of fluorescence of some of the derivatives was found to be ranged from 1.65 to 2.33 ns.

E. Beltran and coworkers [85] synthesized tris(triazolyl)triazine core-based materials **XXVIa-c** by applying "click" reactions [86] of the aromatic alkyne and azide precursors . Aromatic azides and the precursor, 2,4,6-tris(ethynyl)-1,3,5-triazine, were used for the synthesis of the C_3-symmetrical system, 2,4,6-tris(triazolyl)-1,3,5- triazine core, by click-chemistry (scheme 2.13).

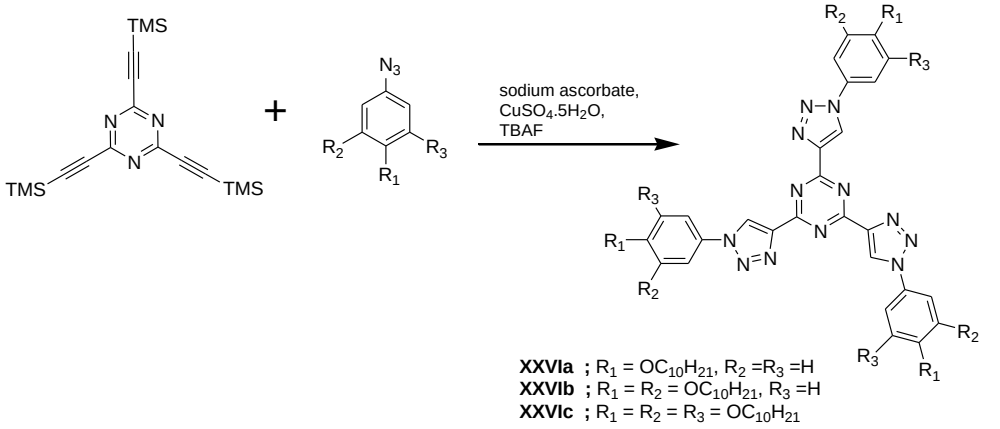

Scheme 2.13 Synthesis of triazine derived liquid crystals **XXVIa-c**

All 2,4,6-tris(triazolyl)-1,3,5- triazine compounds were found to be liquid crystalline. They were thermally stable above their clearing point according to thermogravimetric analysis. **XXVIb-c** displayed textures that were typical for hexagonal columnar phases (Col_h) by polarized optical microscopy. **XXVIa** did not show any characteristic texture in pure state, but a Col_h mesophase was displayed in miscibility tests with **XXVIb**. The maximum absorption wavelengths were located in the UV region, at around 300 nm, and were attributed to π-π* transitions due to the high absorption coefficients. All 2,4,6-tris(triazolyl)-1,3,5- triazine compounds were luminescent and emitted in the blue-green part of the visible spectrum. A remarkable red-shift in the emission maximum was observed as the number of peripheral alkoxy chains increased. The thin films of the compounds also showed luminescence at room temperature with the emission wavelengths similar to those of the solutions. Electrochemical measurements confirmed the electron-deficient nature of this family of compounds and their potential for electron-transport. **XXVIa** showed a reversible reduction process with a half-wave potential of -1.28 V. In addition, an irreversible reduction process was found at -2.24 V. **XXVIb** also showed the similar behaviour, with reversible and irreversible reduction processes (at -1.33 and -2.15 V, respectively). In contrast, only one reversible reduction process was observed, at a half-wave potential of -1.33 V, for **XXVIc.**

Tris(tetrathiafulvalene)- and tris(ferrocene)-1,3,5-triazines **XXVIIa-b** with redox properties were synthesized by A. Garcia *et.al.* (Scheme 2.14) [87].

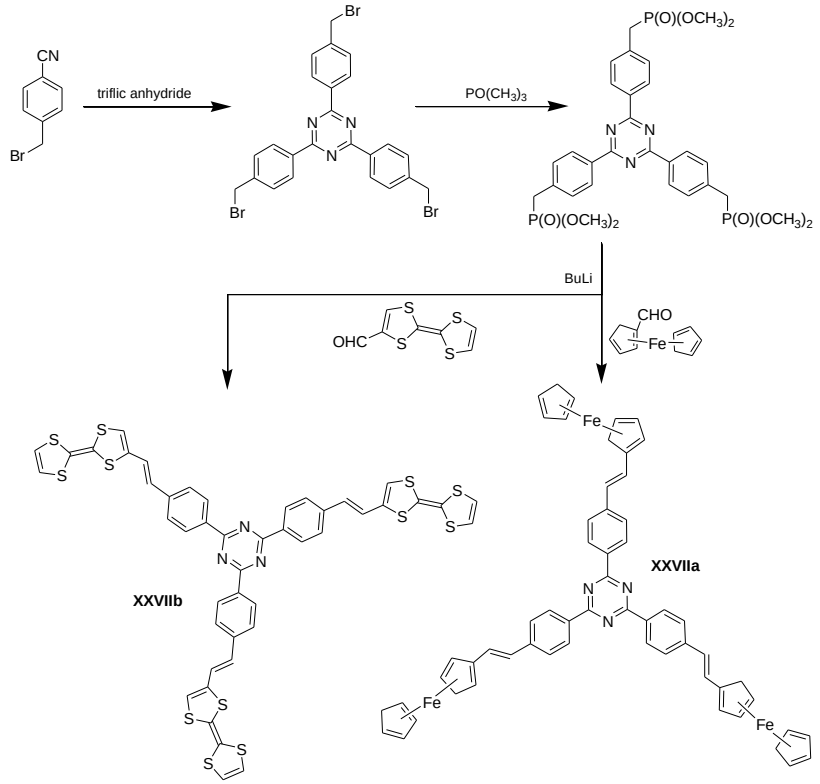

Scheme 2.14 Synthesis of triazine derivatives **XXVIIa-b**

In the absorption spectra of the dilute solutions in $CHCl_3$, the broad band in the visible region at 484 nm for **XXVIIa** and 461 nm for **XXVIIb** evidenced the occurrence of a donor-acceptor ICT. HOMO-LUMO gap was smaller for **XXVIIa** compared to **XXVIIb**. Compounds **XXVIIa-b** showed an amphoteric redox behaviour showing the oxidation features of the electron-donor moiety as well as that of the triazine as the acceptor unit. An electronic communication between the three electron donor units located at the periphery and the electron acceptor triazine core was also observed in the cyclic voltametry studies.

By using palladium-catalyzed 3-fold coupling methodology, π-conjugated molecules **XXVIIIa-e** based on 1,3,5-triazine were synthesized (Scheme 2.15) [88]. The C_3-symmetrical precursor, 2,4,6-tris(5-bromothiophene-2-yl)-1,3,5-triazine, was prepared by trimerization of 5-bromo thiophene-2-carbonitrile. Suzuki-Miyaura cross-coupling reactions of 2,4,6-tris(5-bromothiophene-2-yl)-1,3,5-triazine with three equiv. of the corresponding phenylboronic esters afforded compounds **XXVIIIa-c** in the presence of a catalytic amount of $Pd(PPh_3)_4$. Compound **XXVIIId** possessing three phenylbithiophene arms was synthesized by the Stille cross-coupling reaction. The carbazolyl-substituted compound **XXVIIIe** was obtained *via* Buchwald-Hartwig amination [89] using a mixture of Pd_2-$(dba)_3$ and $[(t\text{-}Bu)_3PH]BF_4$ as the catalyst [90].

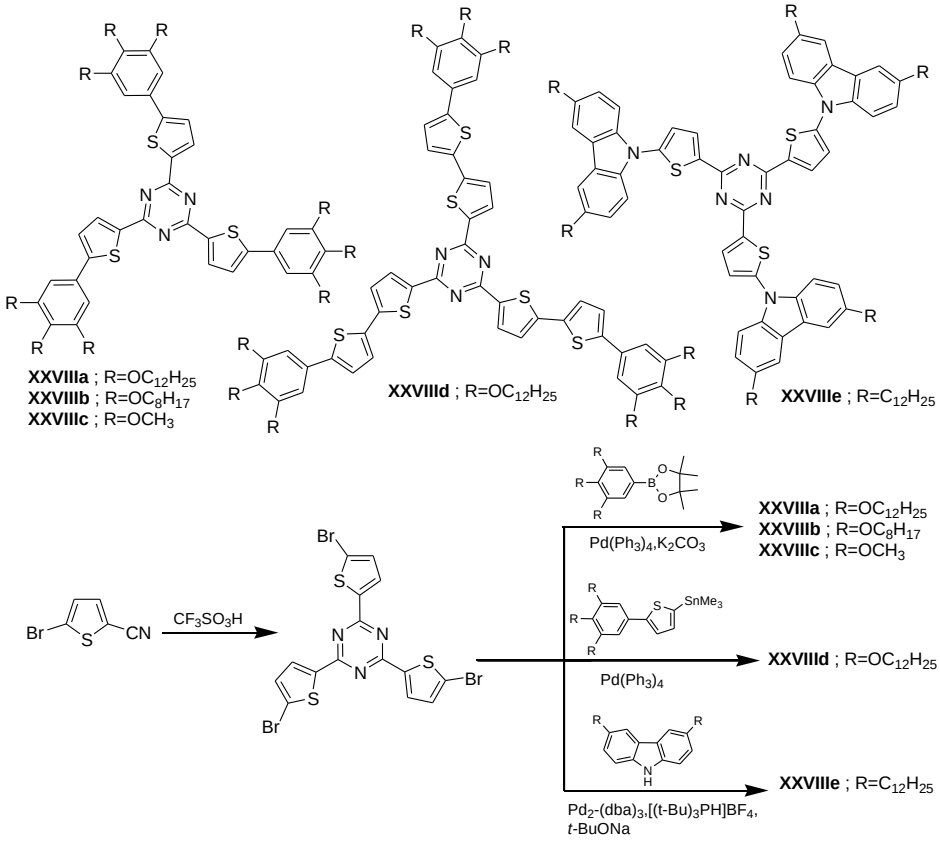

Scheme 2.15 Synthesis of triazine derived liquid crystals **XXVIIIa-e**

Compounds **XXVIIIa, XXVIIIb** and **XXVIIIe** having flexible alkyl chains exhibited columnar liquid crystalline phases from room temperature upon heating, while the columnar phase of **XXVIIId** with an enlarged π-conjugated core existed over relatively higher temperatures in the range of 48-125 ^{o}C. The time-of-flight experiments revealed that these materials were capable of transporting both holes and electrons in the columnar phases; functioning as ambipolar one dimensional conducting materials. The hole and electron mobilities of **XXVIIIa** were estimated to be 3×10^{-5} and 4×10^{-3} cm^2 V^{-1} s^{-1} at 100 ^{o}C, respectively. Compound **XXVIIIb** also exhibited ambipolar conduction behaviour, giving rise to hole and electron mobilities on the order of 10^{-5} and 10^{-3} cm^2 V^{-1} s^{-1}, respectively, in the Col_h phase. The photoconductive properties of these compounds were also examined over a range of temperatures. Low charge carrier mobilities in the order of 10^{-6} cm^2 V^{-1} s^{-1} were observed in the isotropic phase of **XXVIIIa**. As for compound **XXVIIIa**, the hole and electron mobilities discontinuously increased by about 1 and 3 orders of magnitude, respectively, at the isotropic Col_h phase transition upon cooling, reflecting the formation of ordered one dimensional π-stacked structures in the Col_h phase. The mobility of electrons in the Col_h phases of **XXVIIIa-b** was more than 100-times higher than that of holes. This behaviour reported to be originated from the octupolar structure of the propeller-shaped molecules containing both the electron-accepting triazine core and the trigonally ramified electron-donating phenylthiophene units. The observed electron mobilities of **XXVIIIa-b** in the nanostructured liquid crystalline states were 1-4 orders of magnitude higher than those of widely used electron-transporting amorphous materials [91,92]. Due to highly dispersive features of the photocurrents in the experimental conditions distinct electron mobility for compounds **XXVIIId** and **XXVIIIe** could not be evaluated. However, the hole mobilities of both **XXVIIId** and **XXVIIIe** in the Col phases were found to be higher than those of **XXVIIIa-b** and reached values of 1×10^{-3} cm^2 V^{-1} s^{-1}. The enhanced hole mobilities in **XXVIIId** and **XXVIIIe** as compared to **XXVIIIa-b** might be arised from an increased intermolecular π-overlap attributed to the expanded electron-donating segments (the phenylbithiophene units in **XXVIIId** and the carbazolylthiophene units in **XXVIIIe**) within the columns. The lowest energy absorption maxima of **XXVIIIa**, **XXVIIId**, and **XXVIIIe** were observed at 385, 440, and 415 nm, respectively, in the Col phases. It has been revealed that the PL emission colour of the octupolar materials can be tuned from blue-green to orange by changing the electron-donating segments. Compound **XXVIIIe** in the Col phase exhibited an emission maximum at 490 nm, which appeared at a higher energy with a smaller Stokes shift than those of **XXVIIIa** (λ_{em} = 519 nm) and **XXVIIId** (λ_{em} = 585 nm). The redox properties of **XXVIIIa-e** characterized by cyclic voltametry demonstrated that all the compounds underwent both electrochemical oxidation and reduction processes because of their D-A hybrid characteristics.

2.3. Electron-transporting or ambipolar bay substituted perylene bisimides

Perylene bisimides were initially applied for industrial purposes as red vat dyes. Recent applications of perylene bisimide pigments are in the field of electronic materials, among which they are in the group of best n-type or ambipolar semiconductors. Electron-transporting character of perylene bisimides is related to their high electron affinity. Perylene-3,4,9,10-tetracarboxylic dianhydride can be considered as the parent compound of this class of compounds [93]. It was first obtained in the early 1910s. Perylene bisimides with different chemical and physical properties can be obtained by introduction of the substituents, most often in the imide N, N' positions and t 1, 6, 7, and/or 12 positions of the hydrocarbon core, the so called "bay" positions (Figure 2.14). The imide substituents have little influence on molecular-level electronic and optical properties, but can be used to affect aggregation and solubility, whereas bay substituents affect electronic and optical properties [94,95]. Due to the relatively higher reactivity of perylene bisimides at the bay positions towards electrophilic substitutions, they can be easily substituted with various electroactive moieties to improve the molecular properties. Hence, bay substitutions with various electron-donors or with other functional groups are the strategic way of improving the charge-transporting property as well as ambient stability of perylene bisimides.

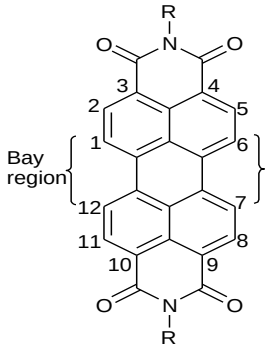

Figure 2.14 Structure of perylene bisimide

B. A. Jones *et.al* [96] reported a series of bay cyanated perylene bisimides exhibiting air-stable n-type carrier mobilities in combination with low threshold voltages and substantial processing versatility. The immediate precursors to the cyanoperylenes were the corresponding bromo derivatives. These bromo derivatives can be readily synthesized by the direct bromination of the parent hydrocarbons. Classical cyanation procedures using CuCN in refluxing DMF failed to produce the desired cyano compound **XXIXa**. By using $Zn(CN)_2$ method in the presence of a Pd(0) catalyst, the authors [96] were able to convert bromoperylene to cyanoperylene quantitatively [97]. **XXIXb** was synthesized by modified core cyanation and N-fluoroalkylation [97,98].

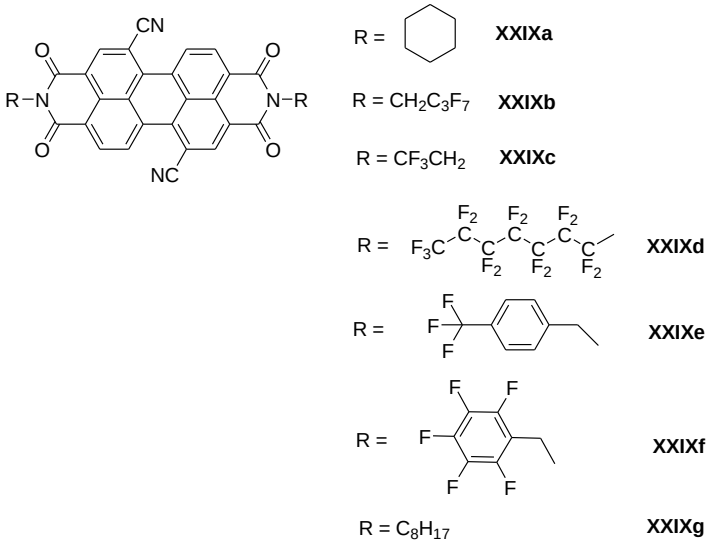

Figure 2.15 Structures of bay cyano functionalized perylene bisimides

The cyano functionalities provided solubility for solution processing and stability of n-type charge carriers by lowering the LUMO to resist ambient oxidation. **XXIXa**-based OFETs displayed electron mobilities as high as 0.1 cm^2V^{-1} s^{-1}, threshold voltages of approximately 15 V, and I_{on}/I_{off} (+100 V/0 V) ~10^5, while **XXIXb**-devices exhibited electron mobilities as high as 0.64 cm^2V^{-1} s^{-1}, threshold voltages between -20 V and -30 V, and I_{on}/I_{off} (+100 V/60 V) as high as 10^4. Devices stored and tested under ambient conditions exhibited negligible degradation in charge mobility, threshold voltage, or I_{on}/I_{off} over six months. The electron-withdrawing N-functionalities further aided charge carrier stability in **XXIXb** by further lowering the LUMO energies; however, might be also induced close molecular packing for increased intermolecular π-overlap and more efficient charge transport [96].

R. T. Weitz *et.al* [99] also reported core-cyanated perylene bisimides end-functionalized with fluorine-containing linear and cyclic substituents for the fabrication of air-stable n-channel OFETs (Figure 2.15). Field-effect mobilities of transistors were found to be depending on the substrate temperature during the vacuum deposition of semiconductors **XXIXb-f.** The best performance was obtained with **XXIXb** deposited at a substrate temperature of 120 °C. This transistor has an electron mobility of 0.1 cm^2V^{-1} s^{-1}, a threshold voltage of -1 V, a subthreshold swing of 0.5 V/decade, and an on/off current ratio of 10^5. For lower substrate temperatures, the films were less ordered and the carrier mobility was lower, whereas the rate of mobility degradation in air was independent of the degree of molecular order in the film. The carrier mobility of the OFETs based on **XXIXb** increased almost monotonically over 4 orders of magnitude as the substrate temperature during the deposition was increased from 25 to 120 °C. OFETs prepared at a substrate temperature of 140 °C; however, have a much smaller drain current than the transistors prepared at 120 °C for **XXIXb.** For OFETs based on **XXIXc**, the

performance peaked at a much lower substrate temperature (25 °C), apparently because of the short substituents which lead to distinct island growth at temperatures as low as 60 °C. However, at a substrate temperature of 25 °C the degree of molecular order in the film was very small, which explained the poor electron mobility at this temperature. OFETs based on **XXIXd** prepared at 140 °C showed relatively good performance. The two compounds with cyclic end groups showed a maximum electron mobility of 0.004 cm^2V^{-1} s^{-1} (**XXIXe**) and 0.002 cm^2V^{-1} s^{-1} (**XXIXf**); both for a substrate temperature of 120 °C. OFETs based on **XXIXe** and **XXIXf** also showed a much more negative threshold voltage than the transistors based on the compounds with linear end groups. The bulkier cyclic end groups in **XXIXe-f** might be leading a different crystal packing that was characterized both by a smaller degree of orbital overlap in the direction of transport in the channel (leading to a poor mobility) and by a greater density of defects (leading to a larger threshold voltage). The shelf life of the OFETs prepared from **XXIXb** through **XXIXf** was also investigated when stored under ambient conditions. All the devices reported to be showed almost the same rate of charge mobility degradation in air.

Single crystal n- channel OFETs using **XXIXb** was also fabricated by A. S. Molinari *et.al* [100]. Typical electrical characteristics of **XXIXb** transistors were tested in vacuum and in air. The electrical characteristics were virtually free of hysteresis and in most cases the threshold voltage was between -5 and +5 V usually close to 0 V. The vacuum field-mobility values ranged from ~6 to 1 cm^2V^{-1} s^{-1} whereas the electron mobility in ambient conditions ranged between ~3 and 0.8 cm^2V^{-1} s^{-1}. The difference between the **XXIXb** thin-film (~0.1 to 0.6 cm^2V^{-1} s^{-1}) and single-crystal (~1 to 6 cm^2V^{-1} s^{-1}) mobility values might have several origins [96, 100]. Efficient charge transport in organic semiconductors required uniform and continuous film morphology; however, vapour/solution-deposited thin films were usually characterized by grain boundaries and random crystallite molecular orientation which limited the device performance. A single crystal represented an almost ideal situation for charge transport characterized by absence of macroscopic grain boundaries, a very smooth and homogeneous surface, and micrometer-extended ordered molecular arrangement. Moreover, the crystal growth process provided an additional purification step by reducing charge traps.

H. Yan and co-workers [101] investigated several n-channel OFET structures fabricated using different dielectric materials and semiconductor film deposition methods. Within the solution-processed films, drop-casting of **XXIXg** afforded OFETs with statistically greater carrier mobilities (0.08–0.005 cm^2V^{-1} s^{-1}) than those fabricated by spin-coating (0.04–0.005 cm^2V^{-1} s^{-1}). However, spin-coated semiconductor films were smoother and afforded more reproducible transistor characteristics. Top-gate OFETs were realized using **XXIXg** in combination with a solution-processed top gate dielectric. These top-gate devices clearly showed n-type transistor behaviour with typical linear and saturation characteristics. The electron mobilities of these devices were ~10^{-3} cm^2V^{-1} $s^{-1}$with I_{on}/I_{off} ratio ~10^4. The long term stability of these top-gate OFETs were investigated by testing the ring oscillator after storage in air for more than 9 months in dark containers. Negligible variation in signal amplitude (~ +3%) and minimal frequency changes (~ -15%)

were recorded; demonstrating the good stability of these ambient-fabricated and unencapsulated devices.

J. H. Oh *et.al* [102] studied the effects of the interplay between energetic and kinetic factors on the air stability of n-channel organic thin-film transistors OFETs using two PBI compounds, N,N'-bis(2,2,3,3,4,4,5,5,5-nonafluoropentyl)-3,4:9,10-tetracarboxylic acid bisimide (PBI-F) and N,N'-bis(cyclohexyl)-1,7-dicyano-perylene-3,4:9,10-tetracarboxylic acid bisimide (**XXIXa**), with distinctly different LUMO levels. On the basis of the empirical energy level windows, PBI-F was at the onset region for air stability (LUMO = -3.84 eV) whereas the other compound **XXIXa** (LUMO = -4.33 eV) was in the air-stable region. Charge-transport behaviours under an inert atmosphere and in air were investigated as a function of active layer thickness. Charge-transport in air was found to be greatly affected by the active layer thickness for both compounds. The ambient stability of the air-unstable PBI-F transistors increased significantly for thicknesses over ~10 monolayers. The previously considered "air-stable" **XXIXa** transistors were not stable in air if the active layer thickness was less than ~4 monolayers. The minimum thickness required for air stability was found to be closely related to the LUMO level, film morphology and film growth mode [102].

M.-M Ling *et.al* [103] also fabricated OFETs using tetrachloroperylene tetracarboxylbisimide. Air-stability measurements were carried out by monitoring the negative charge-carrier mobilities and on/off ratios as a function of time. The mobilities of devices decreased slightly from 0.16 and 0.18 $cm^2V^{-1}s^{-1}$ to 0.08 and 0.04 $cm^2V^{-1}s^{-1}$ after storage in air for 80 days. The devices that were exposed only to air showed a slightly better stability than those that were exposed to both air and ambient light.

R. Schmidt *et.al* [104,105] reported core-halogenated perylene bisimides **XXXa-h** for air-stable n-channel OFETs (Figure 2.16). Core-fluorinated compounds **XXXa** and **XXXb** were obtained by Halex reaction of the corresponding dibrominated derivatives [106,107]. Imidization reactions of perylene dianhydrides with the corresponding amines by employing N-methyl- 2-pyrrolidone together with catalytic amounts of acetic acid as solvent yielded **XXXa-i**.

Compounds that possessed two fluorine substituents at the concomitantly flat PBI core **XXXa** afforded excellent n-channel transistors (0.3 $cm^2\ V^{-1}\ s^{-1}$; $I_{on}/I_{off} > 10^6$). Compounds **XXXc** and **XXXd** bearing more bulky chlorine and bromine atoms at the PBI core exhibited much less field-effect mobilities compared to fluorine-substituted derivative **XXXb**. This was presumably due to the significantly increased torsion angles and the reduced intermolecular π-π interactions that hinder efficient charge transport. The replacement of perfluorinated alkyl side chains by perfluorinated aromatic groups in the imide position improved the charge carrier mobility by ~2 orders of magnitude. In this case the perfluorinated aromatic imide substituents might be provided an additional charge transport path. For distorted core-tetrahalogenated (fluorine, chlorine, or bromine) PBIs, less advantageous solid state packing was observed and high performance OFETs were obtained from only one tetrachlorinated derivative **XXXf**. Perylene bisimide derivative bearing four chlorine substituents in the bay positions **XXXi** exhibited interesting charge carrier

mobility in the liquid crystalline phase [108]. The charge carrier lifetime of **XXXi** was over 100 times greater than that found in the non-chlorinated parent compound. This dramatic increase in lifetime was explained in terms of increased order in the modified material.

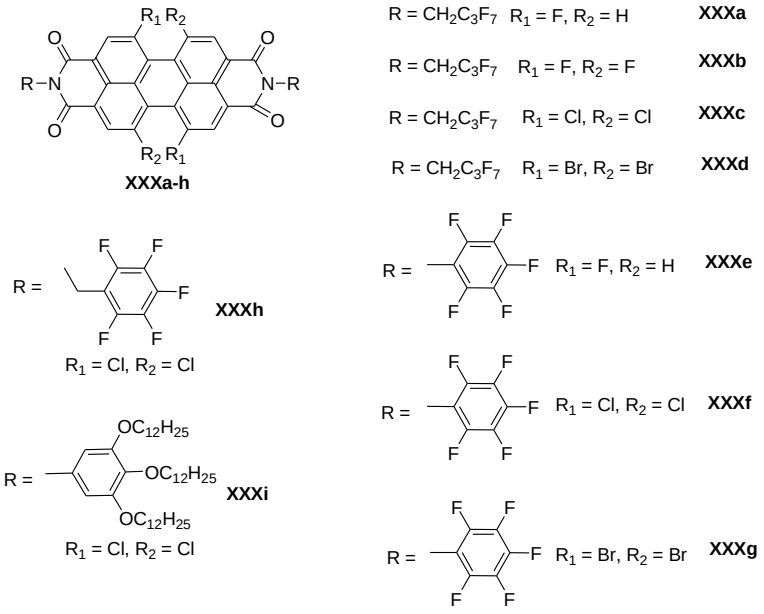

Figure 2.16 Structures of bay halogenated perylene bisimides

S. Vajiravelu *et.al* [109] incorporated electron donating substituents such as 3,4,5-trimethoxy phenyl, thiophene, 6-methoxy naphthyl, 5-hexyl dithiophene and thioanthrenyl moieties at the bay region of *N*,*N*'-dodecylperylene bisimide and evaluated the effect of these substituents on the electron transporting properties of these derivatives by xerographic time-of-flight technique. Figure 2.17 shows the structures of bay donor substituted perylene bisimides **XXXIa-e**. The highest electron mobility of 4.4×10^{-4} cm^2 V^{-1} s^{-1}at 6.4×10^5 Vcm^{-1} was observed for **XXXIa** under ambient conditions.

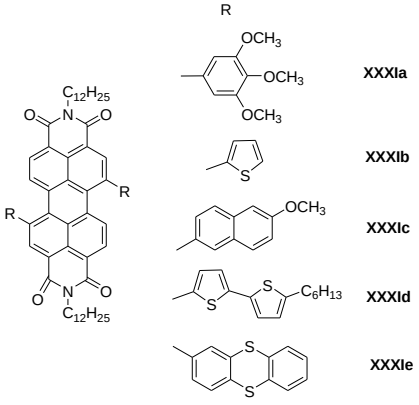

Figure 2.17 Structures of bay donor functionalized perylene bisimides **XXXIa-e**

The same research group [110] also showed the tuning of charge transporting properties by changing substituent positions at the bay region of PBIs. In molecule **XXXIIa**, the linear pentathiophene electron donors were attached to the bay position of the PBI moiety *via* the central thiophene unit through a β-linkage whereas in molecule **XXXIIb** the donor unit (pentathiophene) was cross conjugated and attached to PBI through a central thiophene through an α-linkage (Figure 2.18).

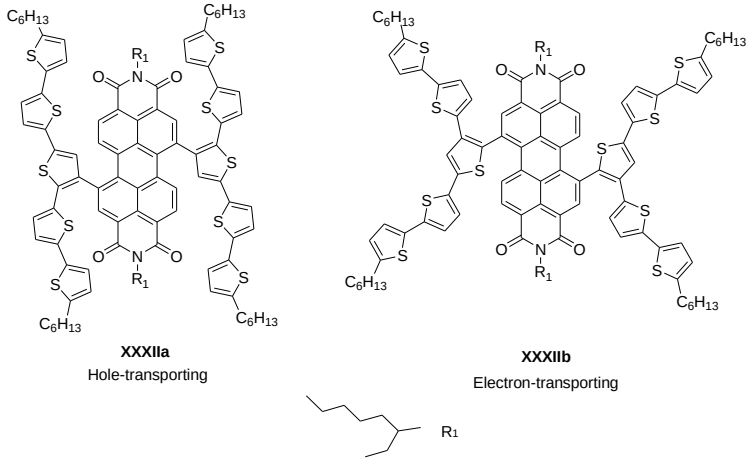

Figure 2.18 Synthesis of hole or electron transporting perylene bisimides **XXXIIa-b**

Bottom contact OFET fabricated by spin coating of **XXXIIa** showed ambipolar behaviour with an electron mobility of 2.23×10^{-7} cm^2 V^{-1} $s^{-1}$and hole-mobility of 6.85×10^{-6} cm^2 V^{-1} s^{-1}, respectively. Compound **XXXIIb** showed electron-transport with an electron mobility of 6.21×10^{-7} cm^2 V^{-1} s^{-1}. Upon annealing, the hole-mobility of **XXXIIa** increased to 1.04×10^{-4} cm^2 V^{-1} s^{-1} and the electron mobility decreased to 9.13×10^{-8} cm^2 V^{-1} s^{-1}, which was attributed to the better ordering of pentathiophene units terminated with hexyl chains resulting in a more effective isolation of PBI units.

2.4. Conclusions of literature review

Symmetric organic materials demonstrate a wide range of interesting physical properties; including effective charge-transport, electroluminescence and high thermal stability. Some low-molar-mass derivatives are capable to form glasses with good morphological stability whereas the compounds containing rigid core and flexible alkyl substituents form organic liquid crystals. Various core-arm combinations in dendritic materials are an interesting methodology for the tunabitity of physical properties, in particular, organic semiconducting and luminescent properties. These compounds can be readily synthesized by applying the so-called "building block approach" together with the use of a variety of cross-coupling reactions. Hence, it is interesting to synthesis and investigate the properties of new thermally stable molecular glasses or room temperature organic liquid crystals with different core-arm combinations, for example, donor-acceptor or donor-donor combinations.

Pyrene, triazine and triphenylamine core-centred organic materials exhibit interesting optical and photoluminescence properties in addition to the excellent redox characteristics and charge-transport. Pyrene- and triphenylamine-based materials represent a class of efficient *p*-type organic semiconductors with excellent luminescence properties. Some triazine-based dendritic organic materials display competent redox and luminescence properties with enhanced charge-transporting characteristics. It is found that the optoelectronic properties of these dendritic materials greatly influenced by both the nature and the number of electron-donor substituents at the rim. Therefore, it is important to synthesis new optically or electrically active organic materials based on the aforementioned aromatic or heteroaromatic cores, and study the effect of substitution of various electron-donor chromophores to these molecular cores in the viewpoint of applications in organic electronics.

Electron-deficient fused heteroaromatic systems, for example, arylene imides, are employed as electron-transporting or ambipolar organic materials in optoelectronic devices, in particular, OFETs. Attachment of electron-donor chromophores to the electron-deficient perylene bisimide core enabled to obtain ambient stable organic materials with the opportunity for the tunability of semiconducting properties. However, the choice of solution processable molecular glasses for n-channel or ambipolar OFETs based on arylene imides is still limited. Therefore, it is of particular importance to synthesis arylene imide based electron-donor substituted organic materials for air-stable OFETs.

3. EXPERIMENTAL

3.1. Instrumentation

The progresses of the reactions were monitored by thin layer chromatography (TLC) on ALUGRAM SIL G/UV245 or POLYGRAM SIL G/UV254 plates in UV light or I_2. Substances in solution were applied to the TLC plates using capillary glass tubes and separation of the substances was carried out using appropriate solvent combinations. Silica gel (grade 60, 70-230 mesh, particle size 0.063 – 0.2 mm, Fluka) was used for column chromatography.

Proton and carbon nuclear magnetic resonance (^{1}H and ^{13}C NMR) spectra were taken on Varian Unity Inova (300MHz (^{1}H), 75.4 MHz (^{13}C)) spectrometer. $(CH_3)_4Si$ (TMS, 0 ppm) was used as an internal standard. All the data are given as chemical shifts in δ (ppm) downfield from TMS. Infrared (IR) spectra were recorded using Perkin Elmer Spectrum GX spectrometer. The spectra of solid materials were performed in KBr pellets. Mass (MS) spectra were obtained on a Waters ZQ (Waters, Milford, USA) and Finnigan MAT 8500 (70 eV) with a MAT 112 S Varian. The molecular weights of some target molecules were determined by MALDI-TOF mass spectrometry using Shimadzu Biotech Axima Performance system. In this case 2, 5-dihydroxybenzoic acid was used as the matrix under reflector mode of operation. Elemental analysis was performed with an Exeter Analytical CE-440 elemental analyzer.

Thermal transition data of synthesized compounds was collected using a TA Instruments Q100, STARe-7 DSC, Perkin-Elmer DSC-7, and Perkin-Elmer Diamond DSC. Samples of 5 – 15 mg as obtained from the synthesis were heated in 40 μL pans at a scan rate of 10 ^{o}C/min or 20 ^{o}C/min under nitrogen flow. During first heating scan the melting points were measured. After melting, the samples were cooled at same scan rate. The resulting glasses were heated again under the same conditions to measure the glass transition temperatures (T_g).

Melting point (m.p.) of the materials were determined using Electrothermal Mel-Temp apparatus.

Thermogravimetric analysis was carried out using a METTLER TOLEDO TGA/SDTA 851e and Netzsch STA 409 with a data acquisition system 414/1. Samples were prepared by filling 6 - 12 mg of substance into alox crucibles. All measurements were performed under nitrogen flow (75cm^3/min) in a temperature range from -30 to 800 °C at a heating rate of 10 ^{o}C/min or 20 ^{o}C/min.

Absorption spectra of the dilute solutions were recorded by UV-Vis-NIR spectrophotometer Lambda 950 (Perkin Elmer). Photoluminescence (PL) of the derivative solutions and thin films was excited by light emitting diode (Nichia NSHU590-B) and measured using back-thinned CCD spectrometer (Hamamatsu PMA-11). For these measurements dilute solutions of the investigated compounds were prepared by dissolving them in spectral grade THF at 1×10^{-4} - 1×10^{-5} M concentration. Neat films of the investigated compounds were prepared from the 1×10^{-3} M THF solutions on the quartz substrates by drop-casting technique. The same technique was also employed to form solid solutions (0.25 wt %) in

polystyrene (PS). Quantum efficiencies were estimated by comparing their spectrally integrated emission intensities with that of the standard [111]. Fluorescence quantum yield (Φ_F) of the samples was estimated by utilizing integrating sphere (Sphere Optics) coupled to the CCD spectrometer using optical fiber. Fluorescence transients were measured using time-correlated single photon counting system PicoHarp 300 (PicoQuant GmbH). Pulsed excitation at 1 MHz repetition rate was provided by picosecond diode laser with the pulse duration of 70 ps.

The ionization potentials (I_p) were measured by the electron photoemission method in air. The samples for the measurements were prepared by dissolving materials in THF and were coated on Al plates pre-coated with ~0.5 mm thick methylmethacrylate and methacrylic acid copolymer adhesive layer. The measurement method is, in principle, similar to the described one in literature [112,113].

Charge drift mobilities of the neat materials or molecular mixtures with a polymer host bisphenol Z polycarbonate (PC-Z) were estimated by xerographic time-of-flight method. The samples for the measurements were prepared by casting the solutions of the compounds or solutions of the mixtures of these compounds with binder materials PC -Z at mass proportion 1:1 in THF. The substrates were glass plates with conductive SnO_2 layer or polyester film with Al layer. After coating the samples were heated at 80 ^oC for 1 hr. Thus the transporting layers of the samples were prepared. In some cases, in order to avoid crystallization, the layers were dried at room temperature for several hours. The thickness of the transporting layer varied in the range of 1–12μm. Electron or hole drift mobility (μ) was measured in the xerographic mode [114,115,116]. Negative or positive corona charging created an electric field inside the material layer. The charge carriers were generated at the layer surface by illumination with pulses of nitrogen laser (pulse duration was 1 ns, wavelength 337 nm). The layer surface potential decrease as a result of pulse illumination was up to 1–5% of initial potential before illumination. The capacitance probe connected to the wide frequency band electrometer measured the speed of the surface potential decrease dU/dt. The transit time t_t for the samples with the transporting material was determined by the kink on the curve of the dU/dt transient in linear scale. In other cases, the dispersion of the transient current was larger and log–log scale was used. The drift mobility was calculated by using the formula: $\mu=d^2/U_0t_t$, where d is the layer thickness, and U_0 the surface potential at the moment of illumination.

Electrochemical investigations were carried out in a dry argon atmosphere on an Autolab potentiostat (Eco Chimie). The data were collected using GPES (General Purpose Electrochemical System) software. The electrolyte medium consisted of the studied semiconducting compounds dissolved in 0.1 M Bu_4NBF_4/CH_2Cl_2 or Bu_4NPF_6/CH_2Cl_2 electrolyte. For cyclic voltametry, following two kinds of three electrode systems were used: i) platinum working electrode of surface area of 3 mm^2**,** platinum wire counter electrode and Ag/AgCl reference electrode (used also for differential pulse voltametry) and ii) glassy carbon working electrode, platinum wire counter electrode and Ag/0.1M $AgNO_3/CH_3CN$ reference electrode.

UV-Vis-near IR spectroelectrochemical analysis was performed on HP Agilent 8453 spectrometer. The spectroelectrochemical cell consisted of indium tin oxide (ITO) covered glass with 1 cm^2 working area as working electrode, Ag wire as quasi-reference electrode and platinum coil as auxiliary electrode.

Electron Spin Resonance (ESR) spectroelectrochemical analysis was performed on JEOL JES-FA200 and the spectroelectrochemical cell was comprised of platinum wire as working electrode, Ag wire as quasi-reference electrode and platinum coil as auxiliary electrode.

The HOMO and LUMO energy levels were calculated from the first onsets of oxidation and reduction potentials, respectively, on the basis of the reference energy standard of ferrocene/ferrocenium redox couple [117,118].

Powder diffractograms were recorded on a X-Pert Pro MPD Philips diffractometer (Co $K\alpha_1$ radiation; λ= 1.789 Å) using Bragg-Brentano ($\theta/2\theta$) reflection geometry. The detector was moved by 2θ steps of 0.04° and the counting time was at least 15s per step. The divergence slit was automatically adjusted giving a constant 10 mm irradiated length. Thin layers (*ca.* 100 nm thick) of the investigated molecules have been deposited on Si wafers by spin-coating. Bragg-Brentano X-ray measurements of these layers have been carried out using the same model of diffractometer and the same cobalt radiation. In these measurements, the divergence slit was fixed at 0.16° while Soller slits were mounted both in the incident beam path (0.04 rad) and in the diffracted beam path (0.01 rad). The 2θ steps were still fixed at 0.04° and the counting time at 15s per step.

The fabrication of field-effect transistors can briefly be described as follows. In the first step 30 nm thick gold source and drain electrodes were vacuum deposited on a poly(ethylene naphthalate) (PEN) substrate and then patterned by photolithography giving a channel width W of 0.9 mm and a channel length L of 40 µm. The surface of the deposited electrode was then modified by oxygen plasma (1 minute) and by treatment with either 4-methoxythiophenol or pentafluorobenzenethiol as recommended [119,120]. In the subsequent step thin layers of the investigated organic semiconductors were spin coated from a chloroform solution (concentration 7 mg/ml, spin speed of 600 rpm during 20 s) and then annealed (10 min at 100 ^oC, under N_2 flow) with the goal to remove the remaining traces of the solvent. Typical thickness of the deposited semiconducting layer as determined by Dektak profilometer was ~100 nm. Commercially available fluorinated polymer, CYTOP, (Asahi glass, Japan) served as the dielectric layer (dielectric constant = 2.1). It was deposited on the top of the semiconducting layer by spin-coating and then dried at 100 ^oC. The deposited, 1 µm thick dielectric layer showed the capacitance of 1.8 nF cm^{-2}. In the last step 500 nm thick gate electrode was deposited by ink-jet using a Dimatix printing head. Commercial suspension of Ag nanoparticles in alcohol (Cabot) was used as a source of silver. A thin layer (<100 nm) of Nafion was used as an adhesion promoter between the highly hydrophobic CYTOP layer (contact angle of water = 110^o) and the silver ink.

Transistors parameters were determined on a HP4155A semiconductor analyzer. The measurements were carried out at ambient atmosphere conditions. The most important transistor parameters such as charge carrier mobility, threshold voltage

and ON/OFF ratio were calculated in the saturation regime as reported elsewhere [121]. The saturation mobilities were taken at the drain voltage of -100 V and +100V respectively for holes and electrons. The average values were extracted on four devices for each condition.

DFT calculations were as implemented in *Gamess US* package [122].Compounds were first geometry optimised using semi-empirical PM6 basis set as implemented in *MOPAC* [123] and these PM6 optimized geometries were further subjected to complete geometry optimization using DFT calculations at the basis B3LYP/6-311G*. Optimized structures were then used to perform single point energy calculations at B3LYP/6-311++G** basis set.

3.2. Material

The solvents were purified and dried using standard procedures [124]. 1, 2-Dichorobenzene, dry THF, dry DCM and other chemicals were purchased from Aldrich and used as received without further purification.

Reagents and catalysts from Aldrich

2-Bromofluorene
Phenothiazine
4-Bromobiphenyl
3, 4: 9, 10-perylenetetracarboxylic anhydride
2, 7-Dibromofluorene
4-Bromo-1, 8-naphthalic anhydride
1, 3, 6, 8 – Tetrabromopyrene
Triphenylamine
4-Bromobenzonitrile
4-Bromomethylbenzonitrile
Triphenyl phosphine
Iodoethane
2-Ethylhexyl amine
n-Dodecylamine
4-(Diphenylamino)phenylboronic acid (**DPB**)
2, 5-thiophenediylbisboronic acid (**TB**)
1-Bromododecane
Tetrabutylammoniumtetrafluoroborate
Methyl-3,4,5-trihydroxybenzoate
Diethyl-4-methoxy benzyl phosphonate
Triethylphosphite
3,4,5-trimethoxybenzaldehyde
Bromine
2-Isopropoxy-4, 4, 5, 5-tetramethyl-1, 3, 2-dioxaborolane
Phosphorus oxychloride
Potassium *ter*-butoxide

n-Butyl Lithium (2.5 M solution in hexane)
Lithium aluminium hydride (2M solution in THF)
Phosphorous tribromide
Trifluoromethane sulfonic acid
Tetra butyl ammonium hydrogen sulfate
Bis(triphenylphosphine) palladium(II) dichloride
18-crown-6 Tetrabutylammoniumhexafluoroborate

From Fluka

Sodium sulfate
Iodine
Potassium carbonate
Potassium hydroxide

From Reakhim

Carbazole

3-Bromo-9*H*-carbazole (1) was prepared using the literature procedure [125]. Yield = 68% (7.5g); White solid (FW = 246.11 g/mol). ^{1}H NMR (300 MHz, DMSO-d^6), δ (ppm): 11.47 (s, 1H, NH), 8.38(s, 1H), 8.19 (d, J = 2.6 Hz, 1H), 7.54-7.41(m, 4H), 7.19 (t, J = 5 Hz, 1H). MS (EI) *m/z* = 246 [M]$^+$.

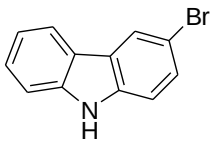

3-Bromo-9-ethyl-9*H*-carbazole (2) was synthesised using the literature procedure [126,127]. The product was purified by column chromatography in silica gel using hexane: ethyl acetate (9:1) as eluent. Yield = 95% (3.15g); White solid (FW = 274.16 g/mol). ^{1}H NMR (300 MHz, DMSO-d^6), δ (ppm): 8.42 (s, 1H), 8.24 (d, J = 2.6 Hz, 1H), 7.65-7.56 (m, 3H), 7.50 (t, J = 5.5 Hz, 1H), 7.23 (t, J = 5.3 Hz, 1H), 4.44 (q, J = 8.1 Hz, 2H, CH_2), 1.30 (t, J = 4.8 Hz, 3H, CH_3). MS (EI) *m/z* = 275 [M + H]$^+$.

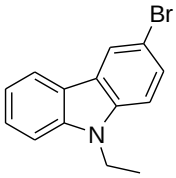

9-Ethyl-9*H*-carbazol-3-yl boronic acid pinacol ester (3). 3-Bromo-9-ethylcarbazole **2** (3g, 10.94 mmol) was dissolved in 60 mL of dry THF under nitrogen. The solution was cooled to -78^{o}C and to which 11 mL of n-BuLi (2.5 M solution in hexane) was added dropwise. The reaction mixture was stirred for 15 min before adding 5.6 mL (27.34 mmol) of 2-isopropoxy-4, 4, 5, 5-tetramethyl-1, 3, 2-dioxaborolane. It was allowed to warm to ambient temperature and stirred for another 12 hours. Water was added slowly into the reaction mixture followed by ethyl acetate and stirred for 10min. Then 2N HCl (20mL) was added and the organic layer was separated. The organic phase was washed with brine and dried over sodium sulfate before the solvent was evaporated. Purification was carried out by column chromatography on silica gel with hexane/ethyl acetate (95/5) as eluent. Yield = 71% (2.48g); White crystals (FW = 321.23 g/mol). ^{1}H NMR (300 MHz, DMSO-d^6), δ (ppm): 8.50 (s, 1H), 8.27 (d, J = 2.6 Hz, 1H), 7.80 (d, J = 3.2 Hz, 1H), 7.62 (t, J = 5.3 Hz, 2H), 7.48 (t, J = 5.5 Hz, 1H), 7.23(t, J = 5.3 Hz, 1H), 4.47(q, J = 7.1 Hz, 2H, CH_2), 1.35-1.29(m,15H, CH_3). MS (EI) *m/z* = 321 [M]$^+$.

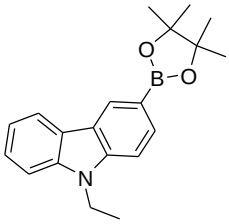

4-Bromo-2-nitrobiphenyl (4) was synthesised using the literature procedure [128]. The product was purified by column chromatography in silica gel with hexane: ethyl acetate (85:15) as eluent. Yield = 34% (6.07g); Yellow solid (FW = 278.11 g/mol); m.p.: 64–65 °C. ^{1}H NMR (300 MHz, $CDCl_3$), δ (ppm): 8.35-8.32 (m, 2H), 7.75-7.72 (m, 2H), 7.67-7.65 (m, 2H), 7.54-7.51(m, 2H). MS (EI) *m/z* = 278 [M]$^+$.

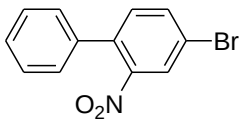

2-Bromo-9*H*-carbazole (5) was synthesised using the literature procedure [128].

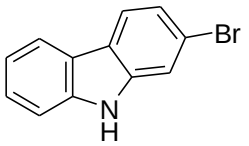

Column chromatography in silica gel was performed to purify the compound using hexane: ethyl acetate (95:5) as eluent. Yield = 70% (2.23g); White solid (FW = 246.11 g/mol); m.p.: 249–250 °C. ^{1}H NMR (300 MHz, DMSO-d^6), δ (ppm): 11.41 (s, 1H, NH), 8.15-8.11(m, 2H), 7.68 (d, J = 1.7 Hz, 1H), 7.54-7.19 (m, 4H). MS (EI) *m/z* = 246 $[M]^+$.

2-Bromo-9-ethyl-9*H*-carbazole (6) was synthesised using the literature procedure [126,127].

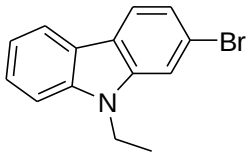

The product was purified by column chromatography in silica gel with hexane: ethyl acetate (95:5) as eluent. Yield = 92% (2.1 g); White solid (FW = 274.16 g/mol). ^{1}H NMR (300 MHz, DMSO-d^6), δ (ppm): 8.19 (d, J = 2.6 Hz, 1H), 8.13 (d, J = 2.7 Hz, 1H), 7.90 (s, 1H), 7.64(d, J = 2.7 Hz, 1H), 7.50 (t, J = 5.5 Hz, 1H), 7.36(d, J = 2.8 Hz, 1H), 7.24 (t, J = 5 Hz, 1H), 4.46 (q, J = 7.1 Hz, 2H, CH_2), 1.30 (t, J = 4.7 Hz, 3H, CH_3). MS (EI) *m/z* = 274 $[M]^+$.

9-Ethyl-9*H*-carbazol-2-yl boronic acid pinacol ester (7) was synthesized using the similar procedure for the preparation of **3**.

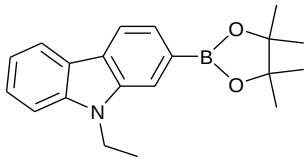

Purification was carried out by column chromatography in silica gel with hexane/ethyl acetate (95/5) as eluent. Yield = 55% (1.28g); White crystals (FW = 321.23 g/mol). ^{1}H NMR (300 MHz, $CDCl_3$), δ (ppm): 8.17-8.14(m, 2H), 7.93(s, 1H), 7.74(d, J = 2.6 Hz, 1H), 7.53(t, J = 4.6 Hz, 1H), 7.47(d, J = 2.8 Hz, 1H), 7.27(t, J = 5 Hz, 1H), 4.47(q, J = 7.2 Hz, 2H, CH_2), 1.48 (t, J = 4.8 Hz, 3H, CH_3), 1.44(s, 12H, CH_3). MS (EI) *m/z* = 321 $[M]^+$.

2-Bromo-9,9-diethyl-9*H*-fluorene (8) was synthesised using the literature procedure [129].

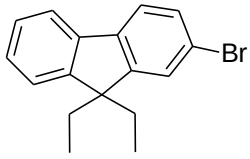

The product was purified by column chromatography in silica gel using hexane: ethyl acetate (96:4) as eluent. Yield = 84% (6.19g); Colourless liquid (FW = 301.23g/mol). ^{1}H NMR (300 MHz, $CDCl_3$), δ (ppm): 7.69-7.54 (m, 2H), 7.46-7.43 (m, 2H), 7.35-7.29 (m, 3H), 2.02 (q, J = 8.9 Hz, 4H, CH_2), 0.31 (t, J = 5 Hz, 6H, CH_3). MS (EI) *m/z* = 302 $[M + H]^+$.

9,9-Diethyl-9*H*-fluoren-2-yl boronic acid pinacol ester (9) was synthesized by using the similar procedure for the preparation of **3** as described above. 2-Bromo-9,9-diethyl-9*H*-fluorene **8** (5g, 16.6 mmol) was used as starting material.

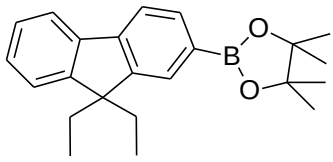

Purification of the product was carried out by column chromatography in silica gel using hexane/ethyl acetate (97/3) as eluent. Yield = 59% (3.4g); White solid (FW = 348.30g/mol). ^{1}H NMR (300 MHz, $CDCl_3$), δ (ppm): 7.82 (d, J = 2.8

Hz, 1H), 7.74-7.69 (m, 3H), 7.34-7.32 (m, 3H), 2.12-1.98(m, 4H, CH_2), 1.38(m, 12H, CH_3), 0.28(t, J = 4.9 Hz, 6H, CH_3). MS (EI) *m/z* = 348 $[M]^+$.

10-Ethyl-10*H*-phenothiazine (10) was synthesised using the literature procedure [130]. The product was purified by column chromatography in silica gel using hexane as eluent. Yield = 55% (2.49g); White crystals (FW = 227.33g/mol). ^{1}H NMR (300 MHz, $CDCl_3$), δ (ppm): 7.18-7.12 (m, 4H), 6.93-6.87 (m, 4H), 3.94 (b, 2H, NCH_2), 1.42 (t, J = 4.7 Hz, 3H, CH_3). MS (EI) *m/z* = 228 $[M + H]^+$.

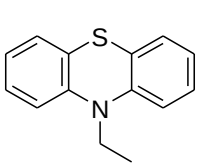

3-Bromo-10-ethyl-10*H*-phenothiazine (11) was synthesised using the literature procedure [131]. The product was purified by column chromatography in silica gel using 95:5 solvent mixture of hexane: ethyl acetate as eluent. Yield = 90% (2.42g); White solid (FW = 306.23g/mol). ^{1}H NMR (300 MHz, DMSO-d^6), δ (ppm): 7.35-7.32 (m, 1H), 7.23-7.12 (m, 2H), 7.03-6.91 (m, 4H), 3.89 (q, J = 6.9Hz, 2H, NCH_2), 1.26 (t, J = 4.6Hz, 3H, CH_3). MS (EI) *m/z* = 307 $[M + H]^+$.

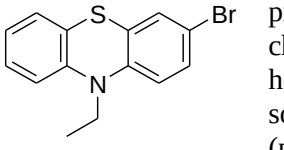

10-Ethyl-10*H*-phenothiazin-3-yl boronic acid pinacol ester (12) was synthesized using the similar procedure for the preparation of **3**. 3-Bromo-10-ethyl-10*H*-phenothiazine **11** (2.3g, 7.5 mmol) was used as starting material. Purification of the product was carried out by column chromatography in silica gel using hexane/ethyl acetate (9/1) as eluent. Yield = 79% (2.1g); White solid (FW = 353.29g/mol). 7.27 (d, J = 2.6 Hz, 1H), 7.18-7.08 (m, 2H), 7.02-6.88 (m, 4H), 3.88 (q, J = 7Hz, 2H, NCH_2), 1.36 (s, 12H, CH_3), 1.27 (t, J = 4.8Hz, 3H, CH_3). MS (EI) *m/z* = 353 $[M]^+$.

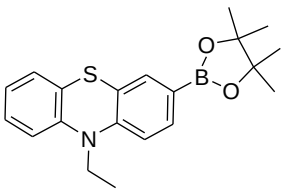

1, 7-Dibromo *N, N'*-2-ethyl hexyl perylene bisimide (13). 3, 4: 9, 10-perylenetetracarboxylic anhydride (5g, 12.7 mmol) was suspended in 100 mL of concentrated sulphuric acid and 250 mg of iodine was added to it. It was heated at 80 ^oC for 45 min followed by dropwise addition of 8 mL of bromine for a period of 30 min and stirred for 24 hrs. Reaction mixture was cooled to room temperature and water was added into it. The precipitated product was filtered, washed with acetone and dried in vacuum. Thus obtained bromo substituted perylene dianhydride (4 g, 7.3 mmol) suspended in 80 mL of N-methyl pyrrolidone and mixed with 40 mL of glacial acetic acid. It was heated at 60 ^oC for 20 min and 2-ethyl hexyl amine (3mL, 18.24 mmol) was added. The temperature was raised to 120 ^oC and stirring was continued for 12 hours under nitrogen atmosphere. The mixture was poured into 600 mL of water and the precipitated product was filtered. It was washed with methanol, subjected to

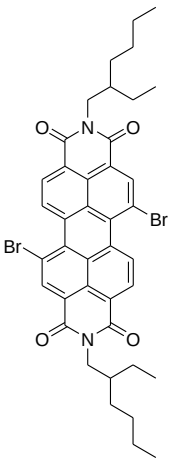

column chromatography (silica gel, eluent- hexane: ethyl acetate, 8: 2) and the desired product was isolated. Yield = 52% (2.94g); Red solid (FW = 772.58 g/mol). ^{1}H NMR (300 MHz, $CDCl_3$, δ ppm): 9.48 (d, J = 2.8 Hz, 2H), 8.91 (s, 2H), 8.70 (d, J = 2.7 Hz, 2H), 4.23-4.11 (m, 4H, NCH_2), 2.03-1.91 (m, 2H, CH), 1.47-1.28 (m, 16H, CH_2), 1-0.91 (m, 12H, CH_3). IR (KBr, υ cm^{-1}): (arene C–H) 3094; (aliphatic C–H) 2958, 2929, 2872; (imide C=O) 1695; (Ar C=C) 1651, 1594; (imide C–N) 1343, 1299. MS (EI) *m/z* = 773 $[M+H]^+$.

1, 7-Dibromo *N, N*'-dodecyl perylene bisimide (14) was synthesized according to the similar procedure for the synthesis of **13**. n-Dodecylamine was used for imidization. Yield = 45% (2.9g); Red solid (FW = 884.80 g/mol). ^{1}H NMR (300 MHz, $CDCl_3$, δ ppm): 9.49 (d, J = 2.7 Hz, 2H); 8.91 (s, 2H), 8.71 (d, J = 2.7 Hz, 2H), 4.27-4.18 (m, 4H, NCH_2), 1.78 (b, 4H, CH_2), 1.44 (b, 4H, CH_2), 1.29 (b, 32H, CH_2), 0.9(t, J = 4.4 Hz, 6H, CH_3). IR (KBr, υ cm^{-1}): (arene C–H) 3090; (aliphatic C–H) 2958, 2927, 2866; (imide C=O) 1695; (Ar C=C) 1651, 1593; (imide C–N) 1342, 1297. MS (EI) *m/z* = 885 $[M+H]^+$.

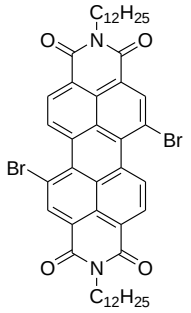

1, 7-Bis (9-ethyl-9*H*-carbazol-3-yl) *N, N*'-2-ethyl hexyl perylene bisimide (15) was obtained by the Suzuki- Miyaura coupling reaction between 1, 7-dibromo *N, N*'-2-ethylhexyl perylene bisimide **13** (300 mg, 0.39mmol) and 9-ethyl-9*H*-carbazol-3-yl boronic acid pinacol ester **3** (276 mg, 0.86mmol, 2.2 molar equ). These compounds were dissolved in a solvent mixture of 15 mL of THF and 2 mL of water. Powdered potassium hydroxide (3.3 molar equ.) was added and the reaction mixture was purged with nitrogen for 10min. Then the reaction vessel was degassed. Bis(triphenylphosphine) palladium(II) dichloride (0.03 molar equ) was added into it and stirred for 8-12 hrs at 80 ^{o}C under nitrogen. After completion, the reaction mixture was diluted with water and extracted with ethyl acetate. The organic layer was dried over sodium sulfate and evaporated. The crude product was purified by column chromatography using silica gel as stationary phase and hexane: ethyl acetate mixture (95:5) as eluent. Yield = 55% (215mg); Black solid (FW = 1001.29g/mol). ^{1}H NMR (300 MHz, $CDCl_3$, δ ppm): 8.69 (s, 2H), 8.33 (b, 4H), 8.01 (d, J = 2.8 Hz, 2H), 7.79-7.73 (m, 2H), 7.59-7.51 (m, 5H), 7.38 (b, 5H), 4.49-4.42 (m, 4H, NCH_2), 4.27-4.12 (m, 4H, NCH_2), 1.99 (b, 2H, CH), 1.55 (t, d=4.8Hz, 6H, CH_3), 149-1.28 (m, 16H, CH_2), 0.99-0.89 (m, 12H, CH_3). ^{13}C NMR (75.5MHz, $CDCl_3$, δ ppm): 164.1, 163.8, 141.9, 140.6, 140.1, 135.9, 134.9, 132.7, 129.8, 129.3, 128.9, 127.1, 126.9, 126.5, 121.9, 121.5, 109.1, 44.6, 38.3, 38.1, 31.1, 29.1, 24.4, 23.3, 14.4, 14.2, 10.9. IR (KBr, υ cm^{-1}): (arene C–H) 3050; (aliphatic C–H) 2954, 2925, 2856; (imide C=O) 1695; (Ar C=C) 1656, 1585; (imide C–N) 1327, 1256. Anal. Calc. for $C_{68}H_{64}N_4O_4$: C, 81.57; H, 6.44; N,

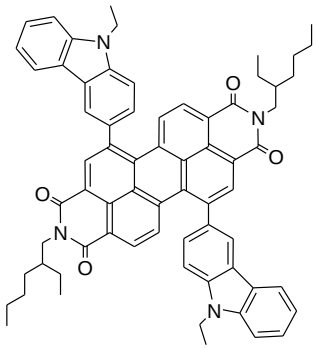

5.60; O, 6.39%. Found: C, 81.46; H 6.75; N, 5.35%. MS (EI) *m/z* = 1001[M]$^+$. MS (MALDI-TOF) *m/z* = 1000.40 (exact mass = 1000.49).

1, 7-Bis (9-ethyl-9*H*-carbazol-3-yl) *N, N*'-dodecyl perylene bisimide (16) was

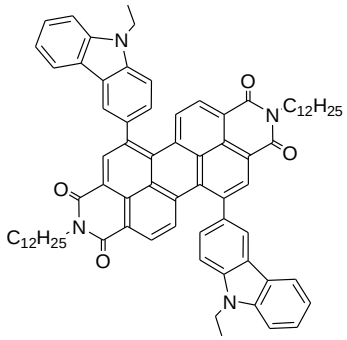

synthesized according to the similar procedure for **15** as described above. 1, 7-dibromo *N, N*'-dodecyl perylene bisimide (300 mg, 0.34mmol) was used for Suzuki- Miyaura coupling reaction. The product was purified by column chromatography using silica gel as stationary phase and hexane: ethyl acetate mixture (9:1) as eluent. Yield = 32% (122mg); Black solid (FW = 1113.51g/mol). ^{1}H NMR (300 MHz, $CDCl_3$, δ ppm): 8.54-8.47 (m, 4H), 8.2 (b, 2H), 8.02 (b, 2H), 7.51 (b, 8H), 7.39 (b, 2H), 7.24 (b, 2H), 4.42-4.3 (m, 8H, NCH_2), 1.82 (b, 4H, CH_2), 1.52-1.29 (m, 42H, CH_2, CH_3), 0.93-0.89(m, 6H, CH_3). ^{13}C NMR (75.5MHz, $CDCl_3$, δ ppm): 163.7, 163.4, 141.9, 140.6, 140, 136.6, 135.8, 135, 132.7, 132, 129.9, 129.3, 128.9, 127.1, 126.9, 126.5, 123.2, 122, 121.5, 119.8, 109.1, 100.2, 72.5, 62.1, 41, 38, 32.1, 29.9, 29.8, 29.7, 29.6, 28.4, 27.4, 22.9, 14.4,14.2. IR (KBr, υ cm^{-1}): (arene C–H) 3051; (aliphatic C–H) 2922, 2851; (imide C=O) 1694; (Ar C=C) 1655, 1586; (imide C–N) 1331, 1256. Anal. Calc. for $C_{76}H_{80}N_4O_4$: C, 81.98; H, 7.24; N, 5.03; O, 5.75%. Found: C, 81.78; H 7.25; N, 4.86%. MS (MALDI-TOF) *m/z* = 1112.18 (exact mass = 1112.62).

1, 7-Bis (9-ethyl-9*H*-carbazol-2-yl) *N, N*'-2-ethylhexyl perylene bisimide (17) was synthesized by using the same procedure of **15** as described above. 9-Ethyl-9*H*-carbazol-2-yl boronic acid pinacol ester **7** was used for Suzuki coupling reaction. The product was purified by column chromatography using silica gel as stationary phase and hexane: ethyl acetate mixture (95:5) as eluent. Yield = 41% (160mg); Black solid (FW = 1001.29g/mol). ^{1}H NMR (300 MHz, $CDCl_3$, δ ppm): 8.64-8.51 (m, 2H), 8.23-7.96 (m, 7H), 7.74-7.46 (m, 7H), 7.34-7.02 (m, 4H), 4.83-4.25 (m, 8H, NCH_2), 1.98-1.94 (m, 2H, CH), 1.39 (b, 16H, CH_2), 1.28 (b, 6H, CH_3), 1.01-0.89 (m, 12H, CH_3). ^{13}C NMR (75.5MHz, $CDCl_3$, δ ppm): 164.0, 163.7, 141.9, 140.9, 139.4, 135.5, 131.8, 130.4, 128.9, 126.5, 125.8, 122.6, 122.1, 121.7, 119.9, 119.6, 109.0, 44.6, 38.4, 31.0, 30.5, 29.9, 29.7, 29.0, 25.0, 24.4, 23.3, 14.4, 10.9. IR (KBr, υ cm^{-1}): (arene C–H) 3051; (aliphatic C–H) 2955, 2924, 2855; (imide C=O) 1695; (Ar C=C) 1652, 1584; (imide C–N) 1326, 1259. Anal. Calc. for $C_{68}H_{64}N_4O_4$: C, 81.57; H, 6.44; N, 5.60; O, 6.39%. Found: C, 81.68; H, 7.21; N, 5.03%. MS (MALDI-TOF) *m/z* = 1000.30 (exact mass = 1000.49).

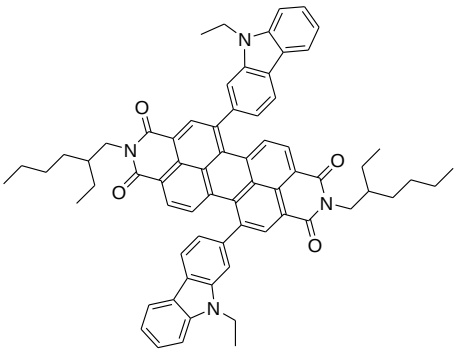

1, 7-Bis [4-(diphenylamino)-phenyl] *N, N'*-2-ethyl hexyl perylene bisimide (18)

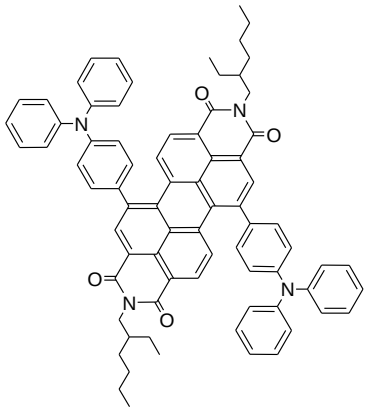

was synthesized according to the same procedure for the preparation of **15** as described above. 4-(diphenylamino)phenylboronicacid was used for Suzuki coupling reaction. The product was purified by column chromatography using silica gel as stationary phase and hexane: ethyl acetate mixture (97:3) as eluent. Yield = 24% (104mg); Black solid (FW = 1101.41g/mol). ^{1}H NMR (300 MHz, $CDCl_3$, δ ppm): 8.63 (s, 2H), 8.24 (d, J = 2.8 Hz, 2H), 8.06 (d, J = 2.7 Hz, 2H), 7.42-7.34 (m, 12H), 7.24-7.1 (m, 16H), 4.26-4.1 (m, 4H, NCH_2), 1.99-1.94 (m, 2H, CH), 1.47-1.31 (m, 16H, CH_2), 0.99-0.92 (m, 12H, CH_3). ^{13}C NMR (75.5MHz, $CDCl_3$, δ ppm): 164.1, 148.7, 147.4, 141.0, 135.6, 135.4, 135.3, 132.5, 130.2, 129.8, 129.6, 129.3, 125.4, 124.0, 123.9, 122.3,122.0, 44.5, 38.2, 31.0, 29.0, 24.3, 23.3, 14.4, 10.9. IR (KBr, υ cm^{-1}): (arene C–H) 3061, 3034; (aliphatic C–H) 2955, 2924, 2856; (imide C=O) 1698; (Ar C=C) 1659, 1586; (imide C–N) 1326, 1270. Anal. Calc. for $C_{76}H_{68}N_4O_4$: C, 82.88; H, 6.22; N, 5.09; O, 5.81%. Found: C, 82.39; H 6.44; N, 4.85%. MS (MALDI-TOF) *m/z* = 1100.29 (exact mass = 1100.52).

1, 7-Bis (9,9-diethyl-9*H*-fluoren-2-yl) *N, N*'- 2-ethyl hexyl perylene bisimide (19)

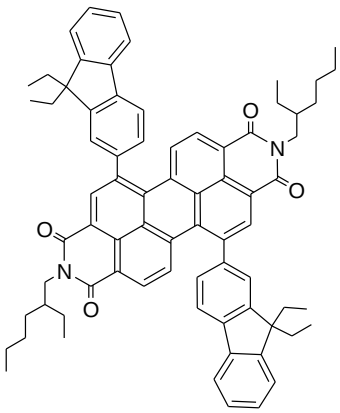

was synthesized by using the same procedure for the synthesis of **15** as described above. *N, N'*-2-ethylhexyl perylene bisimide **13** (300mg, 0.39mmol) and 9,9-Diethyl-9*H*-fluoren-2-yl boronic acid pinacol ester **9** (298mg, 0.86mmol) were used for Suzuki coupling reaction. The product was purified by column chromatography using silica gel as stationary phase and hexane: ethyl acetate mixture (97:3) as eluent. Yield = 40% (164mg); black solid (FW =1055.43g/mol). ^{1}H NMR (300 MHz, $CDCl_3$, δ ppm): 8.69 (s, 2H), 8.09 (d, J = 2.7 Hz, 2H), 7.90-7.80 (m, 6H), 7.57-7.52 (m, 4H), 7.47-7.35 (m, 6H), 4.24-4.11 (m, 4H, NCH_2), 2.16-1.94 (m, 10H, $CH_{2Flourene}$, $CH_{Perylene}$), 1.46-1.32 (m, 16H, $CH_{2Perylene}$), 0.99-0.89 (m, 12H, $CH_{3\ Perylene}$) 0.37 (t, J = 5.1 Hz, 12H, $CH_{3Flourene}$). ^{13}C NMR (75.5MHz, $CDCl_3$, δ ppm): 164.1, 163.9, 152.2, 150.3, 142.6, 141.9, 140.9, 140.8, 135.5, 135.1, 132.7, 130.4, 129.5, 129.4, 128.3, 128, 127.7, 127.4, 123.7, 123.2, 122.3, 121.9, 121.8, 120.4, 72.5, 62.1, 56.8, 44.5, 38.2, 33, 31, 29, 25, 24.3, 23.3, 14.4, 10.9, 8.8. IR (KBr, υ cm^{-1}): (arene C–H) 3059; (aliphatic C–H) 2958, 2924, 2854; (imide C=O) 1697; (Ar C=C) 1656, 1585; (imide C–N) 1326, 1258. Anal. Calc. for $C_{74}H_{74}N_2O_4$: C, 84.21; H, 7.07; N, 2.65; O, 6.06%. Found: C, 83.96; H 7.54; N, 2.61%. MS (MALDI-TOF) *m/z* = 1054.53 (exact mass = 1054.56).

1, 7-Bis (10-ethyl-10*H*-phenothiazin-3-yl) *N, N*'- 2-ethyl hexyl perylene bisimide (20) was synthesized according to the similar procedure for the synthesis of **15** as described above. *N, N'*-2-ethylhexyl perylene bisimide **13** (400mg, 0.52mmol) and 10-Ethyl-10*H*-phenothiazin-3-yl boronic acid pinacol ester **12** (400mg, 1.14mmol) were used for Suzuki coupling reaction. The product was purified by column chromatography using silica gel as stationary phase and hexane: ethyl acetate mixture (9:1) as eluent. Yield = 46% (254mg); Black solid (FW = 1065.42g/mol). ^{1}H NMR (300 MHz, $CDCl_3$, δ ppm): 8.57 (s, 2H), 8.22 (d, J = 2.7 Hz, 2H), 8.06 (d, J = 2.8 Hz, 2H), 7.38-7.26 (m, 4H), 7.24 (d, J = 2.5 Hz, 2H), 7.17 (d, J = 2.5 Hz, 2H), 7.01-6.90 (m, 6H), 4.22-3.99 (m, 8H, NCH_2), 1.94 (b, 2H, $CH_{Perylene}$), 1.52 (t, J = 5.6 Hz, 6H, $CH_{3Phenothiazine}$),1.45-1.28 (m, 16H, $CH_{2Perylene}$), 0.98-0.89 (m, 12H, $CH_{3\ Perylene}$). ^{13}C NMR (75.5MHz, $CDCl_3$, δ ppm): 164.1, 164.0, 145.7, 144.3, 140.1, 136.1, 135.5, 135.2, 132.4, 130.0, 129.7, 129.5, 128.4, 127.8, 127.8, 127.7, 127.6, 126.5, 123.7, 123.1, 122.4, 122.0, 116.3, 115.6, 72.5, 62.1, 44.5, 42.3, 38.2, 31.0, 28.9, 24.3, 23.3, 14.4, 13.2, 10.9. IR (KBr, υ cm^{-1}): (arene C–H) 3057; (aliphatic C–H) 2954, 2926, 2855; (imide C=O) 1692; (Ar C=C) 1648, 1583; (imide C–N) 1327, 1264. Anal. Calc. for $C_{68}H_{64}N_4O_4S_2$: C, 76.66; H, 6.05; N, 5.26; O, 6.01; S, 6.02%. Found: C, 76.77; H 6.29; N, 5.25%. MS (MALDI-TOF) *m/z* = 1063.93 (exact mass = 1064.44).

2, 7-Dibromo-9, 9-diethyl-9*H*-fluorene (21) was synthesised using the literature procedure [129]. Purification of the product was carried out by column chromatography in silica gel using hexane as eluent. Yield = 85% (2.1g); Colourless liquid (FW = 380.13g/mol). ^{1}H NMR (300 MHz, $CDCl_3$), δ (ppm): 7.54-7.51(m, 2H), 7.47-7.44(m, 4H), 2 (q, J = 7.4 Hz, 4H, CH_2), 0.31 (t, J = 4.9 Hz, 6H, CH_3). MS (EI) *m/z* = 380 $[M]^+$.

9,9-Diethyl-9*H*-fluoren-2, 7-yl diboronic acid pinacol ester (22) was synthesized using the similar procedure for the preparation of **3** as described above. 2, 7-Dibromo-9,9-diethyl-9*H*-fluorene **21** (2 g, 5.26 mmol) was used as starting material. Purification of the product was carried out by column chromatography in silica gel using hexane/ethyl acetate (95/5) as eluent. Yield = 43% (1.07g); White crystals (FW = 474.26g/mol). ^{1}H NMR (300 MHz, $CDCl_3$), δ (ppm): 7.82-7.79 (m, 2H), 7.75-7.71 (m, 4H), 2.09 (q, J = 7.4 Hz, 4H, CH_2), 1.38 (s, 24H, CH_3), 0.24 (t, J = 4.9 Hz, 6H, CH_3). MS (EI) *m/z* = 474 $[M]^+$.

4-Bromo-*N*- 2-ethyl hexyl naphthalimide (23). 4-Bromo-1, 8-naphthalic anhydride

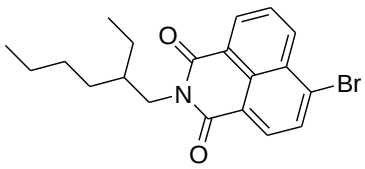

(2g, 7.2 mmol) was dissolved in a solvent mixture of 20 mL of N-methyl pyrrolidone and 10 mL of glacial acetic acid. It was heated at 60 ^{o}C for 20 min and 2-ethyl hexyl amine (1.8mL, 10.8 mmol) was added. The temperature was raised to 120 ^{o}C and stirring was continued for 5 hours under nitrogen atmosphere. The reaction mixture was cooled to room temperature and 100 mL of water was added into it. The crude product was extracted using ethyl acetate. Organic layer was separated and washed with brine. Later on, it was dried over sodium sulfate and evapourated. Purification was carried out by column chromatography using silica gel as stationary phase and hexane: ethyl acetate (9: 1) as eluent. Yield = 93% (2.6g); Yellow solid (FW = 388.31 g/mol). ^{1}H NMR (300 MHz, $CDCl_3$, δ ppm): 8.66 (d, J = 2.8 Hz, 1H), 8.58 (d, J = 3.2 Hz, 1H), 8.42 (d, J = 2.7 Hz, 1H), 8.05 (d, J = 2.6 Hz, 1H), 7.84 (d, J = 5.3 Hz, 1H), 4.17-4.04 (m, 2H, NCH_2), 1.99-1.86 (m, 1H, CH), 1.41-1.25 (m, 8H, CH_2), 0.94-0.84 (m, 6H, CH_3). Anal. Calc. for $C_{20}H_{22}BrNO_2$: C, 61.86; H, 5.71; Br, 20.58; N, 3.61; O, 8.24%. Found: C, 62.25; H, 5.52; N, 3.58. MS (EI) *m/z* = 389 $[M+H]^+$.

4-(9, 9-Diethyl-9*H*-fluoren-2-yl) *N*-2-ethylhexyl naphthalimide (24) was

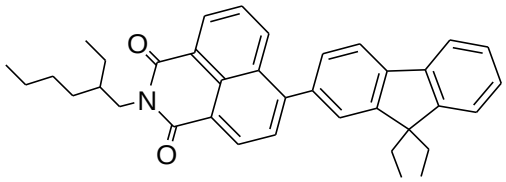

synthesized according to the similar procedure for the synthesis of **15** as described above. 4-Bromo-*N*-2-ethylhexyl naphthalimide **23** (300mg, 0.77 mmol) and 9, 9-diethyl-9*H*-fluoren-2-yl boronic acid pinacol ester **9** (270mg, 0.77 mmol) were used for Suzuki coupling reaction. The product was purified by column chromatography using silica gel as stationary phase and hexane: ethyl acetate (9:1) mixture as eluent. Yield = 73% (370mg); Yellow solid (FW = 529.73g/mol); m.p.: 133-134 ºC. ^{1}H NMR (300 MHz, $CDCl_3$, δ ppm): 8.69 (t, J = 5.3 Hz, 2H), 8.38 (d, J = 3.2 Hz, 1H), 7.92 (d, J = 2.6 Hz, 1H), 7.85-7.72 (m, 3H), 7.53-7.50 (m, 2H), 7.46-7.40 (m, 3H), 4.26-4.14 (m, 2H, NCH_2), 2.13 (q, J = 7.3 Hz, 4H, $CH_{2Fluorene}$), 2.04-1.97 (m, H, $CH_{Naphthlimide}$), 1.49-1.32 (m, 8H, $CH_{2Naphthlimide}$), 1.01-0.90 (m, 6H, $CH_{3Naphthlimide}$), 0.45 (t, J = 4.9 Hz, 6H, $CH_{3Fluorene}$). ^{13}C NMR (75.5MHz, $CDCl_3$, δ ppm): 165.0, 164.8, 150.7, 150.4, 147.7, 142.2, 140.9, 137.7, 132.8, 131.5, 131.1, 130.5, 129.1, 128.2, 127.9, 127.3, 127.0, 124.7, 123.3, 121.8, 120.2, 120.0, 56.5, 44.4, 38.2, 32.9, 31.0, 29.0, 24.3, 23.3, 14.4, 10.9, 8.9. IR (KBr, υ cm^{-1}): (arene C–H) 3063; (aliphatic C–H) 2961, 2929, 2853; (imide C=O) 1698; (Ar C=C) 1659, 1588; (imide C–N) 1353, 1231. Anal. Calc. for $C_{37}H_{39}NO_2$: C, 83.89; H, 7.42; N, 2.64; O, 6.04%. Found: C, 83.60; H 7.74; N, 2.74%. MS (EI) *m/z* = 530$[M+H]^+$.

4, 4'-9, 9-Diethyl-9*H*-fluoren-2, 7-yl-bis (*N*-2-ethylhexyl naphthalimide) (25) 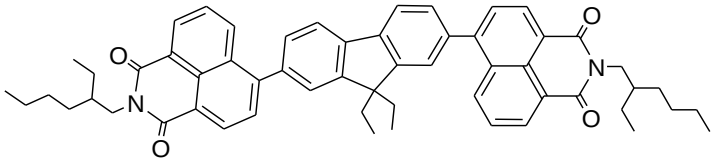 was synthesized according to the similar procedure for the synthesis of **15** as described above. 4-Bromo-*N*-2-ethylhexyl naphthalimide **23** (300mg, 0.77 mmol) and 9, 9-diethyl-9*H*-fluoren-2, 7-yl diboronic acid pinacol ester **22** (182mg, 0.38 mmol) were used for Suzuki coupling reaction. The product was purified by column chromatography using silica gel as stationary phase and hexane: ethyl acetate mixture (9:1) as eluent. Yield = 85% (270mg); Yellow solid (FW = 837.12g/mol); m.p.: 147-149 ºC. ^{1}H NMR (300 MHz, $CDCl_3$, δ ppm): 8.73-8.68 (m, 4H), 8.40 (d, J = 3.2 Hz, 2H), 8.01-7.92 (m, 2H), 7.86 (d, J = 2.5 Hz, 2H), 7.80-7.72 (m, 2H), 7.60-7.54 (m, 4H), 4.27-4.14 (m, 4H, NCH_2), 2.19 (q, J = 7.2 Hz, 4H, $CH_{2Fluorene}$), 2.06-1.95 (m, 2H, $CH_{Naphthlimide}$), 1.49-1.31 (m, 16H, $CH_{2Naphthlimide}$), 1.01-0.90 (m, 12H, $CH_{3Naphthlimide}$), 0.57 (t, J = 4.9 Hz, 6H, $CH_{3Fluorene}$). ^{13}C NMR (75.5MHz, $CDCl_3$, δ ppm): 164.9, 164.7, 151.1, 147.4, 141.4, 138.4, 132.7, 131.5, 131.1, 130.4, 129.4, 129.1, 128.2, 127.1, 124.9, 123.2, 122.0, 120.4, 56.8, 44.47, 38.2, 34.9, 32.9, 31.8, 31.0, 29.0, 27.1, 25.5, 24.3, 23.3, 22.9, 20.9, 14.4, 10.9, 9.1. IR (KBr, υ cm^{-1}): (arene C–H) 3048; (aliphatic C–H) 2958, 2926, 2855; (imide C=O) 1700; (Ar C=C) 1656, 1588; (imide C–N) 1353, 1232. Anal. Calc. for $C_{57}H_{60}N_2O_4$: C, 81.78; H, 7.22, N, 3.35, O, 7.64%. Found: C, 81.48; H, 7.57; N, 3.16%. MS (EI) *m/z* = 837 $[M]^+$.

4, 4'-Thiophen-2,5-yl -bis (*N*- 2-ethyl hexyl naphthalimide) (26) was synthesized by using the same procedure for the synthesis of **15** as described above. 4-Bromo-*N*- 2-ethyl hexyl naphthalimide **23** (450mg, 1.16 mmol) and 2, 5-thiophenediylbisboronic acid (100mg, 0.58 mmol) were used for Suzuki coupling reaction. The product was purified by column chromatography using silica gel as stationary phase and hexane: ethyl acetate mixture (8:2) as eluent. Yield = 49% (200mg); Yellow solid (FW = 698.93g/mol). ^{1}H NMR (300 MHz, $CDCl_3$, δ ppm): 8.77 (d, J = 3.2 Hz, 2H), 8.69-8.60 (m, 4H), 7.94 (d, J = 2.5 Hz, 2H), 7.87-7.77 (m, 2H), 7.50 (s, 2H), 4.21-4.08 (m, 4H, NCH_2), 2.01-1.91 (m, 2H, CH), 1.46-1.25 (m, 16H, CH_2), 0.96-0.86 (m, 12H, CH_3). ^{13}C NMR (75.5MHz, $CDCl_3$, δ ppm): 164.4, 164.1, 141.9, 137.9, 131.8, 131.5, 130.6, 129.7, 129.5, 128.8, 128.6, 127.4, 123.1, 122.4, 44.2, 37.9, 30.7, 28.7, 24.0, 23.0, 14.1, 10.6. IR (KBr, υ cm^{-1}): (arene C–H) 3069; (aliphatic C–H) 2957, 2927, 2857; (imide C=O) 1698; (Ar C=C) 1657, 1587; (imide C–N) 1348, 1233. Anal. Calc. for $C_{44}H_{46}N_2O_4S$: C, 75.61; H, 6.63; N, 4.01; O, 9.16; S, 4.59%. Found: C, 75.18; H 6.72; N, 3.87%. MS (EI) *m/z* = 698 $[M]^+$.

3-Bromo-9-dodecyl-9*H*-carbazole (27) was synthesised using the literature procedure [126, 127]. 1-Bromododecane was used for N-alkylation. The product was purified by column chromatography in silica gel using hexane: ethyl acetate (95:5) solvent mixture as eluent. Yield = 89% (4.48 g); colourless liquid (FW = 414.43g/mol). ^{1}H NMR (300 MHz, $CDCl_3$), δ (ppm): 8.19 (s, 1H), 8.04 (d, J = 2.6 Hz, 1H), 7.53 (dd, J = 3.6 Hz, 1H), 7.48-7.44 (m, 1H), 7.39 (d, J = 2.7 Hz, 1H), 7.27-7.20 (m, 2H), 4.24 (t, J = 4.8 Hz, 2H, CH_2), 1.87-1.78 (m, 2H, CH_2), 1.33-1.22 (m, 18H, CH_2), 0.87 (t, J = 4.5 Hz, 3H, CH_3). MS (EI) *m/z* = 415 $[M+H]^+$.

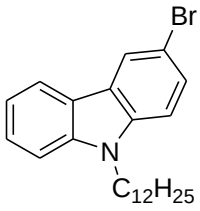

9- Dodecyl-9*H*-carbazol-3-yl boronic acid pinacol ester (28) was synthesized according to the similar procedure for the preparation of **3** as described above. 3-Bromo-9-dodecyl-9*H*-carbazole **26** was used as starting material. Purification was carried out by column chromatography in silica gel with hexane/ethyl acetate (9/1) as eluent. Yield = 52% (2.32g); White solid (FW = 461.50 g/mol). ^{1}H NMR (300 MHz, $CDCl_3$), δ (ppm): 8.42 (s, 1H), 8.24-8.15(m, 2H),, 7.98-7.87 (m, 1H), 7.55 (d, J = 2.7 Hz, 1H), 7.39-7.31 (m, 2H), 4.33 (t, J = 4.8 Hz, 2H, CH_2), 1.91-1.77 (m, 2H, CH_2), 1.41(s, 12H, CH_3), 1.38-1.24 (m, 18H, CH_2), 0.92 (t, J = 4.5 Hz, 3H, CH_3). MS (EI) *m/z* = 462 $[M+H]^+$.

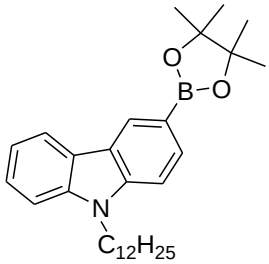

1, 3, 6, 8- Tetra (9-ethyl-9*H*-carbazol-3-yl) pyrene (29) was synthesised by Suzuki- Miyaura coupling reaction. 1, 3, 6, 8 - tetrabromopyrene (200 mg, 0.39mmol) and 9-ethyl-9*H*-carbazol-3-yl boronic acid pinacol ester **3** (526mg, 4.2 molar eq.) were dissolved in a solvent mixture of 20 mL of THF and 2 mL of water. Powdered potassium carbonate (6.6 molar eq.) was added and the reaction mixture was purged with nitrogen for 5 min. The reaction vessel was degassed and then, again purged with nitrogen. Bis(triphenylphosphine) palladium(II) dichloride (0.06 molar eq.) was added into it and stirred for 8-12 hrs at 80 ^{o}C under nitrogen. Then, the reaction mixture was diluted with water and extracted using ethyl acetate. The organic layer was dried over sodium sulfate and evaporated. The crude product was purified by column chromatography using silica gel as stationary phase. The solvent mixture of hexane and ethyl acetate in a volume ratio of 7:3 was used as eluent. Yield = 54% (205mg); Yellow powder (FW = 975.26g/mol). ^{1}H NMR (300 MHz, $CDCl_3$, δ ppm): 8.50 (s, 4H), 8.36 (s, 4H), 8.33 (s, 2H), 8.19 (d, J = 2.3 Hz, 4H), 7.91 (dd, J = 3.4 Hz, 4H), 7.63 (d, J = 2.8 Hz, 4H), 7.55-7.48 (m, 8H), 7.27-7.24 (m, 4H), 4.49 (q, J = 7.1 Hz, 8H, NCH_2), 1.55 (t, J = 4.7 Hz, 12H, CH_3). IR (KBr, υ cm^{-1}): (arene C–H) 3047; (aliphatic C–H) 2974,

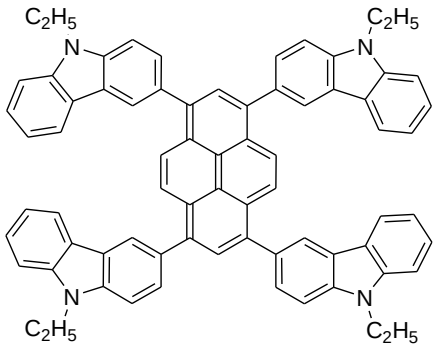

2930, 2890; (Ar C=C) 1625, 1600; (Ar C–N) 1471, 1459. Anal. Calc. for $C_{72}H_{54}N_4$: C, 88.67; H, 5.58; N, 5.74%. Found: C, 88.64; H, 5.79; N, 5.49%. MS (MALDI-TOF) *m/z* = 974.48 (exact mass = 974.43).

1, 3, 6, 8- Tetra (9-ethyl-9*H*-carbazol-2-yl) pyrene (30) was synthesized by using the similar procedure for the synthesis of **29** as described above. 9-Ethyl-9*H*-carbazol-2-yl boronic acid pinacol ester **7** was used for Suzuki reaction. The product was purified by column chromatography using silica gel as stationary phase and hexane: ethyl acetate mixture (1:1) as eluent. Yield = 32% (130mg); Yellow powder (FW = 975.26g/mol). ^{1}H NMR (300 MHz, $CDCl_3$, δ ppm): 8.39 (s, 4H), 8.35 (s, 2H), 8.31(d, J = 2.7 Hz, 4H), 8.23 (d, J = 2.5 Hz, 4H), 7.79(s, 4H), 7.67 (dd, J = 3.2 Hz, 4H), 7.57-7.47 (m, 8H), 7.33-7.28 (m, 4H), 4.50 (q, J = 7.1 Hz, 8H, NCH_2), 1.49 (t, J = 4.8 Hz, 12H, CH_3). IR (KBr, υ cm^{-1}): (arene C–H) 3048; (aliphatic C–H) 2970, 2929, 2890; (Ar C=C) 1626, 1599; (Ar C–N) 1471, 1456. Anal. Calc. for $C_{72}H_{54}N_4$: C, 88.67; H, 5.58; N, 5.74%. Found: C, 88.73; H, 5.39; N, 5.42%. MS (MALDI-TOF) *m/z* = 974.51 (exact mass = 974.43).

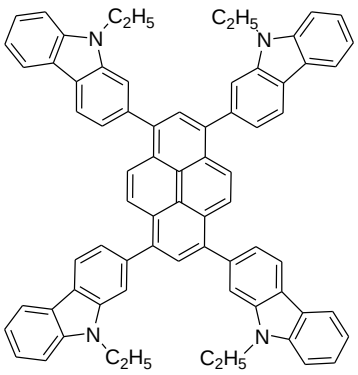

1, 3, 6, 8- Tetra (10-ethyl-10*H*-phenothyazen-3-yl) pyrene (31) was synthesized by using the similar procedure for the synthesis of **29** as described above. 10-Ethyl-10*H*-phenothiazin-3-yl boronic acid pinacol ester **12** was used for Suzuki reaction. The product was purified by column chromatography using silica gel as stationary phase and chloroform as eluent. Yield = 61% (262mg); Yellow powder (FW = 1103.52g/mol). ^{1}H NMR (300 MHz, $CDCl_3$, δ ppm): 8.19 (s, 4H), 7.93 (s, 2H), 7.48-7.44 (m, 8H), 7.23-7.18 (m, 8H), 7.06 (d, J = 2.9 Hz, 4H), 6.98-6.94 (m, 8H), 4.06 (q, J = 7 Hz, 8H, NCH_2), 1.53 (t, J = 4.7 Hz, 12H, CH_3). IR (KBr, υ cm^{-1}): (arene C–H) 3054; (aliphatic C–H) 2970, 2929, 2848; (Ar C=C) 1599, 1575; (Ar C–N) 1488, 1462. Anal. Calc. for $C_{72}H_{54}N_4S_4$: C, 78.37; H, 4.93; N, 5.08; S, 11.62%. Found: C, 78.75; H, 5.12; N, 4.84%. MS (MALDI-TOF) *m/z* = 1102.53 (exact mass = 1102.32).

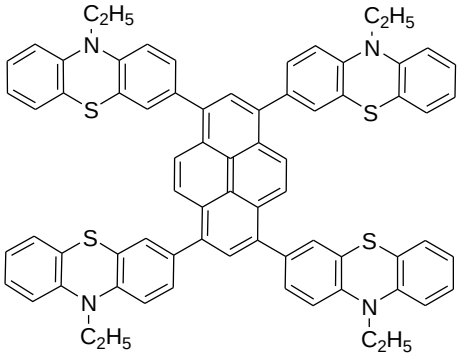

1, 3, 6, 8- Tetra (9-dodecyl-9*H*-carbazol-3-yl) pyrene (32) was synthesized by using the similar procedure for the synthesis of **29** as described above. 9-Dodecyl-9*H*-carbazol-3-yl boronic acid pinacol ester **28** was used for Suzuki reaction. The product was purified by column chromatography using silica gel as stationary phase and hexane: ethyl acetate mixture (9:1) as eluent. Yield = 70% (419mg); Pale yellow solid (FW = 1536.34g/mol). ^{1}H NMR (300 MHz, $CDCl_3$, δ ppm): 8.49 (s, 4H), 8.37 (s, 4H), 8.33 (s, 2H), 8.18 (d, J = 2.6 Hz, 4H), 7.91 (dd, J = 3.4 Hz, 4H), 7.62 (d, J = 2.8 Hz, 4H), 7.55-7.45 (m, 8H), 7.29-7.24 (m, 4H), 4.44-4.31(m, 8H, NCH_2), 2.03-1.88 (m, 8H, CH_2), 1.47-1.28 (m, 72H, CH_2), 0.89 (t, J = 4.2 Hz, 12H, CH_3). ^{13}C NMR (75.5MHz, $CDCl_3$, δ ppm): 141.2, 140.0, 138.2, 132.3, 131.0, 128.9, 128.6, 126.7, 126.0, 125.8, 125.7, 123.3, 123.2, 122.7, 120.8, 119.1, 109.1, 108.7, 43.6, 32.2, 30.6, 29.9, 29.8, 29.7, 29.6, 29.3, 27.7, 25.1, 22.9, 14.4. IR (KBr, υ cm^{-1}): (arene C–H) 3048; (aliphatic C–H) 2922, 2851; (Ar C=C) 1626, 1599; (Ar C–N) 1489, 1465. Anal. Calc. for $C_{112}H_{134}N_4$: C, 87.56; H, 8.79; N, 3.65%. Found: C, 87.30; H, 9.03; N, 3.62%. MS (MALDI-TOF) *m/z* = 1534.91(exact mass = 1535.06).

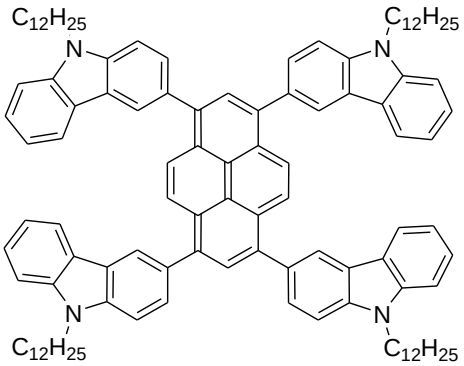

Tris(4-formylphenyl)amine (33) was synthesized by Vilsmeier reaction. 38.7 mL (414.8 mmol) of $POCl_3$ was added dropwise to 33 mL (414.8 mmol) of dry DMF at 0-5 °C under N_2 atmosphere. 5 g (16.5 mmol) of triphenylamine was dissolved in 15mL of DMF and added to the prepared complex at 0 °C. The reaction mixture was stirred at 85°C for 48 hours under nitrogen. Then it was cooled down to the room temperature; poured into ice water and neutralized with potassium hydroxide solution till pH = 6-8. The water solution was extracted with chloroform for several times. The chloroform solution was washed with water followed by brine. The organic layer was dried with anhydrous sodium sulfate, filtered and evaporated. The crude product was purified by silica gel column chromatography (hexane/ethyl acetate, 1/1). Yield = 16% (0.87g); Yellow solid (FW = 329.36 g/mol). ^{1}H NMR (300 MHz, $CDCl_3$), δ (ppm): 9.95 (s, 3H), 7.86 (d, J = 2.8 Hz, 6H), 7.27 (d, J = 3 Hz, 6H). ^{13}C NMR (75.5MHz, $CDCl_3$, δ ppm): 190.4, 151.1, 132.5, 131.4, 124.4. MS (EI) *m/z* = 330 $[M+H]^+$.

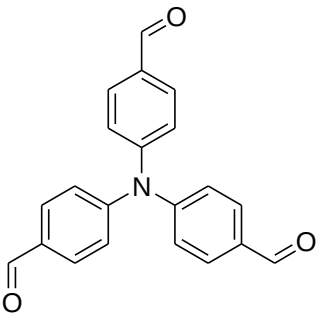

Methyl-3,4,5-tris(dodecyloxy)benzoate (34). Methyl-3,4,5-trihydroxybenzoate (5g, 27.15 mmol) in 200mL of acetone was taken in a 500mL RB flask. Potassium carbonate (13.12g, 95.05mmol) and 18-crown-6 (cat. amount) were added into it and stirred for 10min at room temperature under nitrogen. 1-Bromododecane (21.7mL, 89.59mmol) was added and the stirring was continued for 12 hrs under reflux. Acetone was removed at reduced pressure and the reaction mixture was diluted with water. The crude product was extracted with ethyl acetate. The organic layer was washed with brine and dried over sodium sulfate before the solvent was evaporated. The crude product was cooled at refrigerator and washed with cold methanol, filtered, and dried in vacuum. Yield = 88% (16.38g); White solid (FW = 689.13g/mol). ^{1}H NMR (300 MHz, $CDCl_3$), δ (ppm): 7.25(s, 2H), 4.01 (t, J = 5.1 Hz, 6H, OCH_2), 3.88 (s, 3H, OCH_{3Ester}), 1.89-1.69 (m, 6H, CH_2), 1.45-1.26 (m, 54H, CH_2), 0.88 (t, J = 4.5 Hz, 9H, CH_3). MS (EI) *m/z* = 670 $[M + H]^+$.

(3,4,5-Tris(dodecyloxy)phenyl)methanol (35). Methyl 3,4,5-tris(dodecyloxy)benzoate **34** (10g, 14.5 mmol) in 150mL of dry THF was taken in a 500mL three necked RB flask and allowed to cool at 0 ^oC. Lithium aluminium hydride (2M solution in THF, 21.7mL, 43.5mmol) was added dropwise into it and stirred for 1hr at 0 ^oC under nitrogen. The reaction mixture was allowed to warm to room temperature and stirring was continued for 12 hrs. Water was added dropwise to the reaction mixture followed by ethyl acetate and stirred for 15min. Then 2N HCl was added and the organic phase was separated. The organic layer was washed with brine and dried over sodium sulfate before the solvent was evaporated. The product was washed with cold methanol; filtered, and dried in vacuum. Yield = 92% (8.81g); White solid (FW = 661.11g/mol). ^{1}H NMR (300 MHz, $CDCl_3$), δ (ppm): 6.55(s, 2H), 4.58 (s, 2H, OCH_2), 3.98-3.91 (m, 6H, OCH_2), 1.84-1.69 (m, 6H, CH_2), 1.48-1.26 (m, 54H, CH_2), 0.88 (t, J = 4.5 Hz, 9H, CH_3). MS (EI) *m/z* = 662 $[M + H]^+$.

5-(Bromomethyl)-1,2,3-tris(dodecyloxy)benzene (36). (3,4,5-Tris(dodecyloxy)phenyl) methanol **35** (8g, 12.1 mmol) in 160mL of diethyl ether was taken in a 500mL three necked RB flask and allowed to cool at 0 ^oC. Phosphorous tribromide (1.7mL, 18.15mmol) was added dropwise into it and stirred for 1hr at 0 ^oC under nitrogen. The reaction mixture was allowed to warm to room temperature and the stirring was continued for additional 2 hrs under N_2. Water was added dropwise to the reaction mixture followed by ethyl acetate and stirred for 15min. The organic

layer was separated, washed with brine and dried over sodium sulfate before the solvent was evaporated. The product obtained was dried in vacuum. Yield = 97% (8.49g); White solid (FW = 724.01g/mol). ^{1}H NMR (300 MHz, $CDCl_3$), δ (ppm): 6.57 (s, 2H), 4.43 (s, 2H, Br-CH_2), 3.98-3.91 (m, 6H, OCH_2), 1.83-1.70 (m, 6H, CH_2), 1.48-1.26 (m, 54H, CH_2), 0.88 (t, J = 4.5 Hz, 9H, CH_3). MS (EI) *m/z* = 725 $[M + H]^+$.

Methyl-3,4,5-tris(decyloxy)benzoate (37) was synthesized according to the aforementioned procedure for the synthesis of **34**. Yield = 90% (14.78 g); White solid (FW = 604.96g/mol). ^{1}H NMR (300 MHz, $CDCl_3$), δ (ppm): 7.25(s, 2H), 4.01 (t, J = 5 Hz, 6H, OCH_2), 3.88 (s, 3H, OCH_{3Ester}), 1.85-1.69 (m, 6H, CH_2), 1.52-1.27 (m, 42H, CH_2), 0.88 (t, J = 4.4 Hz, 9H, CH_3). MS (EI) *m/z* = 604 $[M]^+$.

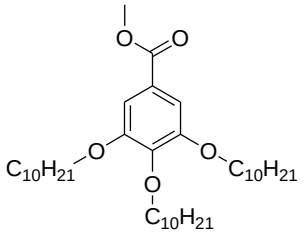

(3,4,5-Tris(decyloxy)phenyl)methanol (38) was synthesized according to the aforementioned procedure for the synthesis of **35**. Methyl 3,4,5-tris(decyloxy)benzoate **37** (8g, 13.2 mmol) was used as starting material. Yield = 95% (7.24 g); White solid (FW = 576.95g/mol). ^{1}H NMR (300 MHz, $CDCl_3$), δ (ppm): 6.55(s, 2H), 4.59 (s, 2H, OCH_2), 3.99-3.91 (m, 6H, OCH_2), 1.83-1.69 (m, 6H, CH_2), 1.51-1.26 (m, 42H, CH_2), 0.88 (t, J = 4.5 Hz, 9H, CH_3). MS (EI) *m/z* = 577 $[M + H]^+$.

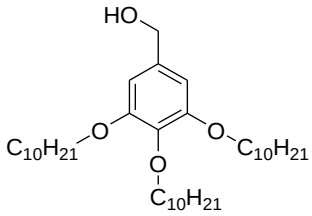

5-(Bromomethyl)-1,2,3-tris(decyloxy)benzene (39) was synthesized according to the aforementioned procedure for the synthesis of **36**. (3,4,5-Tris(decyloxy)phenyl)methanol **38** (5g, 8.6 mmol) was used as starting material. Yield = 98% (5.43 g); White solid (FW = 639.85g/mol). ^{1}H NMR (300 MHz, $CDCl_3$), δ (ppm): 6.57 (s, 2H), 4.43 (s, 2H, Br-CH_2), 3.98-3.91 (m, 6H, OCH_2), 1.87-1.68 (m, 6H, CH_2), 1.48-1.26 (m, 42H, CH_2), 0.88 (t, J = 4.5 Hz, 9H, CH_3). MS (EI) *m/z* = 640 $[M + H]^+$.

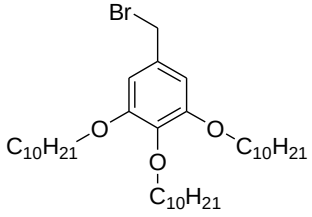

Methyl-3,4,5-triethoxybenzoate (40) was synthesized according to the aforementioned procedure for the synthesis of **34**. Yield = 87% (6.33 g); White solid (FW = 268.31g/mol). ^{1}H NMR (300 MHz, $CDCl_3$), δ (ppm): 7.27(s, 2H), 4.16-4.07 (m, 6H, OCH_2), 3.88 (s, 3H, OCH_{3Ester}), 1.44 (t, J = 4.6 Hz, 6H, CH_3), 1.36 (t, J = 4.7 Hz, 3H, CH_3). MS (EI) *m/z* = 269 $[M+H]^+$.

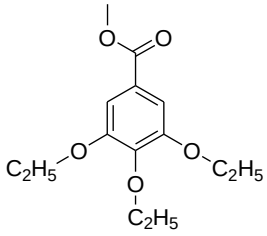

(3,4,5-Triethoxyphenyl)methanol (41) was synthesized according to the aforementioned procedure for the synthesis of **35**. Methyl-3,4,5-triethoxybenzoate **40** (5g, 18.63 mmol) was used as starting material. Yield = 90% (4.03g); White solid (FW = 240.30g/mol). ^{1}H NMR (300 MHz, $CDCl_3$), δ (ppm): 6.58 (s, 2H), 4.57 (s, 2H, OCH_2), 4.12-4.03 (m, 6H, OCH_2), 1.43 (t, J = 4.6 Hz, 6H, CH_3), 1.35 (t, J = 4.7 Hz, 3H, CH_3). MS (EI) *m/z* = 241 $[M+H]^+$.

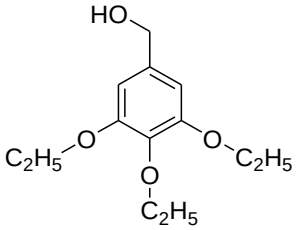

5-(Bromomethyl)-1,2,3-triethoxybenzene (42) was synthesized according to the aforementioned procedure for the synthesis of **36**. (3,4,5-triethoxyphenyl)methanol **41** (3g, 12.48mmol) was used as starting material. Yield = 96% (3.63 g); White solid (FW = 303.20g/mol). ^{1}H NMR (300 MHz, $CDCl_3$), δ (ppm): 6.59 (s, 2H), 4.41 (s, 2H, OCH_2), 4.13-4.05 (m, 6H, OCH_2), 1.43 (t, J = 4.6 Hz, 6H, CH_3), 1.35 (t, J = 4.7 Hz, 3H, CH_3). MS (EI) *m/z* = 304 $[M+H]^+$.

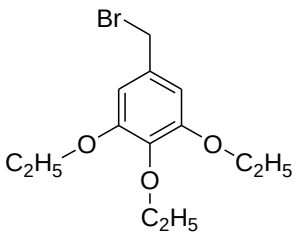

Tris(4-(3,4,5-tris(dodecyloxy)styryl)phenyl)amine (43) was synthesised by Wittig reaction. 5-(Bromomethyl)-1,2,3-tris (dodecyloxy)benzene **36** (1.36g, 1.88 mmol) was dissolved in 35mL of DMF and triphenyl phosphine (0.49g, 1.88 mmol) was added into it. It was refluxed for 12hrs under N_2. DMF was removed at reduced pressure and the crude product was dissolved in 40mL of dry THF. The reaction mixture was cooled to 0 ^oC and to which tris(4-formylphenyl)amine (0.2g, 0.6 mmol) and potassium *ter*-butoxide (0.4g, 3.6 mmol) were added. It was stirred at 0 ^oC for 1hr and then, allowed to warm to room temperature. It was further stirred for 6hrs under N_2 at room temperature. Water was added to the reaction mixture followed by ethyl acetate and the organic layer was separated. The organic phase was washed with brine and dried over sodium sulfate before the solvent was evaporated. The crude product was purified by silica gel column chromatography using hexane/ethyl acetate (97/3) solvent mixture as eluent. Yield = 35% (0.46g); Yellow solid (FW = 2210.66g/mol). ^{1}H NMR (300 MHz, $CDCl_3$), δ (ppm): 7.40 (d, J = 2.9 Hz, 6H), 7.10 (d, J = 2.9 Hz, 6H), 6.92 (s, 6H), 6.69-6.35 (m, 6H), 4.04-3.82 (m, 18H, OCH_2), 1.86-1.70 (m, 18H, CH_2), 1.50-1.26 (m, 162H, CH_2), 0.87 (t, J = 4.4 Hz, 27H, CH_3). ^{13}C NMR (75.5MHz, $CDCl_3$, δ ppm): 153.2, 152.7, 146.6, 132.6, 132.2, 127.7, 127.3, 124.2, 107.5, 105.1, 73.4, 69.0, 31.9, 30.3, 29.7, 29.7, 29.7, 29.6, 29.4, 29.4, 29.3, 29.3,

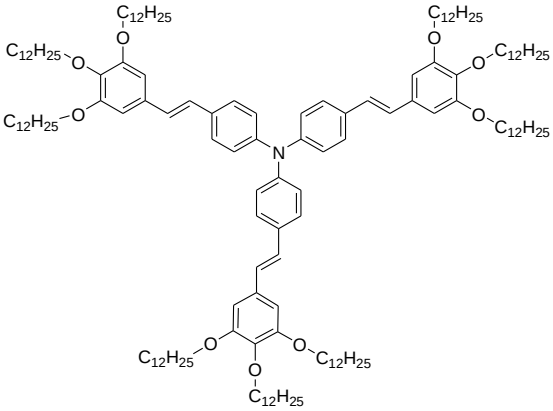

26.1, 26.1, 22.7, 21.7, 14.1. IR (KBr, υ cm^{-1}): (aliphatic C–H) 2955, 2919, 2849; (Ar C=C) 1589, 1511; (C–N stretch) 1240; (C–O stretch) 1122. Anal. Calc. for $C_{150}H_{249}NO_9$: C 81.50; H, 11.35; N, 0.63; O, 6.51%. Found: C, 81.84; H, 11.79; N, 0.79%. MS (MALDI-TOF) *m/z* = 2208.38 (exact mass = 2208.91).

Tris(4-(3,4,5-tris(decyloxy)styryl)phenyl)amine (44) was synthesized according to the aforementioned procedure for the synthesis of **43**. 5-(Bromomethyl)-1,2,3-tris(decyloxy)benzene **39** (1.2g, 1.88 mmol)) was used for the preparation of Wittig reagent. The crude product was purified by silica gel column chromatography using hexane/ethyl acetate (95/5) solvent mixture as eluent. Yield = 50% (0.58 g); Yellow solid (FW = 1958.17g/mol). ^{1}H NMR (300 MHz, $CDCl_3$), δ (ppm): 7.41-6.33 (m, 6H), 7.03-6.87 (m, 6H), 6.69-6.35 (m, 12H), 4.04-3.89 (m, 18H, OCH_2), 1.87-1.69 (m, 18H, CH_2), 1.51-1.27 (m, 126H, CH_2), 0.88 (t, J = 4.4 Hz, 27H, CH_3). ^{13}C NMR (75.5MHz, $CDCl_3$, *δ* ppm): 153.2, 152.8, 146.5, 132.8, 132.2, 127.6, 127.2, 124.2, 107.5, 105.0, 73.4, 69.1, 69.0, 68.8, 31.9, 31.9, 30.3, 29.7, 29.6, 29.6, 29.5, 29.4, 29.4, 29.3, 26.1, 26.1, 22.6, 21.7, 14.1. IR (KBr, υ cm^{-1}): (aliphatic C–H) 2954, 2924, 2853; (Ar C=C) 1589, 1507; (C–N stretch) 1235; (C–O stretch) 1117. Anal. Calc. for $C_{132}H_{213}NO_9$: C, 80.97; H, 10.96; N, 0.72; O, 7.35%. Found: C, 80.55; H, 11.14; N, 0.68%. MS (MALDI-TOF) *m/z* = 1956.46 (exact mass = 1956.62).

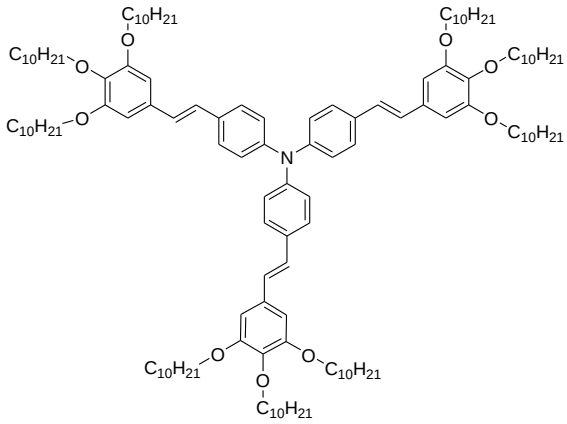

Tris(4-(3,4,5-triethoxystyryl)phenyl)amine (45) was synthesized according to the aforementioned procedure for the synthesis of **43**. 5-(Bromomethyl)-1,2,3-triethoxy benzene **42** (0.57g, 1.88 mmol)) was used for the preparation of Wittig reagent. The crude product was purified by silica gel column chromatography using hexane/ethyl acetate (8/2) solvent mixture as eluent and later on, recrystallization from methanol. Yield = 31% (0.18 g); Yellow crystals (FW = 948.22g/mol). ^{1}H NMR (300 MHz, $CDCl_3$), δ (ppm): 7.41 (d, J = 2.9 Hz, 6H), 7.11 (d, J = 2.9 Hz, 6H), 6.93 (s, 6H), 6.71 (s, 6H), 4.16-4.04 (m, 18H, OCH_2), 1.45 (t, J = 4.7 Hz, 18H, CH_3), 1.37 (t, J = 4.7 Hz, 9H, CH_3). ^{13}C NMR (75.5MHz, $CDCl_3$, *δ* ppm): 153.1, 146.5, 137.9, 132.8, 132.1, 127.5,

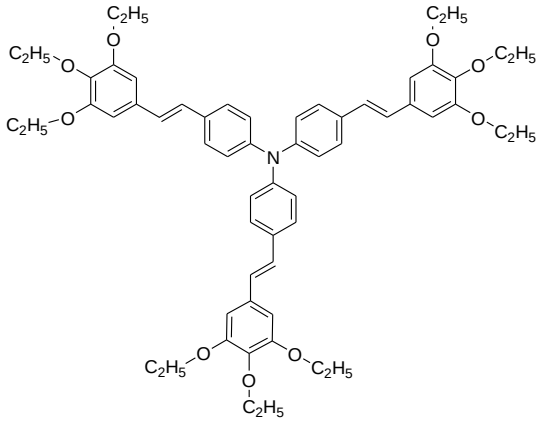

127.2, 127.1, 124.2, 105.2, 68.9, 64.7, 15.6, 15.0. IR (KBr, υ cm^{-1}): (aliphatic C–H) 2948, 2919, 2856; (Ar C=C) 1596, 1516; (C–N stretch) 1238; (C–O stretch) 1114. Anal. Calc. for $C_{60}H_{69}NO_9$: C, 76.00; H, 7.33; N, 1.48; O, 15.19 %. Found: C, 75.88; H, 7.20; N, 1.52 %. MS (EI) *m/z* = 949 $[M+H]^+$.

Tris(4-(4-methoxystyryl)phenyl)amine (46) was synthesised by Wittig-Horner reaction. Diethyl-4-methoxy benzyl phosphonate (0.48g, 1.88 mmol) and tris(4-formylphenyl)amine (0.2g, 0.6 mmol) were dissolved in 30mL of dry THF and cooled to 0^0C. Potassium *ter*-butoxide (0.4g, 3.6 mmol) was added into it and stirred at 0 °C for 1hr under N_2. Then, it was allowed to warm to room temperature and stirred for additional 4hrs under N_2. Water was added to the reaction mixture followed by ethyl acetate and the organic layer was separated. The organic phase was washed with brine and dried over sodium sulfate before the solvent was evaporated. The crude product was purified by silica gel column chromatography using hexane/ethyl acetate (8/2) solvent mixture as eluent. Yield = 72% (0.28g); Yellow crystals (FW = 641.82g/mol); m.p.: 99-101 °C. ^{1}H NMR (300 MHz, $CDCl_3$, δ ppm): 7.45 (d, J = 2.9 Hz, 6H), 7.39 (d, J = 2.9 Hz, 6H), 7.10 (d, J = 2.9 Hz, 6H), 6.96-6.87 (m, 12H), 3.82 (s, 9H, OCH_3). ^{13}C NMR (75.5MHz, $CDCl_3$, δ ppm): 159.1, 146.4, 132.4, 130.3, 127.5, 127.1, 126.9, 126.0, 124.2, 114.1, 55.3. IR (KBr, υ cm^{-1}): (arene C–H) 3024; (aliphatic C–H) 2951, 2927, 2851; (Ar C=C) 1605, 1511; (C–N stretch) 1249; (C–O stretch) 1173. Anal. Calc. for $C_{45}H_{39}NO_3$: C , 84.21; H, 6.12; N, 2.18; O, 7.48%. Found: C, 84.64; H, 5.89; N, 2.28%. MS (EI) *m/z* = 642 $[M+H]^+$.

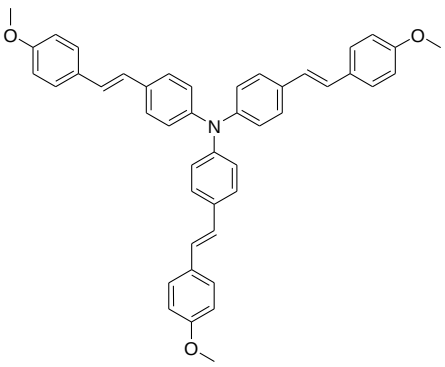

2,4,6-Tris(4-bromophenyl)-1,3,5-triazine (47) Trifluoromethane sulfonic acid (5.8mL, 65.92 mmol) was added to a solution of 4-bromobenzonitrile (4g, 21.97 mmol) in dry chloroform (30 mL) taken in a 250mL RB flask at 0^0C under N_2. The solution was stirred at 0 °C for 2hrs and then, it was allowed to warm to room temperature. The RB flask was closed with Teflon cork and stirring was continued for additional 48hrs. Water was added to the reaction mixture and vigorously stirred for 1 hr. After this period of time, the reaction mixture was carefully neutralized with an aqueous saturated solution of $NaHCO_3$. The precipitated white solid was filtered off and washed with acetone. Yield = 82% (3.28g); White solid (FW = 546.06g/mol). Anal. Calc. for $C_{21}H_{12}Br_3N_3$: C, 46.19; H, 2.22; Br, 43.90; N, 7.70%. Found: C, 46.56; H, 2.85; N, 7.45%. MS (EI) *m/z* = 547 $[M+H]^+$.

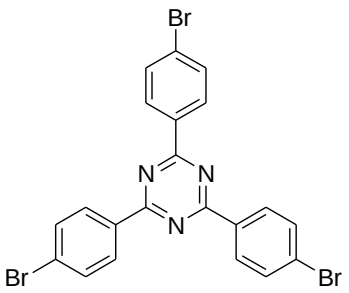

2,4,6-Tris(4-(bromomethyl)phenyl)-1,3,5-triazine (48) was synthesized according to the aforementioned procedure for the synthesis of **47**. 4-bromomethylbenzonitrile (3g, 15.3 mmol)) was used as the starting material. The crude product was further purified by recrystallisation from toluene. Yield = 85% (2.55g); White solid (FW = 588.14g/mol); m.p.: 192-193 ^{o}C. ^{1}H NMR (300 MHz, $CDCl_3$, δ ppm): 8.71 (d, J = 2.9 Hz, 6H), 7.60 (d, J = 2.9 Hz, 6H), 4.58 (s, 6H). MS (EI) *m/z* = 589 $[M+H]^+$.

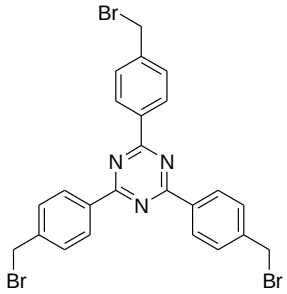

2,4,6-Tris(4-((diethylphosphoryl)methyl)phenyl)-1,3,5-triazine (49) 2,4,6-Tris(4-(bromo methyl)phenyl)-1,3,5-triazine **48** (2.5g, 4.25 mmol) was dissolved in triethylphosphite (5.0 mL) and the mixture was heated to reflux under nitrogen atmosphere during 5 hours. Then, the triethylphosphite excess was removed under reduced pressure. The resulting solid was purified by column chromatography in silica gel using hexane/ethyl acetate (7.5/2.5) solvent mixture as eluent. Yield = 80% (2.58g); White solid (FW = 759.7g/mol). MS (EI) *m/z* = 760 $[M+H]^+$.

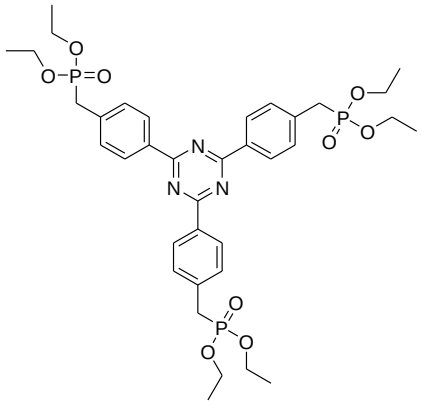

2,4,6-Tris(4-(9,9-diethyl-9*H*-fluoren-2-yl)phenyl)-1,3,5-triazine (50) was synthesised by Suzuki- Miyaura coupling reaction. 2,4,6-Tris(4-bromophenyl)-1,3,5-triazine **47** (300 mg, 0.55mmol) and 9,9-diethyl-9*H*-fluoren-2-yl boronic acid pinacol ester **9** (594mg, 1.70mmol) were taken in a solvent mixture of 30 mL of THF and 2 mL of water. Powdered potassium carbonate (5 molar equ.) was added and the reaction mixture was purged with nitrogen for 5 min. The reaction vessel was degassed and then, again purged with nitrogen. Bis(triphenylphosphine) palladium(II) dichloride (0.06 molar eq.) was added into it and stirred for 8-12 hrs at 80 ^{o}C under nitrogen. Then, the reaction mixture was diluted with water and extracted using ethyl acetate. The organic layer was dried over sodium sulfate and evaporated. The crude product was purified by column chromatography using silica gel as stationary phase. The solvent mixture of hexane and ethyl acetate in a volume ratio of 96:4 was used as eluent. It was further purified by recrystallization from

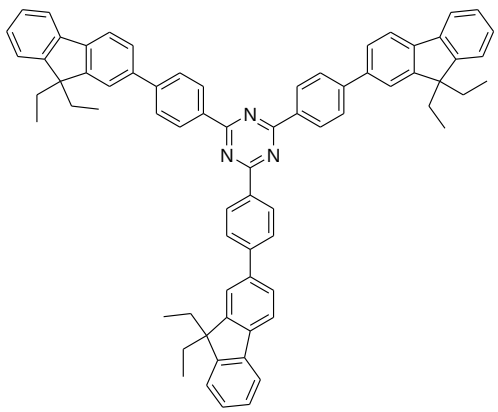

methanol. Yield = 35% (186mg); White solid (FW = 970.33g/mol); m.p.: 148-150 ºC. ^{1}H NMR (300 MHz, $CDCl_3$, δ ppm): 8.96 (d, J = 2.8 Hz, 6H), 7.97 (d, J = 2.8 Hz, 6H), 7.88 (d, J = 2.7 Hz, 3H), 7.82-7.73 (m, 10H), 7.43-7.37 (m, 8H), 2.17 (q, J = 8 Hz, 12H, CH_2), 0.45 (t, J = 4.9 Hz, 18H, CH_3). IR (KBr, υ cm^{-1}): (arene C–H) 3061; (aliphatic C–H) 2961, 2919, 2874; (Ar C=C) 1606, 1580. Anal. Calc. for $C_{72}H_{63}N_3$: C,89.13; H, 6.54; N, 4.33%. Found: C, 88.94; H, 6.78; N, 4.43%. MS (MALDI-TOF) *m/z* = 969.41 (exact mass = 969.5).

2,4,6-Tris(4-(10-ethyl-10*H*-phenothiazin-3-yl)phenyl)-1,3,5-triazine (51) was

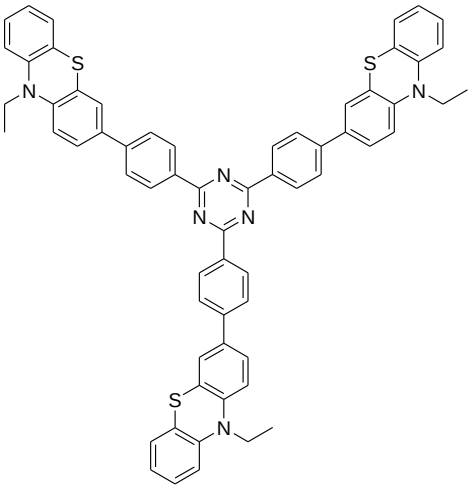

synthesized by using the similar procedure for the synthesis of **50** as described above. 10-Ethyl-10*H*-phenothiazin-3-yl boronic acid pinacol ester **12** was used for Suzuki reaction. The product was purified by column chromatography using silica gel as stationary phase and hexane/ethyl acetate solvent mixture (1:1) as eluent. Yield = 45% (243mg); Yellow crystals (FW = 985.32g/mol); m.p.: 255-256 ºC. ^{1}H NMR (300 MHz, $CDCl_3$, δ ppm): 8.86 (d, J = 2.2 Hz, 6H), 7.79 (d, J = 2.9 Hz, 6H), 7.55-7.72 (m, 6H), 7.23-7.18 (m, 6H), 7.02-6.93 (m, 9H), 4.03 (q, J = 6.8 Hz, 6H, NCH_2), 1.51 (t, J = 4.6 Hz, 9H, CH_3). IR (KBr, υ cm^{-1}): (arene C–H) 3056; (aliphatic C–H) 2975, 2932, 2867; (Ar C=C) 1600, 1577. Anal. Calc. for $C_{63}H_{48}N_6S_3$: C, 76.80; H, 4.91; N, 8.53; S, 9.76%. Found: C, 76.68; H, 4.70; N, 8.63%. MS (MALDI-TOF) *m/z* = 984.35 (exact mass = 984.31).

2,4,6-Tris(4-(9-ethyl-9*H*-carbazol-3-yl)phenyl)-1,3,5-triazine (52) was

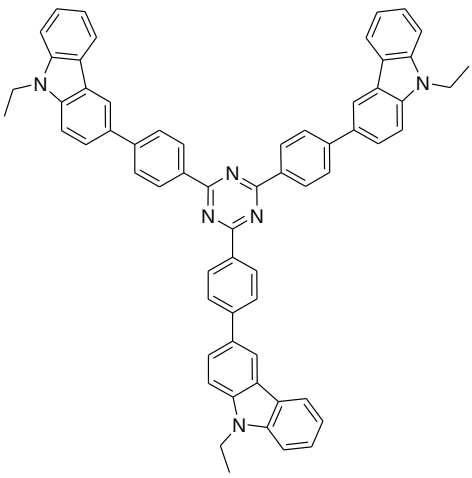

synthesized by using the similar procedure for the synthesis of **50** as described above. 9-Ethyl-9*H*-carbazol-3-yl boronic acid pinacol ester **3** was used for Suzuki reaction. The product was purified by column chromatography using silica gel as stationary phase and chloroform as eluent. Yield = 41% (200mg); Yellow solid (FW = 889.13g/mol); m.p.: 324-326 ºC. ^{1}H NMR (300 MHz, $CDCl_3$, δ ppm): 8.99 (d, J = 2.8 Hz, 6H), 8.51(s, 3H), 8.26 (d, J = 2.6 Hz, 3H), 8.02 (d, J = 2.8 Hz, 6H), 7.92 (d, J = 3.4 Hz, 3H), 7.58-7.48 (m, 9H), 7.33 (t, J = 5.3 Hz, 3H), 4.48 (q, J = 7.1 Hz,

6H, NCH_2), 1.53 (t, J = 4.8 Hz, 9H, CH_3). IR (KBr, υ cm^{-1}): (arene C–H) 3048; (aliphatic C–H) 2968, 2919, 2887; (Ar C=C) 1599, 1568. Anal. Calc. for $C_{63}H_{48}N_6$: C, 85.11; H, 5.44, N, 9.45%. Found: C, 85.24; H, 5.46; N, 9.38%. MS (MALDI-TOF) *m/z* = 888.23 (exact mass = 888.39).

2,4,6-Tris(4-(3,4,5-trimethoxystyryl)phenyl)-1,3,5-triazine (53) was synthesised by Wittig-Horner reaction. 2,4,6-Tris(4-((diethylphosphoryl)methyl) phenyl)-1,3,5-triazine **49** (0.4g, 0.52 mmol) and 3,4,5-trimethoxybenzaldehyde (0.2g, 1.63 mmol) were dissolved in 30mL of dry THF and cooled to 0 °C. Potassium *ter*-butoxide (0.26g, 2.34 mmol) was added into it and stirred at 0 °C for 1hr under N_2. Then, it was allowed to warm to room temperature and stirred for additional 6hrs under N_2. Water was added to the reaction mixture followed by ethyl acetate and the organic layer was separated. The organic phase was washed with brine and dried over sodium sulfate before the solvent was evaporated. The crude product was purified by silica gel column chromatography using hexane/ethyl acetate (1/1) solvent mixture as eluent. Yield = 25% (115mg); Yellow crystals (FW = 886.02g/mol). ^{1}H NMR (300 MHz, $CDCl_3$, δ ppm): 8.77 (d, J = 2.8 Hz, 6H), 7.71 (d, J = 2.8 Hz, 6H), 7.18 (q, J = 15.6 Hz, 6H), 6.80 (s, 6H), 3.95-3.87 (m, 27H). ^{1}H NMR (300 MHz, $CDCl_3$), δ (ppm): 170.9, 153.4, 141.2, 138.3, 135.2, 132.6, 130.5, 129.3, 127.4, 126.5, 103.8, 60.9, 56.1. IR (KBr, υ cm^{-1}): (aliphatic C–H) 2924, 2854; (Ar C=C) 1582, 1506; (C–O stretch) 1121. Anal. Calc. for $C_{54}H_{51}N_3O_9$: C, 73.20; H, 5.80; N, 4.74; O, 16.25%. Found: C, 73.44; H, 5.70; N, 4.54%. MS (EI) *m/z* = 886 $[M]^+$.

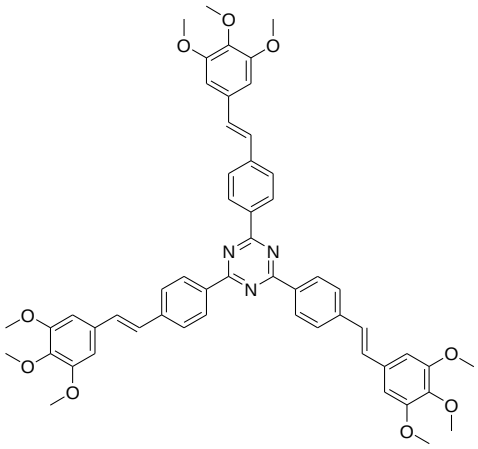

4. RESULTS AND DISCUSSION

4.1. Synthesis and properties of electron-donors substituted arylene imides.

Arylene imides with small aromatic core like naphthalene [132] or perylene imides [133] are promising materials for organic or molecular electronics and more specifically for the fabrication of n-channel or ambipolar field-effect transistors. Perylene and naphthalene anhydrides, the parental compounds of these imides, are readily available and can be easily functionalized in order to improve the processability as well as the physical properties. The electrochemical, photophysical and photoelectrical properties of arylene imides can be tuned and improved by the proper substitution with electroactive chromophores such as electron-donors. The electron-donors can be substituted either at the polycyclic core or at the N-position of the imides. The core-functionalization by using electron-donors is the more effective way of tuning their electronic structure and thus, the physical properties where as the N-functionalization can enhance the solubility which is important for device fabrication [109,110]. Hence, we have substituted the carbocyclic core part of perylene bisimide and naphthalimide with various electron-donor substituents such as carbazole, triphenylamine, fluorene, phenothiazine, thiophene *etc* and the N-position with alkyl substituents and evaluated their physical properties in the viewpoint of application in opto-electronics.

4.1.1. Ambipolar charge transporting bay substituted perylene bisimides

Perylene bisimide derivatives form a class of interesting n-type organic semiconductors owing to excellent charge carrier transport in conjunction with their outstanding chemical, thermal and photochemical stability [134,135,136,137]. Very high electron mobility of perylene bisimide derivatives have qualified them to be widely employed in electronic and optoelectronic devices. Accordingly numerous perylene bisimide derivatives carrying different substituents on the imide positions as well as on the carbocyclic core, the so-called bay region, has been synthesized and investigated [134,135]. However stable ambipolar (transport both hole and electrons) molecular materials based on π-conjugated perylene bisimides have not been explored well and are of still interesting in the perspective of cost effective single layer organic light emitting diodes and filed-effect transistors [138,139,140]. The electron-donors like carbazole, triphenylamine, fluorene and phenothiazine derivatives are well known hole-transporting materials and have extensively been exploited for various optoelectronic applications [17-22]. The combination of these hole-transporting and electron-donating compounds with electron-deficient perylene bisimides at molecular level may lead to novel multichromophoric donor-acceptor molecular materials with interesting and useful optical and charge-transporting properties important for various device applications. Keeping this in mind we have designed and synthesized new 1, 7-bay substituted perylene bisimide derivatives directly linked to various electron-rich chromophores furnishing efficient ambipolar charge-transporting materials possessing excellent photoinduced charge transfer

properties. Moreover, in this chapter we will discuss the thermal, optical, photophysical, electrochemical and photoelectrical characterizations and preliminary quantum chemical calculations of these newly synthesized molecular materials.

Synthesis of bay electron-donor substituted perylene bisimides

Bromination of carbazole with Br_2 usually leads to a variety of brominated carbazole compounds. Due to the electronic structure of the carbazole molecule, the activated 3- and 6-positions are substituted first. Here, we used 1 equiv. of bromine and carefully controlled the reaction temperature at 0 °C in order to obtain 3-bromocarbazole **1** in good yield. The synthesis of 2-bromocarbazole **5** was more complicated. In this case, the bromine has to be introduced before the carbazole skeleton was generated.

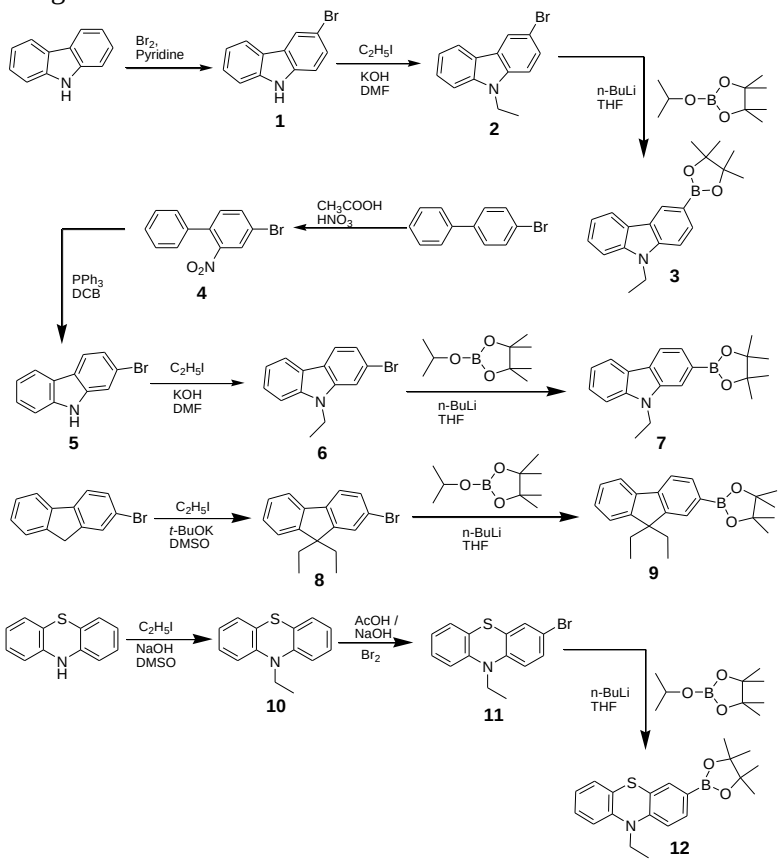

Scheme 4.1 Synthesis of key intermediates **3**, **7**, **9** and **12**.

The boronic acid ester (**3**) for the preparation of compounds **15** and **16** was synthesised from 3- bromo carbazole by N-alkylation and subsequent borylation using n-BuLi and 2-isopropoxy-4, 4, 5, 5-tetramethyl-1, 3, 2-dioxaborolane at -78°C. Compound **7**, the topological isomer of **3**, was obtained from 4-bromo biphenyl by nitration followed by ring closure with triphenyl phosphine and the

consequent N-alkylation and borylation. For the preparation of fluorene derivative **8** potassium *ter*-butoxide was used as the base for alkylation unlike for carbazolyl derivatives; where potassium hydroxide was used. In this case tetra butyl ammonium hydrogen sulfate was used as PTC. The first step for the preparation of **12** was the alkylation of phenothiazine in DMSO in the presence of sodium hydroxide to yield **10**. For the bromination reaction, compound **10** was dissolved in acetic acid /sodium hydroxide mixture and bromine in acetic acid was added continuously with stirring. The synthesis of boronic acid pinacol esters **9** and **12** were quite straightforward like in carbazole derivatives as shown in Scheme 4.1.

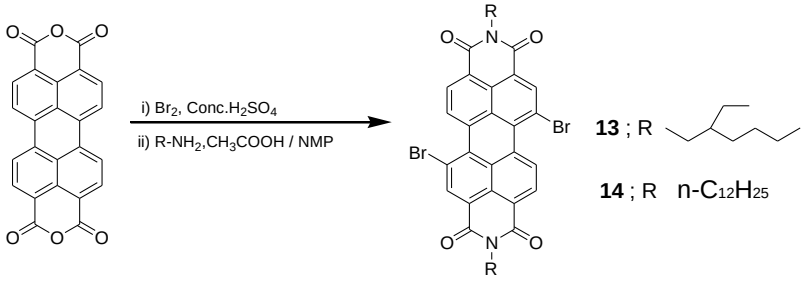

Scheme 4.2 Synthesis of 2,7 dibromo perylene bisimides.

1, 7-dibromo *N, N*'-2-ethylhexyl perylene bisimide (**13**) and 1, 7-dibromo *N, N*'-dodecyl perylene bisimide (**14**) were prepared by the bromination of commercially available 3, 4 : 9, 10 - perylene tetracarboxylic dianhydride followed by the condensation with corresponding alkyl amines, 2-ethyl hexyl amine and n-dodecyl amine, respectively (Scheme 4.2) . The compound **13** was yielded 52% and **14** was yielded 45% after column chromatography.

The donor-acceptor-donor (D-A-D) triads **15-20** were synthesised by the Suzuki-Miyaura coupling reaction of 1, 7-dibromoperylene bisimides (**13** and **14**) with corresponding mono boronic acid or mono boronic acid pinacol ester derivatives (**3**, **7**, **9**, **12** or 4-(Diphenylamino)phenylboronic acid, **DPB**) of electron-donor chromophores. The catalyst, bis(triphenylphosphine) palladium(II) dichloride, using for Suzuki reactions was highly sensitive towards oxygen and hence, all the reactions were perfectly executed under N_2 atmosphere. All the target compounds were purified by column chromatography using hexane/ethyl acetate solvent mixtures at various compositions. The D-A-D **15** was yielded 55% after purification and the compound based on triphenylamine electron-donor **18** gave 24% yield after column chromatography. The D-A-D **16** with longer alkyl chain at the N-position yielded 32% and other derivatives gave ca. 41-46% yield after purification. The synthesis of the newly designed target materials are shown in Scheme 4.3.

The synthesized compounds were characterized by ^{1}H NMR, ^{13}C NMR, IR and mass spectroscopy as well as elemental analysis. For D-A-D **15-20**, MALDI-TOF mass spectroscopy was used for the characterization. The spectral and elemental analysis data were in good agreement with their chemical structures.

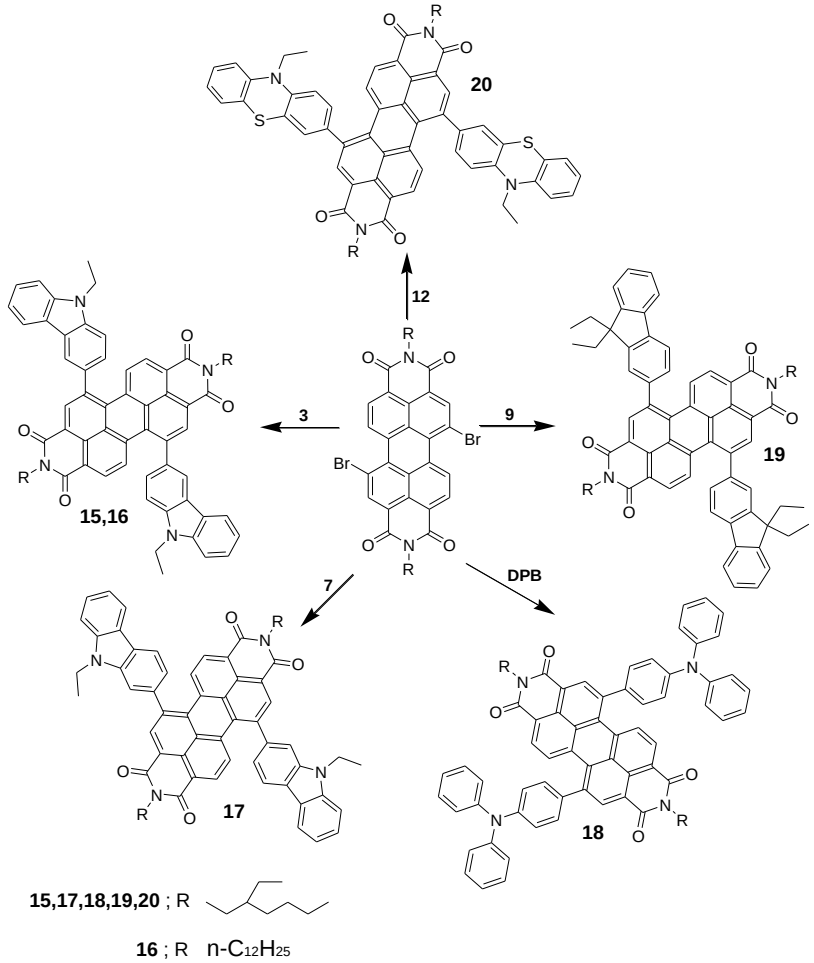

Scheme 4.3 Synthetic route for the preparation of D-A-D derivatives **15-20**. *Reagents and conditions*: $Pd(Ph_3)_2Cl_2$, KOH, THF–H_2O, 80 ^oC, 8–12 h.

^{1}H NMR spectrum of dibrominated perylene bisimide **13** is given in the Figure 4.1. Typical set of peaks for the 1, 7- dibrominated carbocyclic-core appeared in the 9.48 – 8.70 ppm region of the ^{1}H NMR spectrum. It has been reported that the 1, 7-dibrominated product can be contaminated by the trace of 1, 6-dibromoperylene bisimide even after column chromatography since the dibromination reaction of perylene dianhydride is not perfectly regioselective [141]. We have also noted such kind of small contamination in the ^{1}H NMR spectrum of compound **13**. As can be seen in the Figure 4.1, the singlet at 8.91 ppm merged with a small shoulder peak from the regioisomer, i.e. 1, 6 –dibromo substituted perylene bisimide, which can only be separated by repetitive recrystallisation [141]. The peak intensity ratio between the singlet and the shoulder peak is *ca.* 94:6. However after bay substitution of bulky electron-donors regioisomerically pure 1, 7 – substituted compound can be isolated (Figure 4.2) [142,143].

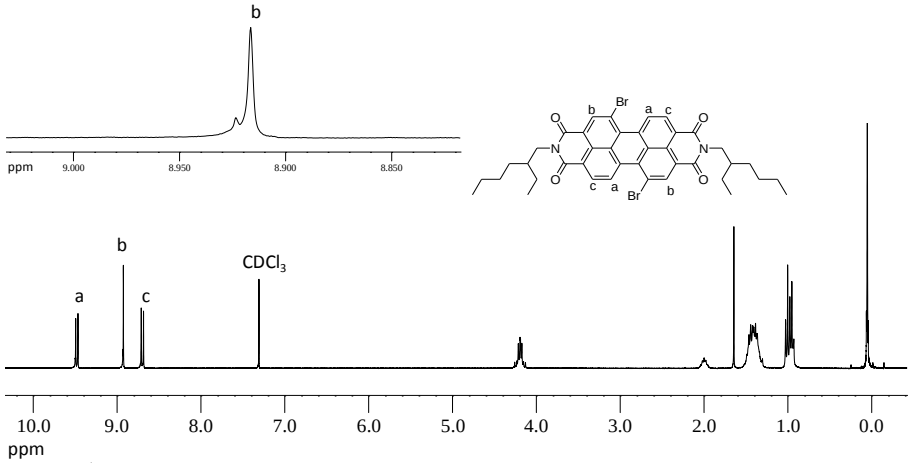

Figure 4.1 ^{1}H NMR spectrum of compound **13**. Aromatic part of the spectrum of interest is shown in the inset.

The ^{1}H NMR spectrum of D-A-D **18** (Figure 4.2) clearly reveals the electron-donating effect of the triphenyl amine bay substituents. The perylene peaks are shielded to 8.63, 8.24 and 8.06 ppm. The considerable shielding effect in the chemical shift value of the proton marked **a** (δ_{shift} = 1.32 ppm) suggests not only the electron-donating capability of triphenylamine but also the influence of diamagnetic ring current in the phenyl substituent of triphenylamine moiety.

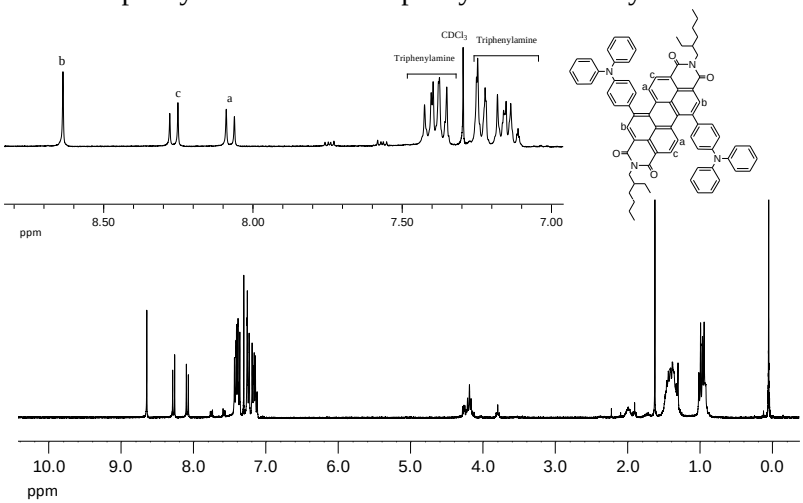

Figure 4.2 ^{1}H NMR spectrum of D-A-D **18**. Aromatic part of the spectrum of interest is shown in the inset.

Thermal characteristics

The glass transition temperatures (T_g) of the synthesized perylene bisimide derivatives are summarised in Table 4.1. They range from 81^{o}C to 95^{o}C. The linking topology of perylene bisimide and carbazole derivatives seems not to have any

substantial influence on their T_g. T_g of 2-carbazolyl substituted derivative (**17**) is comparable to that of its 3-carbazolyl substituted isomer (**15**). The effect of the branched but shorter alkyl chain and longer but linear alkyl chain on the glass transition of 3-carbazolyl substituted derivatives is also comparable. T_g of **15** is close to that of **16**. Bay triphenyl substituted perylene bisimide **18** shows melting transition at 251°C and also crystallise during cooling.

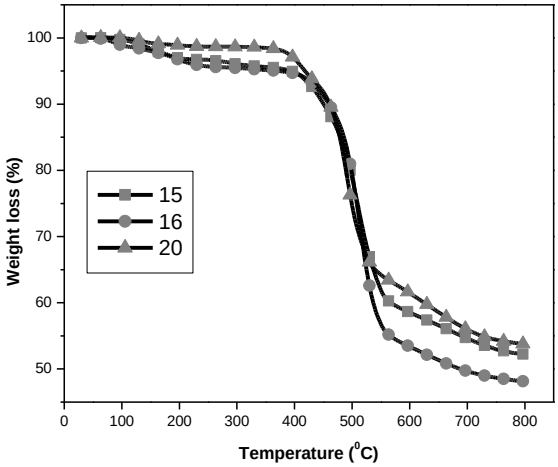

Figure 4.3 TGA traces of D-A-D derivatives at 20°C/min under N_2.

Thermal stability of compounds **15-20** was estimated by thermogravimetric analysis. The TGA traces of D-A-D derivatives are shown in Figure 4.3. All the derivatives demonstrate high thermal stability. The temperatures of the onsets of thermal decomposition (T_{ID}) of perylene bisimide derivatives are collected in Table 4.1. They range from 418 to 471°C. The T_{ID} values of compounds **15, 17, 18** and **19** are comparable irrespective of the bay substituents. The difference in the T_{ID} values of **15** and **16** is pointing towards the influence of N-alkyl substituents on their thermal stability. As can be seen from the Figure 4.3, the weight loss pattern is almost same for all the derivatives irrespective of bay substituents. Hence, the first major weight loss observed from *ca.* 415 to 540 °C for the compounds **15, 16** and **20** may be attributed to the loss of two branched (2-ethyl hexyl) or long (n-dodecyl) alkyl substituents respectively from the imide region [144].

Table 4.1 Thermal characteristics of **1- 4.**

Compound	T_g / °C	T_m / °C	T_{cr} / °C	T_{ID} / °C
15	81	-	-	438
16	82	-	-	471
17	82	-	-	441
18	95	251	194	455
19	85	-	-	448
20	89	-	-	418

Optical and photophysical properties

The synthesized compounds are well soluble in common organic solvents like tetrahydrofuran, dichloromethane, chloroform *etc.* facilitating their optical characterization in solution state. UV-Vis absorption spectra of dilute solutions are shown in Figure 4.4. The wavelengths of absorption maxima are collected in Table 4.2.

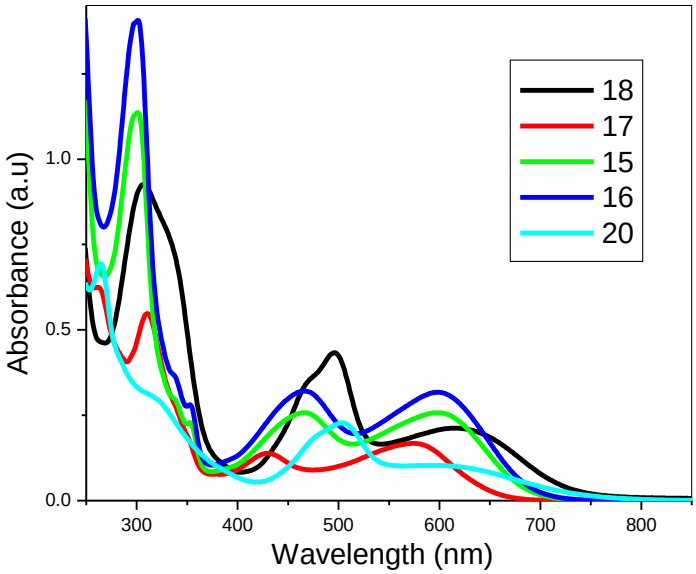

Figure 4.4 UV-Vis absorption spectra of bay substituted perylene bisimides in THF (10^{-4} Mol L^{-1}).

Before analyzing the UV-Vis spectra of the synthesized molecules, it is instructive to discuss the spectroscopic features of arylene bisimides which do not contain chromophore type substituents, for example; perylene bisimides with alkyl groups attached to the imide nitrogen. UV-Vis absorption spectra of these compounds are dominated by a strong band of pronounced vibronic structure, ascribed to the π-π* transition in the perylene core with the *0-0* vibronic peak of the lowest electronic transition being the most intensive [145,146,147]. However, in the case of compounds **15- 20** the vibronic structure is much less resolved. Moreover, a new structureless, relatively broad band appeared with the maxima ranged from 574-617 nm for compounds **15- 18** and **20**. This band, which is common in arylene bisimides core functionalized with electron donating substituents, can be ascribed to a transition of a CT character between the electron-donors, i.e. carbazole, triphenylamine or phenothiazine, and the perylene bisimide core [148,149,150]. The shifts in the peaks positions as well as their significant broadening can be considered as a spectroscopic manifestation of the conjugation between the substituents and the perylene core.

Table 4.2 Optical characterization data of **15-20.**

Compound	Absorption λ_{max}/nm	Emission λ_{max}/nm	Φ_F [a]	E_g^{opt} /eV [b]
15	226, 301, 466, 599	756	0.03	1.74
16	226, 301, 466, 599	756	0.03	1.74
17	224, 311, 430, 574	705	0.004	1.85
18	211, 307, 496, 617	Non-fluorescent	-	1.58
19	251, 312, 428, 572	670	0.57	1.87
20	264, 504, 593	Non-fluorescent	-	1.53

[a]Fluorescence was excited at 570 nm. [b]Calculated from solution absorption edges.

The low energy absorption edges of the newly synthesized compounds range from 1.87 to 1.53 eV and as anticipated for bay substitution by aromatic groups, are red shifted with respect to the unsubstituted parent compound, perylene bisimide (PBI), owing to their greater conjugation [109,140,151]. Moreover, it is found that the least energy absorption band of **18** and **20** carrying triphenylamine and phenothiazine moieties, respectively, at the bay region is bathochromically shifted with respect to that of compounds containing carbazole and fluorene units. This suggests distortion of perylene core, known to occur upon bay substitution, to lesser degree upon substitution by triphenylamine or phenothiazine moieties as well as greater conjugation leading to relatively low optical band gap compared to those of carbazole and fluorene derivatives [109,152]. Furthermore, surprisingly the absorption bands of 3-carbazolyl substituted derivatives (**15** and **16**) are shifted both bathochromically and hyperchromically with respect to that of 2-carbazolyl substituted derivative (**17**) clearly indicating towards different degree of perylene core distortion and/or different torsional angles of bay substituents in these topological isomers.

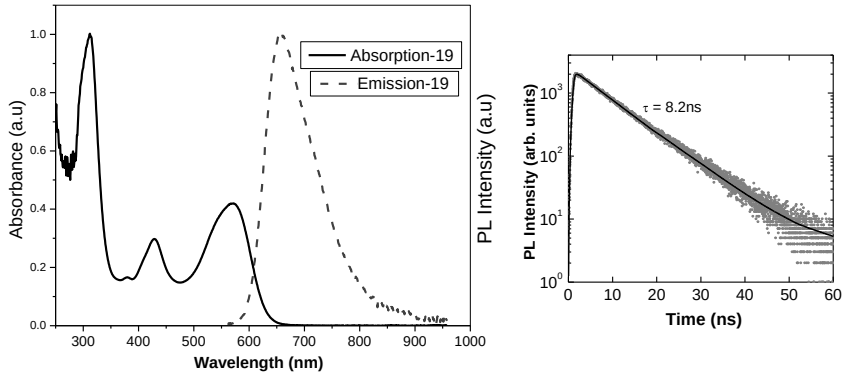

Figure 4.5 (a) Absorption and fluorescence spectra of fluorene-substituted PBI derivative **19** in dilute solution. (b) PL transient of **19** measured at the PL maxima. Lines mark exponential fits to the experimental points with the PL decay time constants (τ), indicated.*

**Fluorescence quantum efficiencies were measured at Institute of Applied Research, Vilnius University by Dr. K. Kazlauskas.*

Investigation of photoluminescent properties of **15-20** yields interesting results on the potential of these multichromophoric D-A-D hybrids. For all the compounds, fluorescence was excited at 570 nm. Fluorescence quantum yield values were estimated by using the integrating sphere method. Complete self-quenching of the fluorescence of compounds **18** and **20** is observed. Compounds **15-17** with carbazolyl substituents at the bay region of perylene bisimides were also almost non-fluorescent with trivial fluorescence quantum yields (Table 4.2). These results suggest that very efficient photo-induced intramolecular electron transfer occurs in these compounds and it is obvious from the absorption spectra. However, fluorenyl derivative **19** showed different behaviour; which exhibits fluorescence and emits at the red region of visible spectrum with the maximum at 670 nm (Figure 4.5). The photoluminescence decay time for **19** was 8.2 ns. For the weakly fluorescent/non-fluorescent PBI derivatives, PL decay should be very fast ($\tau < 0.1$ ns) and hence, it was not measurable because of the restricted time-resolution of our setup. Interestingly, almost non-fluorescent carbazolyl regioisomers **16** and **17** differ in their fluorescence efficiency by a factor of 10 and highly fluorescent **19** with fluorene substituents becomes non-emissive, if fluorenes are exchanged by carbazoles (**17)**. These results imply considerable changes in molecular structure, possibly in orientation of the substituents with respect to the perylene core. Since all these weakly fluorescent/non-fluorescent molecules absorb well in the visible-near IR region of the spectrum with efficient photo-induced intramolecular charge transfer, they can be promising candidates for the application in photovoltaic devices and the fluorescent compound **19** can be exploited for OLEDs.

Electrochemical properties

Perylene bisimides with electrochemically inactive substituents show, in their cyclic voltammograms, two characteristic reduction peaks at E_{red1} and E_{red2}, associated with quasi-reversible reduction of the neutral molecule to a radical anion in the first step and to a spinless dianion in the second one, as shown in Scheme 4.4 [153].

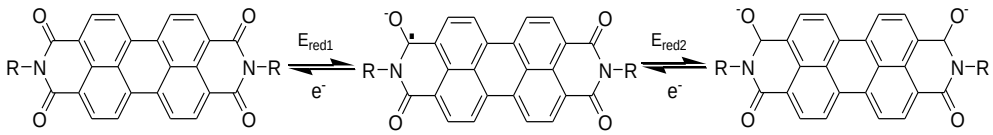

Scheme 4.4 Two step reduction of perylene bisimide.

The spacing between these peaks depends on the size of the arylene core. The addition of an electron in the first reduction step increases the electron density on the carbonyl oxygen of the imide group. The next reduction step, which requires the addition of a second electron, is therefore facilitated by the ability of the aromatic core to delocalize this surplus electron density. This is of course easier in the case of larger arylene core like perylene imides compare to the smaller one such as naphthalimides. Moreover, in large core arylene bisimides Coulombic repulsion between the introduced charges of the same sign is smaller. These two factors cause

that the spacing between the two redox peaks decreases with increasing core size and they eventually merge into one peak in bisimides of very large cores; for example, quaterylene bisimide [152].

Electrochemical properties of compounds **15-18** were studied by cyclic voltametry in order to elucidate the electronic energy levels which determine the energy and electron transfer processes and the reversibility of redox processes [154]. Cyclic voltammograms of **15-18** are given in Figure 4.6. In addition to the expected quasi-reversible redox couples associated with the reduction of the bisimide core new couple(s) appears at positive potentials which can be ascribed to quasi-reversible oxidation of the electron-donor substituents such as carbazole and triphenylamine to radical cation(s).

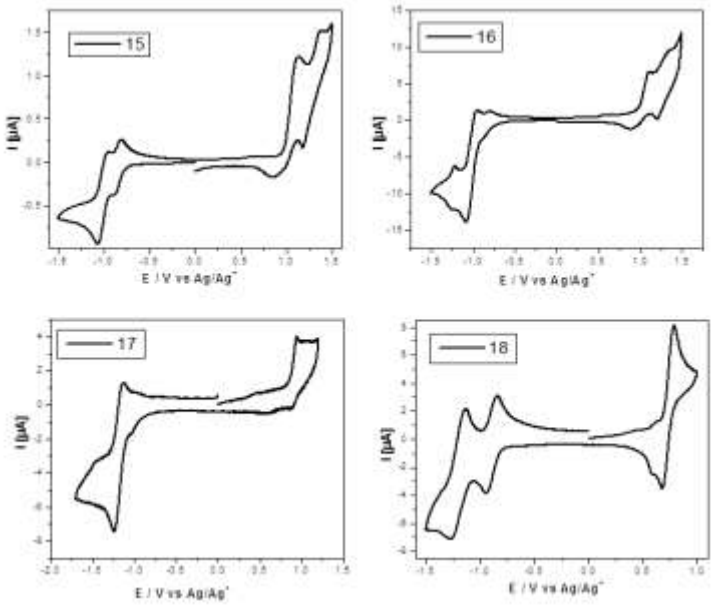

Figure 4.6 Cyclic voltammograms of compounds **15-18**. Electrolyte: n-Bu_4NPF_6 in DCM ($0.01MolL^{-1}$). Working, counter and reference electrodes: Glassy carbon, platinum wire and $Ag/AgNO_3$ (0.01 Mol L^{-1} in acetonitrile) respectively. Scan rate: 100 mV s^{-1}

The half wave potentials and the calculated HOMO-LUMO energy values are summarized in Table 4.3. As can be seen from Table 4.3, compound **17** possesses higher electrochemical band gap than compound **15**, the regioisomeric counterpart of **17**, and the trend is comparable with the optical band gaps. The triphenylamine substituted derivative exhibits narrow band gap compared to carbazolyl derivatives. Relatively high LUMO levels of these electron-donor substituted perylene derivatives compared to other related materials may be attributed to the twisted structure and rather high electron density in the perylene core induced by bulky electron-donating bay substituents [155,156].

Table 4.3 Electrochemical characteristics of compounds **15-18**.

Compound	E_{red}/V	E_{oxi}/V	E_{HOMO}/eV	E_{LUMO}/eV	E_g^{ele} /eV
15	-1.05, -0.87, 0.86, 1.18	-0.96, -0.81, 1.12, 1.37	-5.62	-3.79	1.83
16	-1.07, -0.85, 0.90, 1.20	-0.81, -0.96, 1.12, 1.34,	-5.63	-3.79	1.84
17	-1.24, -1.05, 0.87	-1.13, -0.94, 0.94,	-5.53	-3.66	1.87
18	-1.34, -1.15, 0.51	-1.22, -1.03, 0.59	-5.31	-3.78	1.53

Perylene bisimides without chromophoric bay substituents does not showed any oxidation in the known electrochemical window and the HOMO level calculated using optical band gap was found to be 6.34 eV [109]. For compounds **15-18**, the HOMO levels range from 5.31 to 5.63 eV with the highest value for triphenylamino bay substituted perylene derivative and the lowest for compound **16;** where carbazole is attached through its 3-position to PBI. This significant effect on the HOMO energy level can be considered as a manifestation of the donor-acceptor interactions between the perylene core and the electron-donor substituents. In this case the electron donating effect of the substituent increases the π-electron density in the bisimide core and makes its oxidation easier. The electron accepting effect of the bisimide core shifts, in turn, the oxidation of the triarylamine or carbazole substituents to higher potentials. Hence, it can be assumed that in these core electron-donors substituted bisimides both the components of the molecule interact stronger and subsequently their frontier orbitals should exhibit electron density on both parts of the molecule, i.e., the core and the substituents. DFT calculations *vide ifra* proved these assumptions

Photoelectrical properties

An important characteristic of electro-active compounds used in optoelectronic devices is ionization potential, which characterizes the electron releasing process under illumination. I_p of solid layers of the synthesized compounds were measured by photoelectron spectroscopy. Photoelectron spectra of **15-20** are given in Figure 4.7. The intersection points of the linear parts of the spectra drawn with the abscissa axis give the ionization potential values. I_p values are rather close and range from 5.5eV to 6.1eV. The highest I_p value was observed for fluorenyl substituted derivative (**19**) and the lowest for phenothiazinyl derivative **20**. A small difference is observed in the values of HOMO (I_p) energy levels of these perylene derivatives obtained by PES and electrochemical studies. This is due to the difference in molecular interactions and molecular arrangements in thin solid layers and in dilute solutions of these derivatives. LUMO (E_A) energy levels of compounds **19** and **20** were calculated by subtracting solution absorption edges from the I_p levels and were

found to be 4.23 eV for **19** and 3.97 eV for **20**, respectively. The calculated LUMO energies of these compounds are slightly higher than that of other perylene derivatives obtained from the electrochemical studies.

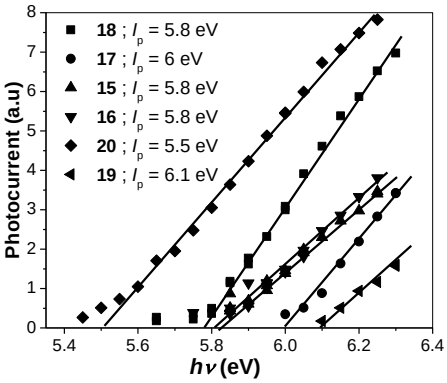

Figure 4.7 Photoelectron spectra and ionization potentials of the thin films of **15-20**.[§]

Xerographic time of flight (XTOF) technique was used for the evaluation of charge-transporting properties of thin layers of compounds **15-18** in air. Compounds **17** and **18** provide good neat thin films. However, thin film preparation for XTOF experiment was not successful for **15** and therefore, a solid solution (1:1; Wt.) was prepared with an inert polymer host, bisphenol Z-polycarbonate (PC-Z). In order to have a fair comparison of charge-transporting properties in neat films between 2- and 3-carbazolyl substituted derivatives, compound **16** with long alkyl substituents was synthesized and found to form good neat film.

All the compounds (**15-18**) exhibited capability of transporting both electrons and holes. This is evidenced by the practically equal amounts of positive and negative charges extracted after the impulse of strongly absorbed irradiation with the wavelength of 337 nm. However, due to the enhanced dispersity of hole-transport we were not able to estimate the hole drift mobilities in the layer of **18.** XTOF charge drift mobility data for **15-18** are summarized in Table 4.4 and representative *dU/dt* transients for the neat films of **16** and **18** are shown in Figure 4.8.

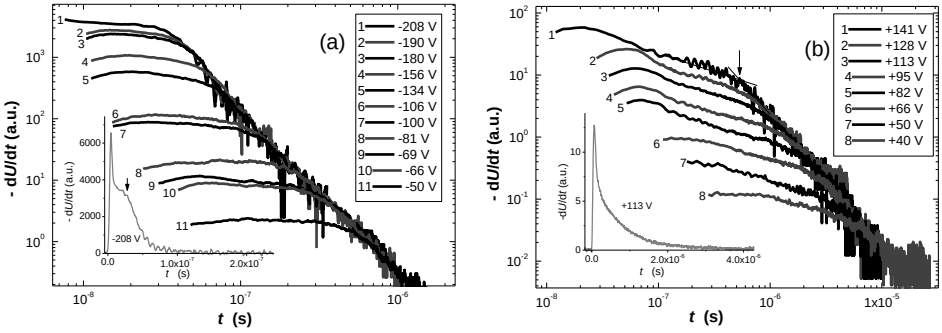

Figure 4.8 XTOF transients for the neat films of perylene derivatives **18** (a) and **16** (b). 1 ns laser operating at 337 nm was used, $T = 25^0$C, Arrows on insets (a) and on main layout (b) indicate transit time of electrons and holes respectively at corresponding surface voltages. [§]

A distinct inflection point indicating transit time with the sign of non-dispersive electron transport was observed in air for the neat film of **18** which was unaltered even after ambient storage for several weeks. Compound **17** also exhibited a non-dispersive electron transport with significantly high electron drift mobility whereas a dispersive and rather slow hole-transport was observed. For compounds **15** and **16**, charge-transport was dispersive; however, the drift mobility values were sufficiently high.

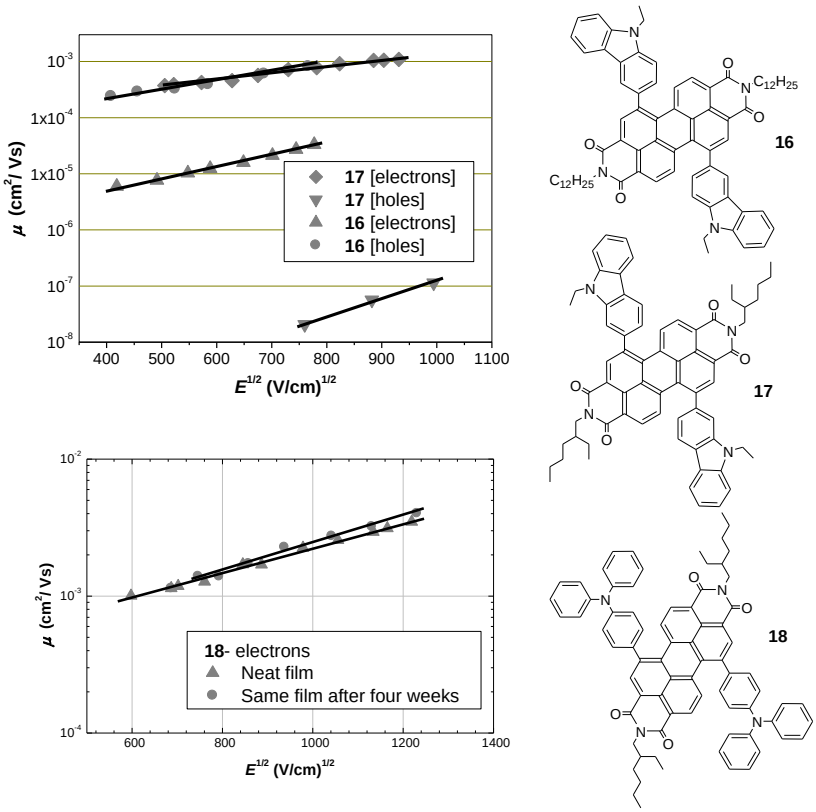

Figure 4.9 The electric field dependencies of charge mobilities of **16-18** in air. [§]

The room temperature electric field dependencies of hole and electron drift mobility values for the thin films of perylene bisimide derivatives **15-18** are given in Figure 4.9. The linear dependencies of hole/electron-drift mobilities on the square root of electric field E are observed. In all cases charge drift mobility may be well approximated by Poole–Frenkel relationship: $\mu = \mu_0 \exp(\alpha\sqrt{E})$, where α is the field dependence parameter and μ_0 is the zero field mobility obtained by extrapolating the linear dependencies to zero electric field [157,158].

Table 4.4 XTOF charge mobility data of **15- 18**.

Compound	Electrons			Holes		
	μ_0	μ	α	μ_0	μ	α
[a]**15**	1.4×10^{-8}	1.2×10^{-6}	0.0045	1.2×10^{-7}	9.2×10^{-6}	0.0044
16	7.3×10^{-7}	8.9×10^{-5}	0.0021	5.8×10^{-5}	1.7×10^{-3}	0.0034
17	9.2×10^{-5}	1.4×10^{-3}	0.0027	8.1×10^{-11}	1.2×10^{-7}	0.007
18	2.8×10^{-4}	2.3×10^{-3}	0.0021	-	-	-

Zero-field mobilities (μ_0) in $cm^2\ V^{-1}\ s^{-1}$, mobilities (μ) in $cm^2\ V^{-1}\ s^{-1}$ at an electric field of 10^6 V cm^{-1} and field dependences (α) in $(cm\ V^{-1})^{1/2}$ of holes and electrons in solid layers. [a]Solid solution [(**15**+ PC-Z) 1:1; Wt.]

The highest electron mobility is observed for **18** containing triphenylamino moiety at the bay region and its value well exceeded 10^{-3} $cm^2V^{-1}s^{-1}$ at high electric fields. Electron drift mobility values of **18** have also been measured after several weeks in order to evaluate the charge-transporting stability in ambient conditions and it was found that they are almost insensitive to ambient storage. The combination of efficient charge carrier mobility and its ambient stability renders **18** particularly attractive for the fabrication of field effect transistors [159,160]. Compounds **15** and **16** exhibited similar pattern of ambipolar charge transportation. However, the magnitude of carrier mobility in the layer of compound **15** is less compared to that of **16** and it may be due to the less amount of chromophores in the solid solution layer of **15** (Table 4.4). It is interesting to compare the electron and hole-drift mobilities in compounds **16** and **17** since they exhibit reverse trends in charge transportation. Compound **17,** in which carbazolyl groups are linked to perylene bay *via* their 2-position, exhibits higher order of electron mobility ($>10^{-3}$ $cm^2\ V^{-1}\ s^{-1}$) than **16** ($>10^{-5}$ $cm^2\ V^{-1}\ s^{-1}$). However compound **16**, in which carbazolyl groups are linked to perylene bay *via* their 3-position, displays higher order of hole mobility ($>10^{-3}$ $cm^2\ V^{-1}\ s^{-1}$) than **17** ($>10^{-7}$ $cm^2\ V^{-1}\ s^{-1}$). It should be noted that **16** and **17** differ in the position of covalent linking of carbazolyl groups to the perylene bisimide core. Therefore the observation of these complementary charge carrier mobilities just by changing the linking topology of the carbazolyl groups to the perylene core is quite remarkable.

[§]*I_p and charge mobilities were measured at Department of Solid State Electronics, Vilnius University.*

DFT Calculations

Quantum chemistry studies were performed for carbazolyl- and triphenylamino-substituted perylene bisimides **15**, **17** and **18** in order to acquire a deeper insight into their frontier molecular orbitals (FMOs), energy distribution, band-gap energies *etc* since these compounds showed interesting optical and electrical characteristics. As demonstrated by quantum chemical calculations, all molecules studied consist of three distinct structural elements: the central, perylene bisimide part and two electron-donor chromophores attached at the bay region. Figure 4.10 shows the structure of **18** identified as minimum on the potential energy surface. The perylene bisimide part was predicted to be planar [161] whereas in bay substituted derivative the planarity of the perylene part was broken: for example, the distortion of the carbon atoms connected to the triphenylamine groups is less than 8^{o} (related to the ring plane).

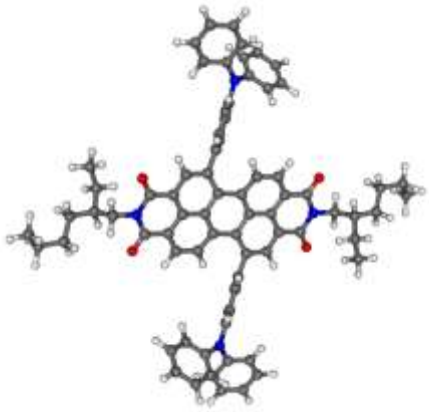

Figure 4.10 Structure of **18** predicted by DFT calculations.

Another interesting feature is the shape of HOMO and LUMO orbitals. For compound **18,** as can be seen from Figure 4.11, the shape of the HOMO orbital suggests that the maximal electron density is mainly on the triphenylamine moiety and also extends to the aromatic core. This is consistent with the spectroscopic and electrochemical data which give strong evidence of the electron donating effect of the amine substituent. However, the LUMO orbital is localised in the electron-deficient perylene bisimide part as reported before [161].

Figure 4.11 (A & B) demonstrates the calculated frontier orbitals for molecules **15** and **17**. HOMO and LUMO energy levels of these molecules established by quantum chemical calculations are summarised in Table 4.5. As seen earlier with the perylenes, these molecules also behave in a similar way with their LUMO mainly localised on the perylene bisimide core [161]. However, there is a considerable difference observed between the HOMO orbitals of species **15** and **17**. In compound **15**, it is seen that the HOMO is distributed evenly on the perylene ring as well as on both the carbazole units. However in **17**, HOMO is more localised on one of the carbazole units unlike in **15**. Figure 4.11(C) demonstrates the FMO for molecule **17** at two different isosurface values; (a) [same as in 4.11(A)] and (b). It clearly shows

that the HOMO being spanned throughout the molecule; but not evenly like in **15** and centred mainly on one of the carbazoles. Thus it is evident that the carbazole substitutions enhance a considerable difference in the HOMO orbitals of **15** and **17**, when there is a difference in their attachment at the bay position of perylene bisimides. Calculated band-gaps for these molecules were found to be 2.33 eV and 2.41 eV respectively for species **15** and **17**. Though the band gap energies calculated seems to deviate by a small factor from the experimentally determined ones, but this owes to the fact that the quantum chemistry calculations are performed at vacuum and the crystalline nature of the model.

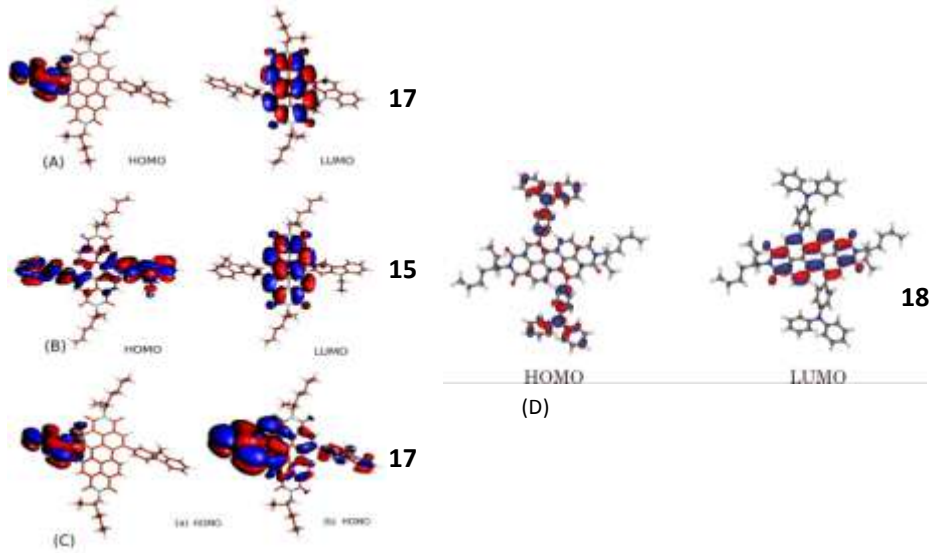

Figure 4.11 HOMO and LUMO orbitals for the molecules **17** (A), **15** (B) and **18** (D) as obtained from DFT calculations. (C) HOMO orbitals for molecule **17** at two different isosurface values.

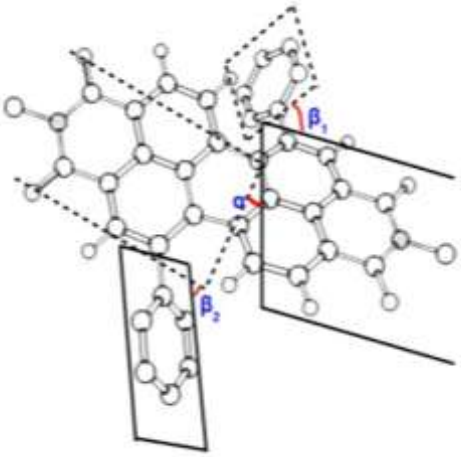

Figure 4.12 Schematic to demonstrate different twist angles in carbazole substituted perylene bisimides. For clarity instead of carbazolyl moieties only phenyl groups are shown.

Another important feature to address here is the twisting of the perylene core (α) and the twisted bay substitution (β) of carbazoles around the perylene bisimide as these parameters play a significant role in defining the properties of these materials. Figure 4.12 demonstrates different twisting angles in these molecules and their values are described in Table 4.5. The calculations imply that the dihedral angle (α) for both **15** and **17** is ~20^0 as reported with perylenes before [161]. As far as the torsional angle (β) is concerned, it's seen that **15** possess a twisting angle of ~57^0 (both β_1 and β_2) and that of **17** is found to be ~56^0 (β_1) and ~62^0 (β_2). Thus here, it can be seen that there is a considerable difference in β angles between **15** and **17**. It is clearly noticeable that β_1 for **15** and **17** are similar, but β_2 shows a deviation by ~6^0. This is also quite visible in their FMOs, as in **17**, for which it can be seen that the electron cloud is much concentrated on one of the carbazoles where it makes more inclination with the perylene core. This might be due to the existence of strong twist between two chromophoric sub units that in turn is limiting the spatial orbital overlap [162]. This could be the reason for the different optical and complementary charge transporting properties of these regioisomers.

Table 4.5 HOMO, LUMO and various angles of **15, 17** and **18** from DFT calculations.

Compound	E_{HOMO}/eV	E_{LUMO}/eV	E_g /eV	α^0	$\beta_1{}^0$	$\beta_2{}^0$
15	-5.61	-3.28	2.33	19.2	57.9	56.03
17	-5.77	-3.36	2.41	20.66	56.77	61.73
18	-5.10	-3.21	1.89	-	-	-

E_g - Band gap. (α) - Perylene core twisting (dihedral) angle. (β_1, β_2) - torsional angles of carbazoles with perylene core.

Supramolecular Organization

Supramolecular organization of compound **18** was thoroughly studied by X-ray diffraction method. Taking into account the shape of this molecule, which contain nonplanar triphenylamine substituents attached to the perylene core, it can be expected that their crystallization may be difficult. The X-ray profiles of **18** are compared in Figure 4.13. Surprisingly, **18** powder seems to crystallize in a 3D structure. Interestingly enough, when this compound is deposited on a Si substrate by spin coating different result is obtained. Compound **18** exhibits some crystallinity and yields a diffraction pattern which is somehow characteristic of liquid-crystal smectic like phase. For such phases the only well-defined Bragg reflections appear at low angles and can be attributed to a long interlayer period. No ordering takes place in the two other directions, as indicated by the poorly defined X-ray profiles for intermediate and high scattering angles values. No evident solution was found for indexing the three low angle Bragg peaks of **18** thin layers on Si centred at 18.1 Å, 26.5 Å and 30.4 Å.

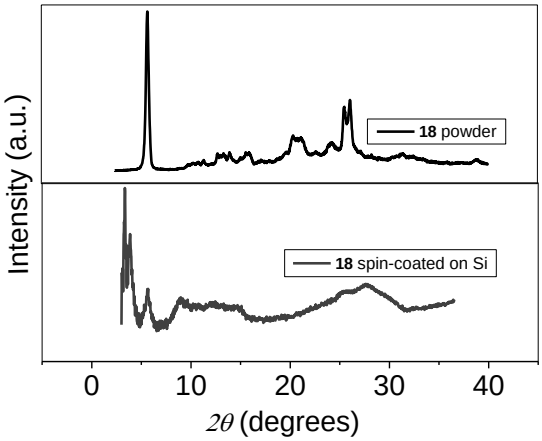

Figure 4.13 X-ray profiles of powder and thin layer of **18**.

It is known that the electronic properties of perylene bisimide-based semiconductors are very sensitive to their supramolecular organization - high electron mobilities are obtained only for well structured layers [163]. Compound **18** can be considered as a hybrid of triphenylamine and perylene bisimide. From this point of view it is tempting to verify how the limited structural organization of its thin layer (smectic liquid crystalline-type) influences the electrical transport properties in this semiconductor. For this reason we have fabricated and tested field-effect transistors based on this semiconductor.

Ambipolar organic field-effect transistor using compound 18 as active layer

Taking into account of the redox characteristics and structural property of compound **18**, it could be considered as a promising candidate for the fabrication of one-component ambipolar transistor. Charge transport behaviour of this semiconducting material has been evaluated in top gate staggered field-effect transistor geometry. The configuration of OFET fabricated using 18 is shown in the Figure 4.14.

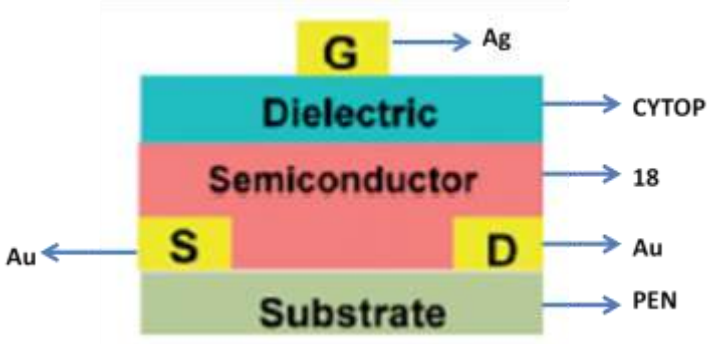

Figure 4.14 Geometry of top gate staggered OFET fabricated using **18**.

Devices have been measured both in p-channel and n-channel biasing conditions. The source and drain electrodes were treated with self-assembled monolayer (SAM) such as 4-methoxythiophenol (4-MTP) and pentafluorobenzenthiol (PFBT) in order to promote the electrons and holes transports, respectively. In the case of **18**, the molecule which is perylene-core substituted with triphenylamine, a well pronounced ambipolar behaviour is observed (see ambipolar transfer characteristics in Figure 4.15).

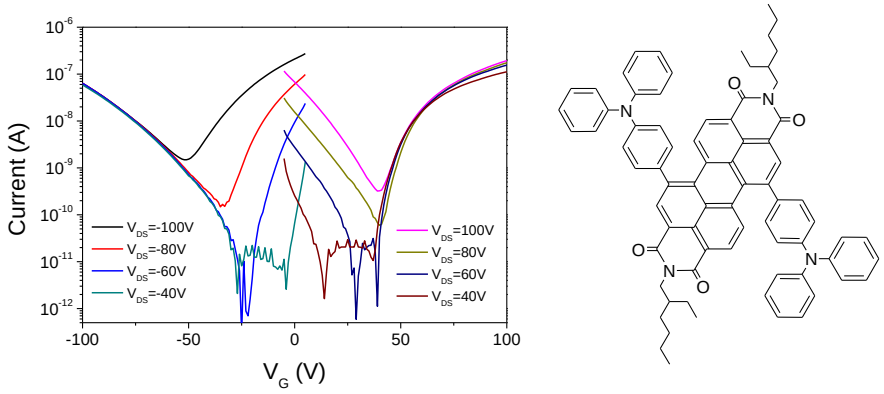

Figure 4.15 Typical ambipolar transfer characteristic of a transistor (L=40µm-W=9mm) made of **18**; source and drain contacts treated with 4-methoxythiophenol (4-MTP).¥

Perfluoronated polymer such as CYTOP, used here as a dielectric layer, tends to minimize trapping of electrons and holes at the dielectric-semiconductor interface and well promotes the ambipolar transport. Both charge polarities mobilities seem to be affected by the injecting electrodes as shown in Table 4.6. The hole-mobility varies by an order of magnitude, from 1.8×10^{-4} to 1.5×10^{-3} $cm^2\ V^{-1}\ s^{-1}$, by changing the work function of gold with SAM treatments. The highest holes mobility is observed with the PFBT. The presence of SAM shifts the gold surface work function to a deeper value [164] and leads to a better electrical match between the gold electrodes work function and the HOMO energy level (~5.31 eV) of **18**. Similar increase in hole-mobility is observed by treating the electrodes with oxygen plasma which also increases the work function of gold [165]. One would expect the electron-mobility to vary inversely to the hole-mobility by shifting the work function of the electrodes. In our case, the electron mobility is less influenced by the electrode pre-treatment. Surprisingly, however, both SAM treatments, i.e., with 4-MTP or with PFBT lead to ca. 2- to 3-fold increase in the electron mobility as compared to transistors in which the electrodes surface has not been activated by the pre-treatment with SAMs. This behaviour has already been observed in other ambipolar devices [165]. One should be aware of the fact that the SAM covered surface could affect the charge carriers mobility in different ways. Apart from the induced modification of contact resistance by changing the metal work function, it could also change the morphology of the semiconductor on the top of the electrode and in the transistor channel [119]. Other factors may influence the mobility such as interfacial tunnelling through the SAMs or a change in the underlying

semiconductor layer thickness induced by the change of the surface tension originating from the presence of SAM [165]. All the above outlined mechanisms could explain why SAMs, which are supposed to degrade the contact resistance for a given type of carriers, can in fact increase their mobility.

Table 4.6 Hole and electron mobilities of ambipolar transistors fabricated from **18** applying different source and drain treatments prior to the semiconductor deposition.

Electrode treatment	Hole mobility ($cm^2 V^{-1}s^{-1}$)	Electron mobility ($cm^2 V^{-1}s^{-1}$)
4-methoxythiophenol	$1.8x10^{-4}$ +/- $8x10^{-5}$	$2.9x10^{-4}$ +/- $4x10^{-5}$
None	$2.0x10^{-4}$ +/- $7x10^{-5}$	$1.3x10^{-4}$ +/- $2x10^{-5}$
Oxygen plasma	$1.0x10^{-3}$ +/- $2x10^{-5}$	$1.2x10^{-4}$ +/- $4x10^{-5}$
Pentafluorobenzenthiol	$1.5x10^{-3}$ +/- $2x10^{-4}$	$3.5x10^{-4}$ +/- $4x10^{-5}$

At the end it should be stressed that the fabricated ambipolar transistors operate in air. Periodical tests carried out during more than 100 days of their storage in laboratory air did not show any sign of the electrical parameters worsening. In view of the fact that organic semiconductors suitable for air operating, one-component ambipolar transistors are still very scarce, the example presented here makes perylene bisimides core substituted with electron-donors; for example, triphenylamine, a promising new class of semiconductors for robust organic electronic devices.

[¥] *Ambipolar OFET was fabricated at Laboratoire d'Electronique Moleculaire Organique et Hybride, CEA Grenoble.*

4.1.2. Fluorene and thiophene substituted naphthalimides

Naphthalimide derivatives, as electron deficient moieties, have been used in supramolecular assemblies, photovoltaic devices and n-type organic field-effect transistors [166,167]. 1, 8-naphthalimide derivatives having an electron-donating substituent at the 4-position are reported to show interesting photophysical properties [168]. N–alkyl naphthalimides can be substituted with different electron donating moieties at the core and it is possible to prepare different coplanar molecular structures containing donor-acceptor hybrids. This kind of substitution may change the glass transitions, shift the photoluminescence wavelengths, change the quantum yields, shift the redox potential and improve the photoelectrical characteristics. Here, we have functionalized 1, 8-naphthalimide with fluorene and thiophene electron-donating moieties and studied the properties of the obtained materials. Electron-donor spacers were sandwiched between naphthalimide moieties *via* the 4-position which enhanced the conjugation length and generated solution processable donor-acceptor hybrids.

Synthesis and Characterization

Fluorene based compound **22** containing boronic acid pinacol ester functionalities at 2, 7- positions was synthesised according to the Scheme 4.5. In the first step, 2, 7-dibromo fluorene was alkylated using excess of iodoethane in DMSO in the presence of potassium *ter*-butoxide. In the next step, borylation reaction was carried out in THF in the presence of n-butyl lithium.

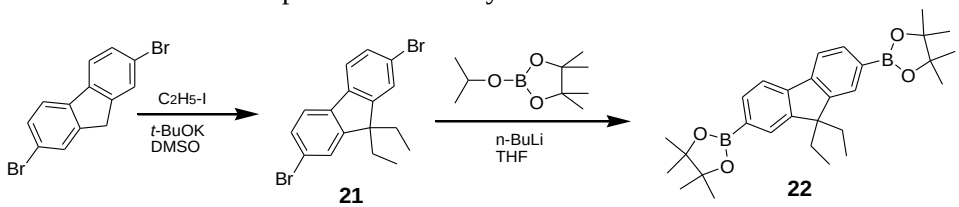

Scheme 4.5 Synthesis of 9,9-Diethyl-9*H*-fluoren-2,7-yl diboronic acid pinacol ester.

The donor-acceptor hybrid materials **24-26** were synthesised by Suzuki-Miyaura coupling reactions as shown in Scheme 4.6. Simple donor-acceptor (D-A) pair **24** containing naphthalimide acceptor and fluorene donor was prepared by the reaction between **23** and mono boronic acid ester derivative **9**. The sandwich-like molecules, acceptor-donor-acceptor (A-D-A), **25** and **26** were synthesised from diboronic acid pinacol ester derivatives of fluorene (**22**) and thiophene (2, 5-thiophenediylbisboronic acid, **TB**), respectively.

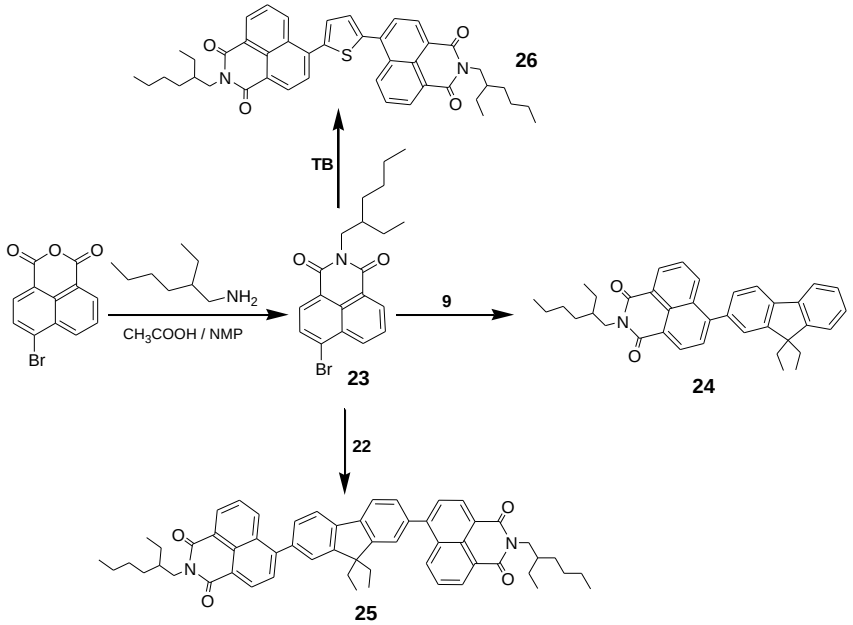

Scheme 4.6 Synthetic route for the preparation of naphthalimides **24-26**. *Reagents and conditions*: $Pd(Ph_3)_2Cl_2$, KOH, THF–H_2O, 80 °C, 8–12 h.

The structures of **24**−**25** were confirmed by IR, ^{1}H NMR, ^{13}C NMR spectra, mass spectrometry and elemental analysis data. ^{1}H NMR spectra of compounds **23** and **26** are compared in the Figure 4.16.

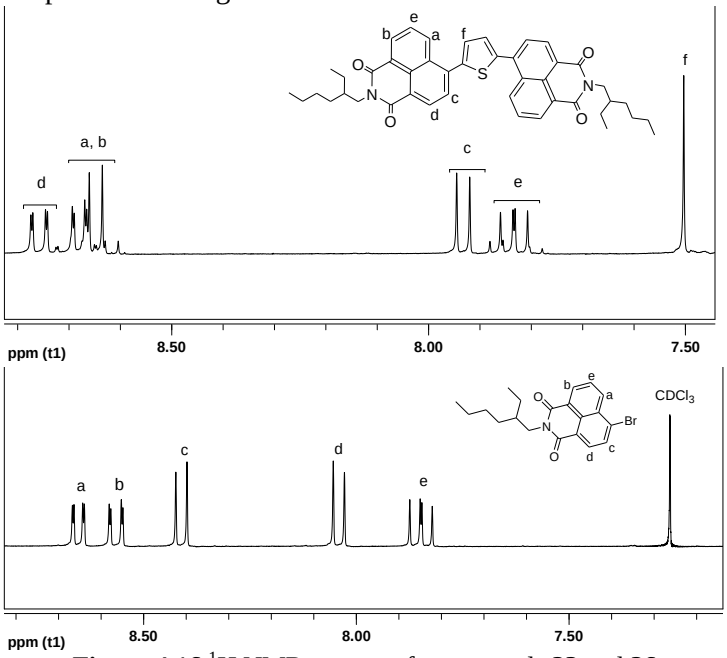

Figure 4.16 ^{1}H NMR spectra of compounds **23** and **26**

The singlet (f) appeared at 7.50ppm, corresponding to two equivalent thiophene protons, together with the large shift in the chemical shift value of naphthalimide confirms the formation of A-D-A compound **26**. Noted shielding (δ_{shift} = 0.49 ppm) of proton marked "**c**" indicates the influence of thiophene electron-donor attached to naphthalimide core. Protons marked "**b** and **d**" are largely deshielded in **26** compared to compound **21** that suggests the strong influence of electron-withdrawing carbonyl groups in the molecule.

Properties of naphthalimide derivatives containing electron-donors

Thermograms of compounds **24-26** as obtained from DSC analysis are shown in Figure 4.17. All the compounds show melting transitions during the first heating scan, which ranged from 143- 179 ^{o}C. When the materials are cooled from the melt, they clearly revealed the glass transition behaviour. T_g of naphthalimide derivatives are in the range of 30-76 ^{o}C (Table 4.7). It is found that both the nature of electron-donor and the molecular size influence the glass transition temperatures of naphthalimide derivatives.

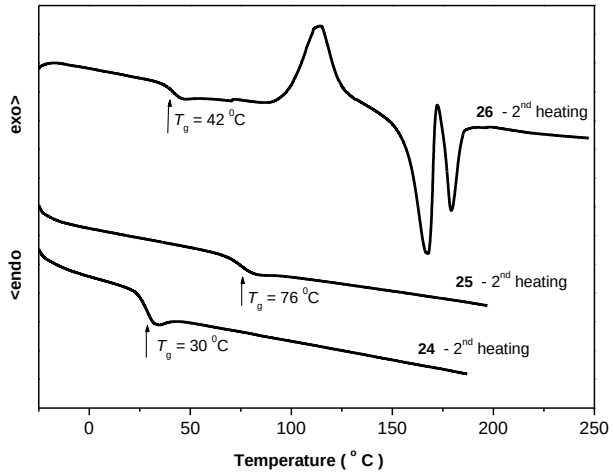

Figure 4.17 DSC thermograms of compounds **24-26**.

Fluorene containing compounds display similar melting transitions whereas the glass transition temperatures differ by 46 ^{o}C; the sandwich compound **25** containing two naphthalimide units shows higher value. Interestingly the thermal behaviour of compound **26** containing thiophene electron-donor moiety is different from that of fluorine-containing compounds **24** and **25**. During the first heating scan, compound **26** showed only endothermic melting transition at 179 ^{o}C. When it was cooled from the melt, it formed amorphous phase by exhibiting a glass transition at 42^{o}C. Upon further heating, this compound crystallised at 114 ^{o}C. During this crystallization process the molecules might be organised in different ways in the crystal lattice and hence, showed two melting transitions at 167 ^{o}C and 179 ^{o}C, respectively, on heating.

Table 4.7 Thermal characteristics of **24- 26.**

Compound	T_g / °C	T_{cr} / °C	T_m / °C
24	30	-	143
25	76	-	145
26	42	114	167, 179

Electrochemical investigation of compounds **24-26** were carried out in dichloromethane in order to elucidate the redox process and to establish HOMO-LUMO energy levels since they are important for device applications. The CV profiles of compounds **24-26** are given in Figure 4.18 and the oxidation and reduction potentials and values of HOMO-LUMO energy levels are collected in the Table 4.8.

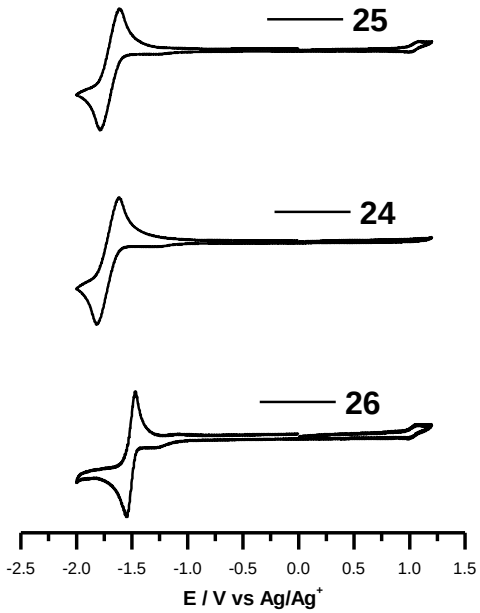

Figure 4.18 Cyclic voltammograms of compounds **24-26**.

As can it be seen from Figure 4.18, all the compounds exhibit a reversible reduction process corresponding to the reduction of naphthalimide moiety to a radical anion. This reduction behaviour clearly demonstrates the electron deficient nature of these naphthalimide derivatives. The reduction potential of fluorene containing compounds is quite similar; whereas for the compound **26** containing thiophene electron-donor moiety, the reduction process is shifted more to the positive voltage side. This observation apparently suggests the less electron affinity and in turn, lowers LUMO energy level of compound **26** compared to those of the fluorine-containing compounds. Compounds **25** and **26** also shows oxidation redox process corresponding to the oxidation of fluorene and thiophene electron-donors,

and their HOMO energy levels are located at 5.58 and 5.60 eV, respectively, with respect to the vacuum level. The LUMO energy levels of compounds **24-26** range between 3.02 eV and 3.21 eV with respect to the vacuum level and are in agreement with those of naphthalimide containing hydrazones [169]. The critical position of LUMO levels suggests the application of these materials as electron-transporting compounds in organic electronics.

Table 4.8 Electrochemical characteristics of compounds **24-26**.

Compound	E_{red}/V	E_{oxi}/V	E_{LUMO}/eV	E_{HOMO}/eV	E_g^{ele} /eV
24	-1.81	-1.61	-3.02	-	-
25	-1.79, 1.01	-1.60, 1.08	-3.04	-5.58	2.54
26	-1.54, 0.99	-1.47, 1.06	-3.21	-5.60	2.39

Xerographic time-of-flight measurements were used to characterize the semiconducting properties of these compounds. It was found that the fluorene-containing naphthalimide derivatives were able to transport electrons. Figure 4.19 demonstrates the electric field dependencies of electron-drift mobilities of the amorphous film of compound **24**.

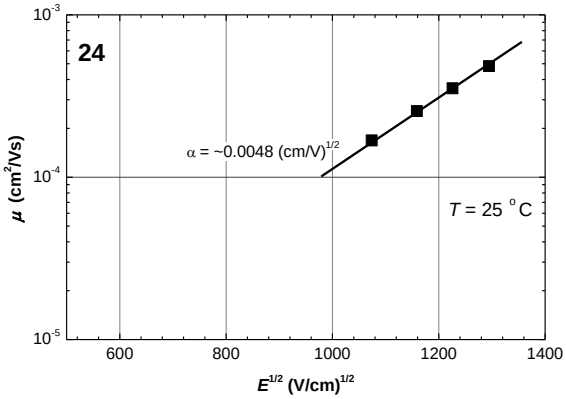

Figure 4.19 Electric field dependencies of electron-drift mobilities of the amorphous film of compound **24**.

Dispersive electron-transport was observed in the amorphous layers of compounds **24** and **25** coated on aluminium by solution processing technique. However, electron-drift mobility in the layer of **25** was not possible to estimate due to the enhanced dispersity of electron-transport. For the amorphous film of compound **25**, the linear dependency of electron drift-mobility on the square root of the electric field was noted at room temperature. This characteristic dependence was observed for the majority of amorphous organic systems and could be attributed to the effects of disorder on charge-transport [170]. The room temperature electron drift-mobility value of fluorene containing naphthalimide **24** well exceeded 10^{-4} cm^2 V^{-1} s^{-1} at high electric field in air.

4.2. Glass-forming carbazolyl- and phenothiazinyl- tetra substituted pyrene derivatives

Dendritic molecules with well defined structure are of high scientific interest since their molecular size reaches the nanometres domain which brings them unique chemical and physical properties important for device applications [171]. The physical properties of star-shaped compounds can be tuned either by changing the core or by changing the arms. Accordingly various functional chromophores with different core-arms combinations have been reported [49,172,173]. Palladium catalyzed cross-coupling reactions like Suzuki reaction, Heck reaction, Stille cross coupling or Sonogashira coupling have successfully been proved as convenient synthetic approaches for the preparation of compounds of such kind.

Organic materials consisting of well-known polycyclic planar aromatic system, pyrene as a core, functionalized with different electron-donating chromophores as arms were employed as hole-transporting materials in various optoelectronic and electronic devices [43,174,175]. Additionally, such kind of architecture could facilitate the hole-injection by tuning the highest occupied molecular orbital (HOMO) energy level. On the other hand, the carbazole molecular moiety as electron-donors has been well exploited for the preparation of both low-molar-mass and polymeric organic electroactive materials since they possess good chemical, environmental and electrochemical stability and the versatility in functionalization [176,177]. The electron-rich phenothiazine derivatives were also extensively exploited in organic electronics because of their unique electro-optical properties and the resulting potential in diverse applications like OLEDs or electrogenerated chemiluminescence [178,179]. Keeping these facts in mind we designed and synthesized pyrene-core based derivatives with the arms of differently linked carbazole (regioisomers) and phenothiazine moieties. Properties of the derivatives were examined by performing thermal, optical, photophysical, electrochemical and photoelectrical measurements.

Synthesis of pyrene compounds with the arms of differently linked carbazoles and phenothiazines

The key intermediate, 9-dodecyl-*9H*-carbazol-3-yl boronic acid pinacol ester **28**, for the preparation of **32** was synthesised from 3-bromo carbazole (Scheme 4.7). N-alkylation of 3-bromo carbazole was carried out in DMF using 1-bromododecane in the presence of potassium hydroxide. Subsequently it was borylated using 2-isopropoxy- 4, 4, 5, 5-tetramethyl-1, 3, 2-dioxaborolane as reported before.

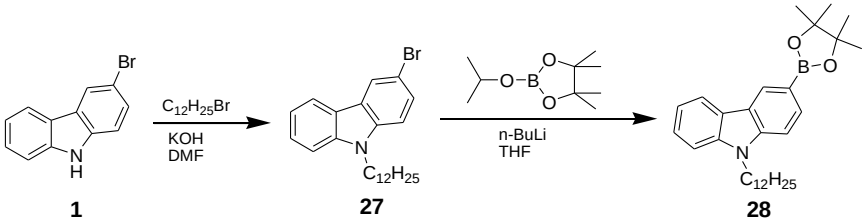

1 **27** **28**

Scheme 4.7 Synthesis of 9-dodecyl-*9H*-carbazol-3-yl boronic acid pinacol ester (**28)**.

The pyrene-core centred materials, i.e. compounds **29-32**, were synthesised from 1, 3, 6, 8-tetrabromopyrene by Suzuki-Miyaura coupling reactions in THF/water mixture in the presence of bis(triphenylphosphine) palladium(II) dichloride catalyst as described in Scheme 4.8.

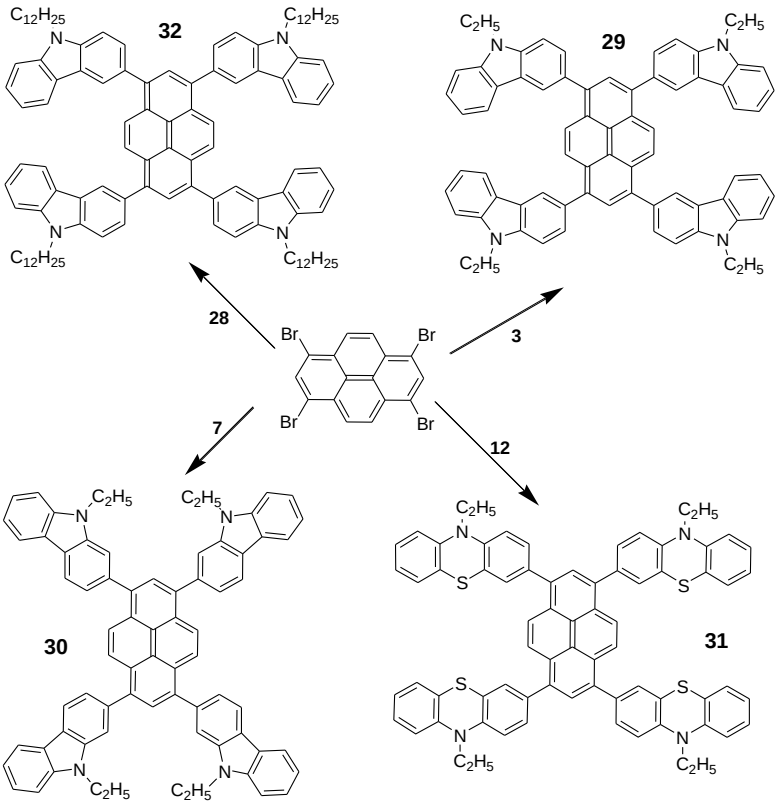

Scheme 4.8 Synthetic route for the preparation of pyrene core-centred compounds **29-32**. *Reagents and conditions*: $Pd(Ph_3)_2Cl_2$, K_2CO_3, THF–H_2O, 80 °C, 8–12 h.

The synthesized compounds were purified by column chromatography and characterized by NMR and IR spectroscopy, MALDI-TOF and elemental analysis. The spectral and elemental analysis data are in good agreement with their chemical structures.

Thermal properties

The behaviour under heating of compounds **29-32** was studied by DSC and TGA under a nitrogen atmosphere. The values of glass transition temperatures (T_g) and the temperatures of the onsets of the thermal decomposition (T_{ID}) are collected in Table 4.9. Figure 4.20 shows DSC thermograms of compound **29**.

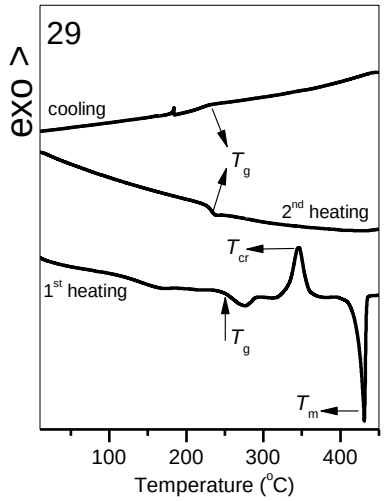

Figure 4.20 DSC thermograms of compounds **29**. Heating/cooling rate: 10 °C min^{-1} under nitrogen atmosphere.

Compounds **30** and **31** were isolated after the synthesis and purification as crystalline materials. However they could be transformed into the amorphous state by cooling from the melt. For compound **29**, the first heating scan showed a glass transition followed by a structural relaxation through crystallization at 345 °C and a melting transition at 431 °C (Figure 4.20). However, the cooling scan and the second heating scan only showed glass transitions and not any other kind of thermal transitions such as crystallization or melting, which clearly demonstrated the transformation of crystalline phase into the morphologically stable amorphous (glassy) phase. Compounds **29-31** showed very high T_g ranging from 211 to 232 °C. Compound **32** was isolated after the synthesis and purification as amorphous material and exhibited T_g just above the room temperature.

Table 4.9 Thermal characteristics of compounds **29-32**.

Compound	T_g °C	T_m °C	T_{ID} °C
29	232	431	537
30	216	409	512
31	211	324	418
32	32	-	452

All the synthesized pyrene derivatives (**29-32**) exhibited high thermal stability with the decomposition onsets ranging from 418 to 537 °C. It was found that both the attached chromophores and the N- alkyl substituents affect the thermal stability of pyrene derivatives. The thermal stability of topological isomers **29** and **30** were comparable whereas the compound **32** with longer N-alkyl substituents displayed lower degradation temperature. The phenothiazinyl derivative exhibited lower thermal decomposition temperature compared to the carbazolyl derivatives.

Optical and photophysical properties

Absorption and PL spectra of dilute solutions in THF, dilute solid solutions in PS and neat films of the pyrene derivatives (**29**-**32**) are depicted in Figure 4.21. The details of the optical properties of the derivatives are summarized in Table 4.10.

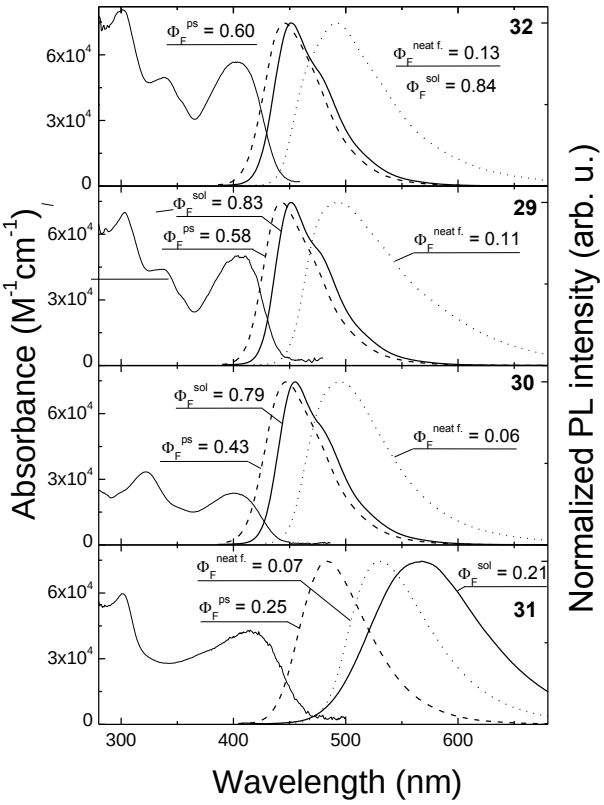

Figure 4.21 Absorption spectra of the pyrene derivatives **29**-**32** in dilute THF solutions (thin solid line) and normalized PL spectra of the derivatives **29**-**32** in dilute THF solutions (thick solid line), dilute solid solutions in PS (0.25 wt %) (thick dashed line) and neat films (thick dotted line). Estimated fluorescence quantum yields (Φ_F) indicated.*

The compounds **29** and **32** differing only in the alkyl chain length of the carbazole moiety shows very similar spectral properties in the dilute solutions, PS matrixes and in the neat films. As expected, Φ_F of the two compounds in a diluted form (in solution or PS matrix) are also nearly the same, i.e. 0.83-0.84 in the solution and 0.58-0.60 in the polymer matrix. Interestingly, a difference in the alkyl chain length of the compounds **29** and **32** has almost no effect on the PL spectrum and PL quantum yield of the neat films, which most likely signifies similar amorphous packing of the films prepared by solution-casting technique**.** The lowest energy absorption band of the carbazole-substituted pyrene derivatives **29, 30** and **32** is located at about 403 nm irrespectively of the linking (2- or 3-position) topology of the carbazole moiety, followed by alike Stokes shifts. This result

indicated similar conjugation length for the carbazol-2-yl as well as for the carbazol-3-yl substituted pyrene derivatives. Note somewhat weaker absorbance of the band at 403 nm for the derivative **30** solution as compared with that for the derivatives **29** and **32.** This correlates with slightly decreased Φ_F (0.79) of the compound **30** solution. Taking into account that the onset of absorption of individual pyrene and carbazole moieties is below 350 nm with PL emerging at 355-375 nm,[180,181,182] the considerably red-shifted spectra of the studied pyrene derivatives clearly point out extension of the pyrene-core conjugation to the carbazole arms. This is also in agreement with a strong enhancement of $S_0 \rightarrow S_1$ transition of pyrene substituted at 1-, 3-, 6- or 8- positions; however, in the case of unsubstituted or 2-, 7-substituted pyrene which has vanishingly small oscillator strength [183]. More detailed analysis of the lowest energy absorption and fluorescence band shapes of the pyrene derivatives **29, 30** and **32** in dilute solutions reveal that they are not mirror images of each other. Particularly, the absorption bands are broad and unstructured, whereas several vibronic modes can be resolved in PL spectra. The presence of the vibronic replicas in the PL indicates enhanced molecule rigidity in the excited state as compared to that in the ground state. It is likely that in the ground state the singly-bridged carbazole substituents are twisted in respect to the pyrene core due to the steric hindrance. Highly non-planar geometry of the molecule facilitates intramolecular torsional motions, which smear out vibronic structure of the absorption band. As opposed to this, in the excited state the twist angle between carbazoles and pyrene core reduces so that molecule becomes more planar, and thus expresses enhanced conjugation and rigidity. To verify the planarization of the pyrene derivatives upon excitation, the derivatives were introduced into rigid polymer matrixes at low concentration (0.25 wt %) where molecule twisting in the excited state was suppressed [184]. Unable to planarize the derivatives exhibited reduced Φ_F as well as slightly blue shifted PL spectra due to reduced conjugation in PS matrix as compared to those in solution (Figure 4.21). This result in turn confirms a tendency of the singly-bonded carbazole-substituted pyrene derivatives **29, 30** and **32** to planarize in the excited state resulting in the increased conjugation and emission efficiency.

Table 4.10 Absorption and fluorescence data of dilute (10^{-5} M) THF solutions, solid 0.25 wt % solutions in PS and neat films of carbazolyl- (**29,30, 32**) and phenothiazinyl- (**31**) substituted pyrene derivatives

	Solution				**Neat film**			**PS film**		
	λ_{abs}, **nm**	λ_{em}, **nm**	Φ_F	**τ, ns**	λ_{em}, **nm**	Φ_F	τ_{avg}, **ns**	λ_{em}, **nm**	Φ_F	**τ, ns**
29	403	451	0.83	1.6	493	0.11	1.7	443	0.58	1.8
30	400	455	0.79	1.5	496	0.06	1.3	446	0.43	1.5
31	415	567	0.21	2.1	533	0.07	0.9	483	0.25	1.6
32	403	451	0.84	1.7	491	0.13	1.8	445	0.60	1.9

PL spectra of the neat films of the pyrene derivatives **29, 30** and **32** are broadened and shifted to the long wavelengths by about 40 nm as compared to those of dilute solutions or solid solitions in PS. This can be attributed to the intermolecular interaction in the neat films. The bathochromic shift accompanied by the 6-13-fold reduction in Φ_F of the neat films in respect to that of the solutions can result from intermolecular coupling of exciton transition dipole moments promoting excitation migration *via* hopping process to nonradiative decay centres (distortions, defects *etc*).

Interestingly, pyrene derivative **31** with more polar phenothiazine arms (with respect to carbazole arms) exhibits different spectral behaviour. The absorption and PL spectra of **31** in dilute solution are much broadened, unstructured and significantly red-shifted. Large Stokes shift (of 150 nm) of the PL band can arise from photoinduced ICT, which is solvent polarity dependent [185]. A presence of ICT character in the derivative **31** was confirmed by spectral measurements in the solvents of different polarity, such as hexane, chloroform and THF. Indeed, the measurements revealed strong bathochromic shift of the PL maximum from 470 nm in non-polar hexane to 570 nm in polar THF while maintaining almost unchanged Φ_F. Since the Φ_F of the pyrene derivative **31** in the dilute solution (non-viscous medium) and in PS matrix (highly viscous medium) are also similar 0.21-0.25, molecular planarization in the excited state is unlikely. Thus, dramatic PL spectral shifts observed for the derivative **31** in different media, i.e. solution, polymer matrix and neat film are a consequence of ICT character of the derivative and results from the changes in polarity of the surroundings.

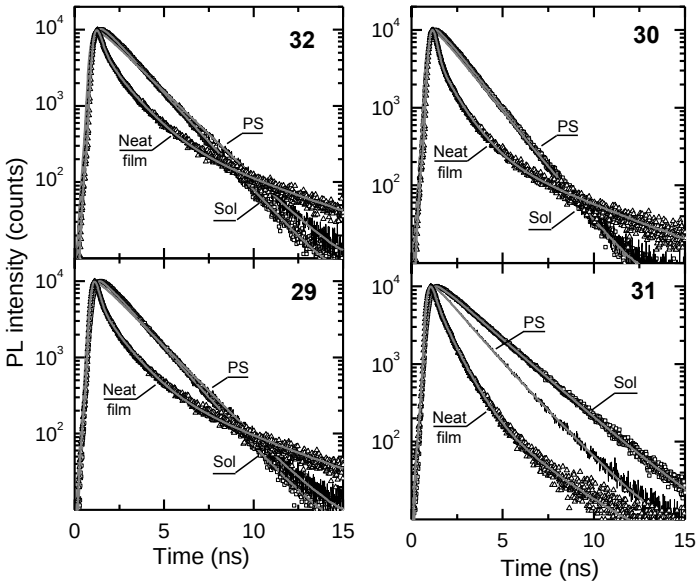

Figure 4.22 PL transients of dilute THF solutions, neat films and PS films (doped at 0.25 wt %) of the carbazole- (**29, 30, 32**) and phenothiazine-substituted (**31**) pyrene derivatives. Lines are single or multi-exponential fits of the data.[*]

[*]*Fluorescence quantum efficiencies were measured at Institute of Applied Research, Vilnius University by Dr. K. Kazlauskas.*

To study excited state relaxation dynamics in carbazole- and phenothiazine-linked pyrene derivatives, PL transients were measured (Figure 4.22). The carbazolyl-substituted derivatives **29, 30** and **32** in dilute solutions exhibited single exponential decay with decay time constants (τ) of 1.5 – 1.7 ns, whereas phenothiazinyl-substituted compound **31** showed slightly longer τ of 2.1 ns. PL decays of all the pyrene derivatives molecularly dispersed in the PS matrix at 0.25 wt % were found to be similar to those of their dilute THF solutions, whereas PL transients of the neat films expressed clearly non-exponential behaviour. The non-exponential transients with rapid excited state relaxation in an early stage (about 1-3 ns after excitation pulse) and prolonged relaxation at a later stage (about 5 ns after excitation) are typically observed in a solid state, where exciton migration and localization at lower energy states take place (spectral diffusion) [184]. During the initial exciton migration stage, migration-induced exciton quenching at nonradiative decay centres occurs, which drastically degrades Φ_F of the neat films of the pyrene derivatives (Figure 4.21). Localized at lower energy states excitons evade fast nonradiative decay, and therefore, exhibit prolonged relaxation times.

Electrochemical properties

The electrochemical behaviour of compounds **29-32** in dichloromethane was examined by cyclic voltametry. It was found that all compounds undergo multi-electron oxidation processes and the redox potentials were dependent on the molecular structure. A reversible redox process was observed for all the derivatives at low oxidation potential region (up to first oxidation peak) and a quasi-reversible characteristic was noted for the second oxidation peak. Figure 4.23 illustrates oxidation process of pyrene derivatives in dichloromethane.

The electrochemical investigation of 1 mM solution of pyrene in 0.1 M Bu_4NBF_4/DCM solution revealed the oxidation potential at 0.54 V versus Ag/AgCl calibrated against Fc/Fc^+ redox couple which suggested that the first oxidation potential of investigated compounds might be from pyrene core [186,187]. For compounds **29**, **30** and **32**, the second oxidation peak was in the range of 0.81 V to 1 V versus Ag/AgCl and was comparable with that of the previously reported carbazole derivatives [188,189]. Hence, the second oxidation process of these compounds can apparently be due to the presence of electron donor-substituents, i.e. carbazoles. Phenothiazinyl-substituted derivative **31** seems to be less stable in the electrochemical environment compared to the carbazolyl-substituted derivatives and assumed to be degraded during successive scanning.

Figure 4.23 shows pronounced increases in anodic current intensity for tetra carbazolyl substituted pyrene derivatives, **29**, **30** and **32**, during the successive voltametric scanning. This observation suggests the occurrence of electro-polymerization on the working electrode. A slight potential shift was observed in the oxidation redox process of compound **32** during the course of electro-polymerization which suggested the hindrance of the doping BF_4^- anions from doping-dedoping processes due to the presence of long dodecyl chains. The phenothiazinyl derivative **31** was not electro-polymerized on the anode. This might

be either due to the low solubility of **31** in dichloromethane since the electro-polymerization reactions are dependent on monomer concentration or due to the presence of less reactive phenothiazinyl tetra substituents unlike carbazoles. For electro-polymerization to be initiated minimum concentration of radical ions should be generated in the reaction medium which might be restricted, in the case compound **31**, due to the decreased availability of electroactive species in less concentrated electrolyte.

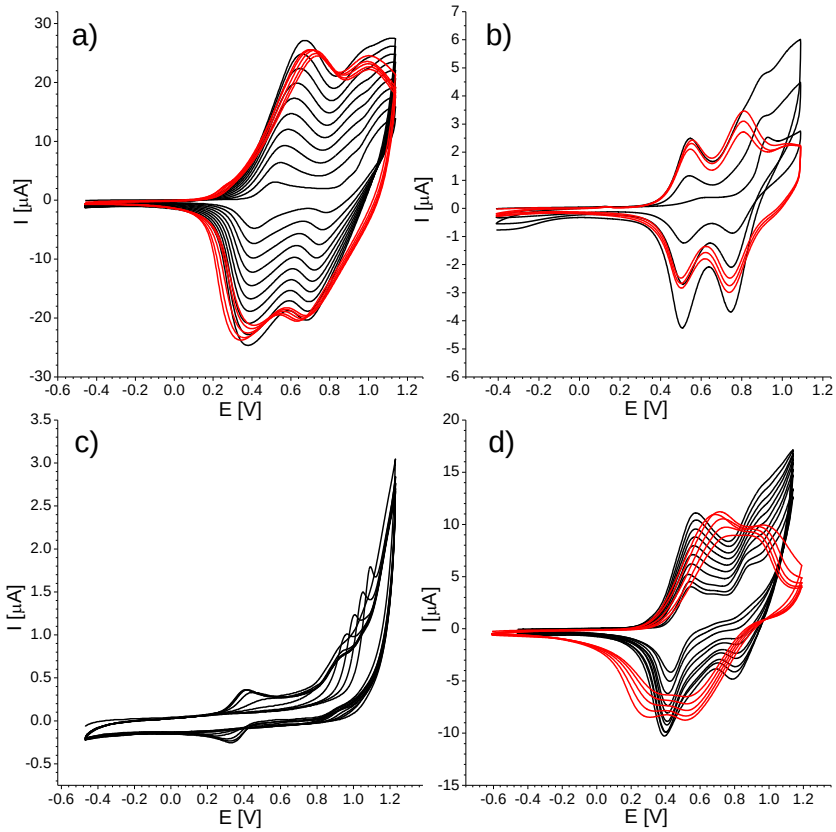

Figure 4.23 Cyclic voltammograms of pyrene derivatives (black lines) showing repetitive anodic sweeps at a platinum electrode immersed in a solution of compounds **29** (a), **30** (b), **31** (c) and **32** (d). Red lines demonstrate doping-dedoping process of their electrodeposited films in monomer free medium. Measurement conditions: scan rate 50 mV/s, Ag/AgCl reference electrode, 0.1 M Bu_4NBF_4/dichloromethane electrolyte.[£]

Figure 4.24 demonstrates the cyclic voltammograms of electrochemically generated polymers of **29**, **30** and **32** (**P29**, **P30** and **P32**, respectively) in monomer-free electrolyte. The redox potentials, HOMO–LUMO energy levels and the electrochemical bandgaps of **P29**, **P30** and **P32** are collected in Table 4.11. HOMO-LUMO values are calculated from the oxidation and reduction potential onsets obtained from cyclic voltametry.

As it can be seen from the CV profiles, carbazolyl-containing polymers are highly conductive and electrochemically stable. Electrochemically synthesized

polymers **P29**, **P30** and **P32** containing carbazole moieties were assumed to possess network like structures. Furthermore, the electro-polymerization might occur at the 6th position of carbazole moieties irrespective of the nature of monomers **29**, **30** and **32** in which carbazolyl groups are linked differently to the pyrene core. It is known that the 3rd and 6th positions of carbazole derivatives are more electron rich and hence, more reactive towards electro-polymerization compared to the 2nd and 7th positions [188]. Polymer **P30** possessed the lowest oxidation potential as compared to those of the other derivatives which might be due to the slight increase in effective conjugation length due to the presence of 2-substituted carbazolyl segments in the polymer backbone [190]. It is interesting to note that **P29** possessed the low-laying HOMO and LUMO levels compared to those of **P30**. Moreover, the electrochemically determined band gap was rather high for **P29** compared to that of **P30**. This observation can be explained by the greater distortion in 3-substituted carbazolyl derivative due to the benzidine-like linkage to pyrene core compared to 2-substituted carbazolyl derivative possessing terphenyl-like linkage which in turn, influences the effective conjugation length of the respective polymers [59,190,191]. Comparatively similar electrochemical band gaps of polymers **P29** and **P32** suggested that the electro-polymerization might occur through the same position (i.e. 6th position) of carbazole moieties albeit they differ slightly in the HOMO-LUMO levels.

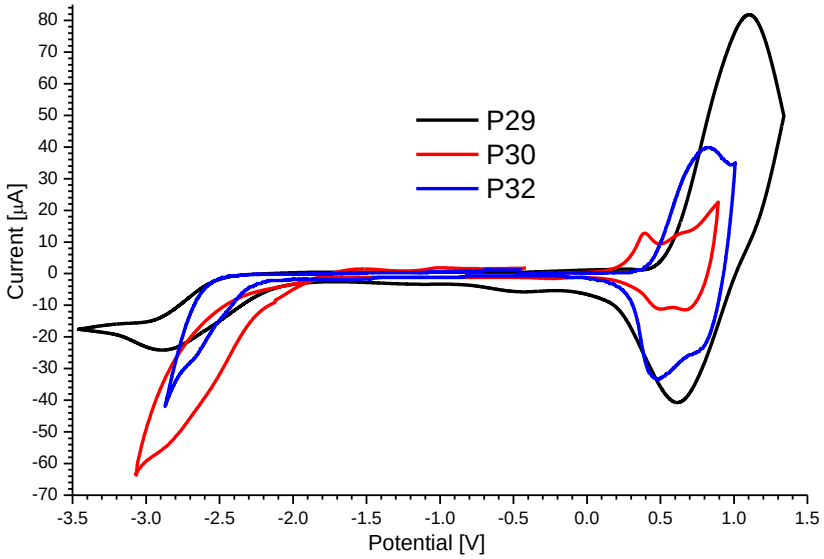

Figure 4.24 Cyclic voltammograms of electrodeposited polymers **P29**, **P30** and **P32** at platinum electrode in monomer free medium. Measurement conditions: scan rate 300 mV/s, Ag/AgCl reference electrode, 0.1 M Bu_4NBF_4/dichloromethane electrolyte. [£]

Table 4.11 Electrochemical characteristics of electro-deposited polymers **P29**, **P30** and **P32** (Potentials vs Ag/AgCl calibrated against Fc/Fc^{+}).

Compound	E_{ox1}/V	E_{red}/V	E_{ox1}^{onset}/V	E_{red}^{onset}/V	HOMO [eV]	LUMO [eV]	E_g^{el} [eV]
P29	1.1	0.61, -2.78	0.53	-2.11	-5.33	-2.69	2.64
P30	0.39	0.47, -2.29	0.3	-2.1	-5.1	-2.7	2.4
P32	0.82	0.45, -2.67	0.42	-2.27	-5.22	-2.53	2.69

DPV spectra of pyrene derivatives (**29**-**32**) are given in Figure 4.25. They give absolute peaks of oxidation processes. For all the pyrene derivatives, oxidation potential peaks are comparable with the oxidation potentials established from the CV profiles. The first oxidation potential is in the range of *ca.* 0.39 – 0.51 V and the second one is in the range of *ca.* 0.79-0.93 V. The oxidation peak located at *ca.* 0.8 V for the derivatives **30** and **32** indicates the presence of carbazolyl groups. The oxidation peak for phenothiazinyl derivative **31** is not as clearly observed as that for carbazolyl-substituted derivatives. This observation can apparently be explained by the lower concentration of **31** in solution.

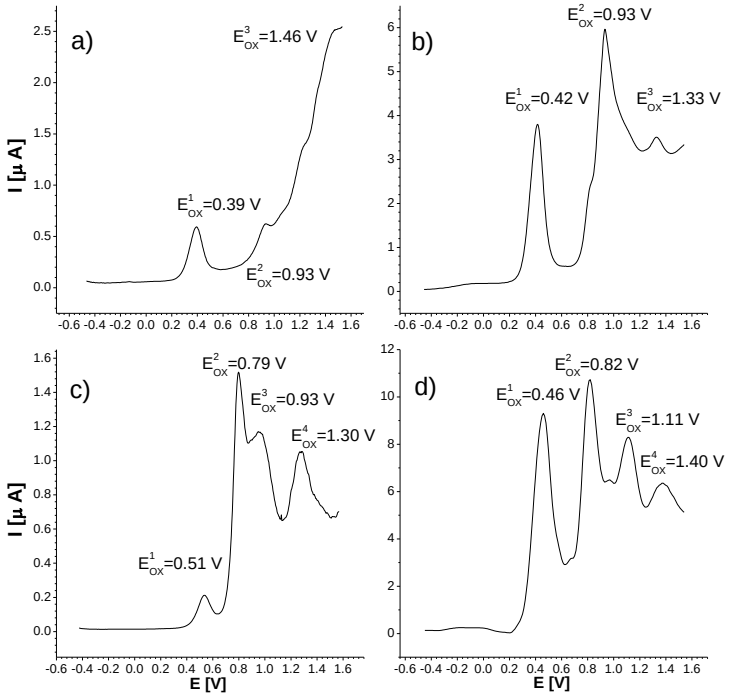

Figure 4.25 DPV profiles of compounds **29** (b), **30** (c), **31** (a) and **32** (d). Measurement conditions: scan rate - 50 mV/s; Ag/AgCl - reference electrode. [£]

Spectroelectrochemical properties of the selected carbazolyl-containing polymers prepared on indium tin oxide (ITO) coated glass electrode were investigated in order to find the relationship between redox processes and UV-Vis absorption. UV-Vis spectra of **P29** and **P30** recorded with increasing applied electrode potential are given in Figure 4.26.

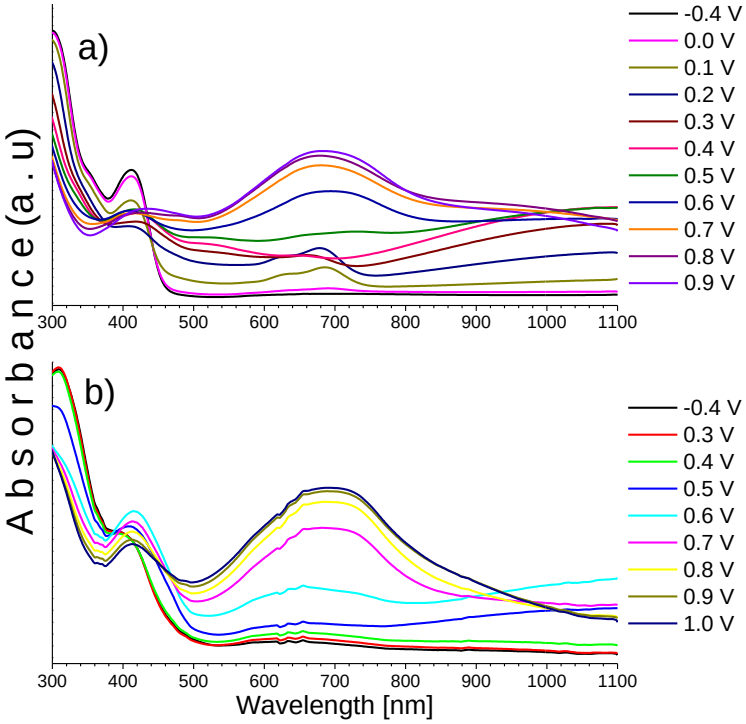

Figure 4.26 UV-Vis spectra recorded during electrochemical oxidation of polymeric films of **P29** (a) and **P30** (b). [£]

It is found that the intensity of absorption band corresponding to the electro-deposited polymers, for example; λ_{max} = 302 nm for **P29** and λ_{max} = 311 nm for **P30**, gradually decreases with the increase of the applied voltage. Moreover for polymers **P29** and **P30**, new definite absorption bands also appeared at *ca*. 418 nm, *ca*. 685 nm and beyond 900 nm during the doping processes. This observation might be explained by the formation of charged species such as polarons and bipolarons [192]. The absorption peak located at *ca*. 685 nm is apparently due to the formation of bipolarons while the spectral bands appeared in lower and higher energy regions might be due to the formation of polaronic species [192, 193]. As a result of p-doping, the color of the electrodeposited films changed from light green to dark violet which implies that these polymeric films have potential for application in electrochromic devices [194].

The formation of polarons and bipolarons was confirmed by the ESR spectroscopy. For recording of ESR spectra the polymers **P29** and **P30** were electro-deposited on platinum electrode. ESR spectra of polymers **P29** and **P30** recorded during the doping processes are demonstrated in Figure 4.27.

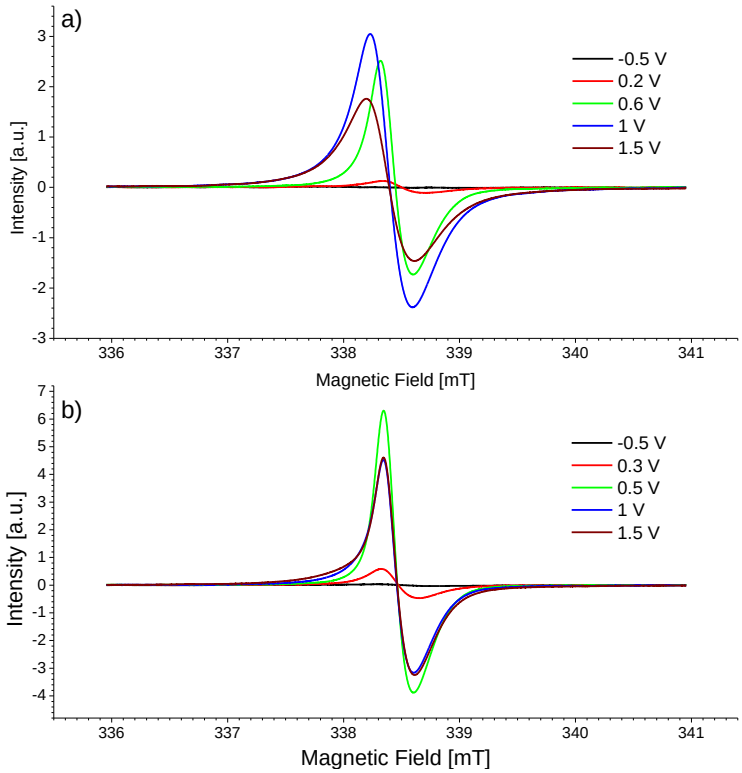

Figure 4.27 ESR spectra of electrochemically doped polymeric films **P29** (a) and **P30** (b) on platinum electrode at various applied potentials in monomer free 0.1 M Bu_4NBF_4/dichloromethane electrolyte. [£]

At low oxidation potentials the electro-deposited polymers showed symmetrical signals corroborating the formation of polarons [195]. On further doping, the increase in the spectral intensity can be attributed to the creation of more poloronic species. The deceased spectral intensity as well as increased spectral broadening at very high doping levels suggested the formation of low-spin bipolarons [195,196].

[£]*Electrochemical measurements were carried out at Faculty of Chemistry, Silesian University of Technology by Premyslaw Data.*

Photoelectrical properties

Ionization potentials (I_p) of thin solid layers of the synthesized compounds were measured by photoelectron spectroscopy. Photoelectron emission spectra of **29-32** are shown in Figure 4.28.The intersection points of the linear parts of the spectra drawn with the abscissa axis give the ionization potential values.

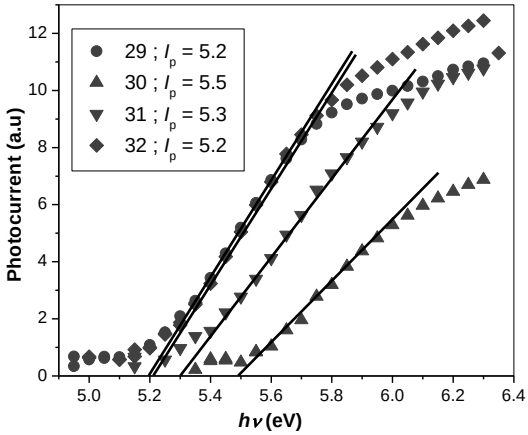

Figure 4.28 Photoelectron spectra and ionization potentials (in eV) of thin films of **29-32**.[§]

Ionization potential values of tetra substituted pyrene derivatives range from 5.2eV to 5.5 eV. Compounds **29** and **32** exhibited similar I_p values as expected whereas **30**, the regioisomer of **29**, demonstrated higher I_p level compared to **29** and **32**. This kind of behaviour of increase in the I_p level of carbazol-2-yl containing compounds compared to carbazol-3-yl containing materials is also noted *vide supra* for perylene bisimide based compounds.

Room temperature hole-drift mobility of thin layer of **32** was measured by xerographic time of flight technique. The representative *dU/dt* transient for the neat film of **32** is demonstrated in Figure 4.29.

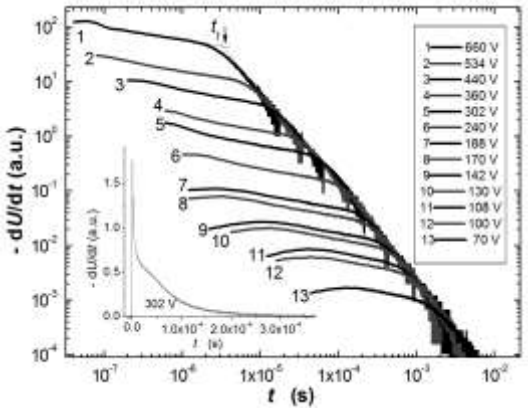

Figure 4.29 XTOF transients for the neat film of **32.** 1 ns laser operating at 337 nm was used, $T = 25^0$C, Arrow mark indicate transit time of holes at respective surface voltage.[§]

It exhibits dispersive hole-transport. The hole-transit times (t_t) needed for the estimation of hole mobilities were established from intersection points of two asymptotes from the double-logarithmic plots.

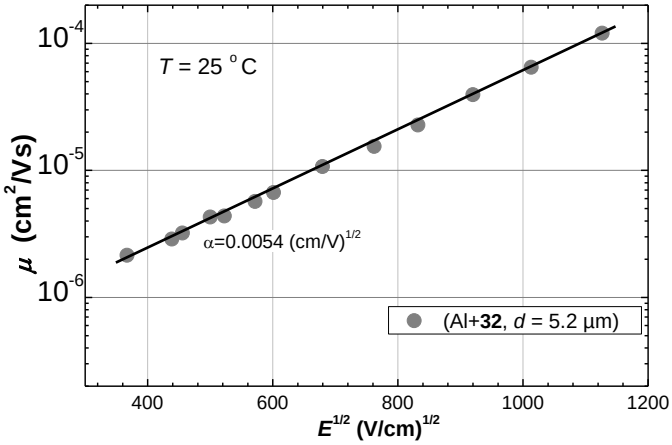

Figure 4.30 The electric field dependency of hole-drift mobility for the layer of **32**.[§]

The electric field dependency of hole-drift mobilities of the thin film of **32** in air is shown in Figure 4.30. The linear dependency of hole-drift mobilities on the square root of electric field (E) is observed. The hole-drift mobility value of 5.8×10^{-5} cm^2 V^{-1} s^{-1} was measured for the thin solid layer of compound **32** at an electric field of 10^6 Vcm^{-1} at 25 °C.

[§] *I_p and hole mobilities were measured at Department of Solid State Electronics, Vilnius University.*

4.3. Synthesis and properties of triphenylamine based dendrimers

Triphenylamino group is highly electron rich and possesses a propeller-shaped structure. Low-molar-mass compounds containing triphenylamino moiety are widely employed as organic hole-transporting materials due to their high hole mobility, electron donating ability and good optoelectronic properties [197,198,199]. However because of the poor film forming property from solution of small molecules, these materials must be used in optoelectronic devices by vacuum evaporation which is not benefit for commercial applications [200]. Triphenylamine-core centred dendrimers are particularly important for solution-processable device applications since they combine good optoelectronic performance and film forming property. We have synthesised and characterised a series of dendritic compounds containing triphenylamino group as central core and electron donating alkoxyphenyl-substituents as arms connected through olefinic spacers.

Synthesis and characterisation

Synthesis of triphenylamine-based compounds ramified with alkoxyphenyl-substituents is described in Scheme 4.9. Tris(4-formylphenyl)amine **33** was synthesized from triphenylamine by Vilsmeier-Haack reaction [61]. Compound **33** was yielded 16% after the column chromatography; however, the diformylated derivative was obtained as major product. For the preparation of alkoxyphenyl-substituents, firstly, methyl-3,4,5-trihydroxybenzoate was *O*-alkylated in acetone using potassium carbonate and corresponding bromoalkane in the presence of catalytic amount of 18-crown-6. In the next reaction, the ester functionality of compounds **34**, **37** and **40** were reduced using lithium aluminium hydride in THF. 3,4,5-Tris(alkyloxy)phenyl)methanols **35**, **38** and **41** were produced in high yeild (~90%) by the lithium aluminium reduction reaction. These derivatives were brominated in the next step using phosphorous tribromide in order to synthesis the respective bromo compounds **36**, **39** and **42**. Wittig reaction of triformyl derivative of triphenylamine with the corresponding alkoxyphenyl-substituents yielded the dendritic materials **43-45**. The Wittig reagent (phosphonium ylide) was prepared *in situ* from the bromine containing compounds **36**, **39** and **42** by refluxing with 1 equivalent of triphenyl phosphine in DMF. Compound **46** was prepared from diethyl-4-methoxy benzyl phosphonate and compound **33** using the modified Wittig conditions.

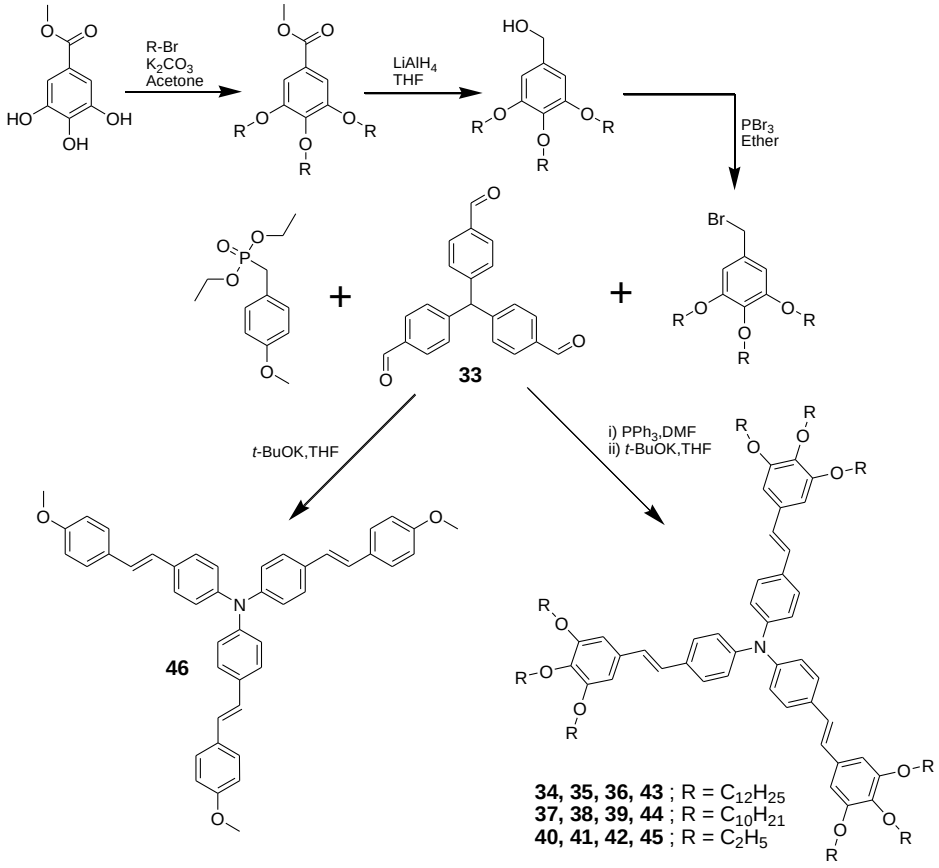

Scheme 4.9 Synthetic route for the preparation of dendritic compounds **43-46**.

Dendritic compounds **43-46** are highly soluble in common organic solvents like dichloromethane, chloroform, toluene or THF; which is benefited from the alkyl-substituents and the olefin spacer. Characterization of these materials by mass spectrometry, elemental analysis, IR spectroscopy and ^{1}H and ^{13}C NMR spectroscopy is therefore easily accomplished. Dendrimers containing long alkyl chains **43** and **44** were characterised by MALDI-TOF mass spectrometry. Experimentally determined and calculated m/z ratios agree perfectly for these compounds within the range of accuracy of the instrument. ^{1}H and ^{13}C NMR spectral data and elemental analysis data are in good agreement with chemical structures of the dendritic compounds **43-46**.

Properties of triphenylamine-core centred dendrimers

The behaviour of compound **46** under heat established by DSC analysis is shown in Figure 4.31. During the first heating scan, compound **46** exhibits a sharp endotherm at 204 °C corresponding to the melting point. When the sample of compound **46** was cooled from the melt, it showed a glass transition at 91 °C.

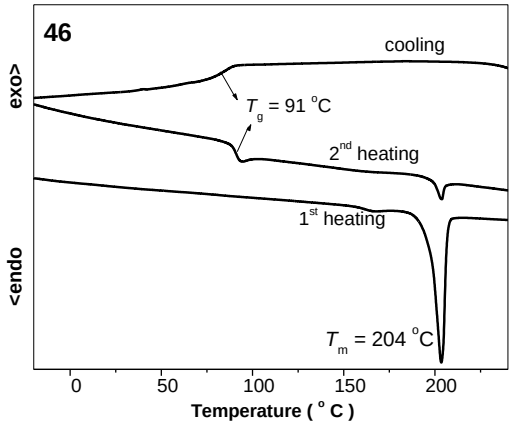

Figure 4.31 DSC thermograms of **46** recorded at a heating/cooling rate of 10 °C min^{-1} under nitrogen atmosphere.

During the first heating scan, compound **45** containing ethyl chains demonstrated glass transition at 107 °C and two endothermic melting transitions at 130 and 168 °C, respectively (Figure 4.32). The appearance of two melting transitions during the heating scan suggested the existence of two types of crystal structure in this compound. However, the cooling scan and the second heating scan of compound **45** did not show any thermal transitions which clearly display its amorphous (glassy) nature.

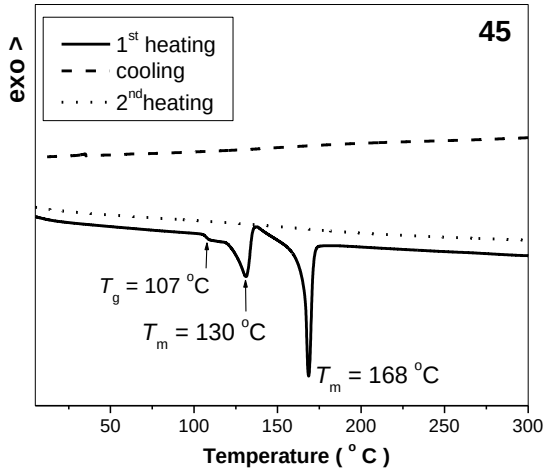

Figure 4.32 DSC thermograms of **45** recorded at a heating/cooling rate of 10 °C min^{-1} under nitrogen atmosphere.

Different DSC curves were observed for compound **43** containing dodecyl alkyl chains at the rim. In both first and second heating cycles three endotherms appeared as shown in Figure 4.33.

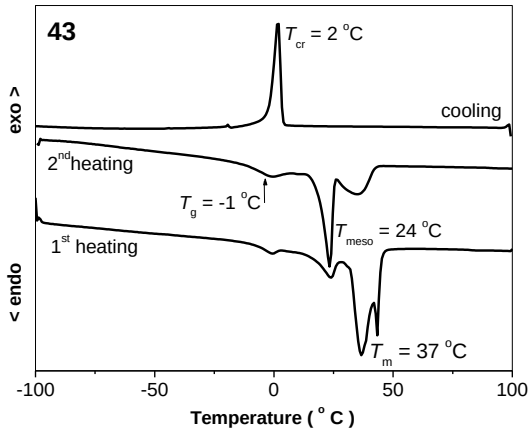

Figure 4.33 DSC thermogram of **43** recorded at a heating/cooling rate of 10 °C min^{-1} under nitrogen atmosphere.

The first one, which is located at -1 ºC can be attributed the glass transition. Upon first heating, other thermal transitions also observed at 24 ºC and 37 ºC with the enthalpy values ΔH = 14.5 KJ/mol and ΔH = 105.3 KJ/mol, respectively. Upon cooling from melt, an exotherm corresponding to the crystallization was observed at 2 ºC (ΔH = 115.6 KJ/mol). During the second heating cycle, the endothermic transitions were again noted at 24 ºC (ΔH = 46.3 KJ/mol) and 35 ºC (ΔH = 32.4 KJ/mol), respectively. Therefore, a liquid-crystalline phase was assumed to be formed on heating and existed between 24 ºC and 35 ºC. However, this mesophase seems to be monotropic since the isotropic melt solidified through a unique exotherm to get the crystalline phase on cooling. This hypothesis was confirmed by polarized optical microscopy (POM) observations.

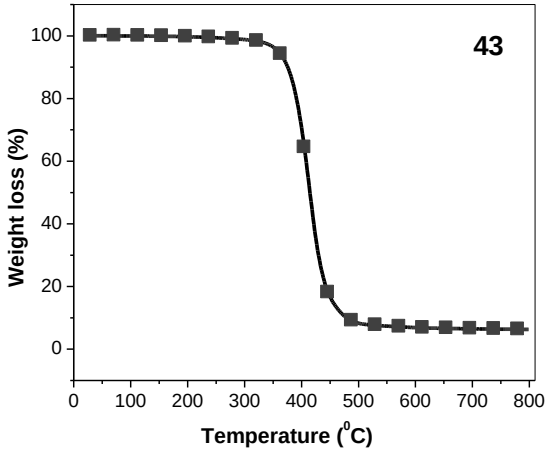

Figure 4.34 TGA trace of compound **43** recorded at a heating rate of 20 °C min^{-1} under N_2

Thermal stability of compound **43** was examined by TGA (Figure 4.34). It was found that compound **43** was stable above the clearing point of liquid crystalline phase transitions with the decomposition onset of *ca*. 375 ºC.

The material **43** was examined using polarizing optical microscopy to determine the nature of the phase transitions. On heating the sample, a viscous anisotropic liquid formed at the expected range of temperatures (24-35 ºC), which proves the existence of the mesophase. Figure 4.35 demonstrates the POM photographs of the mesophase of compound **43** during the warming of the sample at 32 ºC and 34 ºC. Upon heating to 24 °C, the material melts, as it was evidenced by a rapid change in birefringence. At temperatures above 35 ºC, it becomes a low-viscosity (free-flowing) isotropic fluid. The cooling of this isotropic melt did not again lead to the mesophase and the melt remained isotropic up to the room temperature. The sample was observed to be crystalline after storage at *ca.* 20 hours at laboratory temperature. Hence, we can conclude that compound **43** can exist in liquid crystal form (monotropic) over a short range of temperature between 24 ºC and 35 ºC.

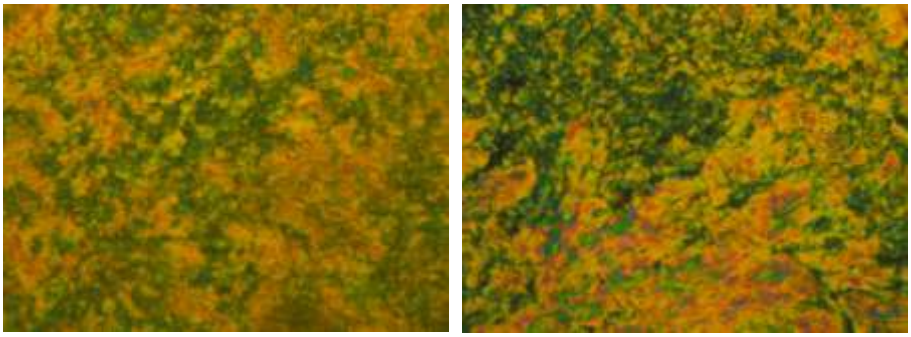

100 x magnified POM photograph at 32 ºC 100 x magnified POM photograph at 34 ºC

Figure 4.35 Photographs showing optical textures of a sample of **43** taken at 32 and 34 °C during the warming of the sample.

To confirm the liquid crystalline structure, X-ray diffraction (XRD) measurements were performed for compound **43**. A representative XRD patterns for **43** in the crystalline and liquid crystalline phase taken under synchrotron radiation are depicted in Figure 4.36. The X-ray diffraction pattern of compound **43** recorded at 15 ºC contains a number of sharp diffractions which indicates the occurrence of a crystalline phase at this temperature. In the pattern recorded at 33 ºC, a broad diffraction at 2θ=20.4º (4.3 Å) appears. This diffraction can be attributed to the planar distance between discotic molecules. Moreover, a broad diffraction of low intensity also appears at 2θ=2.1º (42 Å), which seems to indicate that a short-range columnar order also exists in the mesophase. Therefore, the compound can be recognized to exhibit between 24 ºC and 35 ºC a monotropic nematic discotic (N_D) mesophase, but this mesophase shows a short-range columnar organization (*i.e.* the molecules are stacked on top of each other to some extent).

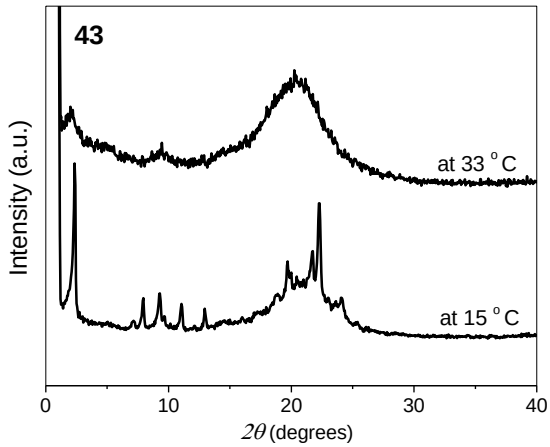

Figure 4.36 High-resolution XRD patterns of **43** in the crystalline phase at 15 ºC and in the N_D mesophase at 33 ºC

Ionization potential values of triphenylamine derivatives measured by photoelectron spectroscopy ranged from 5.21eV to 5.47 eV (Figure 4.37). Compounds **43** and **44** with flexible alkyl chains exhibited similar I_p values whereas compounds containing shorter alkyl substituents demonstrated lower I_p levels of 5.38 eV for **45** and of 5.21 eV for **46**, respectively. It is found that the photocurrent emission from the thin films of compounds **43** and **44** was comparatively lower with respect to that from the layer of **45** and **46**. This observation can apparently be attributed to the relatively lesser amount of chromophores per unit area of thin films due to the presence of long flexible alkyl chains in compounds **43** and **44**.

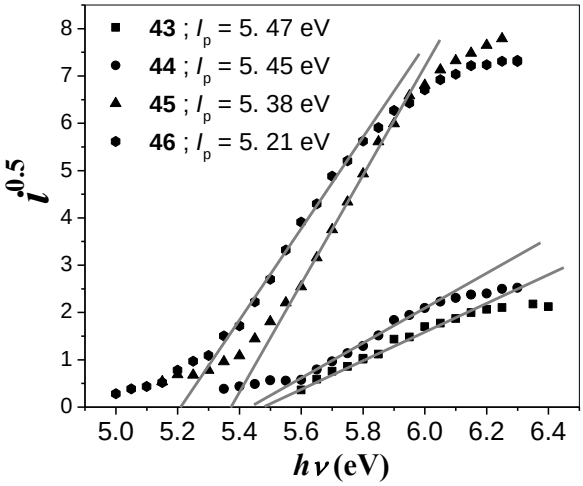

Figure 4.37 Photoelectron spectra and ionization potentials of the thin films of **43-46**. [§]

The electric field dependency of hole-drift mobilities of the thin film of **45** in air is shown in Figure 4.38.

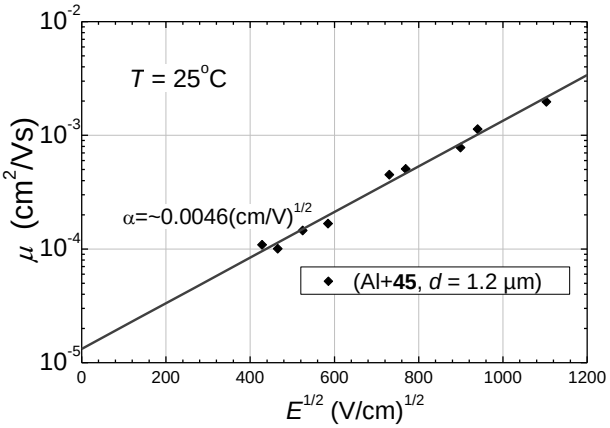

Figure 4.38 The electric field dependency of hole-drift mobility for the layer of **45**.[§]

Hole-drift mobility of 1.3×10^{-3} cm^2 V^{-1} s^{-1} was observed in the amorphous layer of compound **45** at an electric field of 10^6 Vcm^{-1} at 293 K. Due to the formation of crystallites in the thin film we were not able to measure the charge carrier mobility in compound **46**. Compounds **43** and **44** also did not show any photosignal of hole-transport in the thin solid layers.

[§]*I_p and hole mobilities were measured at Department of Solid State Electronics, Vilnius University.*

4.4. Electron-donor-substituted star-shaped 1, 3, 5-triazine derivatives

1, 3, 5-Triazine derivatives have proven their great potential in the rising area of material chemistry, i.e. organic electronics, due to their interesting semiconducting and photophysical properties as well as electrochemical characteristics [76, 88]. Star-like compounds possessing electron-deficient 1, 3, 5-triazine-core scaffold and electron-rich chromophores as side arms are of particular interest. Such kind of architecture enables to produce organic materials possessing intramolecular charge transfer, enhanced luminescent properties and redox characteristics important for device applications. Hence, we have focused our attention on the versatile 1, 3, 5-triazine scaffold as it can be triply functionalized with various electron-donors. We have synthesized and characterized compounds containing triazine, as central core, which possesses an electron affinity considerably larger than that of other aromatic rings [201,202], and carbazole, phenothiazine, fluorene or trimethoxyphenyl- substituents, as electron-donors, at the periphery. Thermal, photophysical and electrochemical properties of the synthesised compounds were evaluated.

Synthesis of 1, 3, 5-triazine derivatives

Compounds **50-52** were synthesized by the Suzuki coupling reaction of 2, 4, 6-tris(4-bromophenyl)-1,3,5-triazine (**47**) with boronic acid pinacol ester derivatives of electron-donors, i.e. fluorene, phenothiazine or carbazole. For the preparation of triazine scaffold **47**, 4-bromobenzonitrile was stirred in chloroform in the presence of excess amount of trifluoromethane sulfonic acid under inert atmosphere. The synthetic route for the preparation of compounds **50-52** is described in the Scheme 4.10.

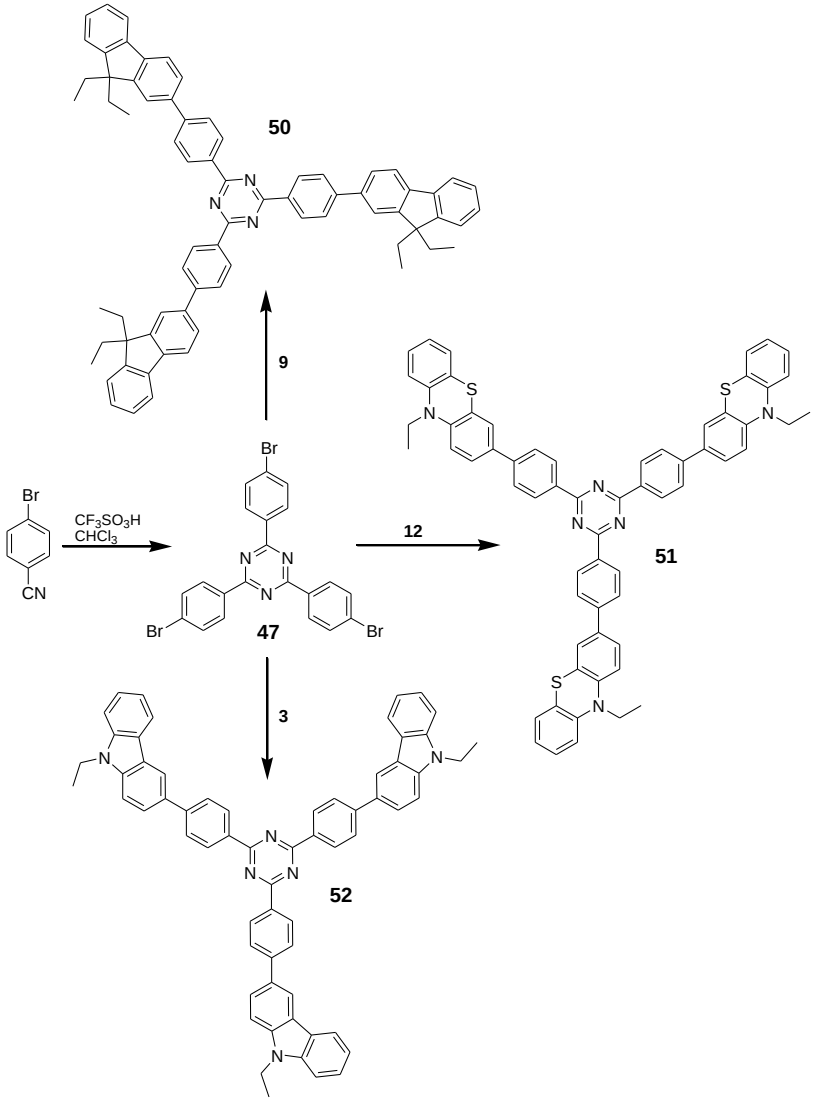

Scheme 4.10 Synthetic route for the preparation of compounds **50**-**52**. *Reagents and conditions*: $Pd(Ph_3)_2Cl_2$, K_2CO_3, THF–H_2O, 80 ^oC, 8–12 h.

Compound **53** containing olefin spacers was synthesised by Wittig-Horner reaction as shown in Scheme 4.11. Triazine intermediate **48** was synthesized from 4-bromomethylbenzonitrile using excess amount of trifluoromethane sulfonic acid as described before. The Wittig reagent **49** was prepared by refluxing compound **48** in excess amount of triethylphosphite under nitrogen. Wittig reaction between compound **49** and 3, 4, 5-trimethoxybenzaldehyde in the presence of potassium *ter*-butoxide in dry THF yielded the triazine derivative **53**.

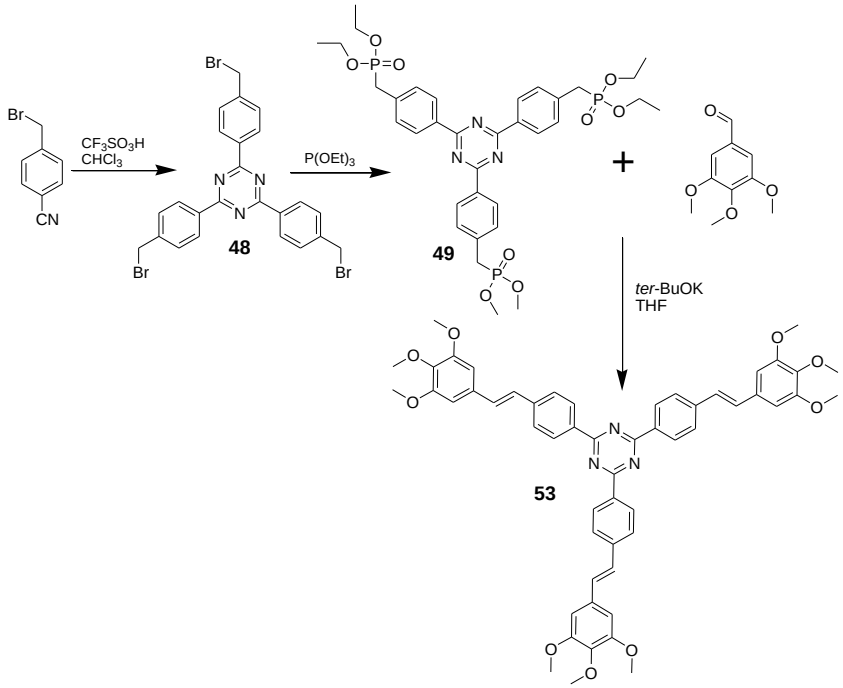

Scheme 4.11 Synthetic scheme for the preparation of compound **53**.

The synthesised compounds were characterised by NMR and IR spectroscopy, mass spectrometry and elemental analysis. Compounds **50-52** were characterised by MALDI-TOF mass spectrometry. The characterisation data are in good agreement with the chemical structures of the synthesised materials.

Thermal properties of triazine derivatives

The behaviour of compounds **50-53** under heat was investigated by DSC and TGA under nitrogen atmosphere. DSC thermograms of compounds **50-52** are shown in Figure 4.39 and the data are summarized in Table 4.12.

All the triazine derivatives possessed high glass transactions (> 148 ^{o}C). Compounds **50** and **51** displayed T_g at 148 and 235 ^{o}C, respectively, indicating the clear influence of donor-substituents on the amorphous character of triazine derivatives. T_g of triazine compound **51** was found to be increased by *ca* 90 ^{o}C compared to that of compound **50** when phenothiazinyl donor substituents were symmetrically replaced by fluorenyl moieties. As seen from Figure 4.39, compound **52** displayed an exothermic transition at 287 ^{o}C representing structural relaxation through crystallization during the first DSC heating cycle. Upon further heating, it melted by showing the sharp endotherm at 344 ^{o}C. In successive cooling scan, compound **52** did not crystallize and demonstrated a clear T_g at 198 ^{o}C suggesting the formation of amorphous phase. Glass forming ability of these triazine derivatives indicated the significant twisting of donor-segments with respect to the

triazine core. Compound **53** was scanned over 400 °C heating/cooling cycles; however, we were not able to observe any kind of thermal transitions.

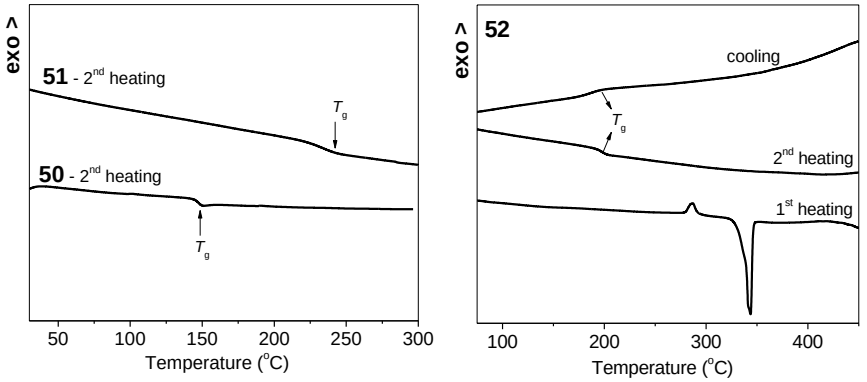

Figure 4.39 DSC thermograms of triazine compounds **50-52** recorded at a heating/cooling rate of 10 °C min^{-1} under N_2.

Table 4.12 Thermal characteristics of compounds **50-52**.

Compound	T_g °C	T_{ID} °C
50	148	442
51	235	390
52	198	514

Triazine derivatives **50-52** exhibited high thermal stability in the TGA experiments. The onset temperatures of thermal decomposition (T_{ID}) range from 390 to 514 °C (Table 1). It is found that not only electron rich substituents but also the phenylene spacer between the triazine core and the donor-substituents greatly affected the thermal behaviour of these triazine compounds.

Photophysical properties

The normalized absorption and fluorescence spectra of the investigated triazine compounds in dilute THF solutions, polystyrene (PS) matrix and neat films are shown in Figure 4.40. The details of the photophysical properties of the compounds **50-52** are summarized in Table 4.13. The lowest-energy absorption bands of the compounds in 10 μM THF solutions were found to range from 351 nm (for fluorene-substituted compound **50**) to 393 nm (for phenothiazine-substituted compound **51**). Since the electron-deficient core (2,4,6-triphenyl-1,3,5-triazine) of the triazine compounds absorbs deep in UV (~270 nm) [76], and furthermore, separate fluorene, carbazole and phenothiazine moieties exhibit absorption below 340 nm [180], substitution of the core with these electron-donating moieties evidently extends π-conjugation of the D-A compounds **50-52** by considerably red-shifting their bands. The gradual increase in the absorption wavelength was accompanied by continuous reduction of extinction coefficient from 1.3×10^5 $M^{-1}cm^{-}$

^{1} (for **50**) to 0.4×10^{5} $M^{-1}cm^{-1}$ (for **51**), which was in agreement with enhanced electron-donating ability of the substituents having a following order: phenothiazine > carbazole > fluorene. The stronger electron-donating ability implies higher electronic delocalization, and thus, stronger ICT character resulting in a more pronounced red shift, and usually, a decrease in oscillator strength [203,204]. Note that the absorption spectra of the compounds **50-52** dispersed in dilute toluene solutions and PS matrixes at low concentration (0.25 wt %) are nearly identical. Only slightly red-shifted absorption spectra of the neat films are caused by intermolecular interactions [205], which are considered to be weak due to nonplanar conformations of the triazine compounds preventing close packing of the molecules in the films. Twisted conformers are likely to originate from steric hindrance effects induced by substitution of the triazine core with bulky electron-donating moieties.

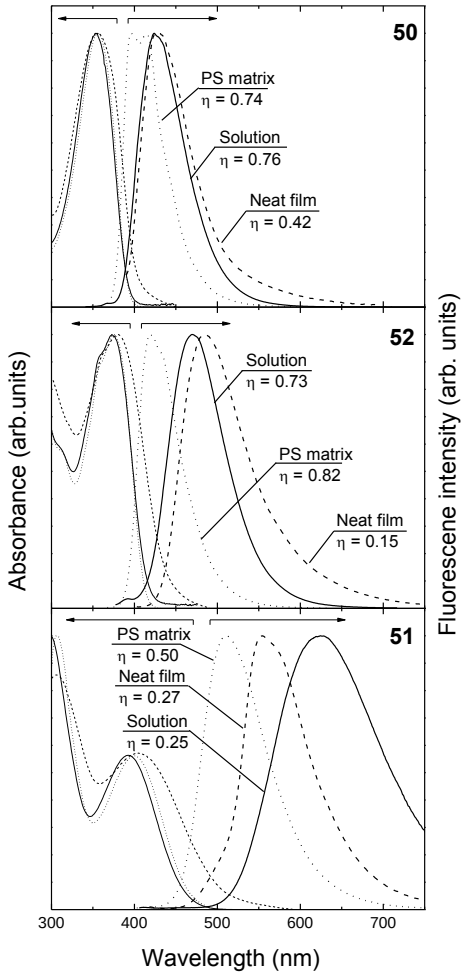

Figure 4.40 Normalized absorption and fluorescence spectra of the triazine compounds **50**, **51** and **52** in 10μM THF solution (solid line), PS matrix at 0.25 wt % concentration (dotted line), and neat films (dashed line). Fluorescence quantum yields (Φ_F) are indicated. *

Dilute solutions of fluorene- and carbazole-functionalized triazine compounds (**50** and **52**) exhibited efficient fluorescence in a blue spectral range with bands peaked at 424 nm and 470 nm, respectively (Figure 4.40). Estimated fluorescence quantum yields (Φ_F) of the compound solutions were as high as 0.76 for **50** and 0.73 for **52**. Measured fluorescence spectra of the neat films of these two compounds were only slightly red-shifted and broadened most likely due to intermolecular interactions as in the case of absorption spectra. Additional long-wavelength shift of the fluorescence spectra can appear as a result of exciton migration towards lower energy sites (e.g. originating from different conformers) in the films with subsequent emission of photons [184]. Indeed, 2-5-fold lower Φ_F values obtained in the neat films as compared to those in solutions suggest that exciton migration and migration-assisted exciton quenching at non-radiative decay sites are important. Three times less efficient fluorescence quenching in the neat film of fluorene-substituted triazine compound **50** as that obtained in the film of carbazole-substituted compound **52** can be attributed to suppressed intermolecular interactions facilitated by out-of-plane twisted two ethyl groups at fluorene C9 position, whereas enhanced quenching observed in **52** is consistent with closer packing of the molecules containing only one ethyl group at carbazole N9 position [206].

In contrast to relatively small Stokes shift (0.6-0.7 eV) estimated for compounds **50** and **52** solutions, the phenothiazine-substituted compound **51** solution expressed considerably enlarged Stokes shift (~1.2 eV) followed by 3-fold reduced fluorescence quantum yield down to 0.25. The latter result is a signature of the well-pronounced ICT occurring between phenothiazine (donating) and triazine (accepting) moieties.

Table 4.13 Photophysical properties of the dilute THF solutions, neat films and polystyrene matrix of 0.25 wt % concentration of compounds **50**, **51** and **52**.

Compound	Solution					Neat film				PS film			
	λ_{abs} [a] (nm) (ε [b], L mol^{-1} cm^{-1})	λ_F^{max} [c] (nm)	Φ_F	τ (ns)	τ_R [d] (ns)	τ_{NR} [d] (ns)	λ_{abs} [a] (nm)	λ_F^{max} [c] (nm)	Φ_F	τ (ns)	λ_{abs} [a] (nm)	λ_F^{max} [c] (nm)	Φ_F	τ (ns)
50	271 (47693) 351 (131397)	424	0.76	1.2	1.6	5	280 355	430	0.42	1.2 [63%] 0.4 [28%] 3.4 [9%]	356	396 415	0.74	1 [97%] 3.1 [3%]
51	299 (67489) 393 (38030)	624	0.25	3	12	4	305 403	554	0.27	3.7 [70%] 1.2 [15%] 10.4 [15%]	306 400	511	0.5	4.4
52	295 (58795) 372 (87660)	470	0.73	2	2.7	7.5	299 380	485	0.15	3.1 [51%] 0.7 [31%] 13.8 [18%]	295 376	419	0.82	1.4 [96%] 3.7 [4%]

[a] Peak wavelength of absorption bands. [b] Molar extinction coefficient. [c] Wavelength at fluorescence band maximum. [d] Radiative and non-radiative decay time constants calculated as τ/Φ_F and $\tau/(1-\Phi_F)$, respectively.

The CT properties of the compound **51** were further assessed by performing solvent polarity dependent measurements of the fluorescence spectrum. Figure 4.41 and Table 4.14 report fluorescence data of the compound **51** dissolved in several solvents of different polarities. Obviously, increasing solvent polarity resulted in remarkable broadening and red-shifting (by 142 nm) of the fluorescence band,

which were accompanied by significantly reduced Φ_F from ~0.6 (in nonpolar solvents) to 0.25 (in polar solvent), and slightly shortened fluorescence decay time (τ) from ~4 ns (in nonpolar solvents) to 3 ns (in polar solvent). Accordingly, the calculated radiative (τ_R) and non-radiative (τ_{NR}) decay time constants were found to increase and decrease, respectively, with increased solvent polarity thereby supporting manifestation of ICT states in the compound **51**. The observed features were likely to originate from the so-called twisted ICT phenomenon imposing twisting of D and A moieties upon charge transfer in the excited state [204,206].

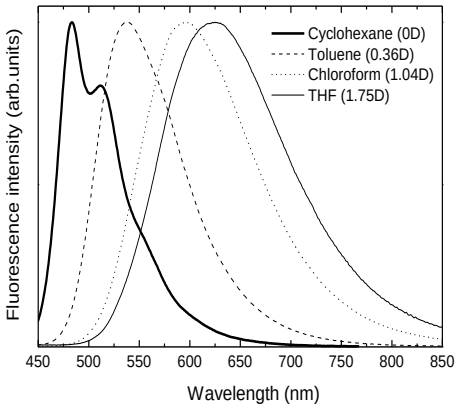

Figure 4.41 Normalized fluorescence spectra of compound **51** in solvents of various polarities: cyclohexane (thick solid line), toluene (dashed line), chloroform (dotted line), THF (thin solid line). Dipole moments of solvents are indicated in brackets. *

Table 4.14 Photophysical properties of compound **51** in solvents of different polarity.

Solvent	Dipole moment (D)	λ_F^{max} [a] (nm)	Φ_F	τ (ns)	τ_R [b] (ns)	τ_{NR} [b] (ns)
Cyclohexane	0	483	0.63	3.9	6.2	10.5
Toluene	0.36	536	0.59	4.2	7.1	10.2
Chloroform	1.04	596	0.62	5	8.1	13.2
Tetrahydrofuran (THF)	1.75	625	0.25	3	12	4

[a] Wavelength at fluorescence band maximum. [b] Radiative and non-radiative decay time constants calculated as τ/Φ_F and $\tau/(1-\Phi_F)$, respectively.

The twisting of the moieties in the excited state were verified by comparing fluorescence properties of the compounds **50-52** in dilute solution with those obtained in rigid PS matrix at low (0.25 wt %) concentration. Incorporation of molecules in rigid polymer matrix highly suppresses their intramolecular twistings in the excited state as opposed to those in a dilute solution, where the molecules are free to change their conformation. Generally, in the absence of excited state twisting, the compounds being in the diluted form either in PS matrix (solid media) or in solution (liquid medium) should exhibit similar fluorescence properties.

Although, the fluorene-substituted triazine compound **50** with the weakest D-A character demonstrate only a small red shift (~25 nm) of the fluorescence spectrum obtained in solution in regard to that in PS matrix, the carbazole-substituted compound (**52**) and, in particular, phenothiazine-substituted compound (**51**) exhibits distinct red shifts (50 nm and 110 nm) of the solution spectra in agreement with an enhanced ICT character, and most likely, more pronounced excited state twisting. The extent of twisted ICT is also reflected in the amount of reduced fluorescence quantum yield associated with the decrease of rigidity of the surrounding medium. For example for the compound **50**, Φ_F values obtained in solution and PS matrix are almost the same implying negligible twisted ICT, whereas in the case of compound **51**, reduction of Φ_F in solution as compared to PS matrix is 2-fold confirming pronounced twisted ICT.

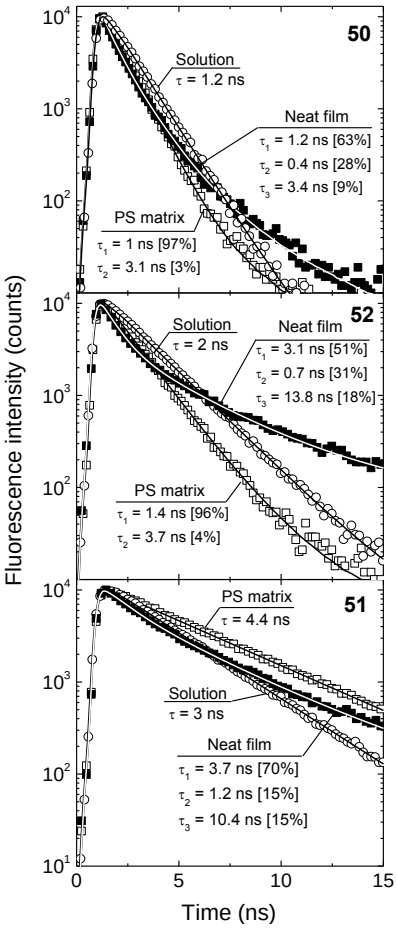

Figure 4.42 Fluorescence transients of the 10μM THF solutions (open circles), PS matrixes at 0.25 wt % concentration (open squares) and neat films (solid squares) of compounds **50**, **51** and **52** measured at the fluorescence band maxima. Lines indicate single or multiple exponential fits to the experimental data. Fluorescence lifetimes (τ) are indicated.*

Fluorescence transients of the studied triazine compounds in the dilute THF solutions, PS matrixes and neat films measured at the band maxima are presented in Figure 4.42. Excited state relaxation of the compounds in a solution was found to follow single exponential decay profile with estimated fluorescence lifetimes (τ) of 1.2, 3 and 2 ns for the compounds **50**, **51** and **52**, respectively. The increase of τ well correlated with enhanced ICT character of the compounds. To evaluate the contribution of radiative and non-radiative decay processes in the studied compounds, radiative and non-radiative decay time constants were estimated (see Table 4.13). As opposed to relatively small variations of τ_{NR} (4 – 7.5 ns) with respect to the substituents attached, the deduced τ_R values were found to vary from 1.6 ns for compound **50** to 12 ns for compound **52** unambiguously indicating substituent-induced alteration of radiative decay processes in dilute solutions. This finding well supports twisted ICT occurring in D-A molecules, since large intramolecular twisting severely modifies electron wave function overlap between the neighbouring conjugated moieties, thus drastically changing the rate of radiative decay. Fluorescence transients of the compounds dispersed in PS matrixes showed similar decay profiles as those of the compound solutions; however, they exhibited slightly non-exponential behaviour due to the differently twisted conformers. The transients of the neat films exhibited even more pronounced deviation from the exponential decay, which was attributed to dispersive exciton hopping through the localized states in the disordered media [207].

[*] *Fluorescence quantum efficiencies were measured at Institute of Applied Research, Vilnius University by Dr. K. Kazlauskas.*

Electrochemical properties

Electrochemical investigations of compounds **50-52** were carried out in 0.1 M Bu_4NBF_4/dichloromethane by performing cyclic voltametry and differential pulse voltametry. DPV profiles for the oxidation and reduction processes of compounds **50-52** are given in Figure 4.43. They give absolute values of oxidation and reduction potentials. The data are summarized in Table 4.15.

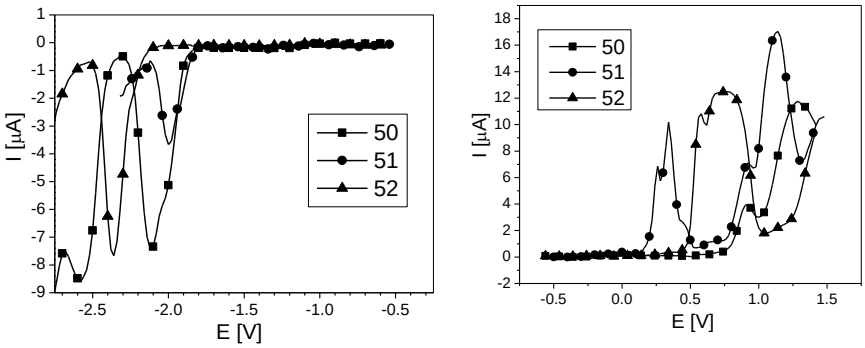

Figure 4.43 Differential pulse voltammogram of **50-52**. Measurement conditions: scan rate 50 mV/s, Ag/AgCl reference electrode calibrated against Fc/Fc^+, 0.1 M Bu_4NBF_4/dichloromethane electrolyte.[ε]

For compounds **50-52**, oxidation potentials range between 0.26 and 1.28 V and the reduction processes range from -2 to -2.58 V. The HOMO and LUMO energies of these materials were calculated from the onset values of the first oxidation and reduction peaks using the referencing standard of Fc/Fc^+ redox couple.

Table 4.15 Electrochemical data of **50-52** obtained from differential pulse voltametry (Potentials vs Ag/AgCl calibrated against Fc/Fc^+).

Compound	E_{oxi} (V)	E_{red} (V)	E^{onset}_{oxi1} (V)	E^{onset}_{red1} (V)	E_{HOMO} (eV)	E_{LUMO} (eV)	E_g^{ele} (eV)
50	0.92, 1.28	-2.12, -2.58	0.78	-1.88	-5.58	-2.92	2.66
51	0.26, 0.34, 0.94,1.15	-2	0.18	-1.83	-4.98	-2.97	2.01
52	0.57, 0.78	-2.36	0.48	-2.17	-5.28	-2.63	2.65

Adequately low laying HOMO energy level is observed for compound **51** containing phenothiazine substituents compared to other triazine derivatives. HOMO energy levels of compounds **50** and **52** are at -5.58 eV and at -5.28 eV, respectively, and are different from the hole-transporting dendritic materials containing carbazole or fluorine moieties [208]. This may be apparently due to the influence of electron-deficient triazine core. However, the HOMO energy level is considerably lowered due to the electro-donor substitutions for compounds **50** and **52** compared to TPZ which do not have electron-donors at the rim [76]. For compounds **50** and **51**, LUMO energy levels are comparable; whereas the triazine

derivative containing carbazole segments shows LUMO at -2.63 eV. Electrochemically determined bandgaps follow the trend as in optical bandgaps for compound **52** displaying the narrow band gap compared to compounds **50** and **52** showing the comparable energy gaps.

Figure 4.44 shows cyclic voltammograms of compounds **50-52** recorded during the oxidation redox processes. Compounds **50** and **52** demonstrate reversible redox processes and compound **51** displays quasi-reversible oxidation redox processes corresponding to the formation radical cations. The oxidation redox potentials range from 0.36 to 0.86 V.

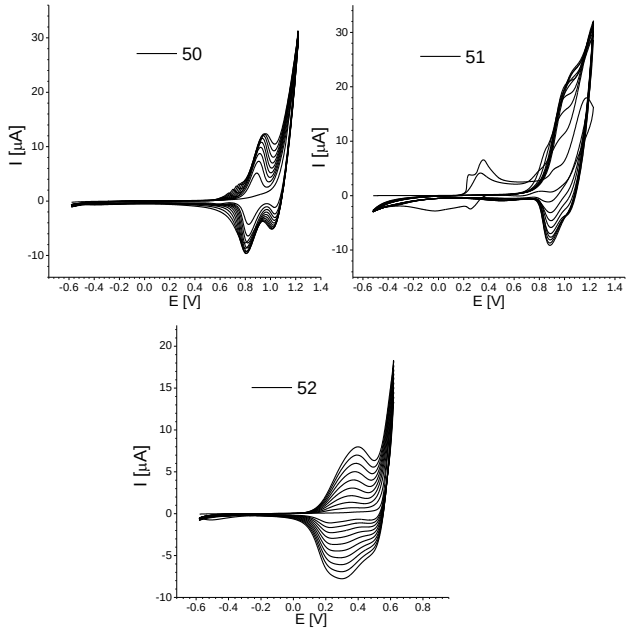

Figure 4.44 Cyclic voltammograms of **50-52.** Measurement conditions: scan rate - 50 mV/s; Ag/AgCl - reference electrode. [£]

Pronounced increase in anodic current intensity suggests the occurrence of electro-polymerization of compounds **50-52** at the working electrode. The diminishing of anodic peaks of phenothiazine containing compound **51** at low potential region during the successive scanning suggests the formation of low conductive polymer layer on the electrode. The electrochemically generated polymers of fluorene (**P50**) and carbazole (**P52**) derivatives show better conductivity and stability during the doping-dedoping processes. The electro-polymerization might have occurred through the 7^{th} -position of fluorene and 6^{th} -position of carbazole, respectively, for compounds **50** and **52** since those positions are more electrochemically active [209]. It is found that the carbazole containing polymer **P52** is electrochemically stable at the doping-dedoping processes and displays two reversible redox couples with the half wave potentials at $E^{1/2}_{ox}$ = 0.38 V and $E^{1/2}_{ox}$ = 0.66 V, respectively. These two redox couples may be attributed to its polaronic and bipolaronic formations, respectively [210]. In Figure 4.45

electrochemical behaviour of triazine derivatives containing carbazole segments, i.e. compound **52** and polymer **P52**, are compared; which clearly show the formation of charged species.

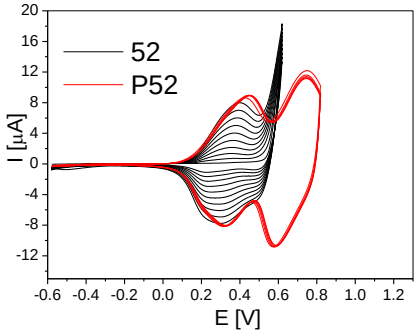

Figure 4.45 Cyclic voltammograms of carbazoles containing triazine derivatives: Black lines demonstrate compound **52** and the red lines display polymer **P52** in monomer free medium. Measurement conditions: scan rate - 50 mV/s; Ag/AgCl - reference electrode. [£]

In order to find the relationship between redox processes and UV-Vis-near IR absorption, spectroelectrochemical properties of the triazine derivatives **50-52** polymerised on indium tin oxide coated glass electrode were investigated. The spectroelectrochemical properties of polymers **P50-P52** upon doping process are compared in Figure 4.46.

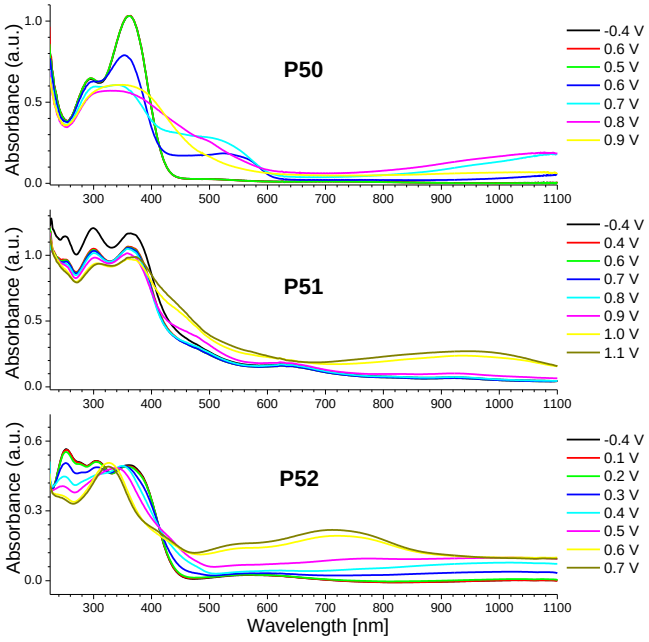

Figure 4.46 Spectroelectrochemical behaviour of **P50-P52** on ITO/glass surface. [£]

[£]*Electrochemical measurements were carried out at Faculty of Chemistry, Silesian University of Technology by Premyslaw Data.*

The low energy absorption bands of neutral polymers **P50-P52** ranged from 361 to 365 nm. Upon oxidation, the absorption maxima of **P50-P52** are gradually decreased up to certain doping levels and new broad absorption bands are intensified; which may be attributed to the formation of polarons and bipolarons in the polymeric films [192]. For polymers **P50**, **P51** and **P52**, the absorption bands developed with increasing potential at *ca.* 340 nm, at *ca.* 373 nm and at *ca.* 328 nm, respectively, and in the near infra-red region (>800 nm) are apparently due to the formation of polaronic species [192,193]. Bipoloronic formations in polymer **P52** is also quiet visible at high doping levels and can be attributed to the absorption peak appeared at *ca.* 712 nm [192,193].

Organic light-emitting devices were fabricated using compound **52** as active layer with the following configurations: Device I - ITO/MoO_3/NPB/**52**(40nm)/LiF/Al and Device II - ITO/MoO_3/NPB/**52** (20nm)/AlQ3(20nm)/LiF/Al. The electroluminescent spectra of these devices I and II are demonstrated in Figure 4.47. EL spectra range from 400 to 750 nm and almost completely cover the total visible region. The emission maxima of both the devices peak at 474 nm with full width at half maxima of 99nm.

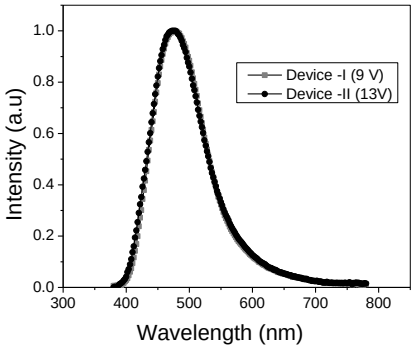

Figure 4.47 EL spectra of Devices I and II at 9V and at 13V, respectively.[¶]

The current-voltage-luminance (*I-V-L*) characteristics of devices I and II prepared using compound **52** are shown in Figure 4.48.

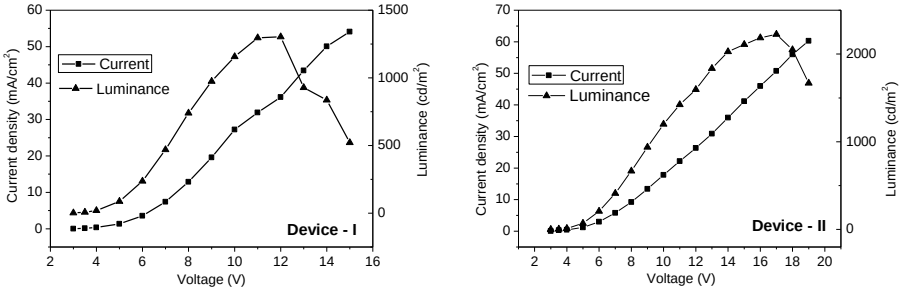

Figure 4.48 Current-voltage-luminance (*I-V-L*) characteristics of devices I and II prepared using **52**. [¶]

[¶]*Electroluminescent devices were fabricated at Nanyang Technological University (Singapore).*

The forward current increases with increasing forward bias voltage and the curves showed typical diode characteristics. The maximal brightness of 1296 cd/m^2 and of 2236 cd/m^2 was observed from the device I and II at a bias voltage of 11 V and of 17V, respectively. The maximal efficiency of both the devices are calculated to be ~0.4 cd/A.

4.5. Comparison of properties of the synthesized donor-substituted compounds

The electron-donor substituents attached to the aromatic or heteroaromatic cores influence the thermal behaviour, optical properties, redox characteristics and photoelectrical properties. Furthermore, most of the synthesized materials are found to be soluble in common organic solvents enabling the solution processing for device fabrication.

The synthesized compounds are thermally stable. The temperatures of the onsets of their thermal degradation range from 390 to 537 ^{o}C. Most of the compounds form molecular glasses and the glass transition temperatures are found to depend on the electron-donor substituents and molecular size of the materials. Perylene bisimide derivatives exhibit glass transitions below 95 ^{o}C; however, the derivatives of pyrene and triazine display T_g higher than 148 ^{o}C. It is also found that the alkyl substituents attached to the chromophore units largely affect the glass-forming capability of molecular glasses. In the case of pyrene derivatives, when the dodecyl chain is repalced by ethyl chain, the T_g is incresed by 200 ^{o}C. Triphenylamino-centred dendritic compounds containing ethyl or methyl chains form molecular glasses whereas derivative containing flexible alkyl (dodecyl) chain forms liquid crystal at the room temperature.

Perylene bisimide derivatives possess wide absorption window and exhibit photo-induced ICT. They also exhibit donor-substituents dependent emission behaviour. Carbazolyl arms in the star-shaped pyrene derivatives are found to be twisted with respect to the pyrene core; however, the molecules tend to planarize in the excited state, thus increasing molecule conjugation and fluorescence quantum yields up to 0.84 in dilute solutions. These compounds also display high fluorescence quantum yields (up to 0.60) when molecularly dispersed in polymer films at low concentration. Meanwhile, in the neat films they show fluorescence decay time shortening (in the initial stage) and considerable drop in fluorescence quantum efficiency which indicates exciton-migration-induced quenching at non-radiative decay sites. The triazine compounds featuring fluorene and carbazole electron-donating moieties also exhibited high fluorescence quantum yields in the dilute solutions (up to 0.76) and polymer matrixes (up to 0.82). Phenothiazinyl-substituted pyrene derivative demonstrates moderate fluorescence quantum efficiency (0.21) and significant PL spectral shifts in different polarity media which indicates the occurance of ICT in this compound. Optical study of triazine compounds performed in different polarity media also revealed an occurrence of excited state twisting followed by ICT (typical for D-A molecules), which is mostly pronounced in phenothiazine-substituted triazine derivative. It is obvious that the

donor-chromophores covalently bonded to the aromatic cores are twisted with respect to the cores and largely affect the electronic communication between the core and the donor-substituents, which in turn, influence the optical characteristics.

LUMO energies of arylene imides are found to be lower than those of other synthesized materials which enabled them to effectively transport electrons in air. Furthermore, the electron-donor substitutions at the core of arylene imides lead to lower the LUMO energies and to higher the HOMO levels with respect to the unsubstituted ones which in turn, rather benefited for ambipolar charge-transport, in particular, for perylene derivatives. I_p levels of solid films of triphenylamine and pyrene derivatives are rather close and similar to commonly used hole-transporting/injection materials. Bay carbazolyl-substituted perylene bisimide derivatives were found to transport both electrons and holes at ambient conditions. It is found that the difference in the linking topology of carbazolyl moieties to the core of perylene bisimides has furnished materials with complementary semiconducting properties. Naphthalimide derivative **24**, however, shows electron-mobility in air which exceeds 10^{-4} cm^2 V^{-1} s^{-1} at higher electric field. Carbazolyl-substituted pyrene derivatives and triphenylamine-based compound **45** represent donor-donor combinations. They transport holes with the drift mobilities ranging from 5.8×10^{-5} $cm^2V^{-1}s^{-1}$ to 1.3×10^{-3} cm^2 V^{-1} s^{-1}, at higher electric fields. The difference in the charge-transporting properties observed in these aromatic or heteroaromatic core based compounds may possibly be related to the critical position of their HOMO-LUMO levels.

5. THE MAIN RESULTS AND CONCLUSIONS

1. Perylene bisimide based new electroactive materials containing electron-donor substituents at the bay positions were designed, synthesized and characterized; their thermal, optical, photophysical, electrochemical and photoelectrical properties have been studied. Frontier molecular orbitals of some of the derivatives were established by DFT level calculations and bay triphenylamino substituted perylene bisimide derivative was tested in OFETs. It was established:
   1.1. The materials possessed high thermal stability and formed uniform films.
   1.2. They displayed a wide absorption window extending to the near infrared region of the spectrum and demonstrated efficient photoinduced intramolecular electron transfer.
   1.3. Ionization potential values of these perylene bisimide derivatives measured by photoelectron spectroscopy ranged from 5.5 to 6.1 eV.
   1.4. Fluorene containing D-A-D compound exhibited red emission in solution with the fluorescent quantum yield of 0.57.
   1.5. The synthesized compounds were capable of transporting both holes and electrons. D-A-D compounds containing differently linked carbazole substituents at the bay region of perylene bisimide exhibited complementary ambipolar charge-transport in air.
   1.6. Compound containing triphenylamine moieties at the bay positions displayed smectic liquid-crystal like phase in film and demonstrated air-stable ambipolar field-effect mobilities of 1.5×10^{-3} $cm^2V^{-1}s^{-1}$ for holes and of 3.5×10^{-4} $cm^2V^{-1}s^{-1}$ for electrons, respectively, in the transistor.
2. Fluorene or thiophene containing naphthalimides were synthesized and characterized as donor-acceptor molecular materials in order to reveal their thermal characteristics, electrochemical behaviour and semiconducting properties. Glass transition temperatures of these materials ranged from 30 to 76 ^oC and were influenced by the electron-donor substituents and molecular size. They exhibited characteristic reversible reduction redox process of n-type organic semiconductors. The fluorene containing naphthalimide derivative displayed time-of-flight electron mobility exceeding 10^{-4} cm^2 V^{-1} s^{-1} at high electric fields in air.
3. Carbazolyl and phenothiazinyl tetra substituted star-shaped pyrene derivatives were synthesized and characterized as molecular materials showing high glass transition temperatures. Thermal, electrochemical, photophysical and photoelectrical properties of these compounds were studied. It was established that:
   3.1. The synthesized compounds exhibited high thermal stability and formed stable amorphous phase with high glass transition temperatures ranged from 32 to 232 ^oC.
   3.2. Pyrene derivatives with carbazole arms were shown to be highly fluorescent in dilute solution (fluorescence quantum yields; Φ_F up to 0.84) and in rigid

polymer matrix (Φ_F up to 0.60). They displayed significant emission quenching and shortening of the fluorescence life time in the neat films.

3.3. Phenothiazinyl-substituted pyrene derivative showed moderate fluorescence quantum efficiency in dilute solution ($\Phi_F = 0.21$) or in polymer matrix ($\Phi_F = 0.25$) and expressed intramolecular charge transfer character.

3.4. The carbazolyl-substituted pyrene derivatives exhibited dicationic behaviour and subsequently underwent electro-polymerization as characterized by cyclic voltametry.

3.5. Ionization potentials of thin layers of pyrene derivatives ranged from 5.2 to 5.5eV and were influenced by the electron donors. Carbazolyl containing topological isomers of pyrene showed a difference in the I_p level of 0.3eV.

3.6. Carbazol-3-yl substituted pyrene compound showed time-of-flight hole-drift mobility of 5.8×10^{-5} $cm^2V^{-1}s^{-1}$ at an electric field of 10^6 Vcm^{-1}.

4. Triphenylamino-centred dendritic compounds ramified with different electron-donating alkoxyphenyl substituents were designed, synthesized and characterised. Compounds containing shorter alkyl chains formed molecular glasses with glass transition temperature exceeding *ca.* 91 ^oC. Triphenylamine derivative containing flexible dodecyl chains formed room temperature liquid crystal and exhibited monotropic nematic discotic (N_D) mesophase with a short-range of columnar organization between 24 and 35 ^oC. Ionization potentials of triphenylamine compounds measured by photoelectron spectroscopy ranged from 5.21 to 5.47 eV. Hole-drift mobility of the amorphous layer of triphenylamine derivative containing ethyl chains at the rim exceeded 1.3×10^{-3} $cm^2\ V^{-1}\ s^{-1}$ at higher electric fields.

5. Triazine-core-based donor-acceptor organic materials were synthesised and characterised in order to reveal the influence of electron-donor substitution on their optical, photophysical and electrochemical properties. It was established that:

5.1. The triazine derivatives formed glasses with high glass transition temperatures.

5.2. The fluorescent quantum yields of dilute solutions of triazine derivatives were influenced by the electron-donor substituents and ranged from 0.25 to 0.76.

5.3. These compounds underwent electro-polymerisation during cyclic voltametry experiments.

5.4. Electroluminescent device fabricated using triazine derivative containing carbazole segments exhibited emission in the border of blue region of visible spectrum with maximum luminance of 2236 cd/m^2 at 17V.

6. **REFERENCES**

1. Zhong, C.; Duan, C.; Huang, F.; Wu, H.; Cao, Y. Materials and devices toward fully solution processable organic light-emitting diodes. *Chemistry of Materials*, 2011, vol. 23, p. 326–340.
2. Thomas, J.; Christenson, C. W.; Blanche, P. –A.; Yamamoto, M.; Norwood, R. A.; Peyghambarian, N. Photoconducting polymers for photorefractive 3D display applications. *Chemistry of Materials*, 2011, vol. 23, p. 416–429.
3. Walker, B.; Kim, C.; Nguyen, T.-Q. Small molecule solution-processed bulk heterojunction solar cells. *Chemistry of Materials*, 2011, vol. 23, p. 470–482.
4. Operamolla, A.; Farinola, G. M. Molecular and supramolecular architectures of organic semiconductors for field-effect transistor devices and sensors: A synthetic chemical perspective. *European Journal of Organic Chemistry*, 2011, p. 423–450.
5. Murayama, T. Organic photoconductive materials used for electrophotographic organic photoreceptors. *Journal of Synthetic Organic Chemistry Japan*. 1999, vol. 57, p. 541-551.
6. Kukuta, A. Infrared absorbing dyes. *Plenum press New York*, 1990, chapter 12.
7. Berner, D.; Houili, H.; Leo, W.; Zuppiroli, L. Insights into OLED functioning through coordinated experimental measurements and numerical model simulations. *Physica Status Solidi A*, 2005, vol. 202, p. 9– 36.
8. Bundgaard, E.; Krebs, F. C. Low band gap polymers for organic photovoltaics. *Solar Energy Materials and Solar Cells*, 2007, vol. 91, p. 954–985.
9. Brown, A. R.; Pomp, A.; Hart C. M.; de Leeuw D. M. Logic gates made from polymer transistors and their use in ring oscillators. *Science*, 1995, vol. 270, p. 972–974.
10. Crone, B.; Dodabalapur, A.; Lin, Y. Y.; Filas, R. W.; Bao, Z.; LaDuca, A.; Sarpeshkar, R.; Katz, H. E.; Li W. Large-scale complementary integrated circuits based on organic transistors. *Nature* 2000, vol. 403, p. 521–523.
11. Crone, B.; Dodabalapur, A.; Gelperin, A.; Torsi, L.; Katz, H. E.; Lovinger, A. J.; Bao, Z. Electronic sensing of vapors with organic transistors. *Applied Physics Letters*, 2001, vol. 78, p. 2229–2231.
12. Someya, T.; Katz, H. E.; Gelperin, A.; Lovinger, A. J.; Dodabalapur, A. Vapor sensing with α,ω-dihexylquarterthiophene field-effect transistors: The role of grain boundaries. *Applied Physics Letters*, 2002, vol. 81, p. 3079–3081.
13. Shirota, Y.; Kageyama, H. Charge carrier transporting molecular materials and their applications in devices. *Chemical Reviews*, 2007, vol. 107, p. 953-1010.
14. Strohriegl, P.; Grazulevicius, J. V. Charge-transporting molecular glasses. *Advanced Materials*, 2002, vol. 14, vol. 1439-1452.
15. Wang, J-L.; Zhong, C.; Tang, Z-M.; Wu, H.; Ma, Y.; Cao, Y.; Pei J. Solution-processed bulk heterojunction photovoltaic cells from Gradient π-conjugated thienylene vinylene dendrimers. *Chemistry: An Asian Journal*, 2010, vol. 5, p. 105–113.
16. Facchetti, A. π-Conjugated polymers for organic electronics and photovoltaic cell applications. *Chemistry of Materials*, 2011, vol. 23, p. 733–758.
17. Kwon, O.; Barlow, S.; Odom, S. A.; Beverina, L.; Thompson, N. J.; Zojer, E.;

Bredas, J-L.; Marder, S. R. Aromatic amines: A comparison of electron-donor strengths. *Journal of Physical Chemistry A*, 2005, vol. 109, p. 9346-9352.

18. Lygaitis, R.; Getautisc, V.; Grazulevicius, J. V. Hole-transporting hydrazones. *Chemical Society Reviews*, 2008, vol. 37, p. 770–788.

19. Grigalevicius, S. 3, 6 (2, 7), 9-Substituted carbazoles as electroactive amorphous materials for optoelectronics. *Synthetic Metals*, 2006, vol. 156, p. 1–12.

20. Liu, Y.; Liu, Y.; Zhan, X. High-mobility conjugated polymers based on fused-thiophene building blocks. *Macromolecular Chemistry and Physics*, 2011, vol. 212, p. 428–443

21. Wong, W-Y.; Chow, W-C.; Cheung, K-Y.; Fung, M-K.; Djurisic, A. B.; Chan, W-K. Harvesting solar energy using conjugated metallopolyyne donors containing electron-rich phenothiazine–oligothiophene moieties. *Journal of Organometallic Chemistry*, 2009, vol. 694, p. 2717–2726.

22. Wallace, J. U.; Chen, S. H. *Advances in Polymer Science: Polyfluorenes.* vol. 212, p. 145-186.

23. Ceroni, P.; Bergamini, G.; Marchioni, F.; Balzani, V. Luminescence as a tool to investigate dendrimer properties. *Progress in Polymer Science*, 2005, vol. 30, p. 453-473.

24. De Schryver F. C.; Vosch, T,; Cotlet, M.; van der Auweraer, M.; Mullen, K.; Hofkens, J. Energy dissipation in multichromophoric single dendrimers. *Accounts of Chemical Research*, 2005, vol. 38, p. 514-522.

25. Puntoriero, F.; Ceroni, P.; Balzani, V.; Bergamini, G.; Vogtle, F. Photoswitchable dendritic hosts: A dendrimer with peripheral azobenzene groups. *Journal of the American Chemical Society*, 2007, vol. 129, p. 10714-10719.

26. Lackowicz, J. R. *Principles of fluorescence spectroscopy*. 2nd Ed., Kluwer Academic/Plenum Publishers: New York, 1999, p. 595-614.

27. Birks J. B. *Photophysics of Aromatic Molecules*, Wiley-Interscience: London, 1970.

28. Ogino, K.; Iwashima, S.; Inokuchi, H.; Harada, Y. Photoelectric emission and electrical conductivity of the cesium complex with pyrene derivatives. *Bulletin of the Chemical Society of Japan*, 1965, vol. 38, p. 473-477.

29. Vollmann, H.; Becker, H.; Corell, M.; Streeck, H.; Langbein Liebigs G. Pyrene and its derivatives. *Justus Liebigs Annalen der Chemie*, 1937, vol. 531, p. 1-159.

30. Zhao, Z.; Li, J-H.; Chen, X.; Wang, X.; Lu, P.; Yang, Y. Solution-processable stiff dendrimers: Synthesis, photophysics, film morphology, and Electroluminescence. *Journal of Organic Chemistry*, 2009, vol. 74, p. 383–395.

31. Sonogashira, K.; Tohda, Y.; Hagihara, N. A convenient synthesis of acetylenes: catalytic substitutions of acetylenic hydrogen with bromoalkenes, iodoarenes and bromopyridines. *Tetrahedron Letters*, 1975, vol. 16, p. 4467–4470.

32. Venkataramana, G.; Sankararaman, S. Synthesis, absorption, and fluorescence-emission properties of 1,3,6,8-tetraethynylpyrene and its derivatives. *European Journal of Organic Chemistry*, 2005, p. 4162-4166.

33. Devadoss, C.; Bharathi, P.; Moore, J. S. Energy transfer in dendritic macromolecules: Molecular size effects and the role of an energy gradient. *Journal of the American Chemical Society*, 1996, vol. 118, p. 9635-9644.

34. Huang, J.; Li, G.; Wu, E.; Xu, Q.; Yang, Y. Achieving high-efficiency polymer white-light-emitting devices. *Advanced Materials*, 2006, vol. 18, p. 114-117.

35. Wan, Y.; Yan, L.; Zhao, Z.; Ma, X.; Guo, Q.; Jia, M.; Lu, P.; Ramos-Ortiz, G.; Maldonado, J. L.; Rodriguez, M.; Xia, A. Gigantic two-photon absorption cross sections and strong two-photon excited fluorescence in pyrene core dendrimers with fluorene/carbazole as dendrons and acetylene as linkages. *Journal of Physical Chemistry B*, 2010, vol. 114, p. 11737–11745.

36. Hu, J.; Era, M.; Elsegood, M. R. J.; Yamato, T. Synthesis and photophysical properties of pyrene-based light-emitting monomers: Highly pure-blue-fluorescent, cruciform-shaped architectures. *European Journal of Organic Chemistry*, 2010, p. 72–79.

37. Anant, P.; Lucasb, N. T.; Ball, J. M.; Anthopoulosc, T. D.; Jacob, J. Synthesis and characterization of pyrene-centered oligothiophenes. *Synthetic Metals*, 2010, vol. 160, p. 1987–1993.

38. Miyaura, N.; Suzuki, A. Palladium-catalyzed cross-coupling reactions of organoboron compounds. *Chemical Reviews*, 1995, vol. 95, p. 2457–2483.

39. Ashizawa, M.; Yamada, K.; Fukaya, A.; Kato, R.; Hara, K.; Takeya, J. Effect of molecular packing on field-effect performance of single crystals of thienyl-substituted pyrenes. *Chemistry of Materials*, 2008, vol. 20, p. 4883-4890.

40. Liu, F.; Lai, W-Y.; Tang, C.; Wu, H-B.; Chen, Q-Q.; Peng, B.; Wei, W.; Huang, W.; Cao, Y. Synthesis and characterization of pyrene-centered starburst oligofluorenes. *Macromolecular Rapid Communication*, 2008, vol. 29, p. 659–664.

41. Liu, F.; Zou, J-H.; He, Q-Y.; Tang, C.; Xie, L-H.; Peng, B.; Wei, W.; Cao, Y.; Huang, W. Carbazole end-capped pyrene starburst with enhanced electrochemical stability and device performance. *Journal of Polymer Science Part A: Polymer Chemistry*, 2010, vol. 48, p. 4943–4949.

42. Xia, R.; Lai, W-Y.; Levermore, P. A.; Huang, W.; Bradley, D. C. Low-threshold distributed-feedback lasers based on pyrene-cored starburst molecules with 1,3,6,8-attached oligo(9,9-dialkylfluorene) arms. *Advanced Functional Materials*, 2009, vol. 19, p. 2844–2850.

43. Sonar, P.; Soh, M. S.; Cheng, Y. H.; Henssler, J. T.; Sellinger, A. 1,3,6,8-Tetrasubstituted pyrenes: Solution-processable materials for application in organic electronics. *Organic Letters*, 2010, vol. 12, p. 3292-3295.

44. Milstein, D.; Stille, J. K. A general, selective, and facile method for ketone synthesis from acid chlorides and organotin compounds catalyzed by palladium. *Journal of the American Chemical Society*, 1978, vol. 100, p. 3636-3638.

45. Gingras, M.; Placide, V.; Raimundo, J-M.; Bergamini, G.; Ceroni, P.; Balzani, V. Polysulfurated pyrene-cored dendrimers: Luminescent and electrochromic properties. *Chemistry- A European Journal*, 2008, vol. 14, p. 10357–10363.

46. Bernhardt, S.; Kastler, M.; Enkelmann, V.; Baumgarten, M.; Mullen, K. Pyrene as chromophore and electrophore: Encapsulation in a rigid polyphenylene shell. *Chemistry- A European Journal* 2006, vol. 12, p. 6117–6128.

47. Brantly, T. B.; Contois, L. E.; Fox, C. J. *Photoconductive Elements Containing Substituted Triarylamine Photoconductors*, 1971, U.S. Patent No. 3567450.

48. Brantly, T. B.; Contois, L. E.; Fox, C. J. *Photoconductive Elements Containing as*

Photoconductors Triarylamines Substituted by Active Hydrogen-Containing Groups. 1972, US Patent No. 3658520.

49. Metri, N.; Sallenave, X.; Beouch, L.; Plesse, C.; Goubard, F.; Chevrot, C. New star-shaped molecules derived from thieno[3,2-*b*]thiophene unit and triphenylamine. *Tetrahedron Letters*, 2010, vol. 51, p. 6673–6676.

50. Ripaud, E.; Rousseau, T.; Leriche, P.; Roncali, J.; Unsymmetrical triphenylamine-oligothiophene hybrid conjugated systems as donor materials for high-voltage solution-processed organic solar cells. *Advanced Energy Materials*, 2011, vol. 1, p. 540–545.

51. Ripaud, E.; Olivier, Y.; Leriche, P.; Cornil, J.; Roncali, J. Polarizability and internal charge transfer in thiophene–triphenylamine hybrid π-conjugated systems. *Journal of Physical Chemistry B*, 2011, vol. 115, p. 9379–9386.

52. Wadsworth Jr, W. S. Synthetic applications of phosphoryl-stabilized anions. *Organic Reactions*, 1977, vol. 25, p. 73-253.

53. Cravino, A.; Roquet, S.; Aleveque, O.; Leriche, P.; Frere, P.; Roncali, J. Triphenylamine−oligothiophene conjugated systems as organic semiconductors for opto-electronics. *Chemistry of Materials*, 2006, vol. 18, p. 2584-2590.

54. Zhang, J.; Deng, D.; He, C.; He, Y.; Zhang, M.; Zhang, Z-G.; Zhang, Z.; Li, Y. Solution-processable star-shaped molecules with triphenylamine core and dicyanovinyl endgroups for organic solar cells. *Chemistry of Materials*, 2011, vol. 23, p. 817–822.

55. Zhang, J.; Yang, Y.; He, C.; He, Y.; Zhao, G.; Li, Y. Solution-processable star-shaped photovoltaic organic molecule with triphenylamine core and benzothiadiazole−thiophene arms. *Macromolecules*, 2009, vol. 42, p. 7619–7622.

56. Jones, G. Knoevenagel Condensation. *Organic Reactions*, 1967, vol. 15.

57. Heck, R. F.; Nolley Jr, J. P. Palladium-catalyzed vinylic hydrogen substitution reactions with aryl, benzyl, and styryl halides. *Journal of Organic Chemistry*, 1972. vol. 37, p. 2320–2322.

58. Ichikawa, M.; Hibino, K.; Yokoyama, N.; Miki, T.; Koyama, T.; Taniguchi, Y. Solution-processable dendric triphenylamine nonamers as hole-transporting and hole-injection materials for organic light-emitting devices. *Synthetic Metals*, 2006, vol. 156, p. 1383–1389.

59. Sonntag, M.; Kreger, K.; Hanft, D.; Strohriegl, P. Novel star-shaped triphenylamine-based molecular glasses and their use in OFETs. *Chemistry of Materials*, 2005, vol. 17, p. 3031-3039.

60. Jiang, K. J.; Sun, Y. L.; Shao, K. F.; Yang, L. M. Synthesis and properties of amorphous hole transport materials of triphenylamine based trihydrazones. *Chemistry Letters*, 2004, vol. 33, p. 50–51.

61. Meth-Cohn, O.; Stanforth, S. P. *Comprehensive Organic Synthesis*, Ed. B. Trost and I. Fleming, Pergamon, Oxford, 1991, vol. 4, p. 777-794.

62. Nam, H.; Kang, D. H.; Kim, J. K.; Park, S. Y. Synthesis of hole-transporting hydrazone dendrimers. *Chemistry Letters*, 2000, vol. 29, p. 1298–1299.

63. Onitsuka, K.; Ohara, N.; Takei, F.; Takahashi, S. Synthesis and redox properties of trinuclear ruthenium–acetylide complexes with tri(ethynylphenyl)amine bridge. *Dalton Transactions*, 2006, p. 3693-3698.

64. Roberts, R. L.; Schwich, T.; Corkery, T. C.; Cifuentes, M. P.; Green, K. A.; Farmer, J. D.; Low, P. J.; Marder, T. B.; Samoc, M.; Humphrey, M. G. Organometallic complexes for nonlinear optics. 45. Dispersion of the third-order nonlinear optical properties of triphenylamine-cored alkynylruthenium dendrimers. *Advanced Materials*, 2009, vol. 21, p. 2318–2322.

65. Satoh, N.; Nakashima, T.; Yamamoto, K. Metal-assembling dendrimers with a triarylamine core and their application to a dye-sensitized solar cell. *Journal of the American Chemical Society*, 2005, vol. 127, p. 13030-13038.

66. Higuchi, M.; Shiki, S.; Yamamoto, K. Novel phenylazomethine dendrimers: Synthesis and structural properties. *Organic Letters*, 2000, vol. 2, p. 3079-3082.

67. Takanashi, K.; Chiba, H.; Higuchi, M.; Yamamoto, K. Efficient synthesis of poly(phenylazomethine) dendrons allowing access to higher generation dendrimers. *Organic Letters*, 2004, vol. 6, p. 1709-1712.

68. Abrahams, B. F.; Batten, S. R.; Hamit, H.; Hoskins, B. F.; Robson, R. A wellsian 'three-dimensional' racemate: eight interpenetrating, enantiomorphic (10, 3)-a nets, four right- and four left-handed. *Chemical Communications*, 1996, p. 1313–1314.

69. Zerkowski, J. A.; Seto, C. T.; Whitesides, G. M. Solid-state structures of rosette and crinkled tape motifs derived from the cyanuric acid melamine lattice. *Journal of the American Chemical Society*, 1992, vol. 114, p. 5473–5475.

70. Chen, H-F.; Yang, S-J.; Tsai, Z-H.; Hung, W-Y.; Wang, T-C.; Wong, K-T. 1,3,5-Triazine derivatives as new electron transport–type host materials for highly efficient green phosphorescent OLEDs. *Journal of Materials Chemistry*, 2009, vol. 19, p. 8112–8118.

71. Ishi, T.; Yaguma, K.; Thiemann, T.; Yashima, M.; Ueno, K.; Mataka, S. High electron drift mobility in an amorphous film of 2,4,6,-tris[4-(1-naphthyl)phenyl]-1,3,5-triazine. *Chemistry Letters*, 2004, vol. 33, p. 1244-1245.

72. Zeng, L.; Lee, T. Y-H.; Merkel, P. B.; Chen, S. H. A new class of non-conjugated bipolar hybrid hosts for phosphorescent organic light-emitting diodes. *Journal of Materials Chemistry*, 2009, vol. 19, p. 8772–8781.

73. Rothmann, M. M.; Haneder, S.; Como, E. D.; Lennartz, C.; Schildknecht, C.; Strohriegl, P. Donor-substituted 1,3,5-triazines as host materials for blue phosphorescent organic light-emitting diodes. *Chemistry of Materials*, 2010, vol. 22, p. 2403–2410.

74. Inomata, H.; Goushi, K.; Masuko, T.; Konno, T.; Imai, T.; Sasabe, H.; Brown, J. J.; Adachi, C. High-efficiency organic electrophosphorescent diodes using 1,3,5-triazine electron transport materials. *Chemistry of Materials*, 2004, vol. 16, p. 1285–1291.

75. Omer, K. M.; Ku, S-Y.; Chen, Y-C.; Wong, K-T.; Bard, A. J. Electrochemical behavior and electrogenerated chemiluminescence of star-shaped D−A compounds with a 1,3,5-triazine core and substituted fluorene arms. *Journal of the American Chemical Society*, 2010, vol. 132, p. 10944–10952.

76. Zhong, H.; Lai, H.; Fang, Q. New conjugated triazine based molecular materials for application in optoelectronic devices: Design, synthesis, and

properties. *Journal of Physical Chemistry C*, 2011, vol. 115, p. 2423–2427.

77. Kulkarni, A. P.; Kong, X.; Jenekhe, S. A. High-performance organic light-emitting diodes based on intramolecular charge-transfer emission from donor–acceptor molecules: Significance of electron- donor strength and molecular geometry. *Advanced Functional Materials*, 2006, vol. 16, p. 1057-1066.

78. Qu, B.; Chen, Z.; Xu, F.; Cao, H.; Lan, Z.; Wang, Z.; Gong, Q. Colour stable white organic light-emitting diode based on a novel triazine derivative. *Organic Electronics*, 2007, vol. 8, p. 529–534.

79. Weder, C.; Wrighton, M. S. Efficient solid-state photoluminescence in new poly(2,5-dialkoxy-*p*-phenyleneethynylene)s. *Macromolecules*, 1996, vol. 29, p. 5157-5165.

80. Pizzoferrato, R.; Ziller, T.; Micozzi, A.; Ricci, A.; Sterzo, C. L.; Ustione, A.; Oliva, C.; Cricenti, A. Suppression of the excimer photoluminescence in a poly(arylene–ethynylene) *co*-polymer. *Chemical Physics Letters*, 2005, vol. 414, p. 234-238.

81. Xu, F.; Wang, Z.; Gong, Q. Synthesis, characterization, and optical properties of two-photon-absorbing octupolar molecule with an *s*-triazine core. *Optical Materials*, 2007, vol. 29, p. 723–727.

82. Jiang, Y.; Wang, Y.; Wang, B.; Yang, J.; He, N.; Qian. S.; Hua, J. Synthesis, two-photon absorption and optical limiting properties of multi-branched styryl derivatives based on 1,3,5-triazine. *Chemistry- An Asian Journal*, 2011, vol. 6, p. 157-165.

83. Jiang, Y. H.; Wang, Y. C.; Hua, J. L.; Tang, J.; Li, B.; Qian, S, X.; Tian, H. Multibranched triarylamine end-capped triazines with aggregation-induced emission and large two-photon absorption cross-sections. *Chemical Communications*, 2010, vol. 46, p. 4689-4691.

84. Idzik, K. R.; Rapta, P.; Cywinskie, P. J.; Beckert, R.; Dunsch, L. Synthesis and electrochemical characterization of new optoelectronic materials based on conjugated donor–acceptor system containing oligo-tri(heteroaryl)-1,3,5-triazines. *Electrochimica Acta*, 2010, vol. 55, p. 4858–4864.

85. Beltran, E.; Serrano, J. L.; Sierra, T.; Gimenez, R. Tris(triazolyl)triazine via click-chemistry: A C_3 electron-deficient core with liquid crystalline and luminescent properties. *Organic Letters*, 2010, vol. 12, p. 1404-1407.

86. Kolb, H. C.; Finn, M. G.; Sharpless, K. B. Click chemistry: Diverse chemical function from a few good reactions. *Angewandte Chemie International Edition*, 2001, vol. 40, p. 2004–2021.

87. Garcia, A.; Insuasty, B.; Herranz, M.; Martinez-Alvarez, R.; Martin, N. New building block for C_3 symmetry molecules: Synthesis of *s*-triazine-based redox active chromophores. *Organic Letters*, 2009, vol. 11, p. 5398-5401.

88. Yasuda, T.; Shimizu, T.; Liu, F.; Ungar, G.; Kato, T. Electro-functional octupolar π-conjugated columnar liquid crystals. *Journal of the American Chemical Society*, 2011, vol. 133, p. 13437–13444.

89. Hartwig, J. F. Transition metal catalyzed synthesis of arylamines and aryl ethers from aryl halides and triflates: Scope and mechanism. *Angewandte Chemie International Edition*, 1998, vol. 37, p. 2046–2067.

90. Netherton, M. R.; Fu, G. C. Air-stable trialkylphosphonium salts: Simple,

practical, and versatile replacements for air-sensitive trialkylphosphines. Applications in stoichiometric and catalytic processes. *Organic Letters*, 2001, vol. 3, p. 4295–4298.

91. Kulkarni, A. P.; Tonzola, C. J.; Babel, A.; Jenekhe, S. A. Electron transport materials for organic light-emitting diodes. *Chemistry of Materials*, 2004, vol. 16, p. 4556–4573.

92. Hughes, G.; Bryce, M. R. Electron-transporting materials for organic electroluminescent and electrophosphorescent devices. *Journal of Materials Chemistry*, 2005, vol. 15, p. 94–107.

93. Herbst W, Hunger K. *Industrial Organic Pigments*, 2nd completely revised ed. Wiley-VCH: Weinhim, 1997.

94. Huang, C.; Barlow, S.; Marder, S. R. Perylene-3,4,9,10-tetracarboxylicacid diimides: Synthesis, physical properties, and use in organic electronics. *Journal of Organic Chemistry*, 2011, vol. 76, p. 2386–2407.

95. Turkmen, G.; Erten-Ela, S.; Icli, S. Highly soluble perylene dyes: Synthesis, photophysical and electrochemical characterizations. *Dyes and Pigments*, 2009, vol. 83, p. 297–303.

96. Jones, B. A.; Ahrens, M. J.; Yoon, M-H.; Facchetti, A.; Marks, T. J.; Wasielewski, M. R. High-mobility air-stable n-type semiconductors with processing versatility: Dicyanoperylene-3,4:9,10-bis(dicarboximides). *Angewandte Chemie International Edition*, 2004, vol. 43, p. 6363 –6366.

97. Ahrens, M. J.; Fuller, M. J.; Wasielewski, M. R. Cyanated perylene-3,4-dicarboximides and perylene-3,4:9,10-bis(dicarboximide): Facile chromophoric oxidants for organic photonics and electronics. *Chemistry of Materials*, 2003, vol. 15, p. 2684-2686.

98. Katz, H. E.; Lovinger, A. J.; Johnson, J.; Kloc, C.; Siegrist, T.; Li, W.; Lin, Y-Y.; Dodabalapur, A. A soluble and air-stable organic semiconductor with high electron mobility. *Nature*, 2000, vol. 404, p. 478-481.

99. Weitz, R. T.; Amsharov, K.; Zschieschang, U.; Villas, E. B.; Goswami, D. K.; Burghard, M.; Dosch, H.; Jansen, M.; Kern, K.; Klauk, H. Organic n-channel transistors based on core-cyanated perylene carboxylic diimide derivatives. *Journal of the American Chemical Society*, 2008, vol. 130, p. 4637-4645.

100. Molinari, A. S.; Alves, H.; Chen, Z.; Facchetti, A.; Morpurgo, A. F. High electron mobility in vacuum and ambient for PDIF-CN_2 single-crystal transistors. *Journal of the American Chemical Society*, 2009, vol. 131, p. 2462–2463.

101. Yan, H.; Zheng, Y.; Blache, R.; Newman, C.; Lu, S.; Woerle, J.; Facchetti, A. Solution processed top-gate n-channel transistors and complementary circuits on plastics operating in ambient conditions. *Advanced Materials*, 2008, vol. 20, p. 3393–3398.

102. Oh, J. H.; Sun, Y-S.; Schmidt, R.; Toney, M. F.; Nordlund, D.; Konemann, M.; Wurthner, F.; Bao, Z. Interplay between energetic and kinetic factors on the ambient stability of n-channel organic transistors based on perylene diimide derivatives. *Chemistry of Materials*, 2009, vol. 21, p. 5508–5518.

103. Ling, M-M.; Erk, P.; Gomez, M.; Koenemann, M.; Locklin, J.; Bao, Z. Air-stable n-

channel organic semiconductors based on perylene diimide derivatives without strong electron withdrawing groups. *Advanced Materials*, 2007, vol. 19, p. 1123–1127.

104. Schmidt, R.; Oh, J. H.; Sun, Y-S.; Deppisch, M.; Krause, A-M.; Radacki, K.; Braunschweig, H.; Konemann, M.; Erk, P.; Bao, Z.; Wurthner, F. High-performance air-stable n-channel organic thin film transistors based on halogenated perylene bisimide semiconductors. *Journal of the American Chemical Society*, 2009, vol. 131, p. 6215–6228.

105. Schmidt, R.; Ling, M. M.; Oh, J. H.; Winkler, M.; Könemann, M.; Bao, Z.; Würthner, F. Core-fluorinated perylene bisimide dyes: Air stable n-channel organic semiconductors for thin film transistors with exceptionally high on-to-off current ratios. *Advanced Materials*, 2007, vol. 19, p. 3692–3695.

106. Pleschke, A.; Marhold, A.; Schneider, M.; Kolomeitsev, A.; Roschenthaler, G-V. Halex reactions of aromatic compounds catalysed by 2-azaallenium, carbophosphazenium, aminophosphonium and diphosphazenium salts: a comparative study. *Journal of Fluorine Chemistry*, 2004, vol. 125, p. 1031–1038.

107. Wurthner, F.; Osswald ,P.; Schmidt, R.; Kaiser, T. E.; Mansikkamaki, H.; Konemann, M. Synthesis and optical and electrochemical properties of core-fluorinated perylene bisimides.*Organic Letters*, 2006, vol. 8, p. 3765–3768.

108. Debije, M. G.; Chen, Z.; Piris, J.; Neder, R. B.; Watson, M. M.; Mullen, K.; Wurthner, F. Dramatic increase in charge carrier lifetime in a liquid crystalline perylene bisimide derivative upon bay substitution with chlorine. *Journal of Materials Chemistry*, 2005, vol. 15, p. 1270–1276.

109. Vajiravelu, S.; Lygaitis, R.; Grazulevicius, J. V.; Gaidelis, V.; Jankauskas, V.; Valiyaveettil, S. Effect of substituents on the electron transport properties of bay substituted perylene diimide derivatives. *Journal of Materials Chemistry*, 2009, vol. 19, p. 4268–4275.

110. Balaji, G.; Kale, T. S.; Keerthi, A.; Pelle, A. M. D.; Thayumanavan, S.; Valiyaveettil, S. Low band gap thiophene−perylene diimide systems with tunable charge transport properties. *Organic Letters*. 2011, vol. 13, p. 18-21.

111. Lakowicz, J. R. *Principles of Fluorescence Spectroscopy*, Kluwer Academic / Plenum Publishers, New York, 1999.

112. Miyamoto, E.; Yamaguchi, Y.; Yokoyama, M. Ionization potential of organic pigment film by atmospheric photoelectron emission analysis. *Electrophotography*, 1989, vol. 28, no. 4, p. 364-370.

113. Grigalevicius, S.; Blazys, G.; Ostrauskaite, J.; Grazulevicius, J. V.; Gaidelis, V.; Jankauskas, V.; Montrimas, E. 3,6-Di(*N*-diphenylamino)-9-phenylcarbazole and its methyl-substituted derivative as novel hole-transporting amorphous molecular materials. *Synthetic Metals*, 2002, vol. 128. p. 127-131.

114. Montrimas, E.; Gaidelis, V.; Pazera, A. The discharge kinetics of negatively charged Se electrophotographic layers. *Lithuanian Journal of Physics*, 1966, vol. 6, p. 569-578.

115. Vaezi-Nejad, S. M. Xerographic time of flight experiment for the determination of

drift mobility in high resistivity semiconductors. *International Journal of Electronics*, 1987, vol. 62, p. 361-384.

116. Archie, Y.; Chan, C.; Juhasz, C. Xerographic-mode transient charge technique for probing drift mobility in high-resistivity materials. *International Journal of Electronics*, 1987, vol. 62, p. 625-632.

117. Gritzner, G. Polarographic half-wave potentials of cations in nonaqueous solvents. *Pure and Applied Chemistry*, 1990, vol. 62, p. 1839-1858.

118. Cardona, C. M.; Li, W.; Kaifer, A. E.; Stockdale, D.; Bazan, G. C. Electrochemical considerations for determining absolute frontier orbital energy levels of conjugated polymers for solar cell applications. *Advanced Materials*, 2011, vol. 23, p. 2367–2371.

119. Boudinet, D.; Benwadih, M.; Qi, Y.; Altazin, S.; Verilhac, J-M.; Kroger, M.; Serbutoviez, C.; Gwoziecki, R.; Coppard, R.; Le Blevennec, G.; Kahn, A.; Horowitz, G. Modification of gold source and drain electrodes by self-assembled monolayer in staggered n- and p-channel organic thin film transistors. *Organic Electronics*, 2010, vol. 11, p. 227-237.

120. Georgakopoulos, S.; Sparrowe, D.; Meyer, F.; Shkunov, M. Stability of top- and bottom-gate amorphous polymer field-effect transistors. *Applied Physics Letters*, 2010, vol. 97, p. 243507-243510.

121. Braga, D.; Horowitz, G. High-performance organic field-effect transistors. *Advanced Materials*, 2009, vol. 21, p. 1473–1486.

122. Schmidt, M. W.; Baldridge, K. K.; Boatz, J. A.; Elbert, S. T.; Gordon, M. S.; Jensen, J. H.; Koseki, S.; Matsunaga, N.; Nguyen, K. A.; Su, S.; Windus, T. L.; Dupuis, M.; Montgomery, J. A. General atomic and molecular electronic structure system. *Journal of Computational Chemistry*, 1993, vol. 14, p. 1347-1363.

123. Stewart, J. J. P. Optimization of parameters for semiempirical methods V: Modification of NDDO approximations and application to 70 elements. *Journal of Molecular Modelling*, 2007, vol. 13, p. 1173-1213.

124. Harwood, L. M.; Moody, C. J.; Percy, J. M. *Experimental Organic Chemistry: Principles and Practice*,. Blackwell Publishing, Oxford 1999.

125. Percec, V.; Obata, M.; Rudick, J. G.; De, B. B.; Glodde, M.; Bera, T. K.; Magonov, S. N.; Balagurusamy, V. S. K.; Heiney, P. A. Synthesis, structural analysis, and visualization of poly(2-ethynyl-9-substituted carbazole)s and poly(3-ethynyl-9-substituted carbazole)s containing chiral and achiral minidendritic substituents. *Journal of Polymer Science, Part A: Polymer Chemistry*, 2002, vol. 40, p.3509–3533.

126. Lengvinaite, S.;Grazulevicius, J. V.; Grigalevicius, S.; Zhang, B.; Yang, J.; Xieb, Z.; Wang, L. Cross-linkable aromatic amines as materials for insoluble hole-transporting layers in light-emitting devices.*Synthetic Metals*, 2008, vol. 158, p. 213–218.

127. Li, Z.; Li, Z.; Di, C.; Zhu, Z.; Li, Q.; Zeng, Q.; Zhang, K.; Liu, Y.; Ye, C.; Qin, J. Structural control of the side-chain chromophores to achieve highly efficient nonlinear optical polyurethanes. *Macromolecules* 2006, vol. 39, p. 6951-696.

128. Freeman, A.W.; Urvoy, M.; Criswell, M. E. Triphenylphosphine-Mediated Reductive Cyclization of 2-Nitrobiphenyls: A Practical and Convenient Synthesis

of Carbazoles. *Journal of Organic Chemistry*, 2005, vol. 70, p. 5014-5019.

129. Kruzinauskiene, A.; Matoliukstyte, A.; Michaleviciute, A.; Grazulevicius, J. V.; Musnickas, J.; Gaidelis, V.; Jankauskas, V. Carbazolyl- and diphenylamino substituted fluorenes as hole transport materials. *Synthetic Metals*, 2007, vol. 157, p. 401–406.

130. Choi, J.; Kim, D.; Lee, B.; Kim, J. H. Synthesis and electro-optical properties of π-conjugated polymer based on 10-hexylphenothiazine and aromatic 1,2,4-triazole. *Bulletin of Korean Chemical Society*, 2009, vol. 30, p. 1933-1938.

131. Ebdrup, S. Preparation of 3-substituted 10-methylphenothiazines. *Journal of Chemical Society: Perkin Transactions 1*, 1998, vol. 1, p. 1147-1150.

132. Sakai, N.; Mareda, J.; Vauthey, E.; Matile, S. Core-substituted naphthalenediimides. *Chemical Communications*, 2010, vol. 46, p. 4225–4237.

133. Li, C.; Wonneberger, H. Perylene imides for organic photovoltaics: yesterday, today, and tomorrow. *Advanced Materials*, 2012, vol. 24, p. 613–636.

134. Wurthner, F. Perylene bisimide dyes as versatile building blocks for functional supramolecular architectures. *Chemical Communications*, 2004, p. 1564-1579.

135. Langhals, H. Control of the interactions in multichromophores: Novel concepts. perylene bis-imides as components for larger functional units. *Helvetica Chimica Acta*, 2005, vol. 88, p. 1309-1343.

136. Avlasevich, Y.; Li, C.; Mullen, K. Synthesis and applications of core-enlarged perylene dyes. *Journal of Materials Chemistry*, 2010, vol. 20, p. 3814-3826.

137. Wurthner, F. Bay-substituted perylene bisimides: Twisted fluorophores for supramolecular chemistry. *Pure and Applied Chemistry*, 2006, vol. 78, p. 2341-2349.

138. Tsuji, H.; Mitsui, C.; Sato, Y.; Nakamura, E. Bis(carbazolyl)benzodifuran: A high-mobility ambipolar material for homojunction organic light-emitting diode devices. *Advanced Materials*, 2009, vol. 21, p. 3776-3779.

139. Liao, Y. L.; Lin, C. Y.; Liu, Y. H.; Wong, K. T.; Hung, W. Y.; Chen, W. J. An unprecedented ambipolar charge transport material exhibiting balanced electron and hole mobilities. *Chemical Communications*, vol. 2007, p. 1831–1833.

140. Hung, W. Y.; Wang, T. C.; Chiu, H. C.; Chen, H. F.; Wong, K. T. A spiro-configured ambipolar host material for impressively efficient single-layer green electrophosphorescent devices. *Physical Chemistry Chemical Physics*, 2010, vol. 12, p. 10685-10687.

141. Wurthner, F.; Stepanenko, V.; Chen, Z.; Saha-Moller, C. R.; Kocher, N.; Stalke, D. Preparation and characterization of regioisomerically pure 1,7-disubstituted perylene bisimide dyes. *Journal of Organic Chemistry*, 2004, vol. 69, p. 7933-7939.

142. Shibano, Y.; Umeyama, T.; Matano, Y.; Imahori, H. Electron-donating perylene tetracarboxylic acids for dye-sensitized solar cells. *Organic Letters*, 2007, vol. 9, p. 1971-1974.

143. Baier, M. C.; Huber, J.; Mecking, S. Fluorescent conjugated polymer nanoparticles by polymerization in miniemulsion. *Journal of the American Chemical Society*, 2009, vol. 131, p. 14267–14273.

144. Sivamurugan, V.; Kazlauskas, K.; Jursenas, S.; Gruodis, A.; Simokaitiene, J.; Grazulevicius, J. V.; Valiyaveettil, S. Synthesis and photophysical properties of glass-forming bay-substituted perylenediimide derivatives. *Journal of Physical Chemistry B*, 2010, vol. 114, p. 1782-1789.

145. Langhals, H.; Jaschke, H. Naphthalene amidine imide dyes by transamination of naphthalene bisimides. *Chemistry- A European Journal*, 2006, vol. 12, p. 2815–2824.

146. Adachi, M.; Murata, Y.; Nakamura, S. Spectral similarity and difference of naphthalenetetracarboxylic dianhydride, perylenetetracarboxylic dianhydride, and their derivatives. *Journal of Physical Chemistry*, 1995, vol. 99, p. 14240–14246.

147. Thalacker, C.; Roger, C.; Wurthner, F. Synthesis and optical and redox properties of core-substituted naphthalene diimide dyes. *Journal of Organic Chemistry* 2006, vol. 71, p. 8098–8105.

148. Chao, C. C.; Leung, M. K.; Su, Y. O.; Chiu, K. Y.; Lin, T. H.; Shieh, S. J.; Lin, S. C. Photophysical and electrochemical properties of 1, 7-diaryl-substituted perylene diimides. *Journal of Organic Chemistry*, 2005, vol. 70, p. 4323–4331.

149. Lin, C. C.; Velusamy, M.; Chou, H. H.; Lin, J. T.; Chou, P. T. Synthesis and characterization of naphthalene diimide (NDI)-based near infrared chromophores with two-photon absorbing properties. *Tetrahedron*, 2010, vol. 66, p. 8629–8634.

150. Velusamy, M.; Shen, J-Y.; Lin, J. T.; Hsieh, C-C.; Lai, C-H.; Lai, C-W.; Ho, M-L.; Chen, Y-C.; Chou, P. T.; Hsiao, J. K. A new series of quadrupolar type two-photon absorption chromophores bearing 11, 12-dibutoxydibenzo[*a*,*c*]-phenazine bridged amines; their applications in two-photon fluorescence imaging and two-photon photodynamic therapy. *Advanced Functional Materials*, 2009, vol. 19, p. 2388–2397.

151. Edvinsson, T.; Li, C.; Pschirer, N. G.; Schoneboom, J.; Eickemeyer, F.; Sens, R.; Boschloo, G.; Herrmann, A.; Mullen, K.; Hagfeldt, A. Intramolecular charge-transfer tuning of perylenes: Spectroscopic features and performance in dye-sensitized solar cells. *Journal of Physical Chemistry C*, 2007, vol. 111, p. 15137-15140.

152. Osswald, P.; Leusser, D.; Stalke, D.; Wurthner, F. Perylene bisimide based macrocycles: Effective probes for the assessment of conformational effects on optical properties. *Angewandte Chemie International Edition*, 2005, vol. 44, p. 250-253.

153. Lee, S. K.; Zu, Y.; Herrmann, A.; Geerts, Y.; Mullen, K.; Bard, A. J. Electrochemistry, spectroscopy and electrogenerated chemiluminescence of perylene, terrylene, and quaterrylene diimides in aprotic solution. *Journal of the American Chemical Society*, 1999, vol. 121, p. 3513–3530.

154. Li, J.; Dierschke, F.; Wu, J.; Grimsade, A. C.; Mullen, K. Poly(2,7-carbazole) and perylene tetracarboxydiimide: A promising donor/acceptor pair for polymer solar cells. *Journal of Materials Chemistry*, 2006, vol. 16, p. 96-100.

155. Chen, S.; Liu, Y.; Qiu, W.; Sun, X.; Ma, Y.; Zhu, D. Oligothiophene-functionalized perylene bisimide system: Synthesis, characterization, and electrochemical polymerization properties. *Chemistry of Materials* 2005, vol. 17, p. 2208-2215.

156. Qu, J.; Pschirer, N. G.; Liu, D.; Stefan, A.; Schryver, F. C. D.; Mullen, K.

Dendronized Perylenetetracarboxdiimides with peripheral triphenylamines for intramolecular energy and electron transfer. *Chemistry- A European Journal*, 2004, vol. 10, p. 528-437.

157. Borsenberger, P. M.; Pautmeier, L.; Bassler, H. Charge transport in disordered molecular solids. *Journal of Chemical Physics* 1991, vol. 94, p. 5447-5454.

158. Bassler, H. Hopping conduction in polymers. *International Journal of Modern Physics B*, 1994, vol. 8, p. 847-854.

159. Wen, Y.; Liu, Y. Recent progress in n-channel organic thin-film transistors. *Advanced Materials*, 2010, vol. 22, p. 1331-1345.

160. Newman, C. R.; Frisbie, C. D.; Filho, D. A. S.; Bredas, J.; Ewbank, P. C.; Mann, K. R. Introduction to organic thin film transistors and design of n-channel organic semiconductors. *Chemistry of Materials* 2004, vol. 16, p. 4436-4451.

161. Geng, Y.; Wang, J.; Wu, S.; Li, H.; Yu, F.; Yang, G.; Gao, H.; Su, Z. Theoretical discussions on electron transport properties of perylene bisimide derivatives with different molecular packings and intermolecular interactions. *Journal of Materials Chemistry*, 2011, vol. 21, p. 134-143.

162. Li, C.; Schoneboom, J.; Liu, Z.; Pschirer, N. G.; Erk, P.; Herrmann, A.; Mullen, K. Rainbow perylene monoimides: Easy control of optical properties. *Chemistry - European Journal*, 2009, vol. 15, p.878 - 884.

163. An, Z.; Yu, J.; Jones, S. C.; Barlow, S.; Yoo, S.; Domercq, B.; Prins, P.; Siebbeles, L. D. A.; Kippelen, B.; Marder, S. R. High electron mobility in room-temperature discotic liquid-crystalline perylene diimides. *Advanced Materials*, 2005, vol. 17, p. 2580–2583.

164. Georgakopoulos, S.; Sparrowe, D.; Meyer, F.; Shkunov, M. Stability of top- and bottom-gate amorphous polymer field-effect transistors. *Applied Physics Letters*, 2010, vol. 97, p. 243507- 243510.

165. Cheng, X.; Noh, Y-Y.; Wang, J.; Tello, M.; Frisch, J.; Blum, R. P.; Vollmer, A.; Rabe, J. P.; Koch, N.; Sirringhaus, H. Controlling electron and hole charge injection in ambipolar organic field-effect transistors by self-assembled monolayers. *Advanced Functional Materials*, 2009, vol. 19, p. 2407–2415.

166. Chen, Z.; Zheng, Y.; Yan, H.; Facchetti, A. Naphthalenedicarboximide- vs perylenedicarboximide-based copolymers. Synthesis and semiconducting properties in bottom-gate n-channel organic transistors. *Journal of the American Chemical Society*, 2009, vol. 131, p. 8-9.

167. Guo, X.; Watson, M. D. Conjugated polymers from naphthalene bisimide. *Organic Letters*, 2008, vol.10, p. 5333-5336.

168. Adam, W.; Qian, X.; Saha-Moller, C. R. Synthesis of photooxygenation of 2,3,6-trimethylfuro[2,3-b][1]naphtho[4a,7a-e,f]pyrida-5,7-dione, a potential chemiluminescent probe for singlet oxygen. *Tetrahedron*, 1993, vol. 49, p. 417-422.

169. Gudeika, D.; Lygaitis, R.; Mimait, V.; Grazulevicius, J. V.; Jankauskas, V.; Lapkowski, M.; Data, P. Hydrazones containing electron-accepting and electron-donating moieties. *Dyes and Pigments*, 2011, vol. 91, p. 13-19.

170. Borsenberger, M.; Weiss, D. S. *Photoreceptors for imaging systems.* New York: Marcel Dekker; 1993.

171. Han, Y.; Fei, Z.; Sun, M.; Bo, Z.; Liang, W. Z. Unusual aggregation of nanosized six-arm star oligofluorenes. *Macromolecular Rapid Communications*, 2007, vol. 28, p. 1017-1023.

172. Kanibolotsky, A. L.; Perepichka, I. F.; Skabara, P. J. Star-shaped π-conjugated oligomers and their applications in organic electronics and photonics. *Chemical Society Review*, 2010, vol. 39, p. 2695-2728.

173. Huang, H.; Fu, Q.; Zhuang, S.; Mu, G.; Wang, L.; Chen, J.; Ma, D.; Yang, C. Solution-processable 1,3,5-tri(9-anthracene)-benzene cored propeller-shaped materials with high T_g for blue organic light-emitting diodes. *Organic Electronics*, 2011, vol. 12, p. 1716-1723.

174. Hirose, T.; Shibano, Y.; Miyazaki, Y.; Sogoshi, N.; Nakabayashi, S.; Yasutake, M. Synthesis and hole transport properties of highly soluble pyrene-based discotic liquid crystals with trialkylsilylethynyl groups. *Molecular Crystals and Liquid Crystals*, 2011, vol. 534, p. 81-92.

175. Xing, Y.; Xu, X.; Zhang, P.; Tian, W.; Yu, G.; Lu, P.; Liu, Y.; Zhu, D. Carbazole–pyrene-based organic emitters for electroluminescent device. *Chemical Physics Letters*, 2005, vol. 408, p. 169-173.

176. Lengvinaite, S.; Grazulevicius, J. V.; Grigalevicius, S.; Gub, R.; Dehaen, W.; Jankauskas, V.; Zhang, B.; Xie, Z. Indolo[3,2-*b*]carbazole-based functional derivatives as materials for light emitting diodes. *Dyes and Pigments*, 2010, vol. 85, p.183-188.

177. Simokaitiene, J.; Grazulevicius, J. V.; Jankauskas, V.; Rutkaite, R.; Sidaravicius, J. Synthesis and properties of glass-forming phenothiazine and carbazole adducts. *Dyes and Pigments*, 2008, vol. 79, p. 40-47.

178. Cao, H.; Chen, Z.; Liu, Y.; Qu, B.; Xu, S.; Cao, S.; Lan, Z.; Wang, Z.; Gong, Q. Undoped yellow-emitting organic light-emitting diodes from a phenothiazine-based derivative. *Synthetic Metals*, 2007, vol. 157, p. 427-431.

179. Lai, R. Y.; Kong, X.; Jenekhe, S. A.; Bard, A. J. Synthesis, cyclic voltammetric studies, and electrogenerated chemiluminescence of a new phenylquinoline-biphenothiazine donor−acceptor molecule. *Journal of the American Chemical Society*, 2003, vol. 125, p. 12631-12639.

180. Simokaitiene, J.; Grigalevicius, S.; Grazulevicius, J. V.; Rutkaite, R.; Kazlauskas, K.; Jursenas, S.; Jankauskas, V.; Sidaravicius, J. Synthesis, photophysical and photoelectrical properties of glass-forming phenothiazinyl- and carbazolyl-substituted ethylenes. *Journal of Optoelectronics and Advanced Materials*, 2006, vol. 8, p. 876-882.

181. Basuray, G.; Chakraborty, I.; Moulik, S. Pyrene absorption can be a convenient method for probing critical micellar concentration (cmc) and indexing micellar polarity. *Journal of Colloid and Interface Science*, 2006, vol. 294, p. 248-254.

182. Romero-Ale, E. E.; Olives, A.I.; Martín, M. A.; del Castillo, B.; López-Alvarado, P.; Menéndez, J. C. Environmental effects on the fluorescence behaviour of carbazole derivatization reagents. *Luminescence*, 2005, vol. 20, p. 162-169.

183. Crawford, A. G.; Dwyer, A. D.; Liu, Z.; Steffen, A.; Beeby, A.; Palsson, L-O.; Tozer, D. J.; Marder, T. B. Experimental and theoretical studies of the photophysical properties of 2- and 2,7-functionalized pyrene derivatives. *Journal of*

the American Chemical Society, 2011, vol. 133, p. 13349-13362.

184. Karpicz, R.; Puzinas, S.; Krotkus, S.; Kazlauskas, K.; Jursenas, S.; Grazulevicius, J. V.; Grigalevicius, S.; Gulbinas, V. Impact of intramolecular twisting and exciton migration on emission efficiency of multifunctional fluorene-benzothiadiazole-carbazole compounds.*Journal of Chemical Physics*, 2011, vol. 134, p. 204508-204516.

185. Acar, N.; Kurzawa, J.; Fritz, N.; Stockmann, A.; Roman, C.; Schneider, S.; Clark, T. Phenothiazine−pyrene dyads: Photoinduced charge separation and structural relaxation in the CT state. *Journal of Physical Chemistry A*, 2003, vol. 107, p. 9530-9541.

186. Zhang, C.; Xu, Y.; Wang, N.; Xu, Y.; Xiang, W.; Ouyang, M.; Ma, C. Electrosyntheses and characterizations of novel electrochromic copolymers based on pyrene and 3,4-ethylenedioxythiophene. *Electrochimica Acta*, 2009, vol. 55, p. 13-18.

187. Xu, L.; Zhao, J.; Liu, R.; Liu, H.; Liu, J.; Wang, H. Electrosyntheses and characterizations of novel electrochromic and fluorescent copolymers based on 2,2′-bithiophene and pyrene. *Electrochimica Acta*, 2010, vol. 55, p. 8855-8862.

188. Ambrose, J. F.; Nelson, R. F. J. Anodic oxidation pathways of carbazoles I. Carbazole and N-substituted derivatives. *Journal of Electrochemical Society: Electrochemical Science*, 1968, p. 1159-1164.

189. Tidwell, C. P.; Alexander, L. A.; Fondren, L. D.; Belmore, K.; Nikles, D. E. Synthesis and characterization of 5, 10, 15, 20-tetra(N-ethyl-3-carbazoyl)porphyrin. *Indian Journal of Chemistry*, 2007, vol. 46, p. 1658-1665.

190. Morin, J-F.; Leclerc, M.; Ades, D.; Siove, A. Polycarbazoles: 25 years of progress. *Macromolecular Rapid Communications*, 2005, vol. 26, p. 761-778.

191. de Halleux, V.; Calbert, J. –P.; Brocorens, P.; Cornil, J.; Declercq, J.–P.; Brédas, J. –L.; Geerts, Y. 1,3,6,8-Tetraphenylpyrene derivatives: Towards fluorescent liquid-crystalline columns? *Advanced Functional Materials*, 2004, vol. 14, p. 649-659.

192. Pomerantz, Z.; Zaban, A.; Ghosh, S.; Lellouche, J-P.; Garcia-Belmonte, G.; Bisquert, J. Capacitance, spectroelectrochemistry and conductivity of polarons and bipolarons in a polydicarbazole based conducting polymer. *Journal of Electroanalytical Chemistry*, 2008, vol. 614, p. 49-60.

193. van Haare, J. A. E. H.; Havinga, E. E.; van Dongen, J. L. J.; Janssen, R. A. J.; Cornil, J.; Bredas, J.-L. Redox states of long oligothiophenes: Two polarons on a single chain. *Chemistry - European Journal*, 1998, vol. 4, p. 1509-1522.

194. Otero, L.; Sereno, L.; Fungo, F.; Liao, Y-Li.; Lin, C-Y.; Wong, K-T. Synthesis and properties of a novel electrochromic polymer obtained from the electropolymerization of a 9, 9'-spirobifluorene-bridged donor-acceptor (D-A) bichromophore system. *Chemistry of Materials*, 2006, vol. 18, p. 3495-3502.

195. Taerum, T.; Lukoyanova, O.; Wylie, R. G.; Perepichka, D. F. Synthesis, polymerization, and unusual properties of new star-shaped thiophene oligomers. *Organic Letters*, 2009, vol. 11, p. 3230-3233.

196. Domagala, W.; Pilawa, B.; Lapkowski, M. Quantitative in-situ EPR spectroelectrochemical studies of doping processes in poly(3,4-alkylenedioxythiophene)s Part 1: PEDOT. *Elecrochimica Acta*, 2008, vol. 53, p.

4580-4590.

197. Adachi, C.; Nagai, K.; Tamoto, N. Molecular design of hole transport materials for obtaining high durability in organic electroluminescent diodes. *Applied Physics Letters*, 1995, vol. 66, p. 2679-2681.

198. Shirota, Y. Photo- and electroactive amorphous molecular materials—molecular design, syntheses, reactions, properties, and applications. *Journal of Materials Chemistry*, 2005, vol. 15, p. 75-93.

199. Thelakkat, M. Star-shaped, dendrimeric and polymeric triarylamines as photoconductors and hole transport materials for electro-optical applications. *Macromolecular Materials and Engineering*, 2002, vol. 287, p. 442-461.

200. Lu, J. P.; Xia, P. F.; Lo, P. K.; Tao, Y.; Wong, M. S. Synthesis and properties of multi-triarylamine-substituted carbazole-based dendrimers with an oligothiophene core for potential applications in organic solar cells and light-emitting diodes. *Chemistry of Materials*, 2006, vol. 18, p. 6194-6203.

201. Barrio, L.; Catalan, J.; de Paz J. L. G. DFT study of ionization potentials for aza-substituted aromatic rings. *International Journal of Quantum Chemistry*, 2003, vol. 91, p. 432–437.

202. Schwab P. F. H.; Smith, J. R.; Michl, J. Synthesis and properties of molecular rods. 2. Zig-Zag rods. *Chemical Reviews*, 2005, vol. 105, p. 1197–1280.

203. Wu, P-T. ; Kim, F. S. ; Champion, R. D. ; Jenekhe, S. A. Conjugated donor−acceptor copolymer semiconductors. Synthesis, optical Properties, electrochemistry, and field-effect carrier mobility of pyridopyrazine-based copolymers. *Macromolecules*, 2008, vol. 41, p. 7021–7028.

204. Grabowski, Z. R.; Rotkiewicz, K.; Rettig, W. Structural changes accompanying intramolecular electron transfer: Focus on twisted intramolecular charge-transfer states and structures. *Chemical Reviews*, 2003, vol. 103, p. 3899–4032.

205. Marini, A.; Muñoz-Losa, A.; Biancardi, A.; Mennucci, B. What is solvatochromism? *Journal of Physical Chemistry B*, 2010, vol. 114, p. 17128–17135.

206. Krotkus, S.; Kazlauskas, K.; Miasojedovas, A.; Gruodis, A.; Tomkeviciene, A.; Grazulevicius J. V.; Jursenas, S. Pyrenyl-functionalized fluorene and carbazole derivatives as blue light emitters. *Journal of Physical Chemistry C*, 2012, vol. 116, p. 7561-7572.

207. Kersting, R.; Mollay, B.; Rusch, M.; Wenisch, J.; Leising, G.; Kauffmann, H. F. Femtosecond site-selective probing of energy relaxing excitons in poly(phenylenevinylene): Luminescence dynamics and lifetime spectra. *Journal of Chemical Physics*, 1997, vol. 106, p. 2850–2864.

208. Promarak, V.; Ichikawa, M.; Sudyoadsuk, T.; Saengsuwan, S.; Jungsuttiwong, S.; Keawin, T. Synthesis of electrochemically and thermally stable amorphous hole-transporting carbazole dendronized fluorene. *Synthetic Metals*, 2007, vol. 157, p. 17–22.

209. Doskocz, J.; Doskocz, M.; Roszak, S.; Soloducho, J.; Leszczynski J. Theoretical studies of symmetric five-membered heterocycle derivatives of carbazole and fluorene: Precursors of conducting polymers. *Journal of Physical Chemistry A*, 2006, vol. 110, p. 13989-13994.

210. Xu, C.; Zhao, J.; Wang, M.; Wang, Z.; Cui, C.; Kong, Y.; Zhang, X. Electrosynthesis and characterization of a neutrally colorless electrochromic material from poly(1,3-bis(9H-carbazol-9-yl)benzene) and its application in electrochromic devices. *Electrochimica Acta*, 2012, vol. 75, p. 28–34.

LIST OF PUBLICATIONS

1. Reghu, Renji Reghu; Bisoyi, Hari Kkrishna; Grazulevicius, Juozas Vidas; Anjukandi, Padmesh; Gaidelis, Valentas; Jankauskas, Vygintas. Air stable electron-transporting and ambipolar bay substituted perylene bisimides // Journal of Materials Chemistry. ISSN 0959-9428. 2011, vol. 21, p. 7811-7819. [ISI Web of Science].
2. Pron, Adam; Reghu, Renji Reghu; Rybakiewicz, Renata; Cybulski, Hubert; Djurado, David; Grazulevicius, Juozas Vidas; Zagorska, Malgorzata; Kulszewicz-Bajer, Irena; Verilhac, Jean-Marie. Triarylamine Substituted Arylene Bisimides as Solution Processable Organic Semiconductors for Field Effect Transistors. Effect of Substituent Position on Their Spectroscopic, Electrochemical, Structural, and Electrical Transport Properties // Journal of Physical Chemistry C. ISSN 1932-7447. 2011, 115, 15008–15017. [ISI Web of Science].
3. Reghu, Renji Reghu; Grazulevicius, Juozas Vidas; Simokaitiene, Jurate; Miasojedovas, Arunas; Kazlauskas, Karolis; Juršenas, Saulius; Data, Przemyslaw; Karon, Krzysztof; Lapkowski, Mieczyslaw; Gaidelis, Valentas; Jankauskas, Vygintas. Glass-Forming Carbazolyl- and Phenothiazinyl-Tetra Substituted Pyrene Derivatives: Photophysical, Electrochemical and Photoelectrical Properties // Journal of Physical Chemistry C. ISSN 1932-7447. Accepted for publication, DOI: 10.1021/jp3019952. [ISI Web of Science].

LIST OF PRESENTATIONS IN INTERNATIONAL CONFERENCES

1. Reghu, Renji Reghu; Grazulevicius, Juozas Vidas; Jankauskas, Vygintas; Gaidelis, Valentas; Kazlauskas, Karolis; Juršenas, Saulius. Synthesis and Properties of Electron-Donor Functionalized Symmetric Compounds Containing Aromatic Polycyclic- or Amino- Core for Organic Electronics // Nanax5: May 7 – 11, 2012, Fuengirola, SPAIN. p. 184.
2. Reghu, Renji Reghu; Grazulevicius, Juozas Vidas; Jankauskas, Vygintas; Gaidelis, Valentas; Kazlauskas, Karolis; Juršenas, Saulius. Synthesis and Properties of Electron-Donor-Substituted Perylene Bisimides and Pyrenes // 10th International Symposium on Functional π-Electron Systems (F-π-10):

October 13 – 17, 2011, Beijing, CHINA / Institute of Chemistry of the Chinese Academy of Sciences, 2011. p. 376.
3. Reghu, Renji Reghu; Grazulevicius, Juozas Vidas; Kazlauskas, Karolis; Juršenas, Saulius; Jankauskas, Vygintas; Gaidelis, Valentas; Data, Przemyslaw; Karon, Krzysztof; Lapkowski, Mieczyslaw. Synthesis and Properties of Dendritic Organic Materials Based on Pyrene, Triphenylamine and Triazine derivatives // Baltic Polymer Symposium (BPS-2011): September 21 – 24, 2011, Pärnu, ESTONIA. Tallinn University of Technology, 2011. p. 76.
4. Reghu, Renji Reghu; Grazulevicius, Juozas Vidas; Reina Lozano, José Antonio. Synthesis and properties of liquid crystalline dendritic organic semiconductors for optoelectronic applications // 11th European Conference on Liquid Crystals (ECLC-2011): February 06 – 11, 2011, Maribor, SLOVENIA / University of Maribor, 2011. ISBN 978-961-6657-19-8. p. P1-17.
5. Reghu, Renji Reghu; Grazulevicius, Juozas Vidas; Jankauskas, Vygintas. Perylene bisimide, pyrene and triazine based organic semiconductors for optoelectronic applications // Baltic Polymer Symposium (BPS-2010): September 08 – 12, 2010, Palanga, LITHUANIA / Kaunas University of Technology, Vilnius Uiversity, 2010. ISBN 978-9955-25-838-4, p. 130.

ACKNOWLEDGEMENTS

Financial support from the European Commission under FP-7 PEOPLE PROGRAMME (MCA–ITN Grant No. 215884) is greatly acknowledged.
Prof. Habil. Dr. J. V. Gražulevičius, Department of Organic Technology, Kaunas University of Technology, is greatly acknowledged for supervising me through my research and for helping me to overcome the usual hurdles of my Doctoral research.
Dr. V. Gaidelis and Dr. V. Jankauskas, Department of Solid State Electronics, Vilnius University, are thanked for the measurements of ionisation potentials and charge carrier mobilities.
Prof. S. Juršenas and Dr. K. Kazlauskas, Institute of Applied Research, Vilnius University, are sincerely thanked for the measurements of fluorescence quantum efficiencies.
Prof. M. Lapkowski and Mr. P. Data, Faculty of Chemistry, Silesian University of Technology, are thanked for electrochemical measurements.
Prof. A. Pron, Laboratoire d'Electronique Moleculaire Organique et Hybride, CEA Grenoble, is greatly acknowledged for OFET fabrication.
Dr. P. Anjukandi, Ruhr-Universität Bochum, is sincerely thanked for DFT level calculations.
Prof. J. A. Reina Lozano, Departament de Química Analítica i Química Orgànica, Universitat Rovira I Virgili, is kindly acknowledged for the polarized optical microscopy.
Prof. A. Kukhta, Nanyang Technological University, is thanked for the fabrication of electroluminescent devices.
Dr. A. Swinarew, Institute of Materials Science, University of Silesia, is thanked for MALDI-TOF spectrometry.
Dr. J. Simokaitiene of Department of Organic Technology, Kaunas University of Technology and Ms. A. Sakalyte of Departament d'Enginyeria Química, Universitat Rovira i Virgili are sincerely thanked for DSC and TGA measurements.
Dr. M. Krenevičienė of Department of Organic Technology, Vilnius University; Dr. K. Rutkauskas, Dr. B. Barvainienė and A. Urbonavičienė of Department of Organic Chemistry; Dr. I. Liutvinienė and Dr. R. Lygaitis of Department of Organic Technology, Kaunas University of Technology are acknowledged for ^{1}H NMR, ^{13}C NMR and IR spectroscopy and elemental analysis.

All the members of “Dendreamers” project consortium are sincerely thanked for the useful discussions and valuable comments that I had during the meetings and schools.
Finally, all the coworkers from the Department of Organic Technology, Kaunas University of Technology are kindly thanked for their helpful advices and for making my stay at Kaunas a memorable one.